

SOIL EROSION IN THE ALPS- CAUSES AND RISK ASSESSMENT

Inauguraldissertation

zur
Erlangung der Würde eines Doktors der Philosophie
vorgelegt der
Philosophisch-Naturwissenschaftlichen Fakultät
der Universität Basel

von

Katrin Meusburger
aus Waldshut (Deutschland)

Basel, 2010

Originaldokument gespeichert auf dem Dokumentenserver der Universität Basel
edoc.unibas.ch



Dieses Werk ist unter dem Vertrag „Creative Commons Namensnennung-Keine kommerzielle Nutzung-Keine Bearbeitung 2.5 Schweiz“ lizenziert. Die vollständige Lizenz kann unter
creativecommons.org/licences/by-nc-nd/2.5/ch
eingesehen werden.

Genehmigt von der Philosophisch-Naturwissenschaftlichen Fakultät
auf Antrag von

Prof. Dr. Christine Alewell
Fakultätsverantwortliche / Dissertationsleiterin

Prof. Dr. Nikolaus J. Kuhn
Korreferent

Basel, den 17.02.2009

Prof. Dr. Eberhard Parlow
Dekan



Namensnennung-Keine kommerzielle Nutzung-Keine Bearbeitung 2.5 Schweiz

Sie dürfen:



das Werk vervielfältigen, verbreiten und öffentlich zugänglich machen

Zu den folgenden Bedingungen:



Namensnennung. Sie müssen den Namen des Autors/Rechteinhabers in der von ihm festgelegten Weise nennen (wodurch aber nicht der Eindruck entstehen darf, Sie oder die Nutzung des Werkes durch Sie würden entlohnt).



Keine kommerzielle Nutzung. Dieses Werk darf nicht für kommerzielle Zwecke verwendet werden.



Keine Bearbeitung. Dieses Werk darf nicht bearbeitet oder in anderer Weise verändert werden.

- Im Falle einer Verbreitung müssen Sie anderen die Lizenzbedingungen, unter welche dieses Werk fällt, mitteilen. Am Einfachsten ist es, einen Link auf diese Seite einzubinden.
- Jede der vorgenannten Bedingungen kann aufgehoben werden, sofern Sie die Einwilligung des Rechteinhabers dazu erhalten.
- Diese Lizenz lässt die Urheberpersönlichkeitsrechte unberührt.

Die gesetzlichen Schranken des Urheberrechts bleiben hiervon unberührt.

Die Commons Deed ist eine Zusammenfassung des Lizenzvertrags in allgemeinverständlicher Sprache:
<http://creativecommons.org/licenses/by-nc-nd/2.5/ch/legalcode.de>

Haftungsausschluss:

Die Commons Deed ist kein Lizenzvertrag. Sie ist lediglich ein Referenztext, der den zugrundeliegenden Lizenzvertrag übersichtlich und in allgemeinverständlicher Sprache wiedergibt. Die Deed selbst entfaltet keine juristische Wirkung und erscheint im eigentlichen Lizenzvertrag nicht. Creative Commons ist keine Rechtsanwaltsgesellschaft und leistet keine Rechtsberatung. Die Weitergabe und Verlinkung des Commons Deeds führt zu keinem Mandatsverhältnis.

SUMMARY

The issue of soil erosion in the Alps has long been neglected due to the low economic value of the agricultural land. However, soil stability is a key parameter which affects ecosystem services like slope stability, water budgets (drinking water reservoirs as well as flood prevention), vegetation productivity, ecosystem biodiversity and nutrient production. In alpine regions, spatial estimates on soil erosion are difficult to derive because the highly heterogeneous biogeophysical structure impedes measurement of soil erosion and the applicability of soil erosion models. However, remote sensing and geographic information system (GIS) methods allow for spatial estimation of soil erosion by direct detection of erosion features and supply of input data for soil erosion models.

Thus, the main objective of this work is to address the problem of soil erosion risk assessment in the Alps on catchment scale with remote sensing and GIS tools. Regarding soil erosion processes the focus is on soil erosion by water (here sheet erosion) and gravity (here landslides). For these two processes we address i) the monitoring and mapping of the erosion features and related causal factors ii) soil erosion risk assessment with special emphasis on iii) the validation of existing models for alpine areas. All investigations were accomplished in the Urseren Valley (Central Swiss Alps) where the valley slopes are dramatically affected by sheet erosion and landslides.

For landslides, a natural susceptibility of the catchment has been indicated by bivariate and multivariate statistical analysis. Geology, slope and stream density are the most significant static landslide causal factors. Static factors are here defined as factors that do not change their attributes during the considered time span of the study (45 years), e.g. geology, stream network.

The occurrence of landslides might be significantly increased by the combined effects of global climate and land use change. Thus, our hypothesis is that more recent changes in land use and climate affected the spatial and temporal occurrence of landslides. The increase of the landslide area of 92% within 45 years in the study site confirmed our hypothesis. In order to identify the cause for the trend in landslide occurrence time-series of landslide causal factors were analysed. The analysis revealed increasing trends in the frequency and intensity of extreme rainfall events and stocking of pasture animals. These developments presumably enhanced landslide hazard. Moreover, changes in land-cover and land use were shown to have affected landslide occurrence. For instance, abandoned areas and areas with recently emerging shrub vegetation show very low landslide densities. Detailed

spatial analysis of the land use with GIS and interviews with farmers confirmed the strong influence of the land use management practises on slope stability. The definite identification and quantification of the impact of these non-stationary landslide causal factors (dynamic factors) on the landslide trend was not possible due to the simultaneous change of several factors.

The consideration of dynamic factors in statistical landslide susceptibility assessments is still unsolved. The latter may lead to erroneous model predictions, especially in times of dramatic environmental change. Thus, we evaluated the effect of dynamic landslide causal factors on the validity of landslide susceptibility maps for spatial and temporal predictions. For this purpose, a logistic regression model based on data of the year 2000 was set up. The resulting landslide susceptibility map was valid for spatial predictions. However, the model failed to predict the landslides that occurred in a subsequent event. In order to handle this weakness of statistic landslide modelling a multitemporal approach was developed. It is based on establishing logistic regression models for two points in time (here 1959 and 2000). Both models could correctly classify >70% of the independent spatial validation dataset. By subtracting the 1959 susceptibility map from the 2000 susceptibility map a deviation susceptibility map was obtained. Our interpretation was that these susceptibility deviations indicate the effect of dynamic causal factors on the landslide probability. The deviation map explained 85% of new independent landslides occurring after 2000. Thus, we believe it to be a suitable tool to add a time element to a susceptibility map pointing to areas with changing susceptibility due to recently changing environmental conditions or human interactions.

In contrast to landslides that are a direct threat to buildings and infrastructure, sheet erosion attracts less attention because it is often an unseen process. Nonetheless, sheet erosion may account for a major proportion of soil loss. Soil loss by sheet erosion is related to high spatial variability, however, in contrast to arable fields for alpine grasslands erosion damages are long lasting and visible over longer time periods. A crucial erosion triggering parameter that can be derived from satellite imagery is fractional vegetation cover (FVC). Measurements of the radiogenic isotope Cs-137, which is a common tracer for soil erosion, confirm the importance of FVC for soil erosion yield in alpine areas. Linear spectral unmixing (LSU), mixture tuned matched filtering (MTMF) and the spectral index NDVI are applied for estimating fractional abundance of vegetation and bare soil. To account for the small scale heterogeneity of the alpine landscape very high resolved multispectral QuickBird imagery is used. The performance of LSU and MTMF for estimating percent vegetation cover is good ($r^2=0.85$, $r^2=0.71$ respectively). A poorer performance is achieved for bare soil ($r^2=0.28$, $r^2=0.39$ respectively) because compared to vegetation, bare soil has a less characteristic spectral signature in the wavelength domain detected by the QuickBird sensor.

Apart from monitoring erosion controlling factors, quantification of soil erosion by applying soil erosion risk models is done. The performance of the two established models Universal Soil Loss Equation (USLE) and Pan-European Soil Erosion Risk

Assessment (PESERA) for their suitability to model erosion for mountain environments is tested. Cs-137 is used to verify the resulting erosion rates from USLE and PESERA. PESERA yields no correlation to measured Cs-137 long term erosion rates and shows lower sensitivity to FVC. Thus, USLE is used to model the entire study site. The LSU-derived FVC map is used to adapt the *C* factor of the USLE. Compared to the low erosion rates computed with the former available low resolution dataset (1:25000) the satellite supported USLE map shows “hotspots” of soil erosion of up to $16 \text{ t ha}^{-1} \text{ a}^{-1}$. In general, Cs-137 in combination with the USLE is a very suitable method to assess soil erosion for larger areas, as both give estimates on long-term soil erosion.

Especially for inaccessible alpine areas, GIS and remote sensing proved to be powerful tools that can be used for repetitive measurements of erosion features and causal factors. In times of global change it is of crucial importance to account for temporal developments. However, the evaluation of the applied soil erosion risk models revealed that the implementation of temporal aspects, such as varying climate, land use and vegetation cover is still insufficient. Thus, the proposed validation strategies (spatial, temporal and via Cs-137) are essential. Further case studies in alpine regions are needed to test the methods elaborated for the Urseren Valley. However, the presented approaches are promising with respect to improve the monitoring and identification of soil erosion risk areas in alpine regions.

CONTENTS

CHAPTER 1

Introduction

- 1.1. Erosion processes in the Urseren Valley
- 1.2. Soil loss assessment
- 1.3. Remote sensing for soil erosion and landslide risk assessment
- 1.4. Aims and outline of the thesis

CHAPTER 2

Methods to describe and predict soil erosion in mountain regions

- 2.1. Introduction
 - 2.2. Site description
 - 2.3. Methods to quantify soil erosion over time
 - 2.4. Methods to describe early stage soil erosion
 - 2.5. New concepts for soil erosion modelling in mountain areas
 - 2.6. Conclusions
- Acknowledgement

CHAPTER 3

Impacts of anthropogenic and environmental factors on the occurrence of shallow landslides in an alpine catchment (Urseren Valley, Switzerland)

- 3.1. Introduction
 - 3.2. Study area
 - 3.3. Materials and Methods
 - 3.4. Results and discussion
 - 3.5. Conclusion
- Acknowledgements

CHAPTER 4

On the influence of temporal change on the validity of landslide susceptibility maps

- 4.1. Introduction
 - 4.2. Study area
 - 4.3. Concept and Method
 - 4.4. Results and Discussion
 - 4.5. Conclusions
- Acknowledgement

CHAPTER 5

Estimating vegetation parameter for soil erosion assessment in an alpine catchment by means of QuickBird imagery

- 5.1. Introduction
- 5.2. Materials and Methods
- 5.3. Results and Discussion
- 5.4. Conclusion

Soil erosion modelled with USLE and PESERA using QuickBird derived vegetation parameters in an alpine catchment

- 6.1. Introduction
- 6.2. Site description
- 6.3. Materials and Methods
- 6.4. Results and Discussion
- 6.5. Conclusion and outlook

Application of in-situ measurement to determine ^{137}Cs in the Swiss Alps

- 7.1. Introduction
 - 7.2. Site
 - 7.3. Analysis
 - 7.4. Method concepts, results & discussion
 - 7.5. Conclusion
- Acknowledgements

Final remarks and outlook

- 8.1. Causes for soil erosion and monitoring
- 8.2. Methodological approach: Erosion monitoring and risk assessment
- 8.3. Outlook

Some additional results

- 10.1. Modelling soil erosion of an alpine grassland
- 10.2. Digital soil mapping – a decision tree approach
- 10.3. Electrical Resistivity Tomography (ERT)

LIST OF FIGURES

Figure 1-1. Different types of soil erosion in the Urseren Valley: sheet erosion (A), landslide (B), rill erosion (D) and cattle trails (E).

Figure 1-2. Main sections of the dissertation.

Figure 2-1. The Urseren Valley, Canton Uri, Switzerland. View from west to east.

Figure 2-2. Examples of landslides and sheet erosion on the (a) calcareous and (b) silicate schists of the south-facing slope of the Urseren Valley, Switzerland.

Figure 2-3. Landslide density histograms dependent on slope and geology. P = permocarbonic, Gr = Granite of the Aare massif, Gn = Gneiss of the Gotthard massif, A = "Altkristallin"(A), M= mesozoic-sediments (Labhart, 1999).

Figure 2-4. Sub-images of aerial photographs in the Urseren Valley (Swisstopo, 2006).

Figure 2-5. Fingerprint hypothesis of soil degradation: if soil erosion from upland A is influencing wetland B significantly, stable isotope signature of B should differ from undisturbed wetland C.

Figure 2-6. Stable isotopes of carbon and nitrogen for the upland soils A (erosion source), wetlands B (erosion sink) and undisturbed wetlands C. Boxplots indicate medians, 10-, 25-, 75- and 90-percentiles. • = outliers.

Figure 2-7. Water flow routing on vaulted area with (a) regular grids using the D8 algorithm and (b) irregular grid using the algorithm presented in Bänninger (2007).

Figure 3-1. Map of Switzerland and the study area (Projection: CH1903 LV03). Dark spots indicate mapped landslides.

Figure 3-2. The landslide density histogram as dependent on (A) geology (for the permocarbonic- (P) and mesozoic-sediments (M), Granite of the Aare massif (Gr), Gneiss of the Gotthard massif (Gn) and "Altkristallin" (Ak), (Labhart, 1999)), (B) avalanche density and (C) slope.

Figure 3-3. Sub-images of air photographs showing the stages of landslide incidence for the years 1959, 1980, 2000 and 2004.

Figure 3-4. Progression of the number of landslides and eroded area by landslides for the entire catchment since 1959. The error of the mapped landslide area is approximately 10%.

Figure 3-5. Increase of the number of landslides in comparison to the frequency of avalanches per year (left) and torrential 3-day-precipitation events (right).

Figure 3-6. Land use intensification (left) and a comparison between the increased landslide - and stocking numbers (right).

Figure 3-7. Pasture maps for the year 1955 and 2006.

Figure 3-8. Progression of landslide affected area on different traditional land use types of 1955.

Figure 4-1. Map of Switzerland and the study area (Projection: CH1903 LV03).

Figure 4-2. Evaluation steps of the logistic regression models of 1959 and 2000. The ellipses show processes and the rectangles results. The numbers and letters refer to the explanation given in the text.

Figure 4-3. Slope section near Hospental showing the overlap of some landslide causal factors: geologic formation, topography, springs, and land use.

Figure 4-4. Final landslide susceptibility map obtained with logistic regression for the 30 km² sub-catchment (Projection: CH1903 LV03).

Figure 4-5. Dependency of modelled landslide susceptibility and actual landslide densities (Spearman's rank correlation coefficient (P);** correlation is significant at a 0.01 level). The landslide density values are based on 411 mapped landslides for the year 2000 (left) and 52 mapped landslides for the period 2000-2004 (right).

Figure 4-6. Differences of susceptibility classes predicted by the logistic regression model based on the inventory maps of 1959 and 2000 (Projection: CH1903 LV03).

Figure 4-7. Frequency distribution of susceptibility deviation zones per land use type. The susceptibility deviation is positive where the susceptibility was one or two zones (1, 2) higher in 1959, negative where the susceptibility was one or two zones (-1, -2) lower in 1959 and zero (0) where no shift of susceptibility occurred.

Figure 5-1. Geographic location of the QuickBird image (false colour). The white lines separate different geologic formations. The white dots show the locations of ground truth measurements of fractional vegetation cover.

Figure 5-2. Sub-image of the QuickBird scene showing (left) the resulting land-cover map compared to land-cover information of the Swisstopo 1:25,000 Vector dataset and (right) normalized abundances of vegetation, bare soil and RMSE for the linear spectral unmixing model. The lighter the colour, the higher the proportion of an endmember (and error) within the pixel.

Figure 5-3. Scatter plot of NDVI versus the ground truth fractional vegetation cover.

Figure 5-4. Scatter plots of linear spectral unmixing and mixture tuned matched filtering-derived abundances versus the ground truth data. Linear regression lines are shown.

Figure 6-1. Geographic location of the QuickBird image (false colour). The white lines separate different geologic formations, the white dots show the locations of the Cs-137 elevation transect and the white rectangles are the slopes used for the model evaluation.

Figure 6-2. Scatter plot of LSU-derived vegetation abundances versus the ground truth fractional vegetation cover. Linear regression line is shown.

Figure 6-3. USLE input factor maps (LS-, R-, K-factor and LSU-derived C factor) and an enlargement for the LSU-derived C factor.

Figure 6-4. Estimated soil loss ($t\ ha^{-1}\ a^{-1}$) by USLE calculated with the low resolution C factor map (based on the swisstopo land-cover dataset) and the C factor based on the QuickBird derived vegetation data. Below: a visible comparison between the high resolved USLE soil erosion map and the pan-sharpened QuickBird image.

Figure 7-1. Aerial photograph of the Urseren Valley in Southern Central Switzerland and location of the sites (numbers), the altitudinal transect (dashed line) and the reference sites (crosses).

Figure 7-2. Nal detector system with its components: (a) detector, (b) pole, (c) control unit, (d) battery and (e) interface to pocket PC.

Figure 7-3. Altitudinal transect between 1500 and 2050 m a.s.l. with trendline (black). Dashed line represents the Cs-137 activity ($146.5 \text{ Bq}\cdot\text{kg}^{-1}$) measured at reference sites. For cluster (a) influence of erosion is possible, cluster (b) is influenced by snow at the time of Cs-137 input.

Figure 7-4. Spatial heterogeneity of the Cs-137 distribution at the calibration site.

Figure 7-5. (a) Cs-137 depth profile for an upland soil measured in the laboratory (GeLi detector). (b) Exponential decrease of the Cs-137 radiation measured at the surface with increasing burial depth of the point source (NaI detector). (c) Exponential decrease of the measured Cs-137 activity with increasing horizontal distance between the point source and the detector (NaI detector).

Figure 7-6. Dependency of Cs-137 on (a) pH, (b) clay content, (c) carbon content and (d) soil moisture (3, 4, 5, 7, 9, 10 stand for different sampling sites).

Figure 7-7. Comparison of Cs-137 activities determined by in-situ (NaI detector) and laboratory measurements (GeLi detector).

Figure 10-1. Locale sensitivities of erosion and runoff in the PESERA model.

Figure 10-2. Decision tree used for the digital mapping of dominant soil types in the Urseren Valley.

Figure 10-3. Digital soil map of the Urseren Valley showing the distribution of the 10 predominant soil types.

Figure 10-4. ERT transect at landslide slope in Hospental (Dipole-dipole | 5 m spacing | 28 electrodes | RMS error 5.7 % | 22.09.06) during dry conditions.

Figure 10-5. ERT transect at landslide slope in Hospental (Dipole-dipole | 5 m spacing | 28 electrodes | RMS error 1.9 % | 26.09.06) during wet conditions.

Figure 10-6. ERT transect at landslide slope in Realp (Dipole-dipole | 5 m spacing | 28 electrodes | RMS error 3.3 % | 26.09.06) during wet conditions.

LIST OF TABLES

Table 3-1. Landslide densities for different land-cover types and areas, that invaded by shrubs since 1959 (new shrub).

Table 4-1. List of air photographs used for the mapping of the landslide inventory maps.

Table 4-2. List of the considered predictors and its data source, search radius applied for the generation of the map, data scale/resolution, evidence of multi-collinearity (O = independent predictors; X = excluded predictors due to multi-collinearity), significance (Sig) of the predictors for the logistic regression model (LRM) of 2000 and 1959 (***) = $P < 0.001$).

Table 4-3. Classification of stable (0) and instable (1) cases (here pixels) by the three most significant predictors of the two logistic regression models (1959 and 2000).

Table 4-4. Regression coefficients (B) and significance (Sig) for the parameters stream density (Denstr), slope, and five geologic units (1 = granite of the Aare system, 2 = Altkristallin, 3 = Mesozoic, 4 = Permocarbone, 5 = gneiss of the Gotthard system) of the two logistic regression models.

Table 5-1. Confusion matrix for the supervised land-cover classification (npv = non-photosynthetic vegetation).

Table 6-1. C factors used for specific land-cover classes (US Department of Agriculture, 1977) for the low resolution land-cover dataset and the QuickBird derived data.

Table 6-2. Used datasets (*npv = non-photosynthetic vegetation).

Table 6-3. Comparison between mean (nine slopes) Cs-137 derived soil erosion rates and mean estimates ($t \text{ ha}^{-1} \text{ a}^{-1}$) of USLE and PESERA for four different model runs with (1) field measured input data at plot scale, (2) 100% FVC, (3) 0% FVC and (4) LSU-derived FVC.

Table 7-1. Cs-137 data of all sites for measurements with GeLi- and NaI detector.

CHAPTER 1

Introduction

Soil loss and its associated impacts is one of the most important, and yet probably the least known, of today's environmental problems (for detailed description, see 2000; Guardian, 2004). This statement is even more true for mountainous regions. Studies on soil erosion quantification in mountainous regions under natural precipitation regimes are scarce (Descroix and Mathys, 2003; Felix and Johannes, 1995; Isselin-Nondedeu and Bedecarrats, 2007). Moreover, soil erosion assessments for the Alps are based on models developed for lowlands that do not consider soil loss by snow processes and landslides and often lack of serious validation.

Soil and slope stability are crucial parameters to preserve the functions of the mountain environment that reach far beyond into the lowland, such as water supply, water retention (to prevent flooding of river plains), nutrient production, biodiversity, aesthetics and cultural heritage. Thus, soil erosion in the Alps was identified as a priority for action by the soil protocol of the Alpine Convention (AlpineConvention, 2005), but a comprehensive assessment of soil erosion of the Alps is still missing (ClimChAlps, 2006).

In comparison to cultivated lowland areas soil erosion damages are a severe problem in mountain ecosystems because soil once erosion has started, it is very often impossible or connected to high efforts to stop the process again by remedial actions due to the extreme topography. Moreover, because of the extreme climate conditions revegetation take usually longer than in lowlands. Assuming a slow rate of soil formation soil erosion causes irreversible damages in the time scale of 50 to 100 years (Van der Knijff et al., 2000). When talking about soil erosion landslides are often excepted. However, landslides are a major source of soil loss in mountain areas, thus, in the following text, the term soil erosion will include the process of landslides.

Soil erosion has been occurring naturally ever since the first soil formed. However, accelerated erosion is of very recent origin triggered by land use and climate change (Dotterweich, 2008).

The European Alps have experienced substantial changes in land-cover and land use during the last centuries. The main agricultural development that influences erosion susceptibility is the abandonment of remote pastures and the parallel intensification through concentration of animals on smaller, accessible areas. This is a general agricultural development in the Swiss Alps (BFS, 2005). The area of summer pastures steadily decreases (from 612619 ha in 1954 to 465519 ha in 2005 (Troxler et al., 2004)) due to abandonment and subsequent emergence of shrubs and reforestation, but simultaneously the stocking numbers increase. The intensification occurs mainly on accessible areas and usually includes increased stocking rates, extended grazing periods, more heavy pasture animals and higher fertilizer inputs. Which development prevails depends on the regions considered. The status and management of the grassland also affects the incidence of landslides (Bunza, 1989; Glade, 2003; Petley et al., 2007; Schauer, 1975; Tasser et al., 2003), although its influence is still discussed controversially in literature with respect to the various mountainous regions (Andre, 1998; Douglas et al., 1996; Krohmer and Deil, 2003; Tasser and Tappeiner, 2002).

Recent projections of climate scenarios indicate that mountains will be the most vulnerable region of Europe (Schroter et al., 2005). An increased frequency and intensity of torrential rainfall events is expected (IPCC, 2007). This may affect the water balance and runoff characteristics resulting in altered sediment yield and frequency of landslides (Asselman et al., 2003; Horton et al., 2006; IPCC, 2007).

Knowledge of present-day soil erosion, and erosion in the past, can be a great help in suggesting where and how future erosion is likely to occur. However, future rates of sheet erosion and landslides are likely to be affected by both climate change, as well as by land use change. The main problem is that rates of water erosion and landslide occurrence may respond to triggering factors, e.g. increases in rainfall in a non-linear manner (Helming et al., 2005). A separation and quantification of the effect of these driving factors on soil erosion is therefore a great future challenge.

Classical techniques to measure soil erosion such as measuring, or estimating sedimentation rates with sediment traps require a long period of continuous measurements impeding estimates for larger regions. New approaches for a better spatially explicit detection and quantification of soil degradation in alpine ecosystems are urgently needed in order to achieve a better conservation of soil resources (EEA, 2000). With the rise in computing power the use of geographical information system (GIS) and remote sensing, for spatially distributed assessments of soil erosion became accessible to a broader community.

Several projects concerning soil erosion in alpine areas are currently running at the University of Basel scaling from qualitative approaches with isotopes over classical erosion measurement with sediment traps to development of new modelling algorithms. An overview of the interdisciplinary approach of new methods to describe and predict soil degradation of mountainous soils with special emphasis on tools for inaccessible regions is presented (chapter 2).

The aim of this dissertation is to address the problem of soil erosion risk assessment in the Alps on catchment scale with remote sensing and GIS tools. The study covers soil loss by landslides (chapter 3 and 4) and sheet erosion (chapter 5 and 6). For both processes, a monitoring and mapping of the erosion features and related causal factors is done and potential causes are discussed. Apart from mapping the second aim was to use the elaborated data soil erosion assessment and quantification. Finally, the validity of the applied models is evaluated.

Methods used range from mapping of erosion features and erosion risk factors with air photographs and satellite imagery (chapter 3, 4, 5, 6), field mapping of soil types and soil characteristics (chapter 4, Appendix), GIS overlay analysis (chapter 3 and 4), application of statistical, empirical and physically based models (chapter 4 and 6) and determination of the radiogenic isotope Cs-137 (chapter 6 and 7). The research focused on the upper Reuss watershed (Urseren Valley) where the soil degradation dramatically affects the valley slopes.

1.1. Erosion processes in the Urseren Valley

Soil Erosion is the displacement soil particles by the agents tillage, wind, water, snow and by down-slope movement in response to gravity (Ahnert, 2003). While tillage erosion is not relevant for sub-alpine and alpine regions, the role of wind transport is so far unknown. Soil loss by water occurs in form of sheet-, rill-, and gully erosion. Soil particles are detached directly by means of rain splash or indirectly by surface flow. Rill and gully erosion typically occur on ploughed fields or deep soils with scarce vegetation in arid or semi-arid regions (Vrieling et al., 2007). For alpine grasslands rill and gully erosion is seldom observed (Strunk, 2003). In the Urseren Valley rill erosion is evident at small intermittent springs. The dominant but often invisible process of water erosion is sheet erosion. Sheet erosion is enhanced by the reduction of vegetation cover, due to climate conditions or land use. Considering land use overgrazing and cattle trails are supposed to have a strong triggering effect. Transport and detachment of soil material seems to be also triggered by the down slope movement of snow (Newesely et al., 2000), which could be observed after snowmelt. Yet, this process is neither measured nor implemented in soil erosion models. The different types of soil erosion observed in the Urseren Valley are displayed in Figure 1-1.

Landslides are a major hazard in mountain regions as they cause large damage to infrastructure and property. In areas affected by landslides, these are a major source of soil erosion (Joint Research Center Ispra, 2008). Landslides are a type of mass movement, which is the down slope movement of earth materials under the influence of gravity (Ahnert, 2003). Material is mobilized when the shear stress imposed on a surface exceeds the shear strength. The –often very sudden – movement of soil packages is along a failure plane, which may be a layer of clay or rock upon which the destabilized surface material sets. Landslides can be triggered

by (natural) physical processes such as heavy or prolonged rainfall, earthquakes, snow melt and slope toe erosion by rivers and by man-made activities such as slope excavation and loading, land use changes, water leakage, etc, or by any combination of natural and man-made processes (Joint Research Center Ispra, 2008). The slopes in the Urseren Valley are mainly affected by shallow landslides. A shallow landslide is a landslide in which the sliding surface is located within the soil mantle or weathered bedrock (typically to a depth from few decimetres to some metres).

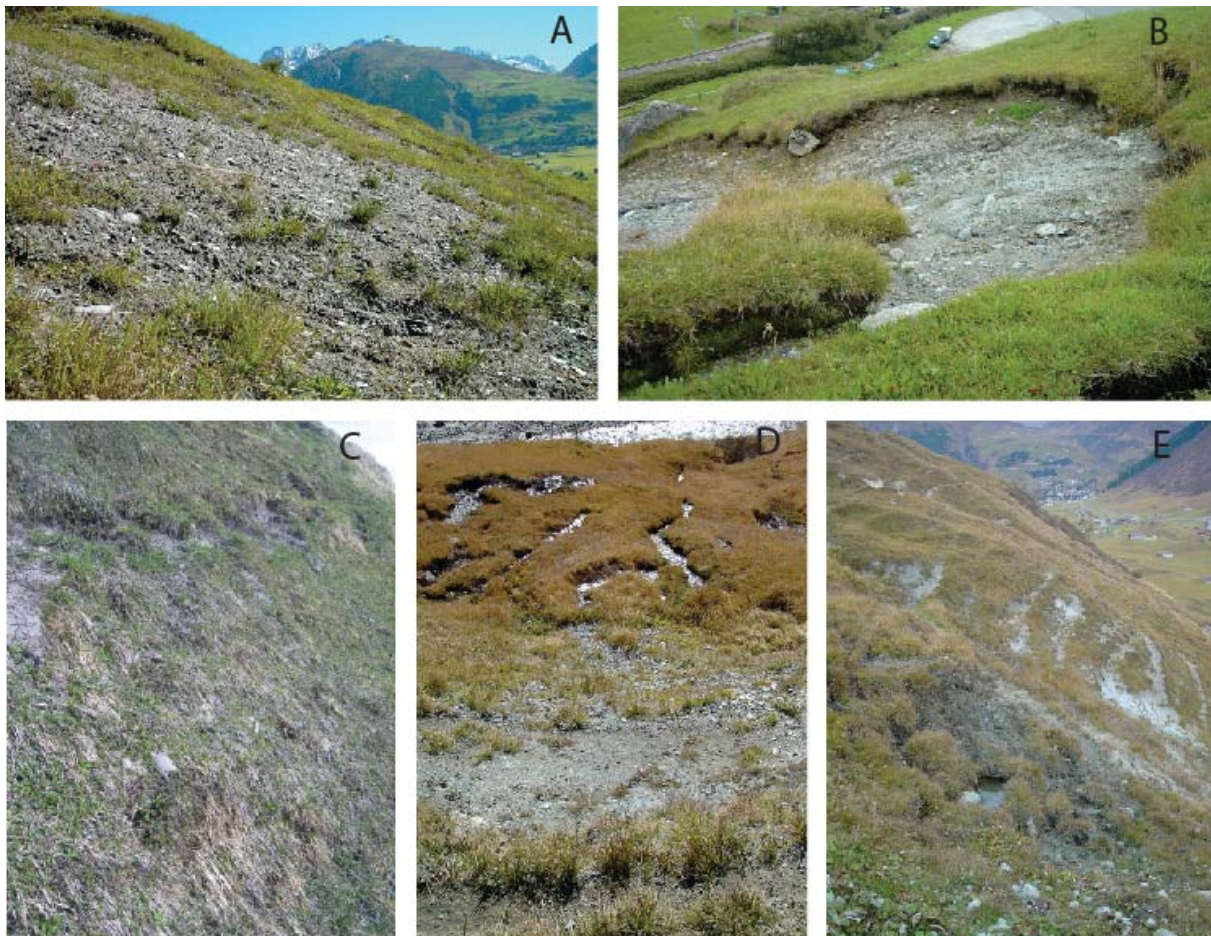


Figure 1-1. Different types of soil erosion in the Urseren Valley: sheet erosion (A), landslide (B), rill erosion (D) and cattle trails (E).

1.2. Soil loss assessment

A reason for the difficulty to predict and control soil erosion is that it is affected by both common and rare events, and so must be studied with high temporal resolution over long time spans. Soil erosion occurs subtle (especially sheet erosion), as a result of many small rainfall events or more event-based, as a result of large but relatively rare storms (especially landslides) (Claessens et al., 2006). Moreover, soil erosion is affected by factors on very small and very large spatial scales (Helming et al., 2005).

At every spatial scale erosion rates can vary greatly as erosion risk factors such as topography and land use change (Helming et al., 2005).

Sheet erosion risk assessment

The focus in erosion research in the Alps has almost entirely been on point measurements (on plots), lumped measurements of hydrographs and sedigraphs at the outlet of the catchment and on sprinkling experiments. These measurements showed that an intact vegetation cover prevents soil loss (Felix and Johannes, 1995; Frankenberg et al., 1995; Langenscheidt, 1995). However, on grassland plots with clear signs of degradation (reduced vegetation cover) a mean erosion rate of $20 \text{ t ha}^{-1} \text{ a}^{-1}$ (during a six year measurement period) could be observed that approximates a profile loss of 3 mm per year (Frankenberg et al., 1995). The plots were located on parent material of Flysch and Molasse in the Allgäuer Alps. In the Bavarian Alps (Kalkalpin), Felix and Johannes (1995) found erosion rates of $4.4 \text{ t ha}^{-1} \text{ a}^{-1}$ (during a two year measurement period) for a grassland test plot with a fractional vegetation cover of 66% due to pasturing. In another region of the Bavarian Alps, Ammer et al. (1995) measured soil erosion rates of approximately $2\text{-}9 \text{ t ha}^{-1} \text{ a}^{-1}$ (during a five year measurement period) after clear-cutting of the small forested catchments, which geologically belong to the formations Flysch and Kalkalpin. A review on erosion measurements on marls in the French Alps names erosion rates of $14\text{-}33 \text{ t ha}^{-1} \text{ a}^{-1}$ (Descroix et al., 2001). In the northern French Alps sediment deposits of 0.6 to 1.8 cm during single events depending on vegetation type and fractional vegetation cover have been measured (Isselin-Nondedeu and Bedecarrats, 2007). Besides, plot measurement sprinkling experiments are often conducted to estimate relative differences of erosion susceptibility, however, extrapolation of measured sediment yield over time is not possible. Several sprinkling experiments conducted in the Bavarian Alps and in South Tyrol showed an increase in runoff and erosion on grassland in the following order: covered vegetation area without grazing or other mechanical impact < covered vegetation area and additional impact (cultivation, grazing...) << areas without vegetation cover (Bunza, 1989; Markart et al., 2000; Schauer, 1981).

All these studies indicate the importance of an intact vegetation cover in order to prevent soil erosion in alpine areas. Thus, for alpine areas with disturbed vegetation cover, we may expect erosion rates that exceed Swiss soil protection guideline ($2\text{-}4 \text{ t ha}^{-1} \text{ a}^{-1}$).

Several models have been developed for soil loss quantification (USLE, RUSLE, LISEM, WEPP, PESERA and EROSION-3D). Water erosion models tended over time to place a greater emphasis on representing the physical processes that are responsible for erosion, still such efforts for the alpine environment are scarce (Cernusca et al., 1998). At European scale the USLE (Universal Soil Loss Equation) and PESERA model (Pan-European Soil Erosion Risk Assessment) are have been commonly used. But the attempts to model soil erosion at a European resulted in too high soil erosion estimates for alpine regions. Thus, the validity of these models has to be carefully

considered for alpine regions (Van Rompaey et al., 2003a; Van Rompaey et al., 2003b). In high relief regions, with rugged topography, a more detailed scale is needed. Jetten et al. (Jetten et al., 2003) even stated that there might be more benefit for soil erosion assessment by improving spatial information for model input and validation rather than by adapting models to a specific landscape.

Landslide risk assessment

Inventories between 1964 and 1999 show a steady increase in the number of landslide disasters worldwide (Nadim et al., 2006). The alpine valleys of Switzerland have always been exposed to a wide variety of natural hazards. Recent landslide events such as those occurring in the Canton of Uri and Graubünden in November 2002, or the Canton Valais in October 2000 led to substantial damage to property, infrastructure and environment.

Most regions already developed methods to assess landslide risk areas and in the framework of the Interreg IIIB catchrisk project (Catchrisk, 2006) efforts have been made to exchange and standardize methods to improve landslide prediction. An open question of the catchrisk project was how to judge and quantify the impact of land use. Also within the Silva-Protect project (SilvaProtect-CH, 2008) endeavours have been made to create a Swiss vulnerability map for natural hazards including the process of landslides. However, the prediction of shallow landslides posed problems and especially in the alpine region the correspondence between observed and modelled instabilities was deficient because of the insufficient spatial resolution of model input parameters (SilvaProtect-CH, 2006).

Carrara et al. (Carrara et al., 1991) and Zhou et al. (2002) mention that prediction of landslides, caused by interaction of factors, which are not always fully understood, and vary over areas and time, pose limitations to the tasks of mapping and analysing the spatiotemporal patterns. Thus, a key concept to improve the understanding of these spatiotemporal patterns is the analysis of temporal data of landslides and the related temporally varying causal factors (called dynamic factors in the following). Studies on the temporal dynamic of landslide activity are scarce (Hufschmidt et al., 2005), even though it is a crucial requirement to understand the actual landslide patterns and to predict future landslide incidence.

The main method to study trends in landslide incidence is based on the application of physical slope stability models, which are applied to simulate former climate and land use conditions (Claessens et al., 2006; Collison et al., 2000; Schmidt and Dikau, 2004; Vanacker et al., 2003). However, this approach is linked to high uncertainties resulting from the up- and downscaling of required input data. Another possible method is to analyse landslide databases in relation to trends in landscape and climate (Meusburger and Alewell, 2008; Petley et al., 2007).

1.3. Remote sensing for soil erosion and landslide risk assessment

The control of soil erosion demands the implementation of biophysical measures at the field and catchment scale. However, the allocation of scarce conservation resources and development of policies and regulations require erosion risk assessment at the regional scale. A limitation to accomplish this task is data availability and quality (Van Rompaey and Govers, 2002). Remote sensing can provide high-resolution data and can assist ground truth erosion mapping in two ways (i) through detection of erosion features (Vrieling et al., 2007; Zinck et al., 2001) or (ii) through the mapping of erosion controlling factors such as climatic characteristics, topography, soil properties, vegetation cover and land management (Okin, 2007; Peng et al., 2003). Traditionally, remote sensing has been used for soil erosion assessment through air photograph interpretation especially for landslide inventory mapping.

With the recent availability of high-resolution satellites such as IKONOS and QuickBird (e.g. resolution of QuickBird-PAN: 0.61 m), options for detecting and monitoring of small-scale erosion features have increased, although results based on this data are not yet reported in literature (Vrieling, 2006). In addition, this high-resolution satellite imagery offers an alternative to manual interpretation techniques; the automatic and detailed mapping of land-cover. Compared to aerial photographs the high-resolution satellites detect the near infrared electromagnetic spectrum that gives valuable information on soil and vegetation cover. Thus, the gradual degradation of grassland by sheet erosion is detectable by means of vegetation indices (for instance the **N**ormalized **D**ifferenced **V**egetation **I**ndex - NDVI) or spectral unmixing algorithms. When the relation between these spectral changes and erosion susceptibility are established satellite data allows spatial and temporal assessment of erosion status (Liu et al., 2004; Shrimali et al., 2001).

1.4. Aims and outline of the thesis

In general, there is still a lack of methods to describe and predict change of alpine ecosystem stability and degradation. The dissertation is part of an overall project on soil erosion in the Alps at the University in Basel. An overview of new approaches to investigate soil loss and soil degradation (chapter 2) is presented precedent to the four main chapters (chapter 3, 4, 5, 6). With this PhD thesis, it is intended to address soil erosion assessment by applying GIS and remote sensing methods for the assessment of soil erosion by landslides and sheet erosion in the Alps. Simultaneously, the study shall give input to identification of main drivers and causal factors for the occurrence of soil erosion. Thematically the work is subdivided into three main sections Figure 1-2. First erosion features and causal factors are mapped by air photograph interpretation and analysis of satellite imagery. Subsequent the objective is to implement the elaborated data in commonly used soil erosion risk assessment models in order to yield estimates on landslide probability and sheet

erosion rates. Finally, the suitability and validity of the models for the alpine environment is tested. These procedures are done separately for the process of landslide and sheet erosion due to the lack of a soil erosion model considering both processes.

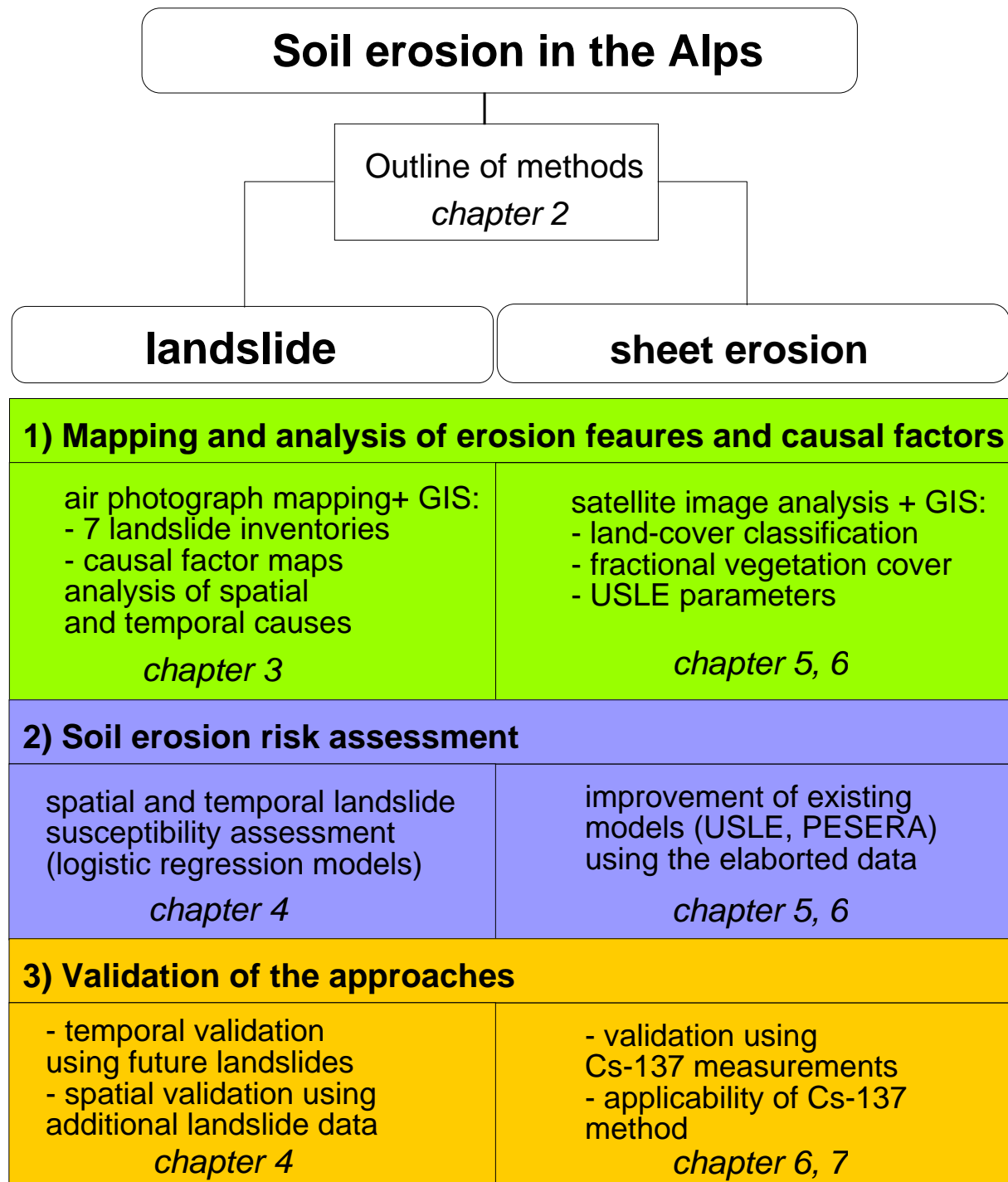


Figure 1-2. Main sections of the dissertation.

For landslides our approach is to compile a series of landslide inventory maps and causal factor maps by air photograph interpretation. The evolution of landslide occurrence is compared to time-series of potential dynamic causal factors (such as

precipitation characteristics, avalanche frequency, land-cover changes, stocking number and pasture regimes). This is done to evaluate, if land use- and climate changes cause a trend in landslide occurrence and to determine the possible causes for the temporal variation (chapter 3). In addition, the impact of static landslide causal factors on the spatial distribution of landslides is assessed by bivariate (chapter 3) and multivariate statistics (chapter 4). Here, static is defined for the considered time span of the study (45 years), e.g. geology, stream network, are factors, which do not change during this time span.

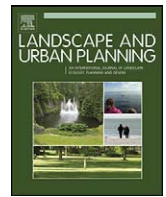
Multivariate statistic models are most commonly used to produce landslide susceptibility maps, however, they neglect the temporal variability of landslide causal factors. Therefore, we aim to assess the impact of dynamic landslide causal factors on the validity of the produced landslide susceptibility maps. The landslide susceptibility maps are derived by logistic regression models based on static landslide causal factors for two points in time (1959, 2000) (chapter 4).

For the process of sheet erosion (chapter 5, 6), the objective is to improve the acquisition of land-cover data and detect vegetation impoverishment. For this purpose, the applicability of the high resolution satellite imagery of the QuickBird sensor is tested. The suitability of vegetation impoverishment in autumn as a proxy for soil erosion is determined with the Cs-137 method. The Cs-137 method is further used to evaluate the improvement of soil erosion estimates that are subsequently calculated using the satellite derived input data for the soil erosion models USLE and PESERA (chapter 6). The improvement is assessed with reference to model runs using the former available low resolution dataset (1:25000; © swisstopo). A suitable measurement routine for measurement of Cs-137 in an alpine environment is established (chapter 7). Finally, the major findings of this thesis are discussed and general directions for future work are given.

CHAPTER 2

Methods to describe and predict soil erosion in mountain regions

This chapter is published in Landscape and Urban Planning as: *Alewell, C., Meusbürger, K., Brodbeck, M., and Bänninger, D.: Methods to describe and predict soil erosion in mountain regions, Landscape and Urban Planning, 88, 46-53, 2008.*



Methods to describe and predict soil erosion in mountain regions

Christine Alewell*, Katrin Meusburger, Monika Brodbeck, Dominik Bänninger

Institute for Environmental Geosciences, University of Basel, Bernoullistrasse 30, CH-4056 Basel, Switzerland

ARTICLE INFO

Article history:

Available online 11 October 2008

Keywords:

Soil degradation
Modelling
Remote sensing
Stable isotopes
The Alps

ABSTRACT

Suitable methods to describe and predict soil degradation in mountain areas with low accessibility, steep topography and extreme climate are urgently needed for suitable planning processes in Alpine regions under global change regime.

Aerial photograph mapping has been proven to be a valuable tool in surveying landslide development over time. However, landslides $< 10 \text{ m}^2$ as well as sheet erosion have been difficult to detect. Thus, the beginning of potentially heavy soil degradation cannot be tracked with aerial photographs.

As an early warning system for soil degradation, we analyzed gradients of stable isotopes of carbon and nitrogen from upland (erosion source) to wetland soils (erosion sink). Oxidic upland soils and anoxic wetlands differ in their isotopic signature, due to differing isotopic fingerprints of aerobic and anaerobic metabolism in soils. Gradients of $\delta^{15}\text{N}$ and $\delta^{13}\text{C}$ in soils reflected erosion of material. However, if soils were fertilized with manure, the $\delta^{15}\text{N}$ profiles were obscured.

To quantify soil erosion, we noted that existing soil erosion models are generally unsuitable for mountain regions. As a first step, we developed a new modelling concept with a special algorithm for spatial discretization with irregular grids. The latter ensures three-dimensional water flow routing that is controlled by topography and not by the underlying algorithm. Regarding quantification of soil erosion an improvement and validation of existing modelling approaches or development of new models is urgently needed.

© 2008 Elsevier B.V. All rights reserved.

1. Introduction

Mountain systems all over the world are unique in their ecology, economy and cultural diversity. However, the extreme topography and climate result in high instability, fragility and sensitivity for these ecosystems (Gellrich and Zimmermann, 2007). Simultaneously, most mountain environments have been exploited by human society to a maximum (Lasanta et al., 2006) with serious degradation since the Middle Ages (Höchtel et al., 2005). Economic, societal and environmental changes are often an immediate threat to mountain systems and careful planning is needed (Lasanta et al., 2006; Höchtel et al., 2005). Transformation rates in the Swiss Alps are very diverse and the spatial and contextual specifics have to be considered (Schneeberger et al., 2007). Thus, methods to describe and predict ecosystem stability in mountain systems are urgently needed (Garcia-Ruiz et al., 1996; Lasanta et al., 2006). One inherent parameter of ecological stability is the status of soils in the ecosystems which affects ecosystem services like slope stability, water budgets (drinking water reservoirs as well as flood preven-

tion), vegetation productivity, ecosystem biodiversity and nutrient production. First priority of most planning processes in Alpine grassland or arable systems is to reduce soil erosion risk (Garcia-Ruiz et al., 1996). Soil degradation is driven by environmental conditions as well as by land management practices (Meusburger and Alewell, 2008). In the near future, soil degradation might be significantly increased by the combined effects of global climate and land use change (Beniston, 2006; Fuhrer et al., 2006). With the projection of further warming the duration of snow cover will be shortened by up to 100 days with earlier snowmelt in spring depending on region and altitude (Beniston, 2006; Horton et al., 2006; Jasper et al., 2004). In Europe, a raising snowline, intensified precipitation during the winter and strong leaching effects with no or sparse vegetation cover in late fall and early spring will result in an increase in erosion especially in the Northern (mainly North-Western) Alps (Fuhrer et al., 2006). Nevertheless, increased erosion is also likely in the Southern Alps where extreme droughts will be followed by rain events of increased intensity (Brunetti et al., 2006; Schmidli and Frei, 2005).

In addition to changes connected with global climate change, European mountain systems have been confronted with a substantial change in land use management during the last decades (Lasanta et al., 2006; Gellrich and Zimmermann, 2007;

* Corresponding author. Tel.: +41 61 2670477; fax: +41 61 2670479.
E-mail address: Christine.alewell@unibas.ch (C. Alewell).



Fig. 1. The Urseren Valley, Kanton Uri, Switzerland. View from west to east.

Schneeberger et al., 2007). Since the late 19th century the forested area is increasing because reforestation was promoted for flood protection and erosion control or because of the abandonment of agricultural sites (Swiss Federal Statistical Office, 2001; Descroix and Mathys, 2003; Piégay et al., 2004; Lasanta et al., 2006; Tasser et al., 2007). Simultaneously, the remaining farm land has been managed with increased intensity (Meusbürger and Alewell, 2008). In the Swiss High Alps, the livestock population has increased from 200 000 to 420 000 sheep during the last 40 years (Troxler et al., 2004). Furthermore, permanent shepherding of cattle and sheep has mostly been abandoned since 1950 and replaced by uncontrolled grazing. The latter has resulted in a significantly higher grazing intensity of high alpine meadows (Troxler et al., 2004). Thus, destabilizing effects on soils can be expected from changes in animal farming practice. In contrast, studies in the Mediterranean mountains like the Spanish Pyrenees state a re-vegetation of lower and medium slopes with shrubs due to land abandonment (Lasanta et al., 2006). Planning tools were developed in these areas to support vegetation clearing to maintain a productive landscape and revitalize the economy. However, the latter was accompanied by an increase in soil erosion risk (Lasanta et al., 2006). Regarding land use changes, it is not yet clear whether we can expect a reduced erosion risk due to reforestation or increased erosion risk due to land use intensification of remaining pastures. Generally, the combined effects of climate and land use change are predicted to increase future soil erosion in Alpine regions (Frei et al., 2007). Modelled estimations of sediment delivery to the river Rhine from alpine regions resulted in more than a 200% increase by the year 2100 (Asselman et al., 2003). Because of the high degree of uncertainty connected to estimating soil erosion in mountainous regions, the demand for methods to describe and predict erosion of alpine soils

from small to large scale has been put forward (Asselman et al., 2003). This need for method development suitable for Alpine systems has already been proposed 15 years ago (Lange, 1994) and planning tools have been developed in the mean time (Lange, 1994; Höchtl et al., 2005; Lasanta et al., 2006; Schneeberger et al., 2007). However, we still lack methods to describe and predict change of alpine ecosystem stability and degradation.

Here, we present an interdisciplinary approach of the combination of new methods to describe and predict soil degradation of mountainous soils qualitatively and quantitatively, with special emphasis on tools for inaccessible or difficult to access regions with low infrastructure. We chose the Urseren Valley (Canton Uri, Switzerland) as our study area, where the relevance of farming and the numbers of farmers have gradually decreased during the last decades and “the traditional principles of land use are dissolving” (Kaegi, 1973).

2. Site description

The catchment of the Furkareuss (80 km², 1400–2500 m a.s.l.) is located in the Urseren Valley (Canton Uri, Switzerland, Fig. 1). The valley corresponds to a fault line that separates the gneiss massif of the Gotthard system to the south from the granite massif and the pre-existing basement (named “Altkristallien” by Labhart (1999)) of the Aare system in the north. Intermediate layers consist of Permocarbone and Mesozoic sediments (Labhart, 1999). The Mesozoic sequences include rauhwacke (Triassic), sandy marble and sandy-schistous marble, calcareous quartzite (Lias), dark clayey schist and quartz schist (Dogger), marble (Callovian-Oxfordian), coprolite and dark schist (Malm) (Wyss, 1986). The whole sequence was deformed at compressive conditions during the Tertiary (for a

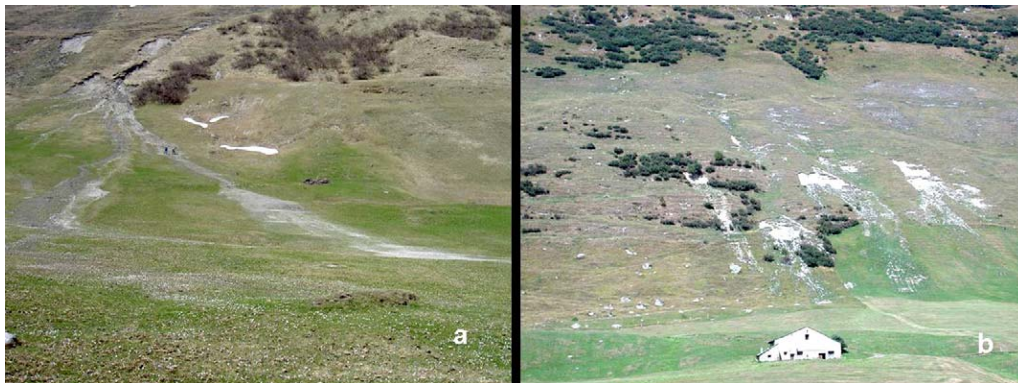


Fig. 2. Examples of landslides and sheet erosion on the (a) calcareous and (b) silicate schists of the south-facing slope of the Urseren Valley, Switzerland.

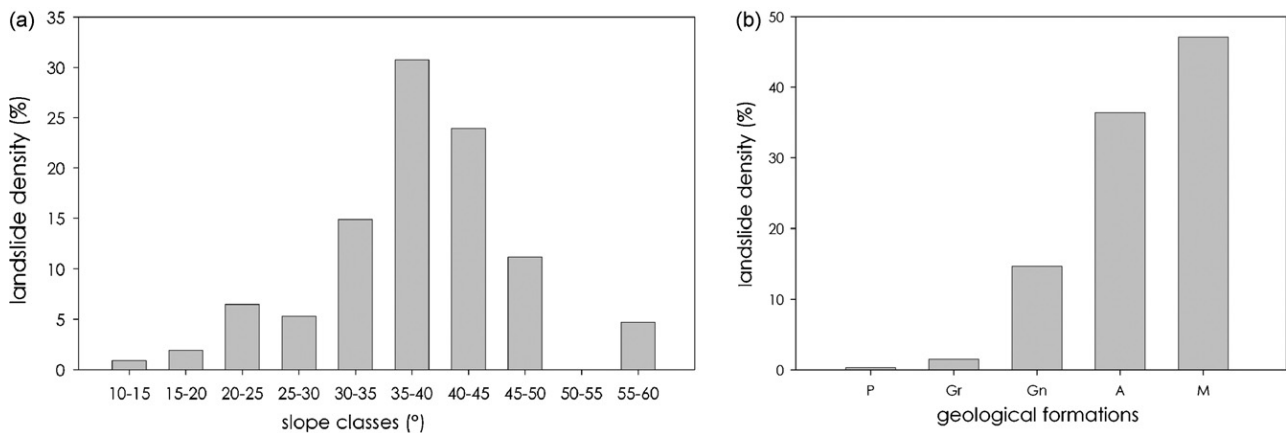


Fig. 3. Landslide density histograms dependent on slope and geology. P = permocarbonic, Gr = Granite of the Aare massif, Gn = Gneiss of the Gotthard massif, A = "Altkristallin" (A), M = Mesozoic-sediments (Labhart, 1999).

detailed discussion of the geology of the region see Wyss (1986)). Weathering of the calcareous material produced clay-rich soils that are prone to landslides and weathering of the silicate schist yields silty soils prone to sheet erosion (Fig. 2). On the valley slopes, quaternary moraines and scree deposits are very common and consist mainly of siliceous loamy gravel material.

Dominant soil types of the catchment classified after World Reference Base for Soil Resources [WRB], 2006 are Podzols, Podzocambisols and Cambisols, partly with stagic properties. Above 2000 m a.s.l. and on steep valley slopes, Leptosols are common (with rendzic Leptosols on the calcareous substrate). At the valley bottom, clayey gleyic Luvisols and Gleysols developed.

The valley is characterized by a high mountain climate with a mean air temperature of 3.1 °C. Mean annual rainfall at the meteorological station in Andermatt of MeteoSchweiz (located at the outlet of the valley, 8°35'/46°38'; 1442 m a.s.l.) is about 1400 mm with a maximum in October and a minimum in February. The valley is typically snow covered for 5–6 months (from November to April), with maximum snow depth in March. Runoff is usually dominated by snowmelt in May and June, with maximum in June. Summer and early autumn floods represent an important contribution to the flow regime (Swiss Federal Environmental Agency, 2007).

The four main types of land cover are (i) alpine grasslands and dwarf-shrubs (64%), (ii) scree (16%), (iii) shrubs (7%) and (iv) bare rock at higher elevations (11%) (Meusbürger and Alewell, 2008). Urban areas and forests cover less than 1% of the valley (70% of the forest was cultivated for avalanche protection above the villages). Natural vegetation is strongly influenced by anthropogenic land use for pasturing over the last centuries. Particularly on the less productive north-facing slope, an invasion of shrubs is evident (mainly by *Alnus viridis*, *Calluna vulgaris*, *Salix appendiculata*, *Sorbus aucuparia* and *Rhododendron ferrugineum*; Kaegi, 1973; Küttel, 1990). On the fertile south-facing slope, *Rhododendron ferrugineum* and *Juniperus sibirica* are the dominant shrubs (Kaegi, 1973; Küttel, 1990).

Land use in the Urseren Valley is dominated by pasturing. The property of the land is divided between the Korporation Urseren and private owners. The alp areas belonging to the Korporation Urseren are traditionally used as summer pastures. The private land serves as hay meadows to feed the cattle during the winter months.

3. Methods to quantify soil erosion over time

Environmental characteristics of ecosystems are one inherent driver of soil erosion and mass movement (Carrara et al., 1991;

Guzzetti et al., 1999). To assess the contribution of catchment characteristics to soil degradation in the Urseren Valley, landslide densities for variable catchment characteristics were calculated (Suezén and Doyuran, 2004). Landslide densities are calculated according to:

$$D_i = \frac{SX_i}{X_i} \times 100 \times \sum_{k=1}^n \frac{X_{i=k}}{SX_{i=k}}$$

in which D_i = landslide density for a variable class, SX_i = number of pixels with landslides within a variable class, X_i = number of pixels within a variable class and n = number of variable classes. To ease the comparability between landslide densities of different classes a normalization with the sum of landslide densities for all classes was done.

To assess the development over time within the Urseren Valley, we used aerial photograph interpretation. A geographic information system (ArcDesktop 9.1, ESRI, Zürich, Switzerland) was used to collect, superimpose and analyze the spatial data layers. Landslides were mapped by visually vectorizing the affected area from aerial photographs. Photographs from 1959 and 2004 were selected from a series of aerial photographs that are available at Swisstopo (BA071108) with a scale of at least 1:12,000. In order to allow for the local comparison of the individual landslides between different years the photographs were georeferenced and orthorectified using the ENVI software package (Version 4.0) with the help of ground control points, the DEM and the camera calibration protocol supplied by Swisstopo (BA071108).

Field verification was done in spring 2005 to check the inventory map produced by aerial photograph interpretation (comparison of photos from autumn 2004). During these field surveys, eight landslides were investigated in more detail to assess the accuracy of the GIS mapping method. The areas of those eight landslides determined during the field survey were compared with the corresponding areas achieved by photo interpretation. The latter resulted in an error of $\pm 10\%$.

There is no doubt that the unstable geology of the south-facing slopes in the Urseren Valley, as well as the steepness of the slopes, is significantly influencing slope instability (Fig. 3a). Erosion peaked at slopes of 35–40° (note that the lower rates of erosion with slopes > 45° are most likely due to thin soil development and low land use pressure). Furthermore, unstable bedrock of the Mesozoic layer was connected to high erosion rates in the catchment (Fig. 3b) and hydrology plays a crucial role because subsurface and return flow within the Mesozoic schists seems to trigger landslides (Meusbürger and Alewell, 2008). However, if environmental char-

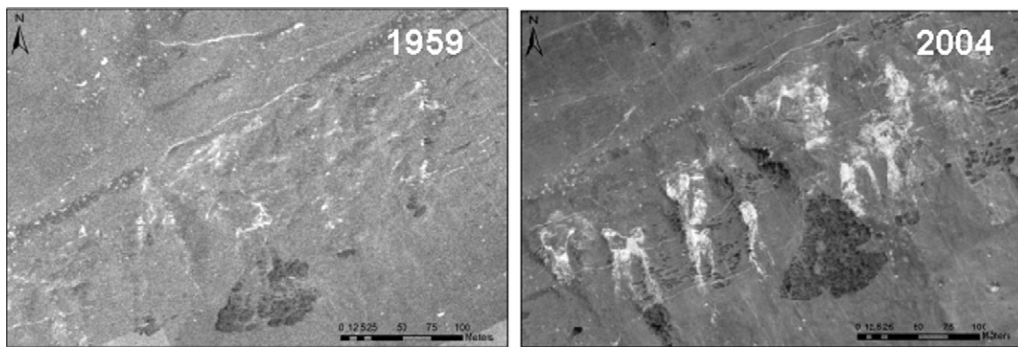


Fig. 4. Sub-images of aerial photographs in the Urseren Valley (Swisstopo, 2006).

acteristics like geology, geomorphology and/or hydrology would be the only or the main driving factors of soil erosion, we would not expect a trend over time. Thus, determining soil erosion over time is not only crucial for assessing the development of ecosystem stability but can also help us with the analysis of cause–effect relationships which is important for planning processes in fragile systems like Alpine grasslands.

Aerial photographs of the Urseren Valley demonstrate that we have had a strong increase in landslides and sheet erosion over the last 45 years (Fig. 4). The aerial size of the smallest landslide that was observable in the catchment in the 1959 photograph is approximately 10 m² and the largest landslide is about 7000 m². Landslides with a minimum area of 25 m² can be accurately digitized from aerial photographs. In 2004, 383 landslides (>25 m²) with an area of 9.42 ha and a mean size of 250 m² were mapped (for a typical landslide see Fig. 2). The total eroded area in the catchment increased by 92% between 1959 and 2004. The causes of this increase are mostly an effect of land use change (increase in intensity as well as change in management practice) but it might also be triggered by climate change (Meusburger and Alewell, 2008). One effect of the latter is the dramatic increase in the intensity of three-day rain events from 200 mm in the seventies to 270 mm today (Meusburger and Alewell, 2008). Prolonged rain events over more than 3 days are known to decrease soil stability and trigger landslide activity.

One disadvantage of erosion mapping with aerial photographs is that the beginning of erosion (e.g., landslides < 10 m², initial forms of sheet erosion) cannot be detected and accurate mapping is only possible with landslides ≥ 25 m². The latter point is crucial, because the extreme climate and topography in mountain regions sets the pre-conditions for self-energizing events: once erosion has started and stability of the slopes has decreased, destabilization of slopes will accelerate. Thus, in mountain systems it is crucial to develop methods to detect the first signs of erosion or even detect erosion before it is visible. The strong increase in slope instabilities in the last decades stresses the need for an early warning system of soil erosion and an implementation of these tools into planning processes.

4. Methods of describing early stage soil erosion (stable isotope fingerprinting)

The influence of soil erosion, weathering and sedimentation to wetlands and groundwater has often been investigated with radioactive isotope tracers like ¹³⁷Cs or ⁷Be (for an overview see Matisoff et al., 2002; Walling et al., 1999; Zapata, 2003). Both tracers are deposited from the atmosphere. A soil inventory of these isotopes that is less than the reference value (soil without erosion) is assumed to indicate erosion whereas an inventory greater than the reference value provides evidence of deposition. The assumed

prerequisites are an originally homogenous distribution with deposition within the catchment, and strong binding of the tracer to soil particles. The first assumption is not always true and might cause problems in data interpretation. The half-life time of ⁷Be is 54 days, thus ⁷Be is only suitable for short term investigations. With the longer half-life time of ¹³⁷Cs (30.2 years) longer term investigations are possible; however, the most recent source for atmospheric ¹³⁷Cs fallout in Europe is the Chernobyl accident in 1986. Thus, for regions with low ¹³⁷Cs deposition, time for using ¹³⁷Cs as an erosion tracer is already running out.

A new tool to detect soil erosion has to be developed. Stable carbon isotopes (¹³C) have been used to track down changes in geomorphology that are coupled to changes from C3 to C4 vegetation (Buck and Monger, 1999; Gibbs et al., 2001). Papanicolaou et al. (2003) used stable carbon and nitrogen signature to track down the origin (forest versus crops soils) of river sediments within catchments. They found differences between sediments from irrigated versus non-irrigated crop soils but not between forest and crop soils (Papanicolaou et al., 2003). In a review done by Amundson et al. (2003) it has been shown that $\delta^{15}\text{N}$ values of soils are dependent on soil age and soil slope. Soil age is correlated with the degree of steady state and the kinetics of N cycling. It has been shown that steeply sloping soils have low residence times. Thus, Amundson et al. (2003) postulated that because steeply sloping soils are far from steady state, they have lower $\delta^{15}\text{N}$ values that approach the atmospheric input. In addition to soil age and soil rejuvenation, the topographic position indirectly plays a key role in isotopic signature of elements, because dissimilatory reduction processes in lowland or wetland anaerobic soils cause significant shifts in carbon, nitrogen and sulfur isotopes (Kendall, 1998; Krouse and Grinenko, 1991; Wang et al., 1998). The latter is most likely due to the lower energy efficiency of dissimilatory processes and slower reduction rates. Low reduction rates are known to cause a greater discrimination of the heavier isotopes and thus a greater fractionation between the isotope ratios of substrate and product (Krouse and Grinenko, 1991). Stable sulfur isotopes have been shown to give a historic fingerprint of prevailing metabolism (aerobic or anaerobic) over time (Alewell and Novak, 2001). Upland soils, which are dominated by assimilatory reduction processes, can generally be expected to have distinctively different isotopes signatures than the associated wetlands and water bodies. The latter has been shown for sulfur (Alewell and Gehre, 1999; Alewell and Novak, 2001; Morgan, 1995), but not yet for nitrogen or carbon isotope dynamics.

We determined transects in stable isotopes from upland soils (oxic environment and erosion source) to lowlands (predominantly anoxic environments and a sink for erosion material, Fig. 5). A second site, the Seebodenalp (near Küsnacht am Rigi, Switzerland; for site description see Rogiers et al., 2005) was investigated for method validation. Soil profiles were taken with a core

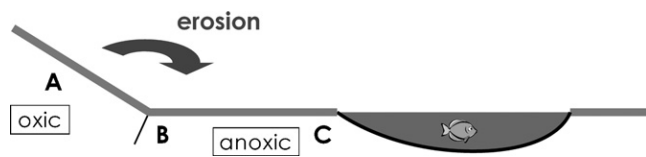


Fig. 5. Fingerprint hypothesis of soil degradation: if soil erosion from upland A is influencing wetland B significantly, the stable isotope signature of B should differ from undisturbed wetland C.

sampler at five sampling points per site and transported to the laboratory where they were stored in a refrigerator at approximately 4°C until further processing. Samples were sieved (2 mm), dried at 40°C for 3 days and ground using a WoC-swing grinder. Inorganic carbon was removed by acid fumigation following the method of Harris et al. (2001). Stable carbon and nitrogen isotope analyses were accomplished on a mass spectrometer (Thermo Finnigan Delta plus XP) coupled with an elemental analyzer (Flash EA 1112 Series).

Stable carbon isotopes in the upper mineral soil (0–15 cm) were significantly different between upland soils in the catchment and undisturbed wetlands (wetlands C; Fig. 6a). At the Urseren Valley, the wetland that was influenced by erosion processes (wetland B) had a mean $\delta^{13}\text{C}$ signature of $-27.51 \pm 0.47\text{‰}$, which was between the upland ($\delta^{13}\text{C} = -26.62 \pm 0.60\text{‰}$) and the undisturbed wetland C ($\delta^{13}\text{C} = -28.29 \pm 0.59\text{‰}$). However, the difference between the upland and wetland $\delta^{13}\text{C}$ signatures was only minor. At some of the sites in the Urseren Valley, erosion features were visible (e.g.,

eroded areas at the upland and/or sediment layers at the wetland). At other sites, no such geomorphic difference was detectable. The difference between $\delta^{13}\text{C}$ of the upland ($-27.67 \pm 0.40\text{‰}$) and the undisturbed wetland C ($-28.33 \pm 0.23\text{‰}$) at Seebodenalp was even smaller, but still significant. The latter site showed no visible soil erosion (e.g., sediment layers in wetland B, or visibly eroded areas at the upland site), but cattle trails and steep slopes on the upland site make leaching of soil and organic material into wetland B very likely. The $\delta^{13}\text{C}$ signature of wetland B ($-28.15 \pm 0.25\text{‰}$) was again between the upland site and the undisturbed wetland C. Thus, at both sites, $\delta^{13}\text{C}$ seems to be a possible tracer for soil erosion processes, but the difference between the $\delta^{13}\text{C}$ signatures of upland and wetland soils was rather small.

Stable isotopes of nitrogen were also significantly different between the upland site and undisturbed wetland C at the Seebodenalp site (Fig. 6d). Confirming the results of the $\delta^{13}\text{C}$ values, $\delta^{15}\text{N}$ of wetland B ($+0.59 \pm 0.46\text{‰}$) was very similar to the $\delta^{15}\text{N}$ values of the upland soil ($+0.75 \pm 0.75\text{‰}$), while $\delta^{15}\text{N}$ of the undisturbed wetland C was significantly different ($-1.08 \pm 0.35\text{‰}$). Thus, influence by nitrogen leaching and erosion from the upland soil to wetland B is very likely at this site. The $\delta^{15}\text{N}$ profiles of Urseren Valley did not show the expected results. Median $\delta^{15}\text{N}$ values of all three sites were very similar. Farmyard manure ($\delta^{15}\text{N} = +5.80 \pm 1.24\text{‰}$) is used very intensively in the Urseren Valley at most of the pastures and meadows, including our sampling sites. The influence of the organic N from the manure generally increases $\delta^{15}\text{N}$ signature of the soils and obviously obscured any differences between upland and wetland sites in the Urseren Valley.

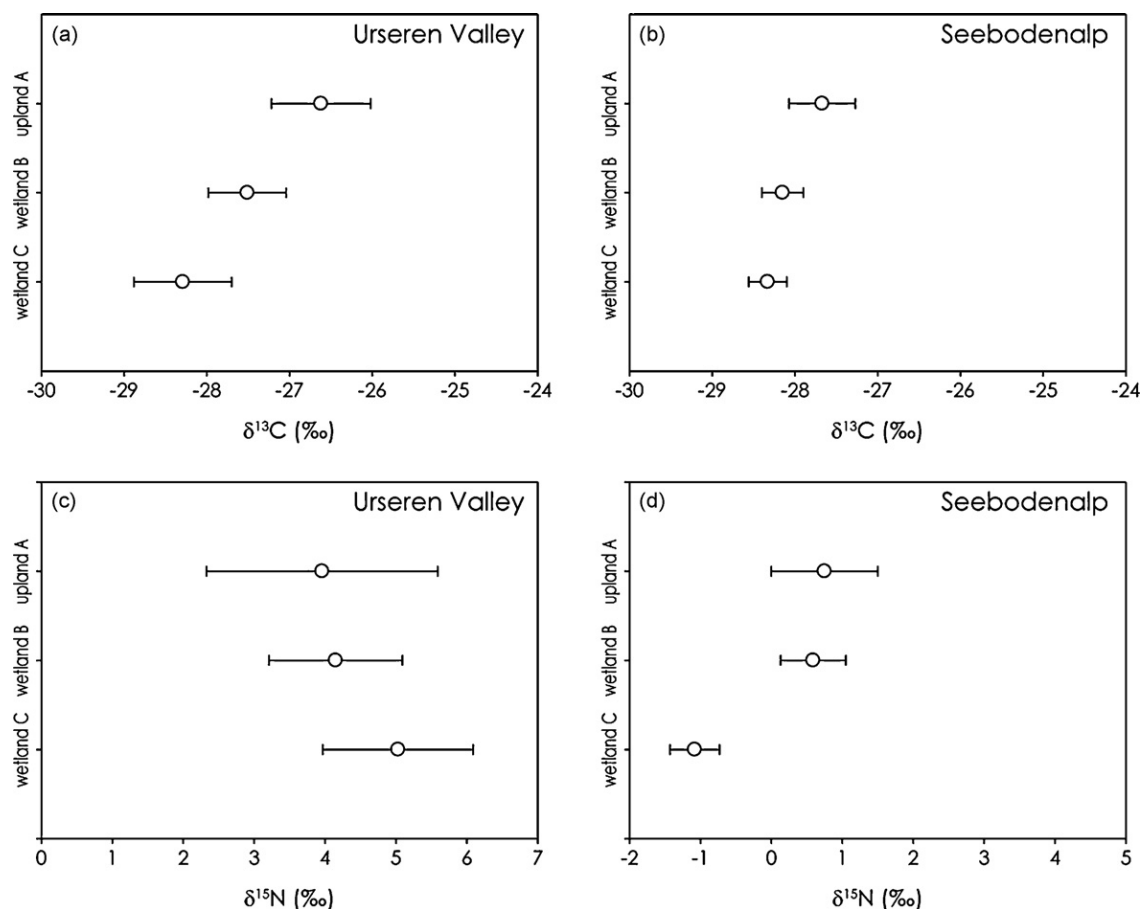


Fig. 6. Stable isotopes of carbon and nitrogen for the upland soils A (erosion source), wetlands B (erosion sink) and undisturbed wetlands C. Boxplots indicate medians, 10-, 25-, 75- and 90-percentiles. • = outliers.

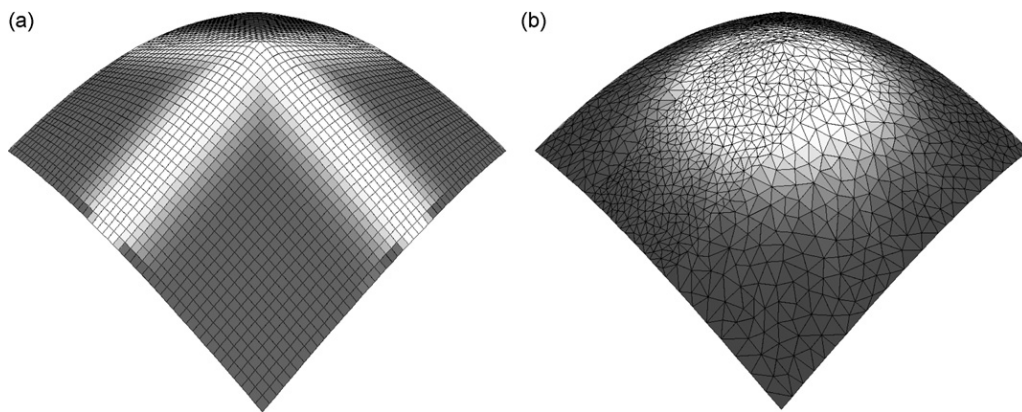


Fig. 7. Water flow routing on a vaulted area with (a) regular grids using the D8 algorithm and (b) irregular grid using the algorithm presented in Bänninger (2007).

In summary, stable isotopes of carbon and nitrogen seem to be a suitable tool to track qualitatively early stage soil erosion and may thus be a promising method for future planning processes. However, stable isotopes are not suitable for the quantitative description of erosion rates.

5. New concepts for soil erosion modelling in mountain areas

Physically distributed and empirically based models have been applied to soil erosion quantification by several nations in Europe (De Jong et al., 1999; Jetten et al., 2003; Millward and Mersey, 1999; Van-Camp et al., 2004; Van der Knijff et al., 2000; Van Rompaey et al., 2003a). The distributed models reflect the spatial variability of processes and outputs in the catchment. They explicitly calculate soil erosion rates within a given landscape and thus provide a more realistic model output than lumped models (Van Rompaey et al., 2001). A sound conceptual soil erosion model is the PESERA. However, it has not been validated for mountain regions yet and comparisons to other models show for Mediterranean regions that PESERA underestimates the erosion rate significantly (De Vente et al., 2008). Generally, major discrepancies between calculated soil erosion and measured erosion were found in mountain watersheds because models were mainly designed for agricultural environment (Van Rompaey et al., 2003a). The extreme topography and climate in mountain regions often cause spatially explicit soil erosion models to fail. Thus, the existing models generally have to be modified for application in mountainous terrain.

We believe that the process of erosion should generally be separated into two sub-processes: detachment and transport. While detachment is mainly dependent on soil texture, soil structure, soil cover, vegetation cover and the kinetic energy of contacting water (rain drop and surface flow), transport is dependent on surface water flow, topography and soil cover. Separating the two sub-processes allows for a more accurate description and sensitivity analysis of crucial input parameters.

To our understanding, one major problem within the algorithms of existing erosion models is the calculation of transport processes, especially of the water flow routing in mountainous terrain with steep slopes. Within the PESERA model (Van Rompaey et al., 2003b), the environmental properties are defined for each grid cell and erosion rates are estimated separately for each grid cell. Mass transfer towards other grid cells is not calculated. Thus, with this model it is not possible to route mass transport on a hill slope. The physically based WEPP model (Nearing et al., 1989) calculates erosion rates

from hill slope profiles but does not consider the three-dimensional spatial extension of the real earth surface. Thus, it is only partly possible to capture influences of the micro-topology on soil erosion (e.g., return flow, which often triggers soil erosion). The soil erosion model LISEM (De Roo and Jetten, 1999) describes the sites of interest by a regular gridded digital elevation model, and water flow routing is calculated with the D8 algorithm. The D8 algorithm searches for the neighbouring cell with the lowest altitude, to which the water is then routed. Water flow routing with D8 works fine for plane hill slopes, but is generally a weak description of the hydrology of undulating hill slopes because this algorithm routes the water preferentially in directions of multiples of 45° (Fig. 7a). The latter is improved within the Erosion3D model (Schmidt et al., 1999) by using an algorithm which weights the outflow to its neighbouring cells according to the altitude difference. However, the directions of water flow routing are still not regulated by multi directional topography but by the possible directions of the underlying algorithm. Thus, new concepts for water flow routing are needed to improve existing approaches.

In a first step we propose two new approaches: (1) spatial discretization is commonly done by taking regular grids. We propose the use of triangulated irregular grids because they have the advantage that small-scaled regions (e.g., transitions from hill slopes to the bottom of a valley) can be discretized by a finer grid resolution than large-scaled regions (e.g., bottom of a valley). The shape and size of the irregular triangular grids have to be optimized according to the given heterogeneity of the digital elevation model. (2) Algorithms like D8 and multiple-direction flows that are based on slopes are often used but are physically imprecise because of the limited number of possible water flow directions (Tarboton, 1997; Fig. 7a). The results of the D8 algorithm are moderate for regular and weak for irregular grids. Thus, using irregular grids – which is favourable for efficient space description – requires an accurate water flow routing algorithm. We developed a new algorithm for regular and irregular grids which routes the water depending on any physically correct topography (within the given grid resolution; Fig. 7b; Bänninger, 2007).

Current modelling approaches of water flow routing can be improved significantly with the described modelling approach. To describe sediment loads and the transport mechanism in space new concepts need to be developed in the same way we did it for water flow routing. This includes the detachment and transport processes of soil particles. Regarding planning processes ecosystem research and planning is still in need for a suitable model to describe and predict soil erosion processes quantitatively in Alpine systems.

6. Conclusions

Because mountain areas are mostly remote regions and are difficult to access, the classical surveying of soil erosion is associated with high investment of labour, time and costs. Remote sensing can overcome these difficulties, and aerial photographs have been shown to be a suitable tool to measure soil erosion over time. We were able to track down landslides $\geq 10 \text{ m}^2$ and heavy cattle trail erosion with aerial photography. Landslides $\geq 25 \text{ m}^2$ can be mapped accurately. However, smaller landslides, which are often the start of steadily or event-based growing degradation, cannot be identified. Furthermore, sheet erosion cannot be detected. Thus, for careful planning processes new techniques in remote sensing are required for future mapping of soil degradation in mountainous regions.

Stable isotopes of carbon and nitrogen seem to be suitable as an early warning system for soil erosion in mountain areas on a plot scale, if transects from upland (erosion source) to wetland soils (erosion sink) are investigated. The method is a retrospective qualitative estimate of erosion. Erosion can be detected based on a single site visit, where spatially distributed information for individual points in the landscape can be assembled. The advantage of the method is its sensitivity, because carbon and nitrogen isotopic fingerprints reflect the displacement of organic matter. Thus, the technique might track erosion processes before they are visible. The technique might become a promising future tool for planning processes in mountain areas prone to erosion if transects from upland oxic to wetland anoxic soils are available for investigation. However, the difference in the $\delta^{13}\text{C}$ signature between erosion sources and sinks was relatively small, so careful planning of sampling design and sufficient replications ($n \geq 5$) have to be taken into account. Stable nitrogen isotopes are not applicable at sites with manure application because the $\delta^{15}\text{N}$ signals of soils will be equalized by the addition of organic fertilizer.

To quantify soil erosion in mountainous regions, an improvement to existing modelling systems is needed. We presented an algorithm which calculates water flow routing and transport in multiple directions on irregular grids. The latter ensures the dependency of the water routing and transport processes on topography and not on the possible flow directions of the underlying algorithm, which is often the case in existing modelling approaches. Similar improvements have to be done in the future for all other processes that are involved in erosion charge generation (e.g., detachment and transport of soil particles). There is no doubt that modelling is the ultimate tool for comprehensive planning processes in mountain regions. However, future work on model development is clearly needed which might include improvement and validation of existing models as well as developing entirely new modelling approaches as we discussed in this study.

Acknowledgements

This study was partly founded by the Swiss National Found (200021-105579) and by the Swiss Federal Office for the Environment.

References

Alewell, C., Gehre, M., 1999. Patterns of stable S isotopes in a forested catchment as indicators for biological S turnover. *Biogeochemistry* 47, 319–333.
 Alewell, C., Novak, M., 2001. Spotting zones of dissimilatory sulfate reduction in a forested catchment: the S-34-S-35 approach. *Environ. Pollut.* 112, 369–377.
 Amundson, R., Austin, A.T., Schuur, E.A.G., Yoo, K., Matzek, V., Kendall, C., Uebersax, A., Brenner, D., Baisden, W.T., 2003. Global patterns of the isotopic composition of soil and plant nitrogen. *Global Biogeochem. Cycles* 17 (1), art. 1031.
 Asselman, N.E.M., Middelkoop, H., van Dijk, P.M., 2003. The impact of changes in climate and land use on soil erosion, transport and deposition of suspended sediment in the River Rhine. *Hydrol. Process.* 17, 3225–3244.

Bänninger, D., 2007. Technical note: water flow routing on irregular meshes. *Hydrol. Earth Syst. Sci.* 11, 1243–1247.
 Beniston, M., 2006. Mountain weather and climate: a general overview and a focus on climatic change in the Alps. *Hydrobiologia* 562, 3–16.
 Brunetti, M., Maugeri, M., Nanni, T., Auer, I., Böhm, R., Schoner, W., 2006. Precipitation variability and changes in the greater Alpine region over the 1800–2003 period. *J. Geophys. Res. -Atmos.* 111 (D11), art. D11107.
 Buck, B.J., Monger, H.C., 1999. Stable isotopes and soil-geomorphology as indicators of Holocene climate change, northern Chihuahuan Desert. *J. Arid. Environ.* 43, 357–373.
 Carrara, A., Cardinali, M., Detti, R., Guzzetti, F., Pasqui, V., Reichenbach, P., 1991. GIS techniques and statistical-models in evaluating landslide hazard. *Earth Surf. Proc. Landscape* 16, 427–445.
 De Jong, S.M., Paracchini, M.L., Bertolo, F., Folving, S., Megier, J., De Roo, A.P.J., 1999. Regional assessment of soil erosion using the distributed model SEMMED and remotely sensed data. *Catena* 37, 291–308.
 De Roo, A., Jetten, V., 1999. Calibrating and validating the LISEM model for two data sets from the Netherlands and South Africa. *Catena* 37, 477–493.
 De Vente, J., Poesen, J., Verstraeten, G., Van Rompaey, A., Govers, G., 2008. Spatially distributed modelling of soil erosion and sediment yield at regional scales in Spain. *Global Planet. Change* 60, 393–415.
 Descroix, L., Mathys, N., 2003. Processes, spatio-temporal factors and measurements of current erosion in the French Southern Alps: a review. *Earth Surf. Proc. Landscape* 28, 993–1011.
 Frei, C., Calanca, P., Schär, C., Wanner, H., Schaedler, B., Haeberli, W. et al., 2007. Basic principles of climate change. In: Fuhrer, J., Beniston, M., Fischlin, A., Frei, C., Goyette, S., Jasper, K. et al. (Eds.). *Climate change and Switzerland—2050. Expected impacts on environment, society and economy*, OcCC Report. OcCC/ProClim, Bern.
 Fuhrer, J., Beniston, M., Fischlin, A., Frei, C., Goyette, S., Jasper, K., Pfister, C., 2006. Climate risks and their impact on agriculture and forests in Switzerland. *Climatic Change* 79, 79–102.
 Garcia-Ruiz, J.M., Lasanta, T., Ruiz-Flano, P., Ortigosa, L., White, S., Gonzalez, C., et al., 1996. Land-use changes and sustainable development in mountain areas: a case study in the Spanish Pyrenees. *Landscape Ecol.* 11, 267–277.
 Gellrich, M., Zimmermann, N.E., 2007. Investigating the regional-scale pattern of agricultural land abandonment in the Swiss Mountains: a spatial statistical modelling approach. *Landscape Urban Plan.* 79, 65–76.
 Gibbs, M., Thrush, S., Ellis, J., 2001. Terrigenous clay deposition on estuarine sand-flats: using stable isotopes to determine the role of the mud crab, *Helice crassa* Dana, in the recovery process. *Isot. Environ. Health Stud.* 37, 113–131.
 Guzzetti, F., Carrara, A., Cardinali, M., Reichenbach, P., 1999. Landslide hazard evaluation: a review of current techniques and their application in a multi-scale study, Central Italy. *Geomorphology* 31, 181–216.
 Harris, D., Horwath, W.R., van Kessel, C., 2001. Acid fumigation of soils to remove carbonates prior to total organic carbon or carbon-13 isotopic analysis. *Soil Sci. Soc. Am. J.* 65, 1853–1856.
 Höchtl, F., Lehninger, S., Konold, W., 2005. “Wilderness” what it means when it becomes a reality—a case study from the southwestern Alps. *Landscape Urban Plan.* 70, 85–95.
 Horton, P., Schaeffli, A., Mezghani, B., Hingray, B., Musy, A., 2006. Assessment of climate-change impacts on alpine discharge regimes with climate model uncertainty. *Hydrol. Process.* 20, 2091–2109.
 Jasper, K., Calanca, P., Gyalistras, D., Fuhrer, J., 2004. Differential impacts of climate change on the hydrology of two alpine river basins. *Climate Res.* 26, 113–129.
 Jetten, V., Govers, G., Hessel, R., 2003. Erosion models: quality of spatial predictions. *Hydrol. Process.* 17, 887–900.
 Kaegi, H.U., 1973. The traditional cultural landscape in the Urseren Valley: a contribution to alpine cultural geography. PhD thesis. University of Zurich, Zurich, Switzerland (in German).
 Kendall, C., 1998. Tracing nitrogen sources and cycling in catchments. In: Kendall, C., McDonnell, J.J. (Eds.), *Isotope Tracers in Catchment Hydrology*. Elsevier Science B.V., Amsterdam, pp. 519–576.
 Krouse, H.R., Grinenko, V.A. (Eds.), 1991. *Scope 43. Stable Isotopes: Natural and Anthropogenic Sulphur in the Environment*. John Wiley & Sons, Chichester.
 Küttel, M., 1990. The subalpine protection forest in the Urseren Valley. *Bot. Helv.* 100, 183–197 (in German).
 Labhart, T.P., 1999. Planning tool: Geological-tectonical Map Aarmassiv, Gotthard-massiv and Tavetscher Massiv. In: Löw, S.W.R. (Ed.), *Pre-exploration and Prediction of the Base Tunnel at the Gotthard and the Lötschberg* (Appendix 1). Balkema A. A., Rotterdam (in German).
 Lange, E., 1994. Integration of computerized visual simulation and visual assessment in environmental planning. *Landscape Urban Plan.* 30, 99–112.
 Lasanta, T., González-Hidalgo, J.C., Vicente-Serrano, S.M., Sferi, E., 2006. Using landscape ecology to evaluate an alternative management scenario in abandoned Mediterranean mountain areas. *Landscape Urban Plan.* 78, 110–114.
 Matisoff, G., Bonniwell, E.C., Whiting, P.J., 2002. Soil erosion and sediment sources in an Ohio watershed using beryllium-7, cesium-137, and lead-210. *J. Environ. Qual.* 31, 54–61.
 Meusburger, K., Alewell, C., 2008. Impacts of anthropogenic and environmental factors on the occurrence of shallow landslides in an alpine catchment (Urseren Valley, Switzerland). *Nat. Hazard. Earth Syst.* 8, 509–520.
 Millward, A.A., Mersey, J.E., 1999. Adapting the RUSLE to model soil erosion potential in a mountainous tropical watershed. *Catena* 38, 109–129.

- Morgan, M.D., 1995. Modeling excess sulfur deposition on wetland soils using stable sulfur isotopes. *Water Air Soil Pollut.* 79, 299–307.
- Nearing, M., Foster, G., Lane, L., Finkner, S., 1989. A process-based soil erosion model for USDA–water erosion prediction project technology. *Trans. ASAE* 32, 1587–1593.
- Papanicolaou, A.N., Fox, J.F., Marshall, J., 2003. Soil fingerprinting in the Palouse Basin, USA using stable carbon and nitrogen isotopes. *Int. J. Sed. Res.* 18, 278–284.
- Piégay, H., Walling, D.E., Landon, N., He, Q.P., Liébault, F., Petiot, R., 2004. Contemporary changes in sediment yield in an alpine mountain basin due to afforestation (The upper Drome in France). *Catena* 55, 183–212.
- Rogiers, N., Eugster, W., Furger, M., Siegwolf, R., 2005. Effect of land management on ecosystem carbon fluxes at a subalpine grassland site in the Swiss Alps. *Theor. Appl. Climatol.* 80, 187–203.
- Schmidli, J., Frei, C., 2005. Trends of heavy precipitation and wet and dry spells in Switzerland during the 20th century. *Int. J. Climatol.* 25, 753–771.
- Schmidt, J., Von Werner, M., Michael, A., 1999. Application of the EROSION 3D model to the CATSOP watershed, The Netherlands. *Catena* 37, 449–456.
- Schneeberger, N., Bürgi, M., Kienast, P.D.F., 2007. Rates of landscape change at the northern fringe of the Swiss Alps: historical and recent tendencies. *Landscape Urban Plan.* 80, 127–136.
- Suezen, M.L., Doyuran, V., 2004. Data driven bivariate landslide susceptibility assessment using geographical information systems: a method and application to Asarsuyu catchment, Turkey. *Eng. Geol.* 71, 303–321.
- Swiss Federal Environmental Agency, 2007. Hydrological data from observation ward Reuss-Andermatt. Swiss Federal Environmental Agency, Bern, <http://www.hydrodaten.admin.ch/d/2087.htm>, access date: 26.09.2008.
- Swiss Federal Statistical Office, 2001. The Changing Face of Land Use. Land Use Statistics of Switzerland. Swiss Federal Statistical Office, Neuchâtel.
- Swisstopo, 2006. Reproduced with allowance from Swisstopo. BA071108. Swisstopo, Zurich.
- Tarboton, D., 1997. A new method for the determination of flow directions and upslope areas in grid digital elevation models. *Water Resour. Res.* 33, 309–319.
- Tasser, E., Walde, J., Tappeiner, U., Teutsch, A., Noggler, W., 2007. Land-use changes and natural reforestation in the Eastern Central Alps. *Agric. Ecosyst. Environ.* 118, 115–129.
- Troxler, J., Chatelain, C., Schwery, M., 2004. Technical and economical evaluation of grazing systems for high altitude sheep pastures in Switzerland. *Grassland Sci. Eur.* 9, 590–592.
- Van-Camp, L., Bujarrabal, B., Gentile, A.-R., Jones, R.J.A., Montanarella, L., Olazabal, C. et al. (Eds.), 2004. Reports of the Technical Working Groups Established under the Thematic Strategy for Soil Protection (EUR 21319 EN, Vol. 2, pp. 187–198). Office for Official Publications of the European Communities, Luxembourg.
- Van der Knijff, J.M., Jones, R.J.A., Montanarella, L., 2000. Soil Erosion Risk Assessment in Italy. European Soil Bureau (European Commission EUR 19022EN). Office for Official Publications of the European Communities, Luxembourg.
- Van Rompaey, A.J.J., Verstraeten, G., Van Oost, K., Govers, G., Poesen, J., 2001. Modelling mean annual sediment yield using a distributed approach. *Earth Surf. Process.* 26, 1221–1236.
- Van Rompaey, A.J.J., Bazzoffi, P., Jones, R.J.A., Montanarella, L., Govers, J., 2003a. Validation of Soil Erosion Risk Assessment in Italy (European Soil Bureau Research Report No. 12, EUR 20676 EN). Office for Official Publications of the European Communities, Luxembourg.
- Van Rompaey, A.J. J., Vieillefont, V., Jones, R.J.A., Montanarella, L., Verstraeten, G., Bazzoffi, P. et al., 2003b. Validation of Soil Erosion Estimates at European scale (European Soil Bureau Research Report No. 13, EUR 20827 EN). Office for Official Publications of the European Communities, Luxembourg.
- Walling, D.E., He, Q., Blake, W., 1999. Use of Be-7 and Cs-137 measurements to document short- and medium-term rates of water-induced soil erosion on agricultural land. *Water Resour. Res.* 35, 3865–3874.
- Wang, Y., Huntington, T.G., Osher, L.J., Wassenaar, L.I., Trumbore, S.E., Amundson, R.G., et al., 1998. Carbon cycling in terrestrial environments. In: Kendall, C., McDonnell, J.J. (Eds.), *Isotope Tracers in Catchment Hydrology*. Elsevier Science B.V., Amsterdam, pp. 498–518.
- World Reference Base for Soil Resources [WRB], 2006. World Soil Resources Reports 103: A framework for international classification, correlation and communication. IUSS Working Group World reference base for soil resources. Food and Agriculture Organization of the United Nations, Rome, Italy.
- Wyss, R., 1986. The Urseren zone: litho-stratigraphy and tectonics. *Eclogae Geol. Helv.* 79, 731–767 (in German).
- Zapata, F., 2003. The use of environmental radionuclides as tracers in soil erosion and sedimentation investigations: recent advances and future developments. *Soil Till. Res.* 69, 3–13.

CHAPTER 3

Impacts of anthropogenic and environmental factors on the occurrence of shallow landslides in an alpine catchment (Urseren Valley, Switzerland)

This chapter has been published in Natural Hazard and Earth system sciences as:
Meusburger, K., and Alewell, C.: Impacts of anthropogenic and environmental factors on the occurrence of shallow landslides in an alpine catchment (Urseren Valley, Switzerland), Volume: 8, 509-520, 2008.

Impacts of anthropogenic and environmental factors on the occurrence of shallow landslides in an alpine catchment (Urseren Valley, Switzerland)

K. Meusburger and C. Alewell

Institute of Environmental Geosciences, University of Basel, Bernoullistrasse 30, 4056 Basel, Switzerland

Received: 4 January 2008 – Revised: 12 March 2008 – Accepted: 9 April 2008 – Published: 19 May 2008

Abstract. Changes in climate and land use pose a risk to stability of alpine soils, but the direction and magnitude of the impact is still discussed controversially with respect to the various alpine regions. In this study, we explicitly consider the influence of dynamic human-induced changes on the occurrence of landslides in addition to natural factors. Our hypothesis was that if changes in land use and climate have a significant influence on the occurrence of landslides we would see a trend in the incidence of landslides over time. We chose the Urseren Valley in the Central Swiss Alps as investigation site because the valley is dramatically affected by landslides and the land use history is well documented. Maps of several environmental factors were used to analyse the spatial landslide pattern. In order to explain the causation of the temporal variation, time-series (45 years) of precipitation characteristics, cattle stocking and pasture maps were compared to a series of seven landslide investigation maps between 1959 and 2004. We found that the area affected by landslides increased by 92% from 1959 to 2004. Even though catchment characteristics like geology and slope largely explain the spatial variation in landslide susceptibility (68%), this cannot explain the temporal trend in landslide activity. The increase in stocking numbers and the increased intensity of torrential rain events had most likely an influence on landslide incidence. In addition, our data and interviews with farmers pointed to the importance of management practice.

1 Introduction

Topographic and climatic extreme conditions make the mountain environment vulnerable to changes of climate and land use (Cernusca et al., 1998). Due to changes of climate

and land use the potential risks of torrents, snow gliding, avalanches, soil erosion and landslides may increase. Soil and slope stability are a crucial precondition to preserve the functions of the mountain environment, for example water supply, nutrient production, biodiversity, aesthetics, and cultural heritage. Landslides endanger slope stability and the resource soil in mountains areas all over the world (Glade, 2003; Ohlmacher and Davis, 2003; Shrestha et al., 2004; Ayalew et al., 2005), as one extreme event can constitute a great proportion of total soil loss while recovery of soil characteristics is very slow (Sparling et al., 2003).

The effect of environmental catchment characteristics on the probability of landslides is well understood and commonly used to predict landslide risk. Most of the investigated triggering factors are quasi-static in time i.e. do not change their characteristics in the considered time-span (such as geology, topography, etc.). Several studies showed the decisive impact of geology and slope as proxies for the physical parameters that describe soil strength properties and gravitational forces (Carrara et al., 1991; Rickli et al., 2001; Dai and Lee, 2002; Zhou et al., 2002; Ohlmacher and Davis, 2003; Santacana et al., 2003; Van Westen and Lulie Getahun, 2003; Suezen and Doyuran, 2004; Ayalew and Yamagishi, 2005; Clerici et al., 2006; Komac, 2006). However, the effect of triggering factors which are variable with time due to anthropogenic influence such as land use and climate (here defined as “dynamic factors”) are only rarely considered.

Even though there is no doubt that land use has a significant effect on the probability of landslides (Schauer, 1975; Bunza, 1984; Glade, 2003; Tasser et al., 2003; Petley et al., 2007), its influence is still discussed controversially in literature with respect to the various mountainous regions (Douglas et al., 1996; Andre, 1998; Tasser and Tappeiner, 2002; Krohmer and Deil, 2003). Overall it is not clear yet, whether we can expect a reduced erosion risk due to reforestation of mountain slopes or an increase due to abandonment and intensification of remote sites in alpine regions.



Correspondence to: K. Meusburger
(katrin.meusburger@unibas.ch)

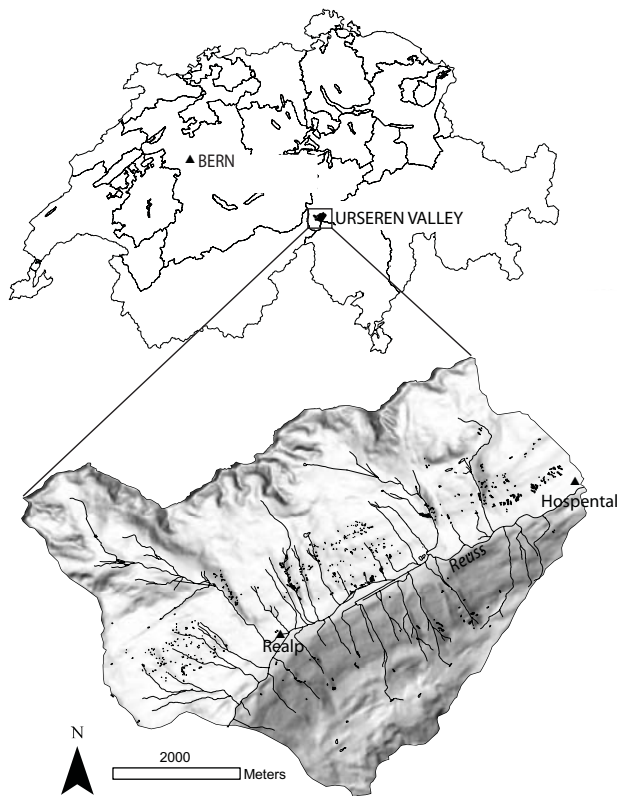


Fig. 1. Map of Switzerland and the study area (Projection: CH1903 LV03).

The assessment of the impact of the above-discussed human-induced changes is a crucial requirement for land managers and policy makers in order to initiate prevention measures. Unfortunately, the impact of the human-induced changes on landslide is difficult to quantify, due to the high natural variability and geomorphic feedback mechanisms. Only few studies exist that could relate actual impact of anthropogenic changes with trends in landslide activity. The main method to study trends in landslide incidence is based on the application of physically based slope stability models, which were applied to simulate former climate and land use conditions (Collison et al., 2000; Vanacker et al., 2003; Schmidt and Dikau, 2004; Claessens et al., 2006). Another possible method is to analyse landslide databases in relation to other human-induced trends in landscape and climate change (Petley et al., 2007). We will pursue the latter approach in our study due to the lack of most of the physical parameters related to the modelling of land use change.

Our aim is to evaluate, if the above described land use- and climate changes cause a trend in landslide occurrence and to determine possible causes for the temporal variation. Our hypothesis is that if anthropogenic changes have had an impact on landslide triggering it will be expressed by a trend in landslide occurrence, since changes of land

use and climate change in the Alps have been evident for decades. For example, the processes of abandonment, extensification and reforestation occur since the early 1960s (Ritzmann-Blickenstorfer, 1996; BFS, 2001; Descroix and Gautier, 2002; Piégay et al., 2004). The process of global warming is most evident in the Alps by the melting glaciers since 1850 (Frei et al., 2007).

The Urseren Valley (Central Swiss Alps) was chosen as investigation site for two reasons; (i) the valley is dramatically affected by landslides and (ii) land use history is well documented. The valley slopes are also affected by sheet erosion, which is addressed and evaluated in other ongoing studies. (Alewell et al., 2008; Brodbeck and Alewell, 2008¹). Here, we explicitly focus on landslides in consequence of soil instability.

2 Study area

The sub-alpine study area (30 km²) is located in the Urseren Valley (Switzerland) and is discharged by the river Reuss (Fig. 1). The wide glaciated valley is characterised by a U-shaped profile and a rugged terrain. Elevation ranges from 1400 to 3200 m a.s.l. The predominant slope angle is approximately 27.2°.

The valley corresponds to a geological fault line that separates the gneiss massif of the Gotthard system to the south from the granite massif and the pre-existing basement (named by “Altkristallin” by Labhart, 1999), of the Aare system in the north. Intermediate vertically dipping layers along the fault line consist of Permocarbone and Mesozoic sediments (Labhart, 1999). During the Permocarbone sandy-clay sediments deposited and during the Mesozoic, different materials from the geological periods Trias (sandstone, rauhwacke and dolomite), Lias (dark clay-marl and marl) and Dogger (clays, marl and limestone) deposited. Throughout the mountain building the material was metamorphosed to schist (Kägi, 1973; Angehrn, 1996). Due to erosion of these soft layers a depression developed (Kägi, 1973). The direction of the strike of these sediments from SW to NE corresponds to the valley axis. Weathering of the calcareous material produced marls that are prone to landslides. Riverbeds are characterised by glaciofluvial deposits. On the valley slopes, Quaternary moraines and talus fans are common and consist mainly of siliceous loamy gravel material. The reader is referred to Wyss (1986) for a detailed description of the tectonic and lithostratigraphical evolution of the region.

Dominant soil types in the catchment, classified according to WRB (2006), are Podzols, Podzocambisols and Cambisols. Above 2000 m a.s.l. and on steep valley slopes, Leptosols are common (with rendzic Leptosols on the calcareous substrates). At the valley bottom and lower slopes,

¹ Brodbeck, M. and Alewell, C.: Stable carbon isotopes as an indicator for soil degradation in an alpine environment (Urseren Valley, Switzerland), *Eur. J. Soil Sci.*, submitted, 2008.

predominantly clayey gleyic Cambisols, Histosols, Fluvisols and Gleysols developed.

The valley is characterised by a high mountain climate with a mean air temperature of 3.1°C (1901–1961). The temperatures of the last years (1961–2006) show a deviation of 1.5°C higher temperatures compared to the long term mean (1901–1961) (Angehrn, 1996). Mean annual rainfall at the climate station in Andermatt (8°35′/46°38′; 1442 m a.s.l.) of MeteoSwiss located at the outlet of the valley is about 1400 mm. The valley is snow covered for 5 to 6 month (from November to April) with the maximum snow height in March (Angehrn, 1996). The rainfall maximum occurs in October, the minimum in February. Runoff is usually dominated by snowmelt in May and June. Nevertheless, summer and early autumn floods represent an important contribution to the flow regime. The peak runoff period is in June (BAFU, <http://www.hydrodaten.admin.ch/d/2087.htm>; Access date: 06.08.2007).

Vegetation shows strong anthropogenic influences due to pasturing for centuries (Kägi, 1973). Particularly on the less productive north-facing slope an invasion of shrubs mainly by *Alnus viridis*, *Calluna vulgaris*, *Salix appendiculata*, *Sorbus aucuparia*, and *Rhododendron ferrugineum* is evident (Kägi, 1973; Küttel, 1990b). Dwarf-shrub communities of *Rhododendron ferrugineum* and *Juniperus sibirica* (Kägi, 1973; Küttel, 1990b) and diverse herbs and grass species dominate on the fertile south-facing slope. The four main land cover types are: 63% alpine grasslands including dwarf-shrubs (mainly consisting of *Calluna vulgaris*, *Rhododendron ferrugineum*, *Juniperus sibirica*), 16% debris (grassland with more than 70% boulders), 11% bare rock at higher elevations, and 8% shrubs (mainly consisting of *Alnus viridis* and *Sorbus aucuparia*) approximately one third of it invaded since 1959 and will be termed “new shrub” in the following. Urban and forest areas each represent less than 1% of total area. Today’s forests were cultivated for avalanche protection above the villages. Deforestation of the valley started in 1100 with the first settlement due to agricultural activities and scarcity of timber. Associated with the deforestation are frequently occurring avalanches (Küttel, 1990a).

The cultural landscape of the valley is dominated by pasturing. Private owners and Korporation Urseren own the land. The alp areas of the Korporation Urseren are traditionally used as summer pastures. The private land serves as hay meadows to feed the cattle during the winter month. Meadows are treated with organic fertilizer and mown once or twice a year. The relevance of farming gradually decreased during the last decades. In addition, the number of full time farmers and farms decreased. Kägi (1973) already observed that, “the traditional principles of land use are dissolving”.

3 Materials and methods

A time-series of landslide inventory maps was generated based on air photographs of seven different years starting in 1959. The occurrence of landslides over time was then tested for a significant trend with the Neumann trend test. The landslide inventory maps were then superimposed with environmental factor maps and analysed with multiple logistic regression. In order to illustrate the relation between landslides and causative factors, bivariate statistic is applied for the factors geology, slope, avalanche density, and land-cover. Finally, the evolution of landslide occurrence over time was compared to time-series of dynamic factors, such as climate (precipitation and avalanches) and land use characteristics (stocking numbers and management practice). The database construction and spatial overlay of the data layers was accomplished with the geographic information system (GIS) software ArcGIS (ESRI) version 9.1.

3.1 Mapping of landslides from air photographs

Landslides in the investigation area (30 km²) were mapped by visually vectorising the affected area from air photographs (Swisstopo, 2006). The photographs had a scale of at least 1:12000 and were available for seven different years: 1959, 1975, 1980, 1986, 1993, 2000, and 2004.

The photographs from 1959 to 1993 are black and white images with no geometrical corrections. In order to allow for local comparison of individual landslides between different years the photographs were georeferenced and orthorectified. The geometrical corrections were done with the help of ground control points, the DEM (25 m grid) and the camera calibration protocols (Swisstopo, 2006). For the years 2000 and 2004 the orthorectified RGB “Swissimages” (air photographs with geometrical corrections) with a pixel resolution of 0.5 m could be directly used without pre-correction. Field verification in 2005 was performed to check the inventory map of 2004. During the field excursions, the maximal width and length of ten landslides was measured and compared to corresponding distances digitised by the photo interpretation mapping method. The resulting deviation between the two methods was approximately 10% which we took as the assumed error of the areal mapping method.

3.2 Mapping of environmental factors

3.2.1 Quasi-static factors

The topographical parameter slope was calculated from the DEM with a three-pixel kernel. A geological map at a scale of 1:200 000 (Labhart, 1999) formed the basis for a revised geological map, that was supplemented by field mapping and air photograph interpretation. This revised geological map, constructed as digital polygons, was then converted to raster format. ArcGIS density functions were used to obtain a raster map of avalanche. The avalanches that occurred

since 1695, recorded by the Swiss Federal Institute for Snow and Avalanche Research Davos, were averaged for each pixel with 500 m moving window to generate the avalanche density map.

3.2.2 Time-series of land use, land-cover and climate data

The present and past land use was determined by a series of pasture maps of the years 1955, 1975, 1990, and 2006 (Russi, 2006) that were digitised and georeferenced. We conducted semi-structured interviews with two farmers concerning changes of land use within the last decades to supplement the pasture map information (FAO, <http://www.fao.org/docrep/x5307e/x5307e08.htm>; Access date: 06.08.2007). One of them was acting as a farmer elected to oversee common lands for 16 years. Quantitative information on stocking on the pastures was obtained from the archive of the Korporation Urseren (Russi, 2006). The stocking numbers together with the pasture maps were used to calculate stocking densities (area per animal) for four different years. In the following we will address the stocking densities (animal/area) as land use intensity. Information on the land-cover was available from the Vector25 dataset (Swisstopo, 2006). The dataset was last actualised in 1993, thus, it was updated with the air photograph of 2004 to display the present-day situation. The land-cover was additionally mapped for the year 1959 (based on air photograph interpretation) to assess potential changes of land-cover with a spatial overlay.

Climate data with daily rainfall was supplied by MeteoSwiss for the Andermatt station from 1971 to 2006. The avalanches that occurred in the valley were summarized for each year to generate a time-series of avalanche frequency.

3.3 Analysis of environmental factors

3.3.1 Quasi-static factors

In order to identify the most relevant environmental factors a multi-collinearity analysis followed by multiple-logistic regression with forward selection method was used.

To illustrate the causative relationship of selected quasi-static factors and landslide occurrence, we used bivariate analysis to produce landslide density histograms (landslide occurrences within each factor map and within each factor map's classes). For bivariate analyses, a categorisation of the continuous factor maps is necessary. The landslide densities are calculated according to equation:

$$D_i = \frac{SX_i}{X_i} * 100 * \sum_{k=1}^n \frac{X_{i=k}}{SX_{i=k}} \quad (1)$$

in which D_i =landslide density for a variable class, SX_i =number of pixels with landslides within a variable class, X_i =number of pixels within variable class and n =number of variable classes. The division of SX by X eliminates the effect of different areal extends of the classes. To

ease the comparability between landslide densities of different classes a normalisation with the sum of landslide densities for all classes was done. ArcGIS 9.1 provides the ready applicable tool "zonal statistic" to simplify the calculation of the ratio between the areas occupied by landslide pixels within each class of a certain factor map. This procedure is repeated for all factor maps.

3.3.2 Time-series of climate data and land use

The mean precipitation data and torrential rainfall events were tested for a trend with the Mann-Kendall's Tau test (Helsel et al., 2006). To assess the influence of dynamic factors, the development of the number of landslides was compared and correlated (Spearman's rank correlation) to the maximum precipitation event (yearly maximum 1 day-events, -3 day-events and -5 day-events; yearly mean precipitation), that occurred in the corresponding period, stocking properties (cumulative stocking and increase of stocking within the years, absolute stocking numbers), and avalanche frequency. In order to avoid pseudo-replication only the number of new landslides (not the increased area of existing slides) between each mapped year was used for the correlation. Thus, increase in landslides means that newly affected areas are spatially separated from older ones.

4 Results and discussion

4.1 Relation of landslides to natural quasi-static factors

In 2004 a total of 383 shallow landslides ($>25 \text{ m}^2$) with a total area of 9.42 ha, an average size of 250 m^2 , and an average slope of the landslide area of 33.9° were mapped with air photograph interpretation. The areal extent of the largest detected landslide is about 7000 m^2 .

A collinearity diagnosis of the quasi-static factors identified several cross-correlations. As was shown by Meusburger and Alewell (2008)². Geology, slope and avalanche density were distinguished as independent factors with variance inflation factors (VIF) <2 . The subsequent multiple-logistic-regression identified the geology as the most dominant factor followed by slope (for both $P<0.0001$). Avalanche density did also significantly ($P=0.002$) improve the explained spatial variance.

Landslide density histograms illustrate the spatial dependence between the mapped landslide pattern and environmental factors (Fig. 2). Regarding geology (Fig. 2a), landslide density was highest in the Mesozoic formation and the Altkristallin (47.1% and 36.4%, respectively). Calcareous rock of the Mesozoic formation, weathered to clay, forming soils with stagnic properties, which are particularly prone

²Meusburger, K. and Alewell, C.: The influence of land use change on the validity of landslide susceptibility maps, *Earth Surf. Proc. Land*, under revision, 2008.

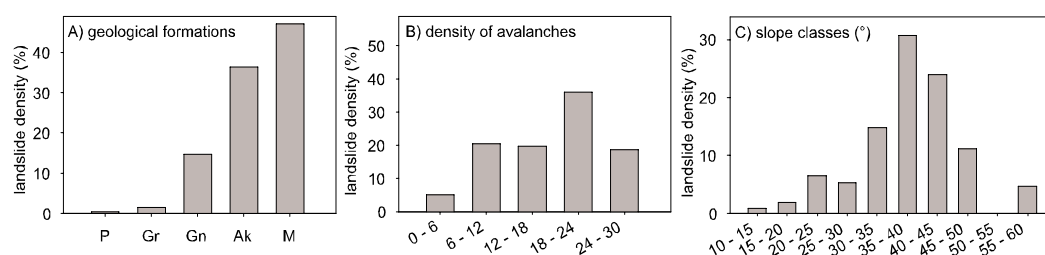


Fig. 2. The landslide density histogram as dependent on (A) geology (for the permocarbonic- (P) and mesozoic-sediments (M), Granite of the Aare massif (Gr), Gneiss of the Gotthard massif (Gn) and “Altkristallin” (Ak) by Labhart, 1999), (B) avalanche density, and (C) slope.

to landslides due to their layered and water ponding character. The Altkristallin, adjacent to the Tavetscher fault line, is a highly deformed and instable clay schist. Both bedrock units of this class occur only along the lower south exposed slope. Even though the Permocarbon is also a sediment layer it shows lowest susceptibility to landslides due to its location at the flat valley floor. Our results seem to confirm the widely recognised view that geology greatly influences the occurrence of landslides as it determines the strength and permeability of rock as well as the resultant cohesion of the soil layer (Carrara et al., 1991; Guzzetti et al., 1999; Dai and Lee, 2002).

Gravitational forces are decisive beside material properties. We observe that the probability of landslides increases with slope angle and peaks at gradients ranging between 35° to 40° (Fig. 2b). This slope angle corresponds well with literature values for other alpine grasslands (Dommermuth, 1995; Rickli et al., 2001; Tasser et al., 2003). For steeper slopes the landslide susceptibility decreases again most likely because soil cover becomes thinner through continuous sheet erosion. A thinner soil cover is less susceptible to landslides because less gravitational forces occur. In general, landslide susceptibility increases with increasing slope angle and soil depth (Carson, 1971).

Avalanche density (since 1695) is a further parameter which might influence landslide distribution. Landslide density increases with increasing avalanche density in the Ursere Valley (Fig. 2c). The exception is the class with the highest avalanche density (24–30) that is located in elevated and steep terrain where soil cover is scarce and rock and debris are dominating land-covers. Interference with geology may be the reason for the increased value of the class with 6 to 12 avalanches. A spatial relationship is evident even though the causal relation is questionable because stability of snow cover depends on similar topographical conditions as the stability of soil cover. The latter will be discussed in more detail in connection with the time-series data in the following chapter.

It is very likely, that the pattern of the mapped landslides is not only showing a statistical correlation but also a causative relationship to the quasi-static, environmental factors geology and slope. Other risk assessment studies also identified

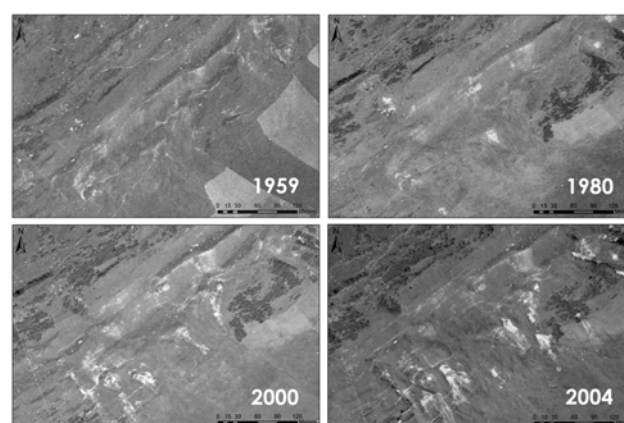


Fig. 3. Sub-images of air photographs showing the stages of landslide hazard for the years 1959, 1980, 2000, and 2004.

geology and slope to be the most decisive quasi-static catchment characteristics (Ohlmacher and Davis, 2003; Suezan and Doyuran, 2004; Ayalew and Yamagishi, 2005). However, beside the static environmental catchment conditions, the relevance of dynamic anthropogenic changes on the temporal evolution of landslide incidence is crucial to know.

4.2 Evolution of landslide incidence compared to human-induced changes

The area affected by landslides increased dramatically since 1959. Figure 3 gives a visual impression of the destabilisation of a lower south-exposed slope over the years. The mapping of the stages of landslide incidence revealed that, once the slope is degraded by trails and landslides, it might take decades to recolonise the bare spots with vegetation.

The Neumann-test shows a significant increasing trend ($P < 0.01$) for landslide numbers and landslide area. While the number of landslides continuously increased with time, the increase of eroded area happened in two phases: from 1959 to 1980 by 45% and from 2000 to 2004 by 32% (Fig. 4). From 1980 to 2000, new landslides occurred but the total affected area did not increase due to partial regeneration of older landslides. In total, the eroded area nearly doubled

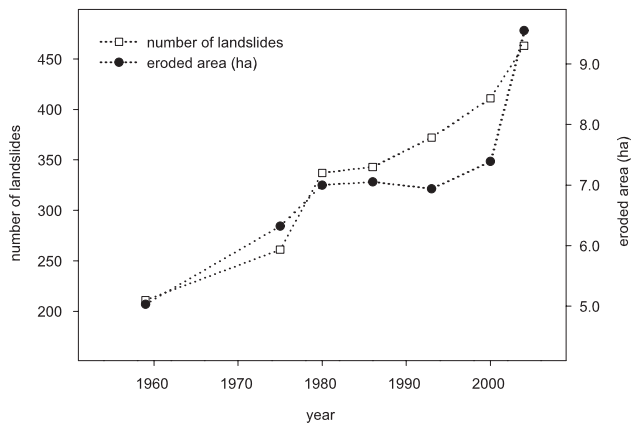


Fig. 4. Progression of the number of landslides and eroded area by landslides for the entire catchment since 1959. The error of the mapped landslide area is approximately 10%.

between 1959 and 2004 (increase of 92%). The average depth of 10 measured landslides was 1.5 m. Given the eroded area and assuming a bulk density of 1.2 t m^{-3} , we estimated a mean sediment rate of $0.6 \text{ t ha}^{-1} \text{ yr}^{-1}$ due to landslides only. According to sheet erosion rates for agricultural low lands, this value is classified as low soil loss. However, due to the higher vulnerability of alpine regions the areal damage is dramatic.

In order to explain the increasing trend, the evolution of landslide incidence is compared to other causative factors that changed over time and have a geophysical association to landslide triggering, as described below. Trends in landslide activity might also be caused by geomorphologic feedback mechanisms i.e. older landslides can undercut and steepen a slope and trigger new landslides. However, the induced feedback mechanisms are not exclusively positive. Claessens et al. (2007) showed that landslides also stabilise some parts of the slope due to the canalisation of the runoff in the eroded area. A quantification of the balance between stabilising and destabilising feedback effects could not be accomplished for the scale considered in our study. Thus, an effect of positive feedback mechanisms might be involved in the observed trend in landslide activity. Moreover, new landslides occurred mostly sideways to older ones or at sites, that were formerly free of landslides (note that triggering interactions show a upslope/downslope shifting pattern (Claessens et al., 2007)). We thus assume that legacy effects are of minor importance. The use of hydropower and accompanying changes of slope humidity can be excluded as possible explanation for the landslide increase, because the hydropower station in Realp was already commissioned in 1913 (EWU, <http://www.ew-ursern.ch/docs/wasserkraft.cfm>; Access date: 06.08.2007).

4.2.1 Climate factors: avalanche frequency and precipitation

The analysis of time-series data showed that several dynamic factors change simultaneously in the Urseren Valley. This impedes the determination of a definite causation of the landslide trend. Moreover, the temporal resolution of the air photographs to analyse the landslides is too low and too irregular, to deduce significant correlations. Nonetheless, in the following correlation coefficients are presented to supplement the graphical illustrations.

Climate change affects soil stability directly via modification of precipitation characteristics and via temperature effects on soils (e.g. melting of permafrost). Indirect effects include the alteration of vegetation cover and snow processes. We evaluated the frequency of avalanches over time as one important proxy for changes in snow dynamics. Avalanches are regarded as potential landslide risk factors because of the additional friction forces that may trigger tension fissures. The time-series of avalanches show a slightly increasing trend of the linear regression. However, the latter is only due to the high number of avalanches in the winter of 1999 (Fig. 5 left). Apart from that extreme event no trend over time is distinguishable. A direct comparison between the time-series of the number of avalanches and number of landslides for single years in the valley did not result in a clear relationship ($r_{sp} = -0.43$, $P = 0.38$). Although there is a connection between spatial pattern of avalanches and landslides (Fig. 2b, see discussion above), no temporal correlation was found, e.g. the winter of 1999 with 30 avalanches did not cause a noticeable rise of the eroded area in 2000. Avalanches might trigger landslide events in subsequent years due to a general destabilisation of slopes. However, the absence of tension fissures in the field and the time-series data lead to the conclusion that avalanches do not directly triggered landslides at our site but rather occur in the same places, because the stability of snow cover and stability of soils are controlled by similar environmental conditions. To conclude, we could not identify avalanches as a causative factor for the landslide trend.

Generally, landslides and precipitation are related by a threshold function (Guzzetti et al., 1999; Zhou et al., 2002) as soil strength properties are a function of soil water content. However, the Spearman correlation coefficients between precipitation characteristics (yearly maximum 1 day-events, – 3 day-events and –5 day-events; yearly mean precipitation) and landslides were not significant. The Mann-Kendall's Tau test was not significant for mean precipitation data of the Andermatt station, too. However, for torrential events $> 150 \text{ mm } 3\text{d}^{-1}$ a significant ($P < 0.05$) increase of $1.32 \text{ mm } 3\text{d}^{-1}$ per year is evident (Fig. 5 right). Thus exceedance of the landslide triggering threshold became more likely.

Farmers confirmed that prolonged rainfall of 2–3 days triggers landslides. The maximum event in the observed period occurred in November 2002 (270 mm in three days), which

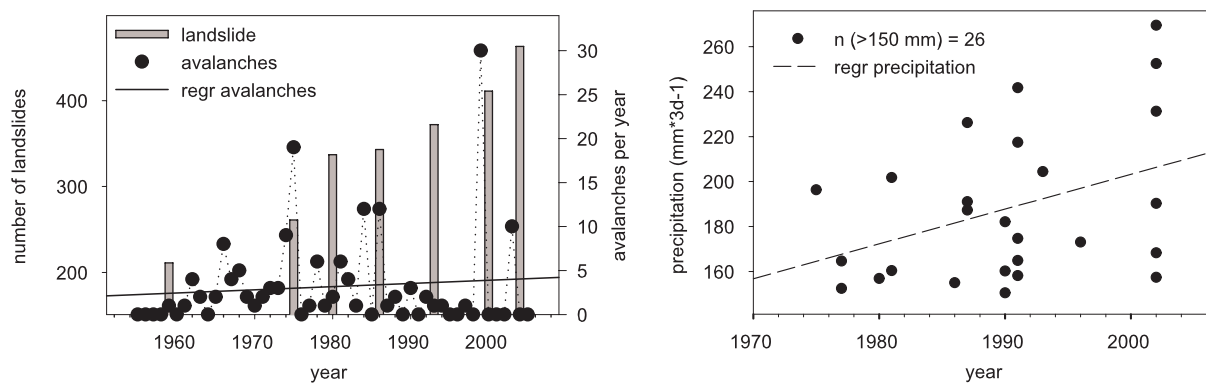


Fig. 5. Increase of the number of landslides in comparison to the climate factors: frequency of avalanches per year (left) and yearly maximum 3-days precipitation events (right).

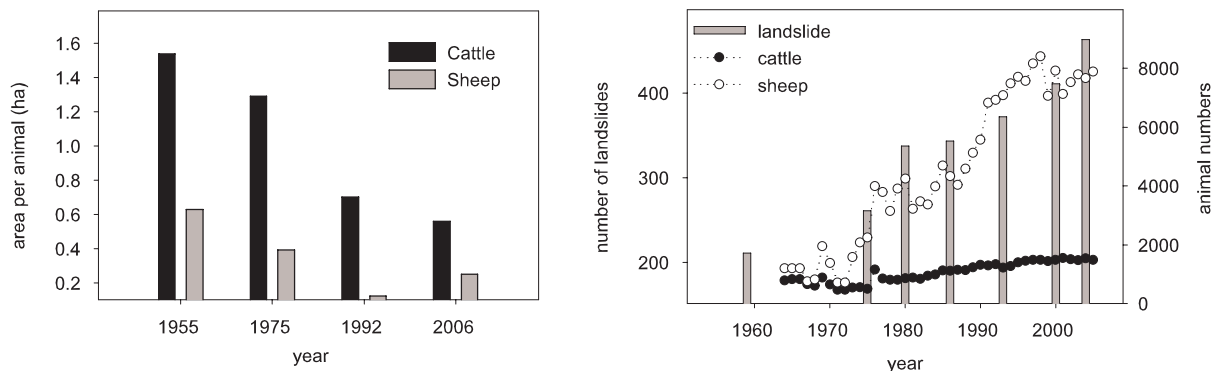


Fig. 6. Land use intensification (left) and a comparison between the increased landslide- and stocking numbers (right).

triggered at least 17 landslides (Berger, August 2005; Swisphoto; personal communication) and mainly contributed to the affected area we observe in 2004. Extreme events from August 1987 (226 mm in three days) and November 1991 (242 mm in three days) also triggered several landslides. However, no triggering event could be observed between 1993 and 2000.

The observed increased frequency and intensity of torrential rainfall events is in correspondence with the generally described climate change effects (IPCC, 2007). Moreover, precipitation is expected to increase more in the winter (Beniston, 2006) when vegetation is sparse. The most severe events were observed in November in the Urseren Valley. On lower altitudes, precipitation will less often fall as snow while for higher altitudes a thicker snow pack in spring is predicted that results in more intense snowmelt events (Beniston, 2006). Thus, landslide hazard can be expected to increase through the described effects (Frei et al., 2007). Our analysis of extreme 3-day precipitation events seem to confirm this statement.

4.3 Land use factors: Intensity, management practices and land-cover

4.3.1 Land use intensity

Besides the climatic factors the triggering of landslides is dependent on intensity and type of land use (Schauer, 1975; Bunza, 1984; Tasser et al., 2003). Land use was mainly intensified in the valley during the last decades, which is shown by the decreasing pasture area per animal (Fig. 6 left). Since 1955, the pasture space per cow steadily decreased for two reasons (i) an increase in cow numbers from 785 to 1482 and (ii) a reduction of cow pasture area. Pasture area per sheep also decreased until 1992 due to an increase of sheep from 1193 in 1955 to 7875 in 2006. The sheep pastures were enlarged in 2006. Goats are of minor importance in the valley and decreased from approximately 550 goats in 1976 to 280 in 2005.

Except between 2000 and 2004, a good correspondence between increase of stocking number and landslides could be observed (Fig. 6 right). However, correlations between the increase of stocking numbers (sheep $r_{sp}=0.10$, $P=0.87$, cattle $r_{sp}=0.35$, $P=0.56$) and new landslides of corresponding

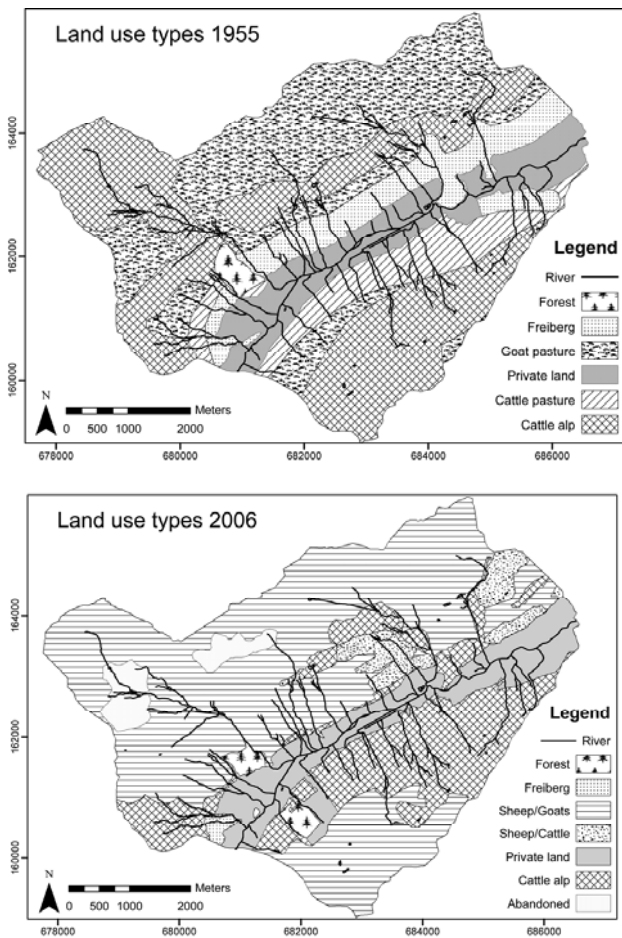


Fig. 7. Pasture maps for the year 1955 and 2006.

years was not significant. One reason is that the interaction with the triggering rainfall event and even the timing of the event needs to be considered. A multiple regression with stocking increase and yearly maximum 3 day-events could improve the explained variance ($R=0.4$) of the landslide development but was still not significant. Both predictors showed similar significance in the multiple regression (stocking number of sheep and cattle $P=0.52$, yearly maximum 3 day-events $P=0.58$). A reason for the low significance of the predictors is the usually non-linear relationship between landslides and its triggering factors. Rainfall events, for example, need to exceed a certain threshold to initialise landslides. Moreover, significant correlations might be obscured by the low temporal resolution of the air photographs (and thus low resolutions of landslide increase).

4.3.2 Land use management practice

Land use management practice is a further dynamic factor. The change of management practice is apparent from the pasture maps of 1955 and 2006 (Fig. 7). The private land

is situated at the valley floor and adjacent slopes. Different forms of pastures (goat, cattle, and sheep) can be found on the slopes. Comparing the two maps, the following developments are noticeable between 1959 and 2006:

- a) Goat pastures disappeared in 2006.
- b) The traditional land use type called “Freiberg” almost disappeared. “Freiberg” areas are pastures, which are used in spring because of the vicinity to the farms and the more advanced vegetation state at this altitudinal level. The 14th June is the appointed date to bring the cattle to the higher pastures. For the rest of the summer the Freiberg is kept as a reservoir in case of an early onset of the winter and is left to regenerate during the main growing season (note that the “Freiberg” were situated in the geological sensitive area of the Mesozoic layer).
- c) Remote and less productive areas were abandoned.
- d) Alpine cattle alps, which are high mountain pastures exclusively used during summer, disappeared completely to give way for sheep pastures.

Interviews with two farmers were conducted to complete the information of the pasture maps. The farmers were asked which kind of land use changes happened and where changes in land use intensity occurred since 1955. The observations and experiences of the farmers can be summarised in two general developments: (i) an intensification of the areas close to the valley (point 1 to 6, see below) and (ii) an extensification of remote areas (point 7 to 9, see below). The developments are ascribed to the following agricultural changes that agree with developments described for other alpine regions (Tasser and Tappeiner, 2002; Troxler et al., 2004; Mottet et al., 2006; Tappeiner et al., 2006; Baur et al., 2007):

- (1) Permanent herding was replaced by uncontrolled grazing within fenced pastures, where animals concentrate on single locations, e.g. at the watering place.
- (2) Steep areas that are difficult to access and that have formerly been mown by hand (wild haying) were converted to pastures.
- (3) The number of external pasture animals delivered from the low lands outside of the valley increased. The animals are delivered to an appointed date independent of the actual vegetation status in the area.
- (4) Compulsory labour that was spent for the maintenance of the pastures was abolished.
- (5) The land use type “Freiberg” was largely abolished. The areas are now pastured throughout the entire season.
- (6) The private land is nowadays more frequently mown with machines and intensely fertilized with organic manure.
- (7) The stocking on the alps with dairy cows was reduced because of increased mother cow husbandry. The latter is mainly proceeded at the valley floor due to difficulties in herding and a more frequent need for veterinarian assistance.
- (8) The shrub cover increased due to cessation of wild haying, firewood collection, and reduced stocking of the alps with cattle and goats. Especially goat grazing hampers the invasion of shrubs (Luginbuhl et al., 2000).
- (9) The number of farmers declined (e.g., in the Urseren Valley from 77 in 1970 to 31 in 2006). Simultaneously, there are less full-time farmers.

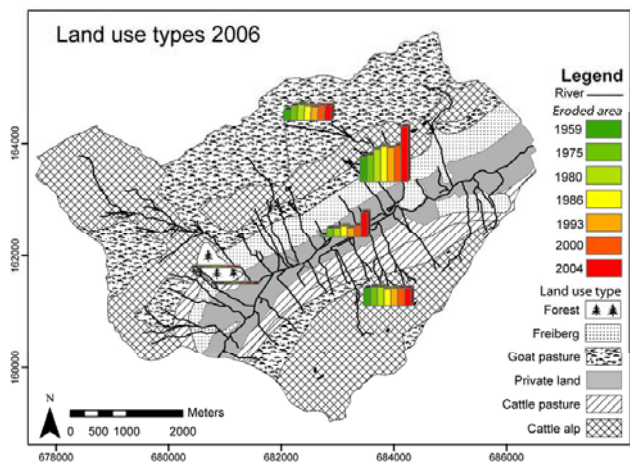


Fig. 8. Progression of landslide affected area on different traditional land use types of 1955.

Most of the changes took place in the beginning of the 1970s as local agriculture became mechanised and traditional farming practices were abandoned. To show the effect of the above described developments on soil stability, the landslide areas for single years are displayed for each traditional land use type of 1955 (Fig. 8). The remote and extensively used pastures were already slightly affected by landslides in 1959, but no increase in landslides could be observed over time. Today these areas are almost exclusively used as sheep pastures. The latter might indicate that sheep are not the main cause of the increase of landslide frequency. However, the data basis does not allow deducing recommendations for a specific pasture animal because the sheep and cattle pastures differ too much in catchment characteristics. Additionally, cattle pastures are temporarily used as sheep pastures; especially in spring when soils are most sensitive. The intensified areas closer to the valley floor (the former “Freiberg” and private land) have clearly destabilised. The “Freiberg” zone was already the most affected zone in 1959 due to its vulnerable geology, whereas the private land at that time was almost undisturbed.

4.3.3 Land-cover: shrub encroachment

Parallel and partly due to the above described changes in grassland management we determined an alteration of land-cover, which manifests in an encroachment of shrubs. Land-cover was not an independent parameter. Nor did it significantly improve the explained variance of the spatial landslide distribution in the multiple logistic regression model. Nonetheless, to evaluate the effect of land-cover change on the landslide trend, landslide densities are presented for the unchanged land-cover types and the areas that changed since 1959 separately (Table 1).

The shrub-cover was the only land-cover category, which showed considerable change over time. The area covered by shrubs increased since 1959 by 30.0%. The landslide density

Table 1. Landslide densities for unchanged land-cover types and areas, that were invaded by shrubs since 1959 (new shrub).

| land-cover | landslide density (%) |
|-----------------------|-----------------------|
| forest | 0.0 |
| debris | 7.5 |
| new shrub | 2.9 |
| shrub | 33.2 |
| grassland/dwarf-shrub | 56.4 |

is 33.2% for the community of old shrubs, but only 2.9% for the new shrubs. The older shrub cover mainly occurs in typical places for *Alnus viridis* i.e. on sites with wet conditions, like tributary channels on the north-facing slope. Especially these wet and steep areas close to channels are susceptible to landslides. The new shrub cover, however, occurred in untypical places for *Alnus viridis* on the plains between the channels and on the south exposed slope. These recently invaded areas show low susceptibility to landslides. The highest landslide densities could be observed for vegetation communities (defined in chapter 2) of dwarf-shrub and grassland (56.4%). Debris is with 7.5% relatively less susceptible to landslide activity, as the inhomogeneous mixture of materials and grain sizes stabilises the soils. The small forested area (0.7% of the catchment) is not affected by landslides.

Extensive investigations have shown that vegetation cover, especially woody shrub type (such as *Alnus viridis*, *Sorbus aucuparia*, *Acer pseudoplatanus*, *Pinaceae* and *Fagaceae*) help to improve stability of the slopes (Schauer, 1975; Newesely et al., 2000). Generally, vegetation has three effects on slope stability: (i) the mechanical anchoring of the soil, (ii) regulation of the soil water budget (iii), and the mechanical resistance to snow or snow gliding. Snow gliding can cause fissures in the soil cover that are potential tear-off lines for landslides (Schauer, 1975; Newesely et al., 2000). *Alnus viridis* constitutes the major species within the shrub category and is known to facilitate snow gliding (Newesely et al., 2000). Nevertheless, this category was less affected by landslides than the grassland/dwarf-shrub category that consists mainly of pastures with high proportions of *Rhododendron ferrugineum* that were found to stabilise the snow cover. We thus conclude that the effect of the land-cover on the landslide probability via the process of snow gliding is most likely of minor importance at our site. The cause for the low landslide susceptibility of the new shrub category can probably be explained by the two other functions of vegetation. *Alnus viridis* is often used in bioengineering to mechanically stabilise slopes with its roots (Graf et al., 2003). In addition, the high evapotranspiration rates of *Alnus* species (Herbst et al., 1999) and the affinity to wet conditions is effective in regulating the soil water budget (Wiedmer and Senn-Irlet, 2006). However, we can not directly deduce a stabilising

effect of *Alnus viridis* from our data and can not exclude that *Alnus viridis* invaded preferably the more stable regions for some unknown reasons.

To summarise, we can see a clear impact of the changed management practice in the Urseren Valley: The accessible, more intensely used areas destabilised whereas areas of extensification to the point of abandonment did not destabilise. The effect of abandonment and the subsequent succession states on slope stability has been discussed in literature in detail (Schauer, 1975; Karl, 1977; Bunza, 1984; Newesely et al., 2000; Tasser et al., 2003). The fact that a reduction of the agricultural use enhances landslides risk is ascribed to increased snow-gliding on these areas (Schauer, 1975), to the higher vulnerability of the succession states and less maintenance (Tasser et al., 2003). For the Urseren Valley, this effect could not be observed. One possible explanation is that an increase of landslides on abandoned land mainly occurs on areas with a slope above 58° inclination (Karl et al., 1985; Mössmer, 1985; Bätzing, 1996), where we could not observe landslides in the Urseren Valley. Furthermore, areas recently (since 1959) colonised by *Alnus viridis* show low landslide density. Mainly species such as *Alnus viridis*, *Sorbus aucuparia* and *Rhododendron ferrugineum* invade in the Urseren Valley, which are believed to increase soil stability. This is crucial information because the invasion of shrubs, is observed for the whole sub-alpine belt of the Swiss Alps. An increase of almost 11.8% was assessed for *Alnus viridis* between 1983/85 and 1993/1995 (Brassel and Brändli, 1999).

We found that the consequence of abandonment of the remote pastures which is the accompanying intensification through concentration of animals on smaller areas in combination with increasing stocking numbers is a greater threat to soil stability than the abandonment itself. Although less pronounced than in the Urseren Valley, this is a general agricultural development in the Swiss Alps (Baur et al., 2007; Troxler et al., 2004). The area of summer pastures steadily decreases (from 612 619 ha in 1954 to 465 519 ha in 2005 BFS, 2005) due to abandonment and subsequent emergence of shrubs and reforestation but simultaneously the stocking numbers increase. For example the summered sheep increased from 200 000 to 420 000 in the last 40 years (Troxler et al., 2004) and the livestock unit from 401 921 in 1954 to 416 566 in 1992 (Baur et al., 2007).

The change in management practice is driven by the decrease of farm numbers and farmers, which resulted in less maintenance and the abandoning of time-consuming traditional farming practices and non-profitable farmland since the early 1960s. In general, this leads on the one hand to abandonment and on the other hand to an intensification of the most profitable and accessible areas in the Swiss Alps and other mountainous regions (Tasser and Tappeiner, 2002; Mottet et al., 2006). These two extreme states of land use intensity are believed to be most vulnerable to landslides (Tasser and Tappeiner, 2002) and will most likely increase in the future.

5 Conclusions

We found a natural susceptibility of the catchment to landslides that has been proved by multivariate analysis. Geology and slope were identified as plausible factors to explain the spatial variation of landslides. However, quasi-static environmental factors like geology, and morphology cannot explain the temporal trend in landslide activity. The increase of the landslide area of 92% within 45 years confirms our hypothesis that dynamic factors like climate and land use decisively influence the landslide pattern that we observe today. The analysis of the time-series of avalanches revealed that avalanches seem to be of minor importance in triggering landslides. The increase of extreme rainfall events and the increased stocking of the pastures are likely to have enhanced the landslide hazard. In order to quantify the proportion of climate change and to separate its impact from land use the application of a deterministic landslide model seems a promising future task (Collison et al., 2000; Schmidt and Dikau, 2004). In addition to stocking numbers, the change in management practices is decisive. Extensively used or abandoned areas with recently emerging shrub vegetation show low landslide densities in the Urseren Valley and were not responsible for the landslide trend.

Land use affected the spatial distribution of landslides and created new landslide risk areas. In this context, it was shown that not abandonment itself but the accompanying intensification of accessible regions poses a major threat to soil stability in the valley. Although we cannot infer quantitative relationships between landslide hazard and anthropogenic impacts, our data indicate an increase of landslide hazard that duplicated the affected area by landslides. The case study in the Urseren Valley clearly highlights the relevance of dynamic anthropogenic driven impacts on landslide hazard. Many of the described developments are representative for other alpine regions, however, it remains to be shown if the impact on landslides is as significant.

Even though estimated soil loss due to landslides might be low compared to arable areas ($0.6 \text{ t ha}^{-1} \text{ yr}^{-1}$ compared to $2\text{--}t \text{ ha}^{-1} \text{ yr}^{-1}$ as a limit value in the Swiss soil protection guideline BAFU, 2001), the areal damage is critical. Thus, there is a strong need, that soil loss through landslides is considered in erosion risk models and for guidelines and limit values adapted to mountain ecosystems.

Acknowledgements. This study was funded by the Swiss Federal Office for the Environment. The authors gratefully acknowledge the supply of data by MeteoSwiss, Korporation Urseren, Swiss Federal Institute for Snow and Avalanche Research (SLF), and Swissphoto. Furthermore, we would like to thank T. Labhart, M. Mueller and the members of the Transdisciplinary Project Urseren (TPU) for valuable support and discussions.

Edited by: K.-T. Chang

Reviewed by: L. Claessens and three other anonymous referees

References

- Ahnert, F.: Einführung in die Geomorphologie, third edition ed., UTB, Stuttgart, 440 pp., 2003.
- Alewell, C., Meusburger, K., Brodbeck, M., and Bänninger, D.: Methods to describe and predict soil erosion in mountain regions, *Landscape and Urban Planning*, in press, 2008.
- Andre, M. F.: Depopulation, land-use change and landscape transformation in the French Massif Central, *Ambio*, 27, 351–353, 1998.
- Ayalew, L. and Yamagishi, H.: The application of GIS-based logistic regression for landslide susceptibility mapping in the Kakuda-Yahiko Mountains, Central Japan, *Geomorphology*, 65, 15, 2005.
- Ayalew, L., Yamagishi, H., Marui, H., and Kanno, T.: Landslides in Sado Island of Japan: Part II. GIS-based susceptibility mapping with comparisons of results from two methods and verifications, *Eng. Geol.*, 81, 432–445, 2005.
- BAFU: Article 18 of the Ordinance of 7 December 1998. Relating to Agricultural Terminology (SR 910.91), Swiss Federal Office for the Environment (German: BAFU), 2001.
- Bätzing, W.: Landwirtschaft im Alpenraum – Ansätze für eine Synthesedarstellung, in: Europäische Akademie Bozen (Hrsg.), *Landwirtschaft im Alpenraum – unverzichtbar, aber zukunftslos*, Blackwell Wissenschaftsverlag, Berlin, 229–242, 1996.
- Baur, P., Müller, P., and Herzog, F.: Alpweiden im Wandel, *AGRAR Forschung*, 14, 254–259, 2007.
- Beniston, M.: Mountain weather and climate: A general overview and a focus on climatic change in the Alps, *Hydrobiologica*, 562, 3–16, 2006.
- BFS: The changing face of landuse. Landuse statistics of Switzerland, Bundesamt für Statistik, Bern, 2001.
- BFS: Arealstatistik Schweiz: Zahlen – Fakten – Analysen, Bundesamt für Statistik, Neuchâtel, 99, 2005.
- Brassel, P. and Brändli, U.: Schweizerisches Forstinventar, Ergebnisse der Zweitaufnahme 1993–1995, Birmensdorf, Eidgenössische Forschungsanstalt für Wald, Schnee und Landschaft, Bundesamt für Umwelt, Wald und Landschaft, Bern, 1999.
- Bunza, G.: Oberflächenabfluss und Bodenabtrag in alpinen Grassökosystemen, *Ver. Ges. Ökol.*, 12, 101–109, 1984.
- Carrara, A., Cardinali, M., Detti, R., Guzzetti, F., Pasqui, V., and Reichenbach, P.: GIS techniques and statistical-models in evaluating landslide hazard, *Earth Sur. Proc. Land*, 16, 427–445, 1991.
- Carson, M. A.: *The mechanics of erosion*, Pion Ltd., London, 174 pp., 1971.
- Cernusca, A., Bahn, M., Chemini, C., Graber, W., Siegwolf, R., Tappeiner, U., and Tenhunen, J.: ECOMONT: a combined approach of field measurements and process-based modelling for assessing effects of land-use changes in mountain landscapes, *Ecological modelling*, 113, 167–178, 1998.
- Claessens, L., Lowe, D. J., Hayward, B. W., Schaap, B. F., Schoorl, J. M., and Veldkamp, A.: Reconstructing high-magnitude/low-frequency landslide events based on soil redistribution modelling and a Late-Holocene sediment record from New Zealand, *Geomorphology*, 74, 29–49, 2006.
- Claessens, L., Schoorl, J. M., and Veldkamp, A.: Modelling the location of shallow landslides and their effects on landscape dynamics in large watersheds: An application for Northern New Zealand, *Geomorphology*, 87, 16–27, 2007.
- Clerici, A., Perego, S., Tellini, C., and Vescovi, P.: A GIS-based automated procedure for landslide susceptibility mapping by the Conditional Analysis method: the Baganza valley case study (Italian Northern Apennines), *Environ. Geol.*, 50, 941–961, 2006.
- Collison, A., Wade, S., Griffiths, J., and Dehn, M.: Modelling the impact of predicted climate change on landslide frequency and magnitude in SE England, *Eng. Geol.*, 55, 205–218, 2000.
- Dai, F. C. and Lee, C. F.: Landslide characteristics and slope instability modeling using GIS, *Lantau Island, Hong Kong*, 42, 213, 2002.
- Descroix, L. and Gautier, E.: Water erosion in the southern French alps: climatic and human mechanisms, *CATENA*, 50, 53–85, 2002.
- Dommermuth, C.: Beschleunigte Bodenabtragungsvorgänge in der Kulturlandschaft des Nationalparks Berchtesgaden. Ursachen und Auswirkungen aufgezeigt am Beispiel des Jennergebiets, *Forstwissenschaftliches Centralblatt*, 114, 285–292, 1995.
- Douglas, T., Critchley, D., and Park, G.: The deintensification of terraced agricultural land near Trevelez, Sierra Nevada, Spain, *Global Ecol. Biogeogr. Lett.*, 4, 258–270, 1996.
- Frei, C., Calanca, P., Schär, C., Wanner, H., Schaedler, B., Haeberli, W., Appenzeller, C., Neu, U., Thalmann, E., Ritz, C., and Hohmann, R.: Grundlagen.Klimaänderungen und die Schweiz 2050 – Erwartete Auswirkungen auf Umwelt, Gesellschaft und Wirtschaft, *OcCC Report*, OcCC Report, 2007.
- Glade, T.: Landslide occurrence as a response to land use change: a review of evidence from New Zealand, *CATENA*, 51, 297–314, 2003.
- Graf, C., Boell, A., and Graf, F.: Pflanzen im Einsatz gegen Erosion und oberflächennahe Rutschungen, *Eidgenöss. Forsch.anst. WSL, Birmensdorf*, 2003.
- Gray, D. H. and Leiser, H. T.: *Biotechnical slope protection and erosion control*, Van Nostrand Reinhold, New York, 288 pp., 1982.
- Greenway, D. R.: *Vegetation and slope stability*, Anderson, M. G. and Richards, K. S., *Slope Stability*, Wiley, Chichester, New York, 187–230, 1987.
- Guzzetti, F., Carrara, A., Cardinali, M., and Reichenbach, P.: Landslide hazard evaluation: a review of current techniques and their application in a multi-scale study, *Central Italy, Geomorphology*, 31, 181, 1999.
- Helsel, D. R., Mueller, D. K., and Slack, J. R.: *Computer Program for the Kendall Family of Trend Tests*, Scientific Investigations Report 2005–5275, 4, 2006.
- Herbst, M., Eschenbach, C., and Kappen, L.: Water use in neighbouring stands of beech (*Fagus Sylvatica* L.) and black alder (*Alnus glutinosa* (L.) Gaertn.), *Ann. For. Sci.*, 56, 107–120, 1999.
- IPCC: *Climate Change 2007: The physical science basis. Summary*

- for policymakers., 661, 10th session of working group I of the IPCC, Paris, 2007.
- Kägi, H. U.: Die traditionelle Kulturlandschaft im Urserental: Beitrag zur alpinen Kulturgeographie, PhD thesis at University of Zurich, Switzerland, 212, 1973.
- Karl, J.: Oberflächenabfluss und Bodenabtrag auf brachliegenden extensiv genutzten Flächen, DVWK (Deutscher Verband für Wasserwirtschaft und Kulturbau), 34, 1977.
- Karl, J., Porzelt, M., and Bunza, G.: Oberflächenabfluss und Bodenabtrag bei künstlichen Starkniederschlägen, DVWK (Deutscher Verband für Wasserwirtschaft und Kulturbau), 71, 37–102, 1985.
- Komac, M.: A landslide susceptibility model using the Analytical Hierarchy Process method and multivariate statistics in perialpine Slovenia, *Geomorphology*, 74, 17, 2006.
- Krohmer, J. and Deil, U.: Dynamic and conservative landscapes? Present vegetation cover and land-use changes in the Serra de Monchique (Portugal), *Phytocoenologia*, 33, 767–799, 2003.
- Küttel, M.: Zur Vegetationsgeschichte des Gotthardgebietes, Mitteilungen der Naturforschenden Gesellschaft Luzern, 31, 100–111, 1990a.
- Küttel, M.: Der subalpine Schutzwald im Urserental – ein inelastisches Ökosystem, *Bot. Helv.*, 100/2, 1990b.
- Labhart, T. P.: Planbeilage: Geologisch-tektonische Übersichtskarte Aarmassiv, Gotthardmassiv und Tavetscher Zwischenmassiv, Balkema A. A., Rotterdam, 1999.
- Luginbuhl, J.-M., Green, J. T., Poore, M. H., and Conrad, A. P.: Use of goats to manage vegetation in cattle pastures in the Appalachian region of North Carolina, *Sheep and Goat Res. J.*, 16, 124–135, 2000.
- Mössmer, E. M.: Einflussfaktoren für die Blaikenerosion auf beweideten und aufgelassenen Almflächen im kalkalpinen Bereich der Landkreise Miesbach und Rosenheim, Forstliche Forschungsberichte München, 1985.
- Mottet, A., Ladet, S., Coque, N., and Gibon, A.: Agricultural land-use change and its drivers in mountain landscapes: A case study in the Pyrenees, *Agriculture, Ecosystems and Environment*, 114, 296–310, 2006.
- Newesely, C., Tasser, E., Spadinger, P., and Cernusca, A.: Effects of land-use changes on snow gliding processes in alpine ecosystems, *Basic Appl. Ecol.*, 1, 61–67, 2000.
- Ohlmacher, G. C. and Davis, J. C.: Using multiple logistic regression and GIS technology to predict landslide hazard in northeast Kansas, USA, *Eng. Geol.*, 69, 331, 2003.
- Petley, D., Hearn, G., Hart, A., Rosser, N., Dunning, S., Oven, K., and Mitchell, W.: Trends in landslide occurrence in Nepal, *Nat. Hazards*, 43, 23–44, 2007.
- Piégay, H., Walling, D. E., Landon, N., He, Q. P., Liébault, F., and Petiot, R.: Contemporary changes in sediment yield in an alpine mountain basin due to afforestation (The upper Drome in France), *CATENA*, 55, 183–212, 2004.
- Rickli, C., Zimmerli, P., and Böll, A.: Effects of vegetation on shallow landslides: an analysis of the events of August 1997 in Sachseln, Switzerland, *International Conference on Landslides, Causes, Impacts and Countermeasures*, Essen, 575–584, 2001.
- Ritzmann-Blickenstorfer, H.: Historische Statistik der Schweiz, Chronos Verlag, Zürich, 1996.
- Santacana, N., Baeza, B., Corominas, J., De Paz, A., and Marturia, J.: A GIS-based multivariate statistical analysis for shallow landslide susceptibility mapping in La Pobla de Lillet area (Eastern Pyrenees, Spain), *Nat. Hazards Earth Syst. Sci.*, 30, 281–295, 2003, <http://www.nat-hazards-earth-syst-sci.net/30/281/2003/>.
- Schmidt, J., and Dikau, R.: Modeling historical climate variability and slope stability, *Geomorphology*, 60, 433–447, 2004.
- Shrestha, D. P., Zinck, J. A., and Van Ranst, E.: Modelling land degradation in the Nepalese Himalaya, *CATENA*, 57, 135, 2004.
- Sparling, G., Ross, D., Trustrum, N., Arnold, G., West, A., Speir, T., and Schipper, L.: Recovery of topsoil characteristics after landslip erosion in dry hill country of New Zealand, and a test of the space for time hypothesis, *Soil Biol. Biochem.*, 35, 1575–1586, 2003.
- Suezen, M. L. and Doyuran, V.: Data driven bivariate landslide susceptibility assessment using geographical information systems: a method and application to Asarsuyu catchment, Turkey, *Eng. Geol.*, 71, 303–321, 2004.
- Swisstopo: Reproduziert mit Bewilligung von swisstopo, BA071108, Zurich, 2006.
- Tappeiner, U., Tasser, E., Leitingner, G., and Tappeiner, G.: Landnutzung in den Alpen: historische Entwicklung und zukünftige Szenarien, *Die Alpen im Jahr 2020, alpine space-man and environment*, 1, 23–39, 2006.
- Tasser, E. and Tappeiner, U.: Impact of land use changes on mountain vegetation, *Appl. Veg. Sci.*, 5, 173–184, 2002.
- Tasser, E., Mader, M., and Tappeiner, U.: Effects of land use in alpine grasslands on the probability of landslides, *Basic Appl. Ecol.*, 4, 271–280, 2003.
- Troxler, J., Chatelain, C., and Schwery, M.: Technical and economical evaluation of grazing systems for high altitude sheep pastures in Switzerland, *Grassland Science in Europe*, 9, 590–592, 2004.
- Van Westen, C. J. and Lulie Getahun, F.: Analyzing the evolution of the Tessina landslide using aerial photographs and digital elevation models, *Geomorphology*, 54, 77, 2003.
- Vanacker, V., Vanderschaeghe, M., Govers, G., Willems, E., Poesen, J., Deckers, J., and De Bievre, B.: Linking hydrological, infinite slope stability and land-use change models through GIS for assessing the impact of deforestation on slope stability in high Andean watersheds, *Geomorphology*, 52, 299–315, 2003.
- Wiedmer, E. and Senn-Irlet, B.: Biomass and primary productivity of an *Alnus viridis* stand – a case study from the Schächental valley, Switzerland, *Bot. Helv.*, 116, 55–64, 2006.
- WRB: IUSS Working Group World reference base for soil resources, Rom, 128 pp., 2006.
- Wyss, R.: Die Urseren-Zone – Lithostatigraphie und Tektonik, *Eclogae Geol. Helv.*, 79, 731–767, 1986.
- Zhou, C. H., Lee, C. F., Li, J., and Xu, Z. W.: On the spatial relationship between landslides and causative factors on Lantau Island, Hong Kong, *Geomorphology*, 43, 197, 2002.

CHAPTER 4

On the influence of temporal change on the validity of landslide susceptibility maps

This chapter has been published in Natural Hazard and Earth system sciences as:
Meusburger, K., and Alewell, C.: On the influence of temporal change on the validity of landslide susceptibility maps, Volume: 9, Pages: 1495-1507, 2009.

On the influence of temporal change on the validity of landslide susceptibility maps

K. Meusburger and C. Alewell

Institute for Environmental Geosciences, University of Basel, Bernoullistrasse 30, 4056 Basel, Switzerland

Received: 27 February 2009 – Revised: 28 July 2009 – Accepted: 4 August 2009 – Published: 28 August 2009

Abstract. The consideration of non-stationary landslide causal factors in statistical landslide susceptibility assessments is still problematic. The latter may lead to erroneous model predictions, especially in times of dramatic environmental change. In this case study in the Central Swiss Alps, we aim to evaluate the effect of dynamic change of landslide causal factors on the validity of landslide susceptibility maps. Logistic regression models were produced for two points in time, 1959 and 2000. Both models could correctly classify >70% of the independent spatial validation dataset. By subtracting the 1959 susceptibility map from the 2000 susceptibility map a deviation susceptibility map was obtained. Our interpretation was that these susceptibility deviations indicate the effect of the change of dynamic causal factors on the landslide probability. The deviation map explained 85% of new landslides occurring after 2000. We believe it to be a suitable tool to add a time element to the susceptibility map pointing to areas with changing susceptibility due to recently changing environmental conditions.

1 Introduction

The alpine terrain with its rugged topography and extreme climatic conditions is naturally disposed to soil erosion. Besides water erosion, mass movements are typical erosion features that constitute an important proportion to total soil loss (Meusburger and Alewell, 2008). Shallow landslides are a type of mass movement highly correlated to extreme events. Thus, unrecognised landslide causal factors can lead to hazardous surface damage and soil loss within one extreme rainfall event. The damages caused by a typical shallow translational landslide with a thickness of 0.3 to 2 m, as defined by Tasser et al. (2003), often persist for several decades

(Meusburger and Alewell, 2008) due to slow vegetation re-settlement, and hampered possibilities for stabilisation measures in the alpine environment.

Landslide hazard assessment, as defined by Varnes (1984), aims at improving the knowledge of processes that lead to slope instability and, in addition, at identifying the locations where and when landslides or potentially instable slopes may occur. According to Carrara et al. (1998) approaches for landslide hazard assessment can generally be grouped into two main categories: the direct, qualitative method that relies on the ability of the investigator to estimate actual and potential slope failures and indirect, quantitative methods that produce numerical estimates (probabilities) of the occurrence of landslide in any hazard zone. The choice of the method mainly depends on the spatial scale (Van Westen, 2000) and, thus, the data availability. To assess landslide susceptibility on a regional scale, multivariate statistical approaches were commonly used in the last decades. Especially discriminant analysis (Carrara et al., 1991, 2003; Davis et al., 2006; Santacana et al., 2003), logistic regression (Ayalew and Yamagishi, 2005; Ayalew et al., 2005; Dai and Lee, 2002; Ohlmacher and Davis, 2003; Tasser et al., 2003; Van Den Eeckhaut et al., 2006; Yesilnacar and Topal, 2005) and neural networks (Ermini et al., 2005; Yesilnacar and Topal, 2005; Kanungo et al., 2006; Gomez and Kavzoglu, 2005) have successfully been applied.

Unconstrained by the statistic method chosen, the basic concept of landslide hazard assessment with statistical methods is to compare the conditions that have lead to landslides in the past with the conditions at regions currently free of landslides (Carrara et al., 1998). The assumption made when using multivariate statistics for landslide hazard prediction is that catchment characteristics leading to landslides in the past will also be susceptible to landslides in the future. This relation (between past and future) may weaken and become invalid when landslide causal factors become variable with time (called “dynamic factors” in the following) and may lead to a loss of model validity under changed



Correspondence to: K. Meusburger
(katrin.meusburger@unibas.ch)

future conditions (Guzzetti et al., 1999). In view of changing climate conditions and agricultural changes the importance of the problem is increasing and validation of landslide prediction maps is essential (Chung and Fabbri, 2003; Zêzere et al., 2004).

Various studies highlight the impact of dynamic factors such as climate and land use on the probability of landslide (Frei et al., 2007; Schauer, 1975; Tasser et al., 2003; Gorsevski et al., 2006; Meusburger and Alewell, 2008). However, compared to the quantity of landslide susceptibility studies, relatively little effort has been made to validate the predictive capability of the obtained maps (Chung and Fabbri, 2003) and even less to generate maps of likely future landslide scenarios (Guzzetti et al., 2006; Irigaray et al., 2007; Zêzere et al., 2004). The latter was done for instance by integrating the susceptibility map with the return period of rainfall (Zêzere et al., 2004). The approach of return period does not account for the non-stationary behaviour of the geomorphologic system (Hufschmidt et al., 2005) and the spatially and temporally nonlinear relationship between landslides and their causative factors (Zhou et al., 2002). Hence, the spatial distribution of susceptibility zones remains unchanged and a change of the spatial susceptibility pattern over time is not considered (Zêzere et al., 2004). A strong element of uncertainty exists, when the importance of landslide causal factors changes rapidly. For instance, human action, mainly land-cover- and land use changes may increase the sensitivity of the geomorphic system to the effects of precipitation and, thus, cause a shift of susceptibility zones. This negligence may impede the identification of new potential susceptibility areas and, hence, may hamper the timely initiation of prevention measures.

The aim of this study is to evaluate the impact of dynamic landslide causal factors on the validity of landslide susceptibility maps. Our hypothesis is that a temporal change of landslide causal factors cause a shift of landslide susceptibility zones. We propose an approach to extract the impact of temporal variation (changing landslide causal factors) on the probability of landslides from multi-temporal data. The sub-catchment of the Urseren Valley (Central Swiss Alps) was chosen as investigation site because of its severe slope degradation by landslides and the evidence of a trend in landslide occurrence (Meusburger and Alewell, 2008).

2 Study area and landslides

The sub-alpine study area (30 km²; Fig. 1) is characterised by rugged terrain with elevations ranging from 1400 m to 3200 m a.s.l. The average slope angle is approximately 27°. The valley is formed by the gneiss massif of the Gotthard system to the south and the granite massif and the pre-existing basement (named “Altkristallin”, Labhart, 1999) of the Aare system in the north. Intermediate vertically dipping layers consist of Permocarbonic and Mesozoic sedi-

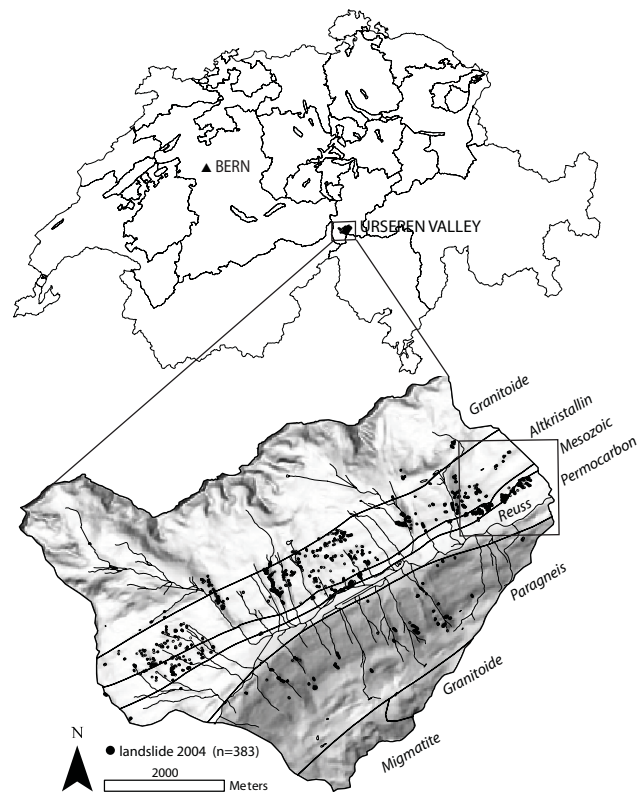


Fig. 1. Map of Switzerland and the study area (Projection: CH1903 LV03). Details on the rectangle area are shown in Fig. 3.

ments (Labhart, 1999). During the Permocarbon sandy-clay sediments deposited while during the Mesozoic, different materials from the geologic periods Trias (sandstone, *rauhwacke* and dolomite), Lias (dark clay-marl and marl) and Dogger (clays, marl and limestone) deposited. Throughout the mountain development the materials were heavily metamorphosed to shale (Kaegi, 1973). Due to erosion of these soft layers a depression developed (Kaegi, 1973). The valley axis corresponds to the direction of the strike of the layers from SW to NE. Weathering of the calcareous material produced clay-rich soils that are prone to landslides. Riverbeds are characterised by glaciofluvial deposits. On the valley slopes, Quaternary moraines and talus fans are common and consist mainly of siliceous loamy gravel material. The reader is referred to Wyss (1986) for a detailed description of the tectonic and lithostratigraphical evolution of the region. Dominant soil types in the catchment classified after WRB (2006) are Podzols, Podzocambisols and Cambisols, often with stagic properties. Above 2000 m a.s.l. and on steep valley slopes, Leptosols are common (with rendzic Leptosols on the calcareous substrates). At the valley bottom and lower slopes, clayey gleyic Cambisol, partly stagic Histosols, Fluvisols and Gleysols developed.

Shallow translational landslides are frequent in the area. The mean area of a single landslide in 2004 is approximately 250 m² with an average slope angle of 33.9°. The single landslides move along planar slip surfaces affecting soil lying upon an impermeable substratum, such as clays and marls or at the contact between regolith and bedrock. The main triggering factor is intense rainfall >150 mm within 3 consecutive days (Meusburger and Alewell, 2008). Sporadic triggering of landslides occurs due to snow movement and snowmelt in spring.

The valley is characterised by a high mountain climate with a mean air temperature of 3.1°C (1901–1961). The mean annual rainfall at the MeteoSwiss climate station in Andermatt (8°35′/46°38′; 1442 m a.s.l.), located at the outlet of the valley, is about 1400 mm year⁻¹. The rainfall maximum occurs in October, the minimum in February. The valley is snow covered for 5 to 6 months (from November to April) with the maximum snow height in March. The river Reuss has a nivo-glacial runoff regime. Nevertheless, summer and early autumn floods represent an important contribution to the flow regime. The peak runoff period is in June (BAFU, 2009).

Vegetation shows strong anthropogenic influences due to grassland farming for centuries. The four main land-cover types are (i) alpine grasslands and dwarf-shrubs (64%), (ii) scree (16%), (iii) at higher elevations bare rock (11%), and (iv) shrubs (8%). Urban areas and forest cover are each less than 1% of the area. The forest was cultivated for avalanche protection above the villages. Frequently occurring avalanches are associated with the scarce forest cover. The valley has been a cultural landscape for centuries. However, land use (grassland management) has undergone decisive changes during the last decades (Meusburger and Alewell, 2008). The main developments are (i) the abandonment of remote areas, which led to an intensification of the accessible areas close to the valley bottom and (ii) a decrease of farmers, which resulted in less maintenance of the grassland areas.

3 Concept and methods

3.1 Logistic regression model (LRM)

Logistic regression predicts the probability distribution of a dichotomy dependent variable (landslide occurrence) through numeric (e.g. elevation) as well as categorical (e.g. geologic formations) predictors. For the categorical predictors dummy variables are used. The strict data requirements of discriminant analysis and linear regression (like e.g. normal distribution) are relaxed. The multiple logistic regression equation (Backhaus, 2006; Ohlmacher and Davis, 2003) is:

$$P(y_i=1)=\frac{1}{1+\exp\left(-\left(b_0+\sum_{p=1}^n b_p x_{pi}+\sum_{q=1}^k b_q z_{qi}\right)\right)} \quad (1)$$

where P is the probability of the occurrence dichotomy dependent variable (here 0 is for stable and 1 for instable conditions), i is the number of observations (here: number of pixels), x_{pi}, \dots, x_{ni} are the values of the independent numeric predictors x_1, \dots, x_n for the i -th observation, b_0, \dots, b_n and b_1, \dots, b_k are the numeric and categorical coefficients of the logistic regression, n is the number of independent numeric predictors, z are values of the independent categorical predictor transformed in dummy variables equal to 1 if the specific class of the categorical predictor is present and 0 if not, and k are the classes of the categorical predictor.

When using multivariate analysis multi-collinearity is a critical point. Multi-collinearity is the undesirable situation when one predictor (here: landslide causal factor) is a linear function of other predictors. Thus, a multi-collinearity diagnosis was applied prior to the logistic regression to reduce redundancy and to improve numerical stability in the subsequent analyses (Backhaus, 2006; Tasser et al., 2003). Predictors with high cross-correlations to several other predictors and with high variance inflation factors (VIF) were excluded in order to reduce collinearity. There is no fixed threshold for VIF values, but as a rule of thumb predictors with $VIF < 2$ can be included (Backhaus, 2006; Tasser et al., 2003). The exclusion process was guided by expert knowledge supported by a field mapping of landslides and related landslide causal factors (see Sect. 4.1). With the remaining set of independent predictors the multivariate logistic regression analysis with a stepwise forward selection method was used. The regression parameters were estimated with the maximum likelihood method.

3.2 Procedure and database construction

Data collection and preparation was accomplished by means of a geographic information system (GIS). We used Arc-Desktop 9.2 by ESRI to visualize, superimpose, and analyse the diverse predictor maps (e.g. geology, slope, elevation, etc.).

3.2.1 Landslide inventory maps

The production of the landslide inventory maps of the study area (30 km²) was done by visually vectorising the landslide source area using aerial photographs of the different years 1959, 2000, and 2004 (Table 1). Landslide source areas >25 m² were mapped, rasterised and included in the analysis. The photographs had a scale of at least 1:12 000. The photographs from 1959 were black and white images that were georeferenced and orthorectified with the help of ground control points, a DEM (25 m grid; vertical accuracy in the Alps of 3 m) and the camera calibration protocols (Swisstopo, 2006). For the years 2000 and 2004 the

Table 1. List of aerial photographs used for the mapping of the landslide inventory maps.

| Aerial photograph | Data source | Resolution | Landslides (>25 m ²) | Landslide area (ha) | Mean area (m ²) | Standard deviation (m ²) |
|-------------------|-----------------------|------------|----------------------------------|---------------------|-----------------------------|--------------------------------------|
| 22 Jul 1959 | ©swisstopo (DV063927) | 1 m | 190 | 5.0 | 263 | 588 |
| 20 Aug 2000 | ©swisstopo (DV043734) | 0.5 m | 324 | 7.3 | 226 | 573 |
| 9 Sep 2004 | ©swisstopo (DV043734) | 0.5 m | 383 | 9.4 | 246 | 566 |

orthorectified RGB “Swissimages” with a pixel resolution of 0.5 m were directly used for landslide mapping without pre-correction. The landslide inventory map resulting from the orthophoto of the year 2004 was verified by ground control during field investigations in 2005. The separation of the landslide database according to landslide type (rotational, translational) was not done, because it could neither be distinguished from aerial photographs nor checked by field investigations for the dataset of 1959. During the field excursions, 27 accessible landslides were investigated in more detail. The landslide inventory map of 1959 could not be verified. However, most of the landslides in 1959 are still present today and could be compared to data of our ground truth measurements. This is due to slow regeneration of the landslides that takes about decades. The quality and reliability of the landslide inventory map generated with aerial photographs was found to be high as all landslides were correctly identified in the field. The aerial photograph interpretation method, that is a standard method for landslides mapping (Wills and McCrink, 2002), was found to be very suitable for the investigation area due to the low percentage of forest cover. In 1959, 190 shallow landslides (>25 m²) were present. In 2000 the number of landslides increased to 324 and in 2004, 383 shallow landslides were mapped.

3.2.2 Landslide causal factors maps

Several of the causal factor maps are derivatives of the DEM (slope aspect, elevation, curvature, morphologic index and slope angle) and were calculated with a three-pixel square kernel. The morphologic index is a classification of the slope and curvature map into the topographic features: peak, ridge, pass, plane, channel, or pit. Further derivatives of the slope and aspect map are the flow direction and the flow length, which is the distance along a flow path. The flow accumulation is based on the number of cells flowing into each cell in the output raster. In addition, topographic wetness index was used, which is defined as $\ln(\alpha/\tan\beta)$ where α is the local upslope area draining through a certain point per unit contour length (here the flow accumulation) and β is the local slope (Beven and Kirkby, 1979). The VECTOR25 dataset of Swisstopo offers vector data of rivers, roads and land-cover. It is based on a 1:25 000 map (position accuracy 3–8 m) of 1993, thus, it was updated with the aerial photograph of 2004 to reflect the present-day land-cover situation. The land-cover map (consisting of the categories grassland, forest, shrub, rock, debris,

snow and water) was converted to raster format (25 m raster resolution). Another land-cover map constructed from the aerial photograph of the year 1959 was used in the logistic regression model of 1959 because land-cover changed during the last decades. Land-cover and the pasture maps (consisting of the categories Freiberg, private land, sheep-, goat- and cattle pasture and cattle alp) were the only causal factor maps variable over time. The remaining causal factor maps were identical and used for the logistic regression of both years, 1959 and 2000. Raster maps of the distance from river and roads were obtained with ArcGIS distance and density functions (with a 500 m moving window). Point density and line density calculate the quantity that falls within the identified neighbourhood (here 500 m) and divide that quantity by the area of the neighbourhood. ArcGIS density functions were also used to obtain a raster map of avalanche density. The avalanches that occurred since 1695 (data source: Swiss Federal Institute for Snow and Avalanche Research) were averaged for each pixel with a 500 m moving window to generate the avalanche density map. The factor map geology was created based on the definition of geologic formations by Labhart (1999) and refined by field and aerial photograph mapping. Thus, for the lower accessible formations (Mesozoic, Permocarbon) mapping scale could be improved from 1:200 000 to 1:25 000. A geomorphologic map (consisting of the categories alluvium, debris fan, moraine, hillside colluvial deposit and solid rock) was generated based on a Quaternary map with a scale of 1:33 000 (Fehr, 1926) and the aerial photographs. The revised geologic and geomorphologic maps, originally in vector format, were then converted to raster format. Tectonic fault lines were digitized (Labhart, 1999) and the map of the distance from those was calculated and stored as a raster map. The present and past land use was determined with pasture maps of the years 1955 and 2006 (Russi, 2006) that were digitised, georeferenced, and rasterised. The precipitation map used is based on long-term (1961–1991) mean precipitation data (©Hydrological Atlas of Switzerland, Swiss Federal Office for the Environment). The resolution of data points is very coarse (1 km), thus, inverse distance weighted (IDW) interpolation was used to determine cell values. This map shows an east-west gradient, ranging from about 1800 mm year⁻¹ in the western part, to about 1400 mm year⁻¹ in the eastern part. No elevation gradient is evident. Further information about these maps and data origins is presented in Table 2.

Table 2. List of the considered predictors and search radius applied for the generation of the map, data scale/resolution, evidence of multi-collinearity (O = independent predictors; X = excluded predictors due to multi-collinearity), significance (Sig) of the predictors for the logistic regression model (LRM) of 2000 and 1959 (***) = $P < 0.001$).

| No. | Predictors | Data source | Search radius | Scale/ Resolution | Inde- pen- dent | Sig LRM 2000 | Sig LRM 1959 |
|-----|---------------------------|---|-----------------|------------------------|-----------------------|--------------------|--------------------|
| 1 | Elevation | DHM25@swisstopo (DV002234.1) | 3 raster kernel | 1:25 000 | X | | |
| 2 | Aspect | DHM25@swisstopo (DV002234.1) | 3 raster kernel | 1:25 000 | O | | |
| 3 | Slope | DHM25@swisstopo (DV002234.1) | 3 raster kernel | 1:25 000 | O | *** | *** |
| 4 | Curvature | DHM25@swisstopo (DV002234.1) | 3 raster kernel | 1:25 000 | X | | *** |
| 5 | Flow length | DHM25@swisstopo (DV002234.1) | | 1:25 000 | X | | |
| 6 | Morphologic index | DHM25@swisstopo (DV002234.1) | 3 raster kernel | 1:25 000 | X | | |
| 7 | Flow accumulation | DHM25@swisstopo (DV002234.1) | | 1:25 000 | O | 0.07 | |
| 8 | Flow direction | DHM25@swisstopo (DV002234.1) | 3 raster kernel | 1:25 000 | X | | |
| 9 | Topographic wetness index | DHM25@swisstopo (DV002234.1) | | 1:25 000 | X | | |
| 10 | Stream-density | VECTOR25@swisstopo (DV002213) | 500 m | 1:25 000 | O | *** | *** |
| 11 | Distance to stream | VECTOR25@swisstopo (DV002213) | | 1:25 000 | O | | |
| 12 | Road-density | VECTOR25@swisstopo (DV002213) | 500 m | 1:25 000 | O | *** | |
| 13 | Distance to roads | VECTOR25@swisstopo (DV002213) | | 1:25 000 | O | 0.03 | |
| 14 | Land-cover 2000 | based on VECTOR25@swisstopo (DV002213) and aerial photograph (2000) | | <1:25 000 | X | | |
| 15 | Land-cover 1959 | based on aerial photograph (1959) | | <1:25 000 | | | |
| | Geologic formation | changed after Labhart (1999) | | 1:25 000; 1:200 000 | O | *** | *** |
| 16 | Distance to fault line | Labhart (1999) | | 1:200 000 | X | | |
| 17 | Quaternary | based on Fehr (1926) | | 1:33 000 | X | | |
| 18 | Mean precipitation | © Hydrological Atlas of Switzerland | | 1 km grid | X | | |
| 19 | Avalanche density | Swiss Federal Institute for Snow and Avalanche Research (SLF) | 500 m | | O | 0.002 | *** |
| 20 | Pasture maps 1955, 2006 | Korporation Urseren; Andermatt | | 1:25 000 | X | | |

3.2.3 Data analysis

All georeferenced raster maps (landslide causal factor maps and landslide inventory maps) were resampled with a reference raster to guarantee a correct allocation of the pixel centroids of the different maps. The grid cells of the reference raster contained unique integer values. The reference raster was superimposed with the causal factors and the landslide inventory maps by the ArcGIS function “combine”. The result is a numbered data matrix where the rows represent the number of grid-cells and the columns contain the attributes of the predictor maps at the grid location plus the information of the inventory map. The resulting two data matrices (1959, 2000) were randomly split into a calibration and validation data set. More details on the model validation is given in the next section. For the logistic regression analysis we used the statistical software package SPSS (version 15.0). Finally, the logistic regression equation was entered in the ArcDesktop raster calculator to produce the landslide susceptibility map for the entire region by means of the most significant landslide causal factors. The predicted probabilities for the

investigation area were classified into five different susceptibility zones with very low susceptibility for probabilities between 0.0 and 0.15, low susceptibility for 0.15 to 0.35, medium from 0.35 to 0.65, high between 0.65 and 0.85 and very high susceptibility for probability of 0.85 to 1.0.

3.3 Validation based on temporal and spatial strategies

The success rate is commonly used in evaluating cell-based landslide susceptibility model performance. It is based on the ratio of successfully predicted landslide sites over total actual landslide sites. However, Fabbri et al. (2003) pointed out that this is not a verification of the predictive value. For validation of the predictive power of the model, a comparison between the map (model) obtained and independent landslide data, which is more recent than the used model set is necessary. The comparison can be qualitative – for instance by a visual overlay – or quantitative, using different indices such as area of a class affected by landslides per total area of class (Suezen and Doyuran, 2004; Yesilnacar and Topal, 2005; Zhou et al., 2002), a confusion matrix (Carrara, 1983;

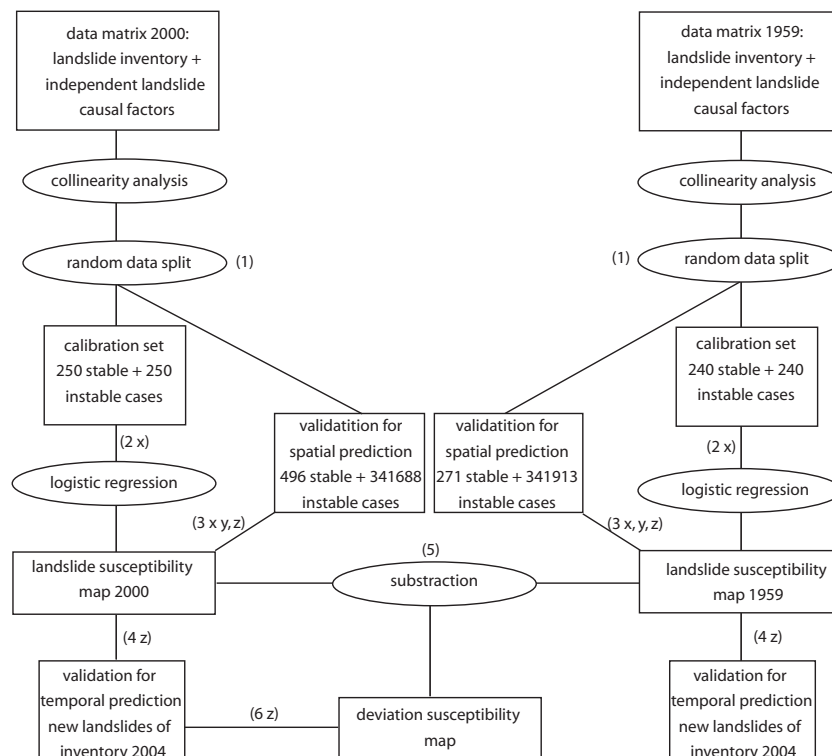


Fig. 2. Evaluation steps of the logistic regression models of 1959 and 2000. The ellipses show processes and the rectangles results. The numbers and letters refer to the explanation given in the text.

Carrara et al., 2003) or by using the Receiver Operating Characteristic (ROC) curve (Chung and Fabbri, 2003; Fabbri et al., 2003). We applied these methods to assess the accuracy of the susceptibility maps. With the statistical software the percentage of correctly classified instable and stable grid cells is given as weighted average in a confusion matrix (x, Fig. 2) and ROC curves of the predicted probabilities were plotted (y, Fig. 2). With the GIS the Spearman's rank correlation between the modelled susceptibility zones and observed percentage landslide density in these zones is assessed (z, Fig. 2). Chung and Fabbri (2003) proposed three strategies to obtain an independent validation dataset: (a) landslides of the study area are randomly split into two groups, one for analysis (calibration) and one for validation (b) the analysis is carried out using landslides occurred in a certain period and validation is performed by means of landslides occurred in a different period (c) the analysis is carried out in a part of the study area and the obtained map (model) is validated in another part. The temporal validation strategy (b) permits testing the predictive capability of a model (Remondo et al., 2003). In this study, we used the random split approach (a) to test the validity of the prediction for extrapolation in space and the approach (b) to test the validity of the model for the extrapolation over time. The following six evaluation steps were executed (Fig. 2):

1. We applied a random split of the entire dataset (for 1959 and 2000 data separately). Approximately 33% of instable grid cells and an equal amount of stable ones were used to setup the LRMs. The remaining dataset was retained for spatial validation.
2. We setup LRMs for the years 1959 and 2000 and determined the “goodness of the fit” or “success rate” of both models by means of maximum likelihood classification with the independent causal factor maps. The number of “selected cases”, here grid cells randomly selected for the model setup are shown in Table 3. A comparison between the number of stable (0) and instable (1) predictions between model and inventory data is shown as percentage in the third column.
3. Validation of the LRM for the spatial prediction, was done with the independent data set obtained by the random split (“unselected cases”, Table 3). The percentage of correct predictions is shown in the 6th column.
4. To evaluate the predictability of the LRM of 1959 and 2000 for extrapolation in time, we used the independent 52 new landslides that occurred between 2000 and 2004 (Table 1). These landslides were mapped on the aerial photograph of 2004.

Table 3. Classification of stable (0) and instable (1) cases (here pixels) by the three most significant predictors of the two logistic regression models (1959 and 2000).

| Observed | | | Selected Cases | | | Unselected Cases | | |
|----------|--------------------|---|----------------|---------------|----------------|------------------|---------------|----------------|
| | | | 0 stable | 1 instable | correct (%) | 0 stable | 1 instable | correct (%) |
| 2000 | | | | | | | | |
| Step 1 | Geologic formation | 0 | 131 | 119 | 52.4 | 183 280 | 158 408 | 53.6 |
| | | 1 | 35 | 215 | 86.0 | 42 | 454 | 91.5 |
| | Overall percentage | | | | 69.2 | | | 53.7 |
| Step 2 | Slope | 0 | 169 | 81 | 67.6 | 232 275 | 109 413 | 68.0 |
| | | 1 | 40 | 210 | 84.0 | 55 | 441 | 88.9 |
| | Overall percentage | | | | 75.8 | | | 68.0 |
| Step 3 | Stream-density | 0 | 176 | 74 | 70.4 | 240 328 | 101 360 | 70.3 |
| | | 1 | 40 | 210 | 84.0 | 67 | 429 | 86.5 |
| | Overall percentage | | | | 77.2 | | | 70.4 |
| Step 7 | Overall percentage | | | | 81.4 | | | 74.5 |
| 1959 | | | | | | | | |
| Step 1 | Geologic formation | 0 | 140 | 100 | 58.3 | 200 717 | 141 215 | 58.7 |
| | | 1 | 25 | 215 | 89.6 | 27 | 244 | 90.0 |
| | Overall percentage | | | | 74.0 | | | 58.7 |
| Step 2 | Slope | 0 | 171 | 69 | 71.3 | 248 111 | 93 821 | 72.6 |
| | | 1 | 33 | 207 | 86.3 | 38 | 233 | 86.0 |
| | Overall percentage | | | | 78.8 | | | 72.6 |
| Step 3 | Stream-density | 0 | 185 | 55 | 77.1 | 255 641 | 86 291 | 74.8 |
| | | 1 | 49 | 191 | 79.6 | 51 | 220 | 81.2 |
| | Overall percentage | | | | 78.3 | | | 74.8 |
| Step 5 | Overall percentage | | | | | 82.3 | | 76.3 |

5. In order to extract the influence of dynamic landslide causal factors on landslide susceptibility, the susceptibility zones of LRM of 1959 were subtracted from the ones of the LRM of 2000. We know that in 1959, the traditional land use was still present (Russi, 2006) and assume that the effects of climate change were less than today (IPCC, 2007). Hence, the susceptibility map of 1959 shows more the traditional long established susceptibility situation compared to today’s situation. In contrast, the susceptibility zones, based on the landslide inventory map of 2000 already include new susceptibility zones due to impact of dynamic factors. This map is already a combination of the initial traditional and “human-induced” susceptibility. Thus, we hypothesise that by subtracting the susceptibility zones of the LRM of 1959 from the LRM of 2000 the obtained map (called “deviation susceptibility map”) displays the shift of susceptibility zones over time. This shift over time is due to the influence of dynamic landslide causal factors, e.g. the relevance of landslide causal factors change over time.

6. To confirm this hypothesis, the obtained deviation susceptibility map is validated with the set of 52 new landslides that occurred between the year 2000 and 2004.

4 Results and discussion

4.1 Field mapping of potential landslide causal factors

In the Urseren Valley, many potential landslide causal factors are spatially correlated, thus, prior to the statistical analysis a mapping of potential landslide causal factors in the field was done to assist the exclusion process of inter-correlated predictors (Fig. 3). In the Urseren Valley (shallow) translational landslides are predominant. These landslides are very frequent in the foot zone of the south-facing slope, where return flow in form of small springs causes relatively high water saturation in the soils. The highly instable calcareous material of the Mesozoic layer weathers to clay minerals, which further favours the development of layered stagnic soils. During field observations, we found that about 80% of the 27 landslides had small springs and stagnic soils at the tear-off line. In addition, land use type changes within this

zone. Where the slopes become too steep for mowing by machines they are intensively pastured. A fence separates the meadows close to the valley floor from the pastures. Pasturing was observed to have several effects possibly related to soil stability (Pietola et al., 2005): trampling leads to (i) a compacting of the soil and the development of a water retaining horizon, (ii) the retention of water is further raised by the micro topography of the trails, and (iii) the reduction of the vegetation cover. Stagnic soils and the occurrence of return flow would probably be good predictors for landslides. However, to derive these parameters for the entire catchment would be very work intensive. Furthermore, most of the area is difficult to access. Therefore, these parameters need to be replaced by other related parameter maps that could be spatially derived from GIS tools. For example the likelihood of return flow can be represented by the topographic wetness index (Beven and Kirkby, 1979).

4.2 Results of the logistic regression analysis

The setup of the logistic regression model of 2000 (LRM 2000) was accomplished based on the landslide inventory map of 2000 and 20 static causal factor maps. During multi-collinearity analysis, 11 predictors were excluded from further analysis due to multi-collinearity. Column 5 in Table 2 displays the inter-correlating predictors. For instance, an inter-correlation between elevation and land-cover was observed; the higher the area the less grass- and the more rock surfaces are present. However, there is no causal relationship between landslide occurrence and elevation. Hence, the elevation was excluded from further analysis. After the model generation with the stepwise forward selection method, seven of nine predictors were included due to a significant explanation of the variance (Table 2): geology, slope, stream-density, road-density, avalanche density, distance to roads and flow accumulation. With this set of seven predictors, a success rate of 81.4% was achieved (selected cases; Table 3). The logistic regression model of 1959 (LRM 1959) identified five significant predictors (geology, slope, stream-density, avalanche density, and curvature) with a success rate of 82.3%. The three most significant predictors are identical to the LRM of 2000.

Both pasture maps are highly correlated with the geologic map. Including the pasture map of 1955 instead of geology into the LRM of 2000 achieved a success rate of 68.6%. The described effects of pasturing on the conditioning of landslides (Sect. 4.1) are related to trampling and, thus, to pasture intensity. However, the pasture maps do not display pasture intensity and its variability within the single classes of the map. Moreover, even within same classes management was not static. For the single pasture maps as well as derived land use change maps could not be quantified and, thus, were no suitable predictors for the multivariate analysis. Nonetheless, the pasture map information is useful to interpret the deviation susceptibility map (see below).

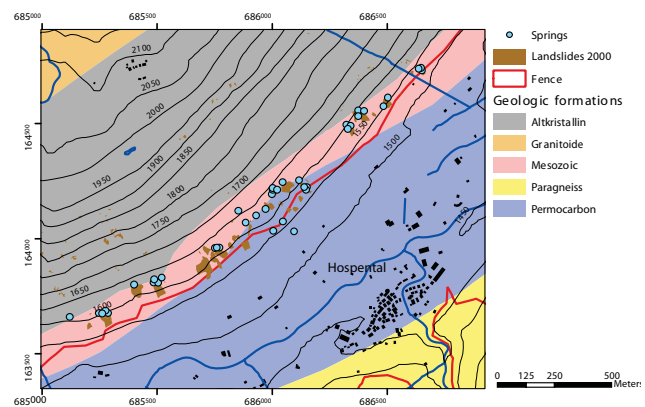


Fig. 3. Slope section near Hospental showing the overlap of some landslide causal factors: geologic formation, topography, springs, and land use (below the fence meadows; above the fence pasturing). The location of the area is shown by rectangle in Fig. 1.

We found, that in correspondence to many other studies the most significant predictors are slope and geology to explain landslide susceptibility (Ayalew and Yamagishi, 2005; Carrara et al., 1991; Clerici et al., 2006; Dai and Lee, 2002; Komac, 2006; Ohlmacher and Davis, 2003; Santacana et al., 2003; Van Westen and Lulie Getahun, 2003; Zhou et al., 2002; Rickli et al., 2001; Suezzen and Doyuran, 2004). These predictors can be physically explained with the equation for the critical altitude H_c for slopes (Carson, 1971):

$$H_c = \frac{4c \sin \chi \cos \Phi}{\gamma * (1.0 - \cos(\chi - \Phi))} \quad (2)$$

where c is cohesion, γ is bulk density, χ is slope and Φ is friction angle. The equation describes slope stability as a function of soil strength (cohesion and friction angle) and shear forces (density and slope). A slope/soil becomes unstable if the actual height/thickness exceeds the critical height. The higher the slope angle and the greater the soil depth, the higher becomes shear force and the less stable becomes the slope.

A further significant predictor in our study is stream-density. The balance between soil strength and shear force is a function of soil water content (Kemper and Rosenau, 1984). Wet places and hollows where water can infiltrate are especially prone to landslides (Fig. 3). Stream-density as well as flow-accumulation are proxy variables for the important physical parameter of “soil water content” in the statistical model. With increasing density of the stream network, water saturation and the occurrence of return flow increases, which results in two processes that potentially decrease soil stability: positive pore water pressure, which reduces cohesion of soil particles (c), and heavier soils that increase the bulk density (γ).

Furthermore, soil strength parameters are influenced by parent material, which is represented by geology in the

model. Geology was found to be the most important predictor as it appears to be most important for the material properties and additionally effects runoff generation. Minor improvements of the model are yielded by the predictor maps distance to roads and road density, which explain the occurrence of few landslides due to constructional interferences. Road distance and road density maps may show high variability over time (Petley et al., 2007). However, in Urseren Valley where the road networks remained basically identical during the last fifty years.

Avalanche density (since 1695) is a further predictor, which improved the explained variance of the landslide distribution. Avalanches are regarded as potential landslide causal factors because of the additional friction forces that may trigger tension fissures. A spatial relationship is evident even though the causal relation is questionable because stability of snow cover depends on similar topographical conditions as the stability of soil cover (Meusburger and Alewell, 2008).

4.3 Validation of the landslide susceptibility model for spatial predictions

With all seven predictors 74.5% of the validation data set for the LRM of 2000 could be correctly predicted. If the three most significant predictors (geology, slope and stream-density) were used for the production of the susceptibility map (selected cases), the validation procedure (unselected cases, see Table 3) produced only slightly worse results. In total 70.4% of the observations could be accurately classified, thereof 70.3% of the non-erodible sites and 86.5% of the erodible sites were correctly assigned. Overall, 53.7% of the observations were correctly classified with geology alone. Slope increased the explained spatial variance to 68.0% and stream-density to 70.4%. Areas, which are stable today, but were predicted as being instable by the model, can be interpreted as the hazard zones for future management considerations.

In addition to the regression coefficients (Table 4, for discussion see below), the logistic regression model yields a map of probabilities expressed by numbers that are constrained to fall between 0 and 1. The closer the numbers are to 1, the higher is the probability for a landslides. We chose a subdivision of the probabilities obtained into five susceptibility zones. A visual comparison between the landslide susceptibility map and the landslide inventory map of 2000 indicates a good agreement (Fig. 4). The exceptions are two clusters of landslides located at the border of geologic formation of the Altkristallin and the granite of the Aare system. This might be due to the lower spatial accuracy of the geologic map in the upper part of the study area, as explained in Sect. 3.2. To evaluate the performance of the susceptibility mapping methods, the method of the Relative Operating Curve (ROC) was used (Table 5; Fig. 5; left panel). The area under the curve for the LRM 1959 and 2000 is 0.86, which

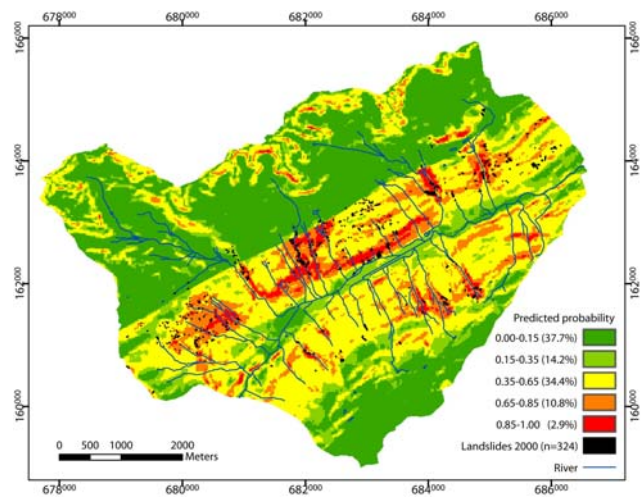


Fig. 4. Final landslide susceptibility map obtained with logistic regression model of 2000 for the 30 km² sub-catchment (Projection: CH1903 LV03).

Table 4. Regression coefficients (*b*) and significance (*Sig*) for the parameters stream-density (Denstr), slope, and five geologic units (1 = granite of the Aare system, 2 = Altkristallin, 3 = Mesozoic, 4 = Permocarbon, 5 = gneiss of the Gotthard system) of the two logistic regression models.

| Predictors | Model 2000 | | | Model 1959 | | |
|------------|------------|------------|------------------|------------|------------|------------------|
| | <i>b</i> | <i>Sig</i> | Exp (<i>b</i>) | <i>b</i> | <i>Sig</i> | Exp (<i>b</i>) |
| Denstr | 2.15-E01 | 3.54-E05 | 1.24+E00 | 4.50-E01 | 1.17-E10 | 1.57+E00 |
| Slope | 1.21-E01 | 1.30-E15 | 1.13+E00 | 1.18-E01 | 3.27-E13 | 1.13+E00 |
| Geo | | 3.56-E10 | | | 5.09-E13 | |
| Geo (1) | 2.96+E00 | 8.14-E01 | 1.93+E01 | 1.75+E01 | 9.99-E01 | 4.15+E07 |
| Geo (2) | 5.59+E00 | 6.57-E01 | 2.67+E02 | 2.04+E01 | 9.99-E01 | 7.24+E08 |
| Geo (3) | 5.90+E00 | 6.39-E01 | 3.66+E02 | 1.86+E01 | 9.99-E01 | 1.17+E08 |
| Geo (4) | 5.87+E00 | 6.41-E01 | 3.55+E02 | 1.81+E01 | 9.99-E01 | 7.18+E07 |
| Geo (5) | 5.38+E00 | 6.69-E01 | 2.17+E02 | 2.00+E01 | 9.99-E01 | 5.06+E08 |
| Constant | -9.37+E00 | 4.56-E01 | 8.49-E05 | -2.44+E01 | 9.99-E01 | 2.60-E11 |

is very satisfactory (it is quite close to the ideal value of 1.0). Also as seen from the table the asymptotic significance is less than 0.0001, which means that using the probability model is much better than guessing.

Also the comparison between the modelled landslide probability and the actual landslide density in 2000 (Fig. 5; middle panel) showed good correspondence, which is expressed in a significant correlation ($P < 0.01$) between observed landslide density and predicted landslide probability.

The prediction for the extrapolation in space with the three most significant predictors of the LRM of 1959 produced slightly better validation results of 74.8% correct predictions (see unselected cases in Table 3). The regression coefficients (*b*) of the two LRMs are presented in Table 4 together with the odds ratio (Exp (*b*)) and the significance.

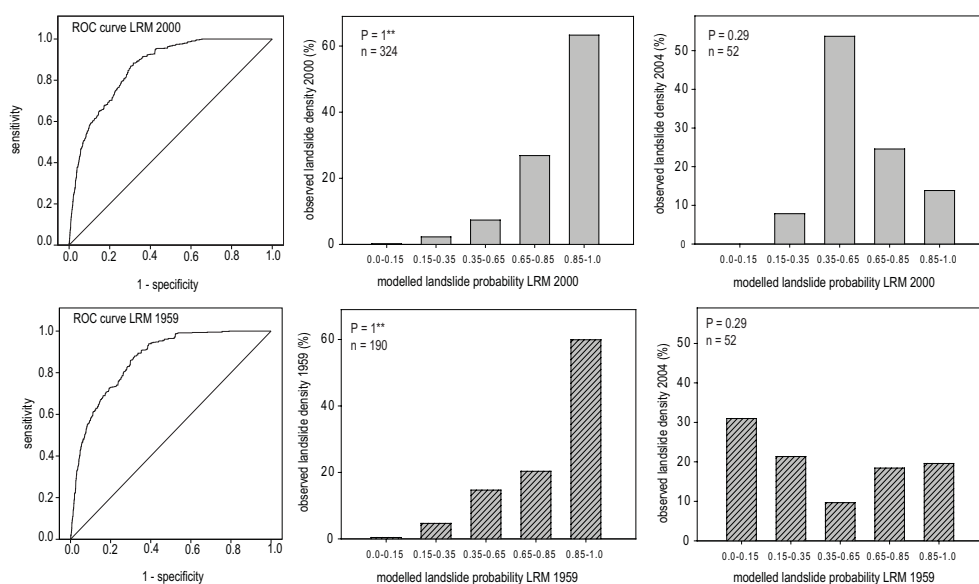


Fig. 5. Receiver operating characteristic (ROC) curves for the two logistic regression models (left) and dependency of modelled landslide susceptibility and actual landslide densities (Spearman's rank correlation coefficient (P); ** correlation is significant at a 0.01 level). The landslide density values are based on 324 mapped landslides for the year 2000 (upper part), 190 mapped landslides for the year 1959 (lower part), and 52 mapped landslides for the period 2000–2004 (right).

Table 5. Test result variable “predicted probability” by LRM 2000 and 1959.

| LRM | Area | Std. Error | Asymptotic Sig. ^a | Asymptotic 95% Confidence Interval | |
|------|------|------------|------------------------------|------------------------------------|-------------|
| | | | | lower bound | upper bound |
| 2000 | .861 | .005 | .000 | .851 | .872 |
| 1959 | .864 | .006 | .000 | .852 | .876 |

^a Null hypothesis: true area = 0.5.

4.4 Validation of the landslide susceptibility model for temporal predictions

To test the suitability of the model for the prediction of future events, we compared the produced landslide susceptibility map of 2000 with the “new landslides” that occurred after 2000 until 2004. It is presumed that a spatial database containing the distribution of all the landslides over a period can be used to predict the distribution of future landslides over a period of the same length (Fabbri et al., 2003). This presumption is critical for the LRM of 1959. Accordingly there is no relation between the observed new landslides in 2004 and the predicted probability by the LRM 1959 (Fig. 5, right panel). For the LRM of 2000 the presumption is valid, nonetheless, the prediction of the new landslides was rather unsatisfactory. This is illustrated by the weak relationship ($P=0.29$) and the loss of significant correlation (at the 0.01

level) between predicted landslide probability and observed landslide density in 2004 (Fig. 5, right panel). The new landslides occurred mainly in the zone that was predicted with only medium susceptibility. This could indicate a loss of prediction quality and the decrease of predictive power of the landslide causal factors with time.

Temporal validation adds a time element to susceptibility maps and makes the transfer to a landslide hazard map possible (Remondo et al., 2003). However, the susceptibility map failed to predict the new landslides. Thus, another approach was needed to introduce a temporal component to the susceptibility map in order to allow prediction of future landslides.

4.5 Effect of temporal change on the probability of landslides

In order to confirm our hypothesis that the recent landslides are a result of the increasing influence of dynamic factors and not an accidental deviation of the predicted probability, we subtracted the modelled susceptibility zones of the LRM of 2000 from the zones of the LRM of 1959. The result is a map, which shows the deviations of the susceptibility zones between the two LRMs and, thus, the change of susceptibility over time (Fig. 6). The values are negative where the landslide susceptibility zones was lower (indicating less landslide probability) in 1959 and positive where it was higher. The landslide susceptibility mainly increased near the valley bottom and the adjacent lower slopes, a decrease is visible for the more remote slopes except for the higher elevated areas with high rock and debris content that behaved unchanged.

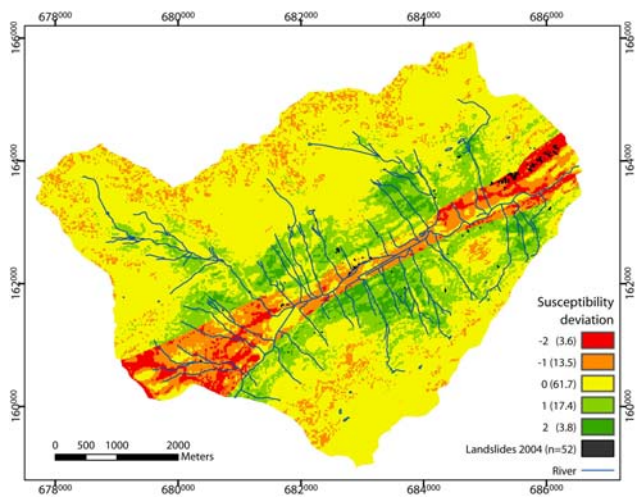


Fig. 6. Differences of susceptibility zones between the logistic regression models of 1959 and 2000 (Projection: CH1903 LV03).

The deviation susceptibility map shows good correspondence with the new landslides that predominantly occurred at the foot of the slope after 2000 (Fig. 6). About 85% of the new landslides occurred in the zone with the highest susceptibility deviation (value: -2) towards an increased landslide probability over time. We interpreted the obtained agreement of the deviation susceptibility map with the occurrence of the new landslides as a validation of our approach. With this multi-temporal data analysis the temporal shift of susceptibility zones could be spatially captured and visualized. Thus, it is possible to add a spatial explicit time element to susceptibility maps in order to improve the assessment of future landslide susceptibility zones.

The pattern of the deviation zones may give information about the dynamic landslide causal factors, that caused the shift of susceptibility zones. The deviation susceptibility map includes the combined effect of temporal environmental change. An increase of maximum 3-day rainfall events was observed (Meusburger and Alewell, 2008). Prolonged rainfall mostly triggers zones with already high susceptibility. Nevertheless, it is necessary to stress that different rainfall amount-duration combinations and difference in rainfall distributions can produce different landslide patterns (Zêzere et al., 2004). To which extend altered snow processes change the susceptibility zones was not evaluated in this study. Geomorphologic feedback mechanism may have effects on landslide susceptibility. On the one hand, susceptibility may decrease over time due to the “emptying” of the slope (Hufschmidt et al., 2005), on the other hand susceptibility may increase over time due to a steepening and undercutting of slopes (Claessens et al., 2007).

The most plausible explanation of a local shift in susceptibility zones is the change in land use types between 1955 and 2006 (Fig. 7). A detailed description of the land use changed that occurred in the valley is given in Meusburger

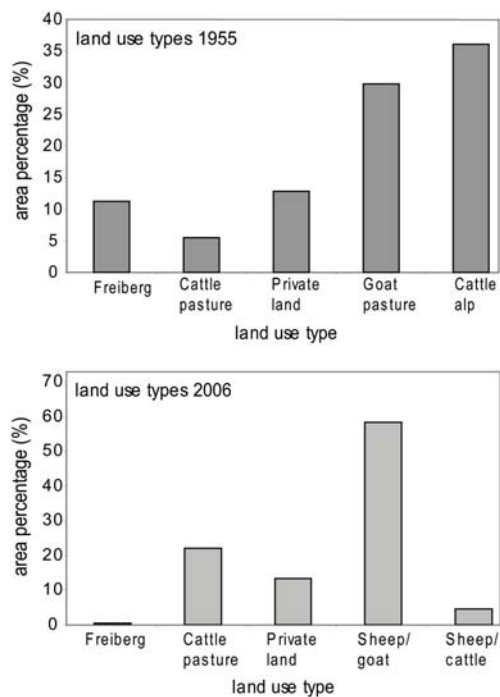


Fig. 7. Difference in area percentage of land use types in 1955 and 2006.

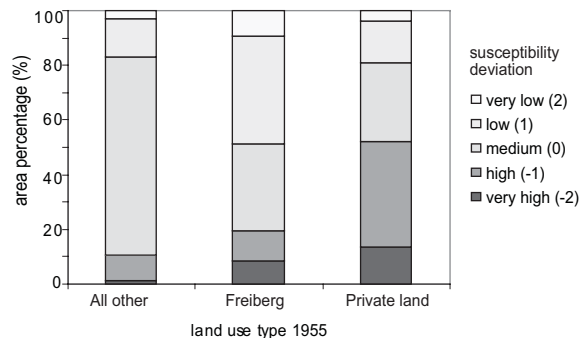


Fig. 8. Frequency distribution of susceptibility deviation zones per land use type. The susceptibility deviation is positive where the susceptibility was one or two zones (1, 2) higher in 1959, negative where the susceptibility was one or two zones (-1, -2) lower in 1959 and zero (0) where no shift of susceptibility occurred.

and Alewell (2008).The percentage of susceptibility deviation zones per land use type of 1955 is given in Fig. 8. The majority of new high susceptibility zones (with a deviation of -2) are located within two land use types (Freiberg and Private land). These two land use types were intensified during the last decades. “Freiberg” is a special pasture, which is used only part time of the season. Since the early 70ties, this land use type was replaced by a permanent pasture. This led to severe degradation of the pasture mainly along the lower fence. It is typical for permanent pastures that the pasture intensities are heterogeneously distributed due to the influence of topography and the location of the water sites. Thus,

in other parts there is also a decrease of susceptibility. The Private land is used as meadow and is nowadays more frequently mown with machines and intensely fertilized with organic manure. Especially the addition of organic fertilizers may be a reason for the enhanced landslide susceptibility, because it favours species with flat rooting (Von Wyl, 1988). For all other land use types, there is no distinct shift of landslide susceptibility zones evident. Generally, land use change seems to be the plausible dynamic causal factor explaining the spatial shift of landslide susceptibility zones over time.

5 Conclusions

Geology, slope and stream-density were the most significant and reliable static parameters for the logistic regression models of 1959 and 2000 and their assessment warrant good potential for spatial landslide susceptibility predictions. Yet, for more recent landslides (since 2000) model prediction was not successful, which confirmed our proposed hypothesis that the predictive capability of statistical susceptibility models may decrease over time. Discrepancies between predicted susceptibility and observed landslides may be due to various dynamic landslide causal factors (e.g. changes in snow and precipitation dynamics, surface cover change). However, the influence of land use changes seemed to be the most likely causal factor in the Urseren Valley. With the proposed new method to analyse multi-temporal data we were able to extract the effect of changing landslide causal factors on the probability of landslides and could improve the prediction for future landslides.

This study implies that the validity of commonly used static landslide susceptibility maps under changing environmental conditions is questionable. Slopes that are predicted as stable can rapidly and mostly unnoticed increase in landslide susceptibility. Thus, a update of the susceptibility maps or a consecutively validation with new landslide data is necessary. Generally, it was shown that it is of decisive impact to understand the dynamic of landslide causal factors in order to guarantee validity of landslide susceptibility maps. The objective of future work would be to develop regional scale models that can include temporal variations of landslide causal factors and, thus, account for changes in landslide susceptibility zones.

Acknowledgements. This study was funded by the Swiss Federal Office for the Environment (Contract-no.: StoBoBio/810.3129.004/05/0X).

Edited by: A. Guenther

Reviewed by: M. Rossi and two other anonymous referees

References

Ayalew, L. and Yamagishi, H.: The application of GIS-based logistic regression for landslide susceptibility mapping in the Kakuda-

Yahiko Mountains, Central Japan, *Geomorphology*, 65, 15 pp., 2005.

Ayalew, L., Yamagishi, H., Marui, H., and Kanno, T.: Landslides in Sado Island of Japan: Part II. GIS-based susceptibility mapping with comparisons of results from two methods and verifications, *Eng. Geol.*, 81, 432–445, 2005.

Backhaus, K.: *Multivariate Analysemethoden: Eine anwendungsorientierte Einführung*, Springer, Berlin, 11th edn., 830 pp., 2006.

BAFU: Hydrological foundations and data. Real time and historical data: <http://www.hydrodaten.admin.ch/d/2087.htm>, access: 7 January 2009.

Beven, K. and Kirkby, M.: A physically based, variable contributing area model of basin hydrology, *Bulletin of Hydrologic Sciences*, 24, 43–69, 1979.

Carrara, A.: Multivariate models for landslide hazard evaluation, *J. Int. Ass. Math. Geol.*, 15, 403–426, 1983.

Carrara, A., Cardinali, M., Detti, R., Guzzetti, F., Pasqui, V., and Reichenbach, P.: GIS techniques and statistical-models in evaluating landslide hazard, *Earth Surf. Proc. Land.*, 16, 427–445, 1991.

Carrara, A., Guzzetti, F., Cardinali, M., and Reichenbach, P.: Current limitations in modeling landslide hazard, *Proceedings of IAMG'98*, 195–203, 1998.

Carrara, A., Crosta, G., and Frattini, P.: Geomorphological and historical data in assessing landslide hazard, *Earth Surf. Proc. Land.*, 28, 1125–1142, 2003.

Carson, M. A.: *The mechanics of erosion*, Pion Ltd., London, 174 pp., 1971.

Chung, C. F. and Fabbri, A. G.: Validation of spatial prediction models for landslide hazard mapping, *Nat. Hazards*, 30, 451–472, 2003.

Claessens, L., Schoorl, J. M., and Veldkamp, A.: Modelling the location of shallow landslides and their effects on landscape dynamics in large watersheds: An application for Northern New Zealand, *Geomorphology*, 87, 16–27, 2007.

Clerici, A., Perego, S., Tellini, C., and Vescovi, P.: A GIS-based automated procedure for landslide susceptibility mapping by the Conditional Analysis method: the Baganza valley case study (Italian Northern Apennines), *Environ. Geol.*, 50, 941–961, 2006.

Dai, F. C. and Lee, C. F.: Landslide characteristics and slope instability modeling using GIS, Lantau Island, Hong Kong, *Geomorphology*, 42, 213 pp., 2002.

Davis, J. C., Chung, C. J., and Ohlmacher, G. C.: Two models for evaluating landslide hazards, *Comput. Geosci.*, 32, 1120–1127, 2006.

Ermini, L., Catani, F., and Casagli, N.: Artificial Neural Networks applied to landslide susceptibility assessment, *Geomorphology*, 66, 327 pp., 2005.

Fabbri, A. G., Chung, C.-J. F., Cendrero, A., and Remondo, J.: Is prediction of future landslides possible with a GIS?, *Nat. Hazards*, 30, 487–503, 2003.

Fehr, W.: *Geologische Karte der Urserenzone*, Kommissionsverlag: A. Franke A.G., Bern, 1926.

Frei, C., Calanca, P., Schär, C., Wanner, H., Schaedler, B., Haeblerli, W., Appenzeller, C., Neu, U., Thalmann, E., Ritz, C., and Hohmann, R.: *Grundlagen. Klimaänderungen und die Schweiz 2050 – Erwartete Auswirkungen auf Umwelt, Gesellschaft und*

- Wirtschaft, OcCC Report, 2007.
- Gomez, H. and Kavzoglu, T.: Assessment of shallow landslide susceptibility using artificial neural networks in Jabonosa River Basin, Venezuela, *Eng. Geol.*, 78, 11–27, 2005.
- Gorsevski, P. V., Gessler, P. E., Boll, J., Elliot, W. J., and Foltz, R. B.: Spatially and temporally distributed modeling of landslide susceptibility, *Geomorphology*, 80, 178–198, 2006.
- Guzzetti, F., Carrara, A., Cardinali, M., and Reichenbach, P.: Landslide hazard evaluation: a review of current techniques and their application in a multi-scale study, Central Italy, *Geomorphology*, 31, 181 pp., 1999.
- Guzzetti, F., Reichenbach, P., Ardizzone, F., Cardinali, M., and Galli, M.: Estimating the quality of landslide susceptibility models, *Geomorphology*, 81, 166–184, 2006.
- Hufschmidt, G., Crozier, M., and Glade, T.: Evolution of natural risk: research framework and perspectives, *Nat. Hazards Earth Syst. Sci.*, 5, 375–387, 2005, <http://www.nat-hazards-earth-syst-sci.net/5/375/2005/>.
- IPCC: Climate Change 2007: The physical science basis. Summary for policymakers, 661 10th session of working group I of the IPCC, Paris, 2007.
- Irigaray, C., Fernández, T., El Hamdouni, R., and Chacón, J.: Evaluation and validation of landslide-susceptibility maps obtained by a GIS matrix method: examples from the Betic Cordillera (southern Spain), *Nat. Hazards*, 41, 61–79, 2007.
- Kaegi, H. U.: Die traditionelle Kulturlandschaft im Urserental: Beitrag zur alpinen Kulturgeographie, Ph.D. thesis, University of Zurich, Switzerland, 212 pp., 1973.
- Kanungo, D. P., Arora, M. K., Sarkar, S., and Gupta, R. P.: A comparative study of conventional, ANN black box, fuzzy and combined neural and fuzzy weighting procedures for landslide susceptibility zonation in Darjeeling Himalayas, *Eng. Geol.*, 85, 347–366, 2006.
- Kemper, W. D. and Rosenau, R. C.: Soil cohesion as affected by time and water-content, *Soil Sci. Soc. Am. J.*, 48, 1001–1006, 1984.
- Komac, M.: A landslide susceptibility model using the Analytical Hierarchy Process method and multivariate statistics in perialpine Slovenia, *Geomorphology*, 74, 17 pp., 2006.
- Labhart, T. P.: Planbeilage: Geologisch-tektonische Übersichtskarte Aarmassiv, Gotthardmassiv und Tavetscher Zwischenmassiv, Balkema A. A., Rotterdam, 1999.
- Meusburger, K. and Alewell, C.: Impacts of anthropogenic and environmental factors on the occurrence of shallow landslides in an alpine catchment (Urseren Valley, Switzerland), *Nat. Hazards Earth Syst. Sci.*, 8, 509–520, 2008, <http://www.nat-hazards-earth-syst-sci.net/8/509/2008/>.
- Ohlmacher, G. C. and Davis, J. C.: Using multiple logistic regression and GIS technology to predict landslide hazard in northeast Kansas, USA, *Eng. Geol.*, 69, 331 pp., 2003.
- Petley, D., Hearn, G., Hart, A., Rosser, N., Dunning, S., Oven, K., and Mitchell, W.: Trends in landslide occurrence in Nepal, *Nat. Hazards*, 43, 23–44, 2007.
- Pietola, L., Horn, R., and Yli-Halla, M.: Effects of trampling by cattle on the hydraulic and mechanical properties of soil, *Soil Till. Res.*, 82, 99–108, 2005.
- Remondo, J., González, A., De Terán, J. R. D., Cendrero, A., Fabri, A., and Chung, C.-J. F.: Validation of Landslide Susceptibility Maps; Examples and Applications from a Case Study in Northern Spain, *Nat. Hazards*, 30, 437–449, 2003.
- Rickli, C., Zimmerli, P., and Böll, A.: Effects of vegetation on shallow landslides: an analysis of the events of August 1997 in Sachseln, Switzerland, International Conference on Landslides. Causes, Impacts and Countermeasures, 575–584, 2001.
- Russi, A.: Erhebung der Viehzahlen in Urseren, Korperation Urseren: Talkanzlei Urseren, Andermatt, 2006.
- Santacana, N., Baeza, B., Corominas, J., De Paz, A., and Marturia, J.: A GIS-based multivariate statistical analysis for shallow landslide susceptibility mapping in La Pobla de Lillet area (Eastern Pyrenees, Spain), *Nat. Hazards*, 30, 281–295, 2003.
- Schauer, T.: Die Blaikenbildung in den Alpen, Schriftreihe Bayerisches Landesamt für Wasserwirtschaft, 1–29, 1975.
- Suezen, M. L. and Doyuran, V.: Data driven bivariate landslide susceptibility assessment using geographical information systems: a method and application to Asarsuyu catchment, Turkey, *Eng. Geol.*, 71, 303–321, 2004.
- Swisstopo: Reproduziert mit Bewilligung von swisstopo, 2006.
- Tasser, E., Mader, M., and Tappeiner, U.: Effects of land use in alpine grasslands on the probability of landslides, *Basic Appl. Ecol.*, 4, 271–280, 2003.
- Van Den Eeckhaut, M., Vanwalleghem, T., Poesen, J., Govers, G., Verstraeten, G., and Vandekerckhove, L.: Prediction of landslide susceptibility using rare events logistic regression: A case-study in the Flemish Ardennes (Belgium), *Geomorphology*, 76, 392–410, 2006.
- Van Westen, C. J.: The modelling of landslide hazard using GIS, *Surv. Geophys.*, 21, 241–255, 2000.
- Van Westen, C. J. and Lulie Getahun, F.: Analyzing the evolution of the Tessina landslide using aerial photographs and digital elevation models, *Geomorphology*, 54, 77 pp., 2003.
- Varnes, D. J.: Landslide hazard zonation: A review of principles and practice, Paris, 63 pp., 1984.
- Von Wyl, B.: Düngung an steilen Hängen vergrößert das Risiko von Erdrutschen, Mitteilungen der Naturforschenden Gesellschaft Luzern, 30, 324–335, 1988.
- Wills, C. J. and McCrink, T. P.: Comparing landslide inventories: The map depends on the method, *Environ. Eng. Geosci.*, 8, 279–293, 2002.
- WRB: IUSS Working Group World reference base for soil resources, Food and Agriculture Organization of the United Nations, Rom, 128 pp., 2006.
- Wyss, R.: Die Urseren-Zone – Lithostatigraphie und Tektonik, *Eclogae Geol. Helv.*, 79, 731–767, 1986.
- Yesilnacar, E. and Topal, T.: Landslide susceptibility mapping: A comparison of logistic regression and neural networks methods in a medium scale study, Hendek region (Turkey), *Eng. Geol.*, 79, 251 pp., 2005.
- Zêzere, J. L., Reis, E., Garcia, R., Oliveira, S., Rodrigues, M. L., Vieira, G., and Ferreira, A. B.: Integration of spatial and temporal data for the definition of different landslide hazard scenarios in the area north of Lisbon (Portugal), *Nat. Hazards Earth Syst. Sci.*, 4, 133–146, 2004, <http://www.nat-hazards-earth-syst-sci.net/4/133/2004/>.
- Zhou, C. H., Lee, C. F., Li, J., and Xu, Z. W.: On the spatial relationship between landslides and causative factors on Lantau Island, Hong Kong, *Geomorphology*, 43, 197–207, 2002.

CHAPTER 5

Estimating vegetation parameter for soil erosion assessment in an alpine catchment by means of QuickBird imagery

This chapter has been published in International Journal of Applied Earth Observation and Geoinformation as: *K. Meusburger, D. Bänninger and C. Alewell: Estimating vegetation parameter for soil erosion assessment in an alpine region by means of QuickBird data, 12, 201-207, 2010.*



Contents lists available at ScienceDirect

International Journal of Applied Earth Observation and Geoinformation

journal homepage: www.elsevier.com/locate/jag

Estimating vegetation parameter for soil erosion assessment in an alpine catchment by means of QuickBird imagery

K. Meusburger*, D. Bänninger, C. Alewell

Institute for Environmental Geosciences, University of Basel, Bernoullistrasse 30, CH-4056 Basel, Switzerland

ARTICLE INFO

Article history:

Received 16 March 2009

Accepted 18 February 2010

Keywords:

Soil erosion

Mountain

Remote sensing

Spectral unmixing

QuickBird

NDVI

ABSTRACT

Soil erosion rates in alpine regions are related to high spatial variability complicating assessment of risk and damages. A crucial parameter triggering soil erosion that can be derived from satellite imagery is fractional vegetation cover (FVC). The objective of this study is to assess the applicability of normalized differenced vegetation index (NDVI), linear spectral unmixing (LSU) and mixture tuned matched filtering (MTMF) in estimating abundance of vegetation cover in alpine terrain. To account for the small scale heterogeneity of the alpine landscape we used high resolved multispectral QuickBird imagery (pixel resolution = 2.4 m) of a site in the Urseren Valley, Central Swiss Alps (67 km²). A supervised land-cover classification was applied (total accuracy 93.3%) prior to the analysis in order to stratify the image. The regression between ground truth FVC assessment and NDVI as well as MTMF-derived vegetation abundance was significant ($r^2 = 0.64$, $r^2 = 0.71$, respectively). Best results were achieved for LSU ($r^2 = 0.85$). For both spectral unmixing approaches failed to estimate bare soil abundance ($r^2 = 0.39$ for LSU, $r^2 = 0.28$ for MTMF) due to the high spectral variability of bare soil at the study site and the low spectral resolution of the QuickBird imagery. The LSU-derived FVC map successfully identified erosion features (e.g. landslides) and areas prone to soil erosion. FVC represents an important but often neglected parameter for soil erosion risk assessment in alpine grasslands.

© 2010 Elsevier B.V. All rights reserved.

1. Introduction

One of the most crucial factors to determine soil erosion rates is vegetation cover. Vegetation cover prevents soil erosion by reducing the impact of falling raindrops, increasing infiltration of water into the soil, reducing the speed and the force of the surface runoff, stabilizing the soil mechanically and improving the physical, chemical and biological properties of the soil (Descroix et al., 2001; Elwell and Stocking, 1976). Grassland is the dominant land use type in the Alps above 1500 m a.s.l. (BFS, 2005). Usually, vegetation cover is regionalized by assigning uniform values from literature or field measured data to a classified land-cover map (Folly et al., 1996; Morgan, 1995; Wischmeier and Smith, 1978). The latter method results in constant values for alpine grasslands, and does not account for spatial variation in fractional vegetation cover.

Remote sensing allows a survey of erosion features such as gullies, landslides or vegetation disturbance to collect input data for soil erosion models even in remote areas (De Jong, 1994; Vrieling, 2006). Most commonly used techniques to assist erosion assessment are image classification, spectral indices and spectral

unmixing. Spectral indices and especially spectral unmixing are useful to derive vegetation abundances (Vrieling, 2006). Spectral indices such as the Normalized Difference Vegetation Index (NDVI) have been used for the direct mapping of vegetation cover (Liu et al., 2004; Thiam, 2003) or to improve the mapping of C factor, which represents the effects of all interrelated cover and management variables in the Universal Soil Loss Equation, by establishing regression analysis (De Jong, 1994; De Jong et al., 1999). For some regions vegetation indices were found to have low correlation with the C factor (De Jong, 1994; Tweddles et al., 2000) due to the sensitivity of the NDVI to vitality of vegetation (De Jong, 1994). The problem was overcome by using linear spectral unmixing (LSU). Asner and Heidebrecht (2000) could successfully map non-photosynthetic vegetation using the LSU technique. Linear spectral unmixing also proved to be superior to NDVI for mapping the C factor by regression analysis (De Asis and Omasa, 2007; De Asis et al., 2008). So far, LSU has been used with satellite systems with a medium spatial resolution and medium to high spectral resolution due to the higher number of spectral bands. The alpine environment exhibits a spatially complex and heterogeneous biogeophysical structure, where abundances of bare soil, vegetation, and rock vary at small scales making it difficult to map these key parameters for soil erosion assessments. A possible solution to account for the problem of spatial heterogeneity might be the usage of very high resolution satellite imagery as high resolution vegetation cover data is

* Corresponding author. Tel.: +41 61 2673631; fax: +41 61 2670479.
E-mail address: Katrin.Meusburger@unibas.ch (K. Meusburger).

crucial for soil erosion modelling (Meusburger et al., submitted for publication).

The objective of this study is to test the suitability of high resolution QuickBird imagery in estimating vegetation cover abundances in an alpine catchment. In many regions, vegetation cover is characterised by strong temporal dynamics that needs to be considered for erosion assessment (Vrieling, 2006). In alpine areas temporal dynamics are less important because disturbances in vegetation cover due to trampling, overgrazing, cutting, snow transport and landslides recover slowly and do not follow a seasonal dynamic as on arable land, where ploughing and harvesting is applied. The QuickBird image was taken in autumn, because we assume that fractional vegetation cover mapped in autumn is a decisive parameter for soil erosion risk. Bare soil areas that have not recovered during the growing season are persistent and are prone for winter damages and subsequent snowmelt, when highest erosion rates can be expected (Konz et al., 2009). In our study site, sheet erosion and landslides are dominant. Rill erosion is scarce, which might be mostly due to the high content of skeleton in the soil. Fractional vegetation cover (FVC) in the field is defined here as the percentage of an area covered by grass. The inverse of FVC equals to the fraction of bare soil. We aim to map FVC for grassland areas by NDVI, linear spectral unmixing (LSU) and mixture tuned matched filtering (MTMF) and relate this to ground truth measurements. Prior to the unmixing analysis a supervised land-cover classification of the image is done to allow for stratified evaluation of the image.

2. Materials and methods

2.1. Site description

The study site is located in the Urseren Valley, Central Swiss Alps (46.36°N, –8.32°E) and covers approximately 67 km². Elevation of the U-shaped valley ranges from 1400 m to 3200 m a.s.l. The valley has heterogeneous geologic formations which correspond to a geological fault line with NW–SE extension (Fig. 1). The climate is alpine with a mean air temperature of 3.1 °C and a mean annual

rainfall of about 1400 mm per year measured at the climate station in Andermatt (1901–1961; 1442 m a.s.l.; data from MeteoSwiss). The valley is snow covered for 5–6 months (from November to April) with the maximum snow height in March and drained by the river Reuss. Its nivo-glacial runoff regime is replenished by summer and early autumn floods with peak runoff in June (BAFU, 2009). The main land-cover types of the 67 km² study site in 2000 were 64% alpine grasslands and dwarf-shrubs, 26% scree and bare rock mainly at higher elevations, and 5% shrubs. The remaining 5% are covered by glacier, forest or settlement (Swisstopo, 2006). For a more detailed description of the study site, see Meusburger and Alewell (2008).

2.2. Pre-processing of the QuickBird image

QuickBird standard imagery was acquired on October 17, 2006 (10:51 UTC), under clear sky conditions. The sun elevation at the time of capture was 34.1° with a nadir view angle of 16.1°. The imagery was geo-corrected by the satellite data providers with a published spatial accuracy of 14 m root mean square error (RMSE). The imagery contains four multispectral bands with a 2.4 m spatial resolution: the wavelength of the respective bands is 0.45–0.52 μm (blue); 0.52–0.60 μm (green); 0.63–0.69 μm (red); 0.76–0.90 μm (near infrared). The QuickBird panchromatic band (0.45–0.90 μm) has a 0.6 m spatial resolution. Standard QuickBird imagery is already radiometrically corrected. The correction accounts for instrument specific errors only, consequently further image correction is necessary.

The image correction procedure requires three steps (Edwards et al., 1999): conversion of the digital number (DN) recorded at the sensor to satellite radiance; conversion of satellite radiance to satellite reflectance at the sensor, and finally the conversion to ground reflectance by removal of topographic- and atmospheric (absorption and scattering) effects. The conversion from DN values to radiances was performed according to the technical note from Digital Globe (Krause, 2003). For the conversion of satellite radiance to apparent reflectance $\rho(-)$ the following equation was used

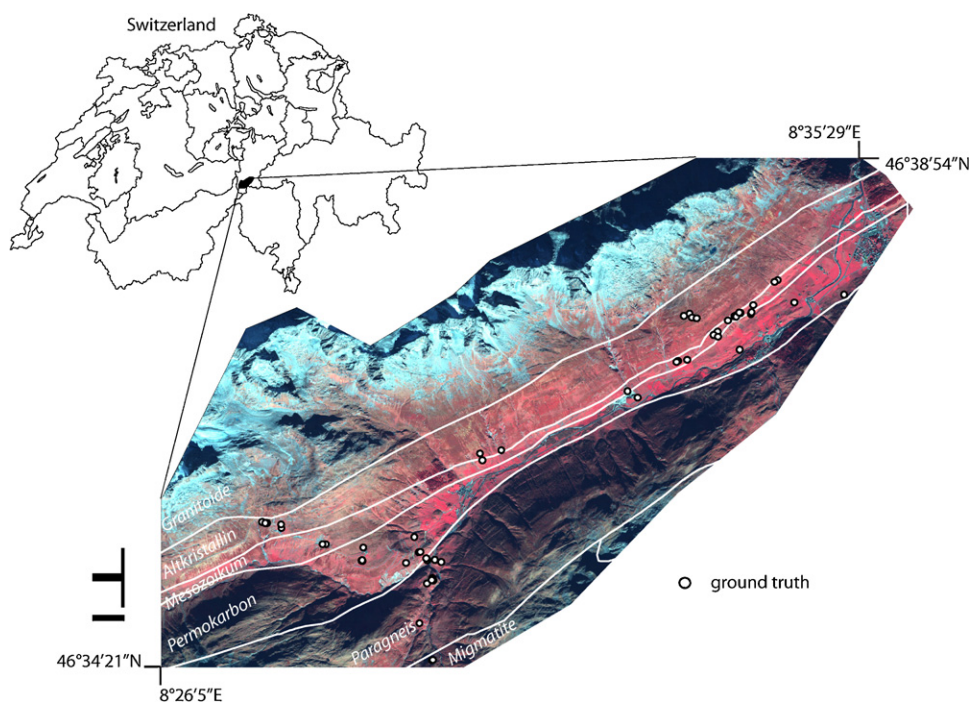


Fig. 1. Geographic location of the QuickBird image (false colour). The white lines separate different geologic formations. The white dots show the locations of ground truth measurements of fractional vegetation cover.

(Edwards et al., 1999):

$$\rho = \frac{\pi \times L \times d^2}{ESUN \times \cos(\theta_s)} \quad (1)$$

L = satellite radiance ($\text{mW cm}^{-2} \text{ster}^{-1} \mu\text{m}^{-1}$), d = earth–sun distance (AU), $ESUN$ = mean solar irradiance ($\text{mW cm}^{-2} \mu\text{m}^{-1}$), θ_s = sun zenith angle in radians. The earth–sun distance (d) is calculated using the following equation:

$$d = (1 - 0.01674 \times \cos(0.9856 \times (\text{JD} - 4))) \quad (2)$$

where JD is the Julian Day of the image acquisition.

The image was corrected for topographic effects only, due to a high visibility (>50 km) during image acquisition and lacking additional information on atmospheric conditions. The topographic correction was done with a DEM (25 m grid; ± 3 m vertical accuracy in the Alps; (Swisstopo, 2006)) and the TOPOCOR module of the Atcor3 software package (Richter, 2005). The correction factor is:

$$f = 1 - \left(1 - \frac{\cos\theta_s}{\cos\beta}\right) \times w, \quad \text{if } \lambda < 1.1 \mu\text{m} \quad (3)$$

β is the local zenith angle and w a wavelength (λ) depending weighting coefficient. For $\lambda \geq 1.1 \mu\text{m}$ w becomes 1 (Richter, 2005). Furthermore, the factor f includes a bound to prevent overcorrection.

2.3. Field measurements

2.3.1. Ground truth measurements

The FVC for 43 plots along two elevation gradients (ranging from 1450 m to 2150 m a.s.l.) and along the valley transect (Fig. 1) was measured two weeks after the image was taken. Sites showing impact of sheet erosion, trampling overgrazing or cutting were chosen for ground truth sites with low FVC. A mesh with 10×10 cells

(cell size 100 cm^2) was put on the earth surface to measure FVC. For each cell, the FVC was visually estimated and averaged over the total mesh area. The geographic position of each ground truth site was determined using Garmin eTrex Summit GPS (3 m accuracy; Garmin International Inc., Olathe, KS, USA). Because of the geolocalization uncertainty of the QuickBird image and the effects of surrounding pixel radiance, ground truth plots with a homogenous surface characteristic for at least $5 \text{ m} \times 5 \text{ m}$ were chosen. The single coordinates of the ground truth sites were measured together with the coordinates of characteristic identifiable features in the image (e.g. boulders, crossroads etc.) to allow better localisation using the pan-sharpened image. The ground truth values did not show a normal distribution, because of a limited availability of ground truth sites with low FVC especially at higher elevation with lower land use intensity.

2.4. Image land-cover classification

All image analysis was performed using ENVI 4.3 software (Research Systems Inc., Boulder, CO). We used supervised classification with a maximum likelihood classifier for land-cover mapping. Land-cover was classified into the following nine categories: forest, shrub, dwarf-shrub, grassland, non-photosynthetic vegetation, snow, water, bare soil, and rock. The artificial category shadow was introduced because of the distinct topography of the study area. For each land-cover class the maximum likelihood classifier was trained on three locations in the valley with 144–1876 pixels per training class. For the land-cover type grassland a higher probability threshold (of 0.75) was used in order to include grassland with reduced FVC. To measure the accuracy of the classification, the kappa coefficient (κ) and overall accuracy were calculated. In total, 3217 independent pixels with five ground truth locations per class were used to assess the classification accuracy.

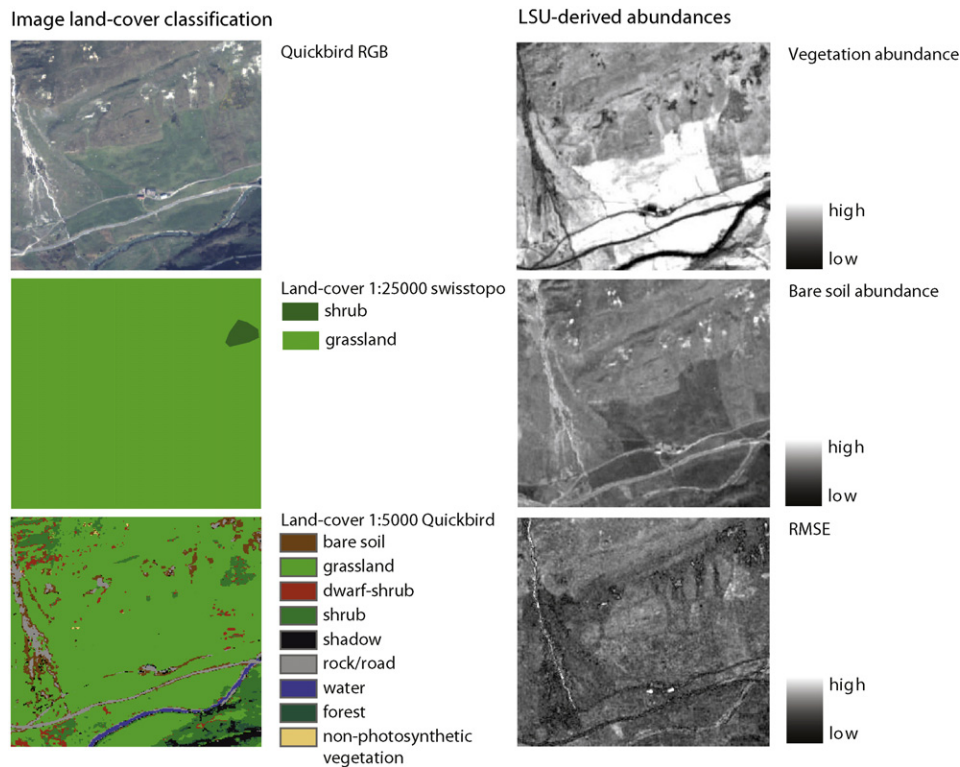


Fig. 2. Sub-image of the QuickBird scene showing (left) the resulting land-cover map compared to land-cover information of the Swisstopo 1:25,000 Vector dataset and (right) normalized abundances of vegetation, bare soil and RMSE for the linear spectral unmixing model. The lighter the colour, the higher the proportion of an endmember (and error) within the pixel.

2.5. Mapping of fractional vegetation cover

We compared the performance of the Normalized Difference Vegetation Index (NDVI) with that of two spectral unmixing approaches. The NDVI is the most widespread spectral ratio of near infrared and red bands and is used for monitoring global vegetation cover (Tucker, 1979).

The spectral unmixing assumes that the reflectance of each pixel is a combination of spectral endmembers (Adams et al., 1995). Most rural land endmember combinations are green vegetation, non-photosynthetic vegetation, bare soil, rock, and shadow (Adams et al., 1995; Roberts et al., 1993; Theseira et al., 2003). A crucial step in spectral unmixing analysis is the determination of spectral endmembers that are pure elements located at the corners of the spectral space. Endmember spectra combine to produce all of the spectra in the image.

The Pixel Purity Index (PPI) algorithm is a common method to find the most “spectrally pure” (extreme) pixels in multispectral images (Boardman and Kruse, 1994). It is computed by repeatedly projecting n -dimensional scatter plots onto a random unit vector. The ones falling at the extremes of each vector line are recorded. After many repeated projections, the total number of times each pixel is marked as extreme is noted. The pixels that count above a certain cut-off threshold are declared “pure” and are the potential endmember spectra. We used 5000 iterations with a threshold of 2.5. Before the PPI is applied, a “noisewhitening” dimensionality reduction step is performed by using a Minimum Noise Fraction (MNF) transformation (Green et al., 1988). Previous studies have shown that the use of the MNF transform can improve the quality of fraction images through decorrelation (Van der Meer and De Jong, 2000). The MNF transformation is in principle a two-phase principal component analysis that segregates the noise from the data resulting in a reduced number of bands containing the most meaningful information. A dark shadow part of the image behind the main mountain ridge was used to steer the MNF algorithm. The dimensionality of the QuickBird image was not reduced by the procedure. We selected the pixels with the highest PPI values as candidate endmembers. The final endmembers were then selected by referring to the QuickBird image and the field survey (e.g. vegetation with homogenous canopy and without boulders). Average reflectance of selected representative pixels (average of 2–81 pixels) with high PPI values that correspond to selected endmembers were used in the subsequent unmixing analysis. Five endmembers were identified for the study site: snow, vegetation, rock, bare soil, and water/shadow. We used two spectral unmixing approaches: linear spectral unmixing (LSU) and mixture tuned matched filtering (MTMF). The LSU method is limited by the assumption that pixel composition is made up of a limited number of elements, because of mathematical reasons, the number of elements cannot exceed the number of spectral bands plus one (Adams et al., 1995). Considering the correlations between the visible bands of the QuickBird imagery, the approach is limited to three endmembers. In order to bypass this limitation the results of the land-cover classification were used to stratify the image in advance. The following categories were masked prior to the LSU analysis: forest, shrub, dwarf-shrub, snow, water and rock. Grassland, bare soil and shadow were used as endmembers. An advantage of LSU is the supply of a residual error for each pixel in the image. The residual error is the difference between the measured and modelled spectrum in each band. Averaged residuals over all bands give an RMSE, which is useful to check for the validity of selected endmembers. The unmixing was constrained to fix the fraction of any endmember between 0 and 1, and the sum of fractions for each pixel equal to 1. In regions with steep topography, shadowed areas are present in the image. However, because shadow is not a physical component, it was removed by normal-

ization (Adams et al., 1995; Hill and Foody, 1994; Smith et al., 1992).

MTMF is another type of spectral unmixing that performs a ‘partial’ spectral unmixing by identifying only a single endmember at a time without knowing the other background endmember signatures (Boardman, 1998). From spectral mixture modelling, it takes over the leverage arising from the mixed pixel model, the constraints on feasibility including the unit-sum and positivity requirements. The response of the endmember of interest is maximized and the unknown background is suppressed (Harsanyi and Chang, 1994). The MTMF and LSU score indicate how well the image pixel compares to the reference spectrum and measures how spectrally abundant a material is in the image pixel. Provided that spectra of the single components mix linearly, spectral abundance in an image pixel corresponds to physical abundance in the same location on the ground.

The advantage of the MTMF compared to LSU is that it is unnecessary to identify all endmembers in a scene (Glenn et al., 2005; Harris and Asner, 2003; Mundt et al., 2005; Parker Williams and Hunt, 2002). Consequently the number of endmembers is independent from the number of spectral bands (Boardman, 1998). For our study area, the sum of the MTMF scores at each pixel was usually less than unity probably due to unidentified background material within the pixel. Because MTMF routine projects the mean of the background data to zero negative MTMF scores or MTMF scores greater than 1 (for at least one of the four endmembers) were present on many pixels for our study site. These values are physically meaningless and were re-scored as 0 or 1 (Robichaud et al., 2007). For the MTMF approach, two ground truth sites were excluded due to high infeasibility values. In contrast to the LSU that was performed using the masked image, the MTMF analysis was applied for the entire image. Finally, all mapped abundances were multiplied by 100 to express as % parallel to the percentage ground data.

3. Results and discussion

3.1. Mapping of land-cover by image classification

At higher elevations the problem aroused that spectral signature of bare soils and non-photosynthetic vegetation are very similar because siliceous geology with podsollic soils is predominant. The rusty colour of the podsollic soils is similar to the colour of non-photosynthetic vegetation. With the available training data either classifying landslide areas in low elevations as non-photosynthetic vegetation or non-photosynthetic vegetation at higher elevations as bare soil was possible. At higher elevation NDVI of non-photosynthetic vegetation training areas was above 0.2 while bare soil areas were below. Thus, subsequent to the supervised classification all pixels classified as bare soil above 2000 m a.s.l. with a NDVI greater than 0.2 were changed to non-photosynthetic vegetation. The elevation above 2000 m a.s.l. was chosen because it produced best classification results compared to the ground truth data. The problem of the discrimination between non-photosynthetic vegetation and soil might be solved by using multi-temporal QuickBird imagery. In the summer season (July, August) the elevated non-photosynthetic vegetation is green vegetation.

The achieved overall accuracy of land-cover classification using the independent pixel dataset is 93.3% (3000/3217 Pixels) and the $\kappa = 0.92$. In total, 0.81% of the dataset remained unclassified. The land-cover classes of bare soil (after correction), grassland, rock, snow, water, forest, and shadow have high classification accuracies (82–100%), while classes of dwarf-shrub, shrub, and non-photosynthetic vegetation have lower classification accura-

Table 1

Confusion matrix for the supervised land-cover classification (npv = non-photosynthetic vegetation).

| Class | Bare soil | Grassland | Dwarf-shrubs | Shrubs | Rock | Snow | Water | Forest | npv | Shadow | Total | Producers accuracy (%) | User accuracy (%) |
|--------------|-----------|-----------|--------------|--------|------|------|-------|--------|-----|--------|-------|------------------------|-------------------|
| Unclassified | 0 | 0 | 0 | 0 | 0 | 0 | 26 | 0 | 0 | 0 | 26 | | |
| Bare soil | 214 | 0 | 0 | 0 | 4 | 1 | 0 | 0 | 4 | 0 | 223 | 97.27 | 95.96 |
| Grassland | 0 | 332 | 0 | 7 | 0 | 0 | 0 | 0 | 0 | 0 | 339 | 92.22 | 97.94 |
| Dwarf-shrubs | 0 | 0 | 160 | 14 | 0 | 0 | 0 | 0 | 30 | 0 | 204 | 74.77 | 78.43 |
| Shrubs | 0 | 28 | 54 | 217 | 0 | 0 | 0 | 21 | 0 | 0 | 320 | 91.18 | 67.81 |
| Rock | 6 | 0 | 0 | 0 | 411 | 0 | 6 | 0 | 0 | 0 | 423 | 99.04 | 97.16 |
| Snow | 1 | 0 | 0 | 0 | 0 | 235 | 0 | 0 | 0 | 0 | 235 | 99.58 | 100.00 |
| Water | 0 | 0 | 0 | 0 | 0 | 0 | 216 | 0 | 0 | 0 | 216 | 83.72 | 100.00 |
| Forest | 0 | 0 | 0 | 0 | 0 | 0 | 6 | 248 | 0 | 1 | 255 | 90.51 | 97.25 |
| npv | 0 | 0 | 0 | 0 | 0 | 0 | 0 | 0 | 122 | 0 | 122 | 78.21 | 100.00 |
| Shadow | 0 | 0 | 0 | 0 | 0 | 0 | 4 | 5 | 0 | 845 | 854 | 99.88 | 98.95 |
| Total | 220 | 360 | 214 | 238 | 415 | 236 | 258 | 274 | 153 | 846 | 3217 | | |

cies (67–78%) (Table 1). Percentage values of each land-cover class within the study site could not be determined due to large shadowed areas. In comparison to the former available low resolution land-cover dataset (1:25,000 of Swisstopo), it was possible to derive more details (Fig. 2, left). Of special interest for erosion mapping is the detection of bare soil areas that have the highest potential erosion rates. In addition, it was possible to map dwarf-shrub vegetation that has lower erosion potential than grassland (Konz et al., 2009).

Detailed mapping of land-cover and separation of different vegetation types is crucial for soil erosion assessment because different vegetation types produce different sediment yields (Isselin-Nondedeu and Bedecarrats, 2007). The supervised classification of the image worked well. However, in an area with distinct elevation gradients, changes in spectral signature of a class due to altering vegetation composition, nutritional status or of soil genesis may occur. For instance, for higher elevated areas the discrimination between non-photosynthetic vegetation and bare soil becomes difficult. The main problem is the classification of bare soil with high spectral variability depending on soil genesis (reductive, oxidative conditions), erosion status and parent material due to the limited number of spectral bands of QuickBird imagery. Sufficient ground truth data is needed that may serve for knowledge-based correction algorithms as was applied here.

3.2. Mapping of bare soil and vegetation abundance relative to ground truth measurements

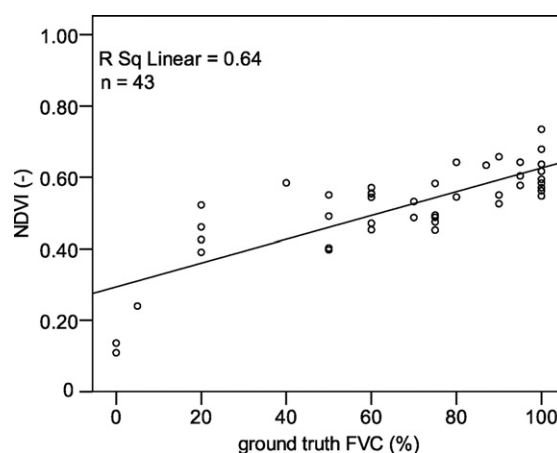
The abundance images derived using LSU for vegetation, bare soil and RMSE are shown in Fig. 2 (right). The figures show high spatial variability that represents the different cover conditions in the study area. Vegetation abundance is highest close to the valley bottom. The evident bare soil areas correspond to landslides, overgrazed areas, road- and river-banks and areas affected by sheet erosion. The RMSE image shows no recognizable pattern for the grassland areas indicating that the chosen endmembers are valid. High RMSE values are evident for areas covered with rock, landslides with rock outcrops and shrubs. These land-cover types were subsequently masked. The mean RMSE value for the masked image is 0.52.

The scatter plot between the ground truth FVC and the NDVI (Fig. 3) has difficulties discerning different levels of ground truth FVC for high abundances (40–100%). The low abundances (0–5%) are overestimated by NDVI. Linear regression yielded an overall coefficient of determination of $r^2 = 0.64$.

The disadvantage of mapping FVC by NDVI is its dependence on the vitality of the vegetation (De Jong, 1994). Spectral indices enhance the spectral contribution of green vegetation in images while minimizing contributions from bare soil, atmosphere and illumination angle. Although spectral indices produce

reliable estimates of green vegetation cover, the accuracy of non-photosynthetic vegetation is less satisfactory (De Jong, 1994). Moreover, quantification of low FVC using NDVI is weakened by the increasing influence of the variability of background bare soil albedo (Harris and Asner, 2003). The chosen ground truth sites showed minor influence of non-photosynthetic vegetation. Larger errors might be expected for grassland with a higher proportion of non-photosynthetic vegetation. While NDVI utilizes only the visible and near infrared band, the unmixing approach makes use of the entire spectral reflectance (De Asis and Omasa, 2007).

Scatter plots between ground truth FVC and percentage bare soil and abundances determined with LSU and MTMF are given in Fig. 4. Using linear regression between ground truth data and the satellite derived abundances could be described with a coefficient of determination of r^2 of 0.85 for LSU and 0.71 for MTMF. Low, but still significant (at a 0.01 level) regression was obtained between bare soil abundance and ground truth bare soil fractions with $r^2 = 0.28$ for LSU and $r^2 = 0.39$ for MTMF. The abundances of vegetation and bare soil do not sum up to 100% because of the high RMSE of the unmixed images caused by the confusion between bare soil and shadow. Only residues of the regression between FVC and LSU-derived vegetation abundance have no significant (at a 0.05 level) difference to a normal distribution. The LSU- and MTMF-derived abundances represent a physical percentage of a material on the ground-surface and should lie on a 1:1 line with the values measured on the ground. The measured ground truth values were generally higher than the corresponding LSU- and MTMF-derived abundances. For the FVC this can be explained by the choice of the grassland endmember that was located on a golf course situated in the study site. Different runs using other grassland endmember spectra yielded higher grassland abundance, however, the linear regression to the

**Fig. 3.** Scatter plot of NDVI versus the ground truth fractional vegetation cover.

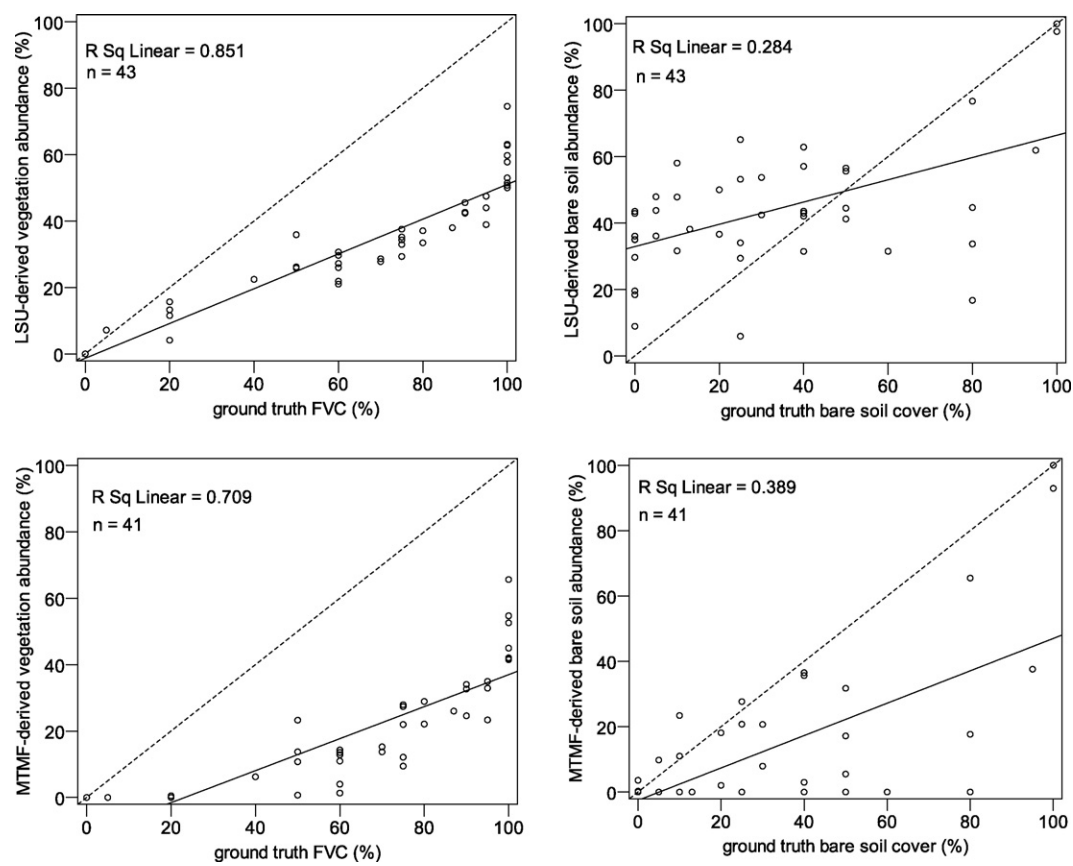


Fig. 4. Scatter plots of linear spectral unmixing and mixture tuned matched filtering-derived abundances versus the ground truth data. Linear regression lines are shown.

ground truth data and RMSE was worse. The better performance of the golf course endmember might be due to the absence of non-photosynthetic vegetation. In October (time of image capture) the chlorophyll content in natural grassland already decreased compared to the irrigated golf course. The unmixing might work also with a generic grassland endmember, which would spare the procedure for local image selection. Still a direct application (without the correction for the deviation from the 1:1 line) in soil erosion models would not be feasible due to the underestimation of the physical percentage. Using the regression equation established between the vegetation abundance maps and the ground truth data it is possible to convert the vegetation abundance map to the FVC map.

For the MTMF-derived abundances, we observe even stronger deviations, which might be due to the partial unmixing algorithm, where the abundances were not constrained to sum to unity. If an endmember is not found in the pixel, the pixel is classified as background material (Boardman, 1995). In our case not every endmember is found in every pixel, which caused zeros on the scatter plots, especially for the bare soil abundance (Fig. 4).

The high coefficient of determination yielded for the mapping of vegetation abundances may be due to the very distinct reflectance curves of vegetation if they are compared with reflectance of bare soil, rock and water. The less distinct spectral signature of bare soil is probably the main reason for the worse estimates of bare soil abundances. Another explanation is the higher spectral variability of the soil depending on its genesis and erosion status. Regarding the abundance of bare soil, we believe the obtained results are not precise enough for further application.

In general, QuickBird is not the 'optimal' sensor for unmixing approaches due to the small number of spectral bands. For the mapping of bare soil abundances the systems seems to reach its limits. This is mainly due to the lack of short wave infrared channels

that are important for mineral and rock discrimination since minerals have numerous absorption bands in this wavelength range. This problem might be solved by using images of the WorldView-2 satellite (launched in October 2009) that provides 8 spectral bands at 1.8 m resolution at nadir. Nonetheless, the results from the linear regression show that the ground measured FVC and the abundances mapped by LSU and MTMF had a significant correlation. Especially the LSU-derived linear regression equation between vegetation abundance and ground truth FVC may be used to quantitatively predict ground FVC. The FVC map allows for a first allocation of potential soil erosion risk areas and improves estimates of soil erosion models (Meusburger et al., submitted for publication).

4. Conclusion

The supervised classification identified the typical land-cover types of alpine regions successfully with an overall accuracy of 93.3%. Relative abundance of vegetation cover could be mapped for grassland areas using NDVI, linear spectral unmixing and mixture tuned matched filtering with coefficients of determination between ground truth and derived FVC of $r^2 = 0.64$ for NDVI, $r^2 = 0.85$ for LSU, and $r^2 = 0.71$ for MTMF. The spectral unmixing approaches (LSU, MTMF) failed to map bare soil abundance, which might be due to the low spectral resolution of the QuickBird imagery and the high variability of the spectral signature of bare soil. The small scale heterogeneity and extreme topography make high demands for the remote sensing of an alpine environment. High spatial resolutions are needed that only few satellite systems such as IKONOS and QuickBird offer. The disadvantage of these systems is the small spectral resolution that causes difficulties in separating bare soil areas from non-photosynthetic vegetation and rock. Sufficient ground truth data is required to handle these difficul-

ties. The produced abundance maps of vegetation are preferable to only parameterising thematic land-cover classes because it retains spatial and distributional information.

Acknowledgement

This study was funded by the Swiss Federal Office for the Environment (Contract No.: StoBoBio/810.3129.004/05/0X).

References

- Adams, J.B., Sabol, D.E., Kapos, V., Almeida Filho, R., Roberts, D.A., Smith, M.O., Gillespie, A.R., 1995. Classification of multispectral images based on fractions of endmembers: application to land-cover change in the Brazilian Amazon. *Remote Sensing of Environment* 52, 137–154.
- Asner, G.P., Heidebrecht, K.B., 2000. Spectral unmixing of vegetation, soil and dry carbon cover in arid regions: comparing multispectral and hyperspectral observations. In: *International Workshop on Land Cover/Land Use Change and Water Management in Arid Regions*, Beer Sheva, Israel.
- BAFU, 2009. BAFU: Hydrological Foundations and Data. Real Time and Historical Data. Swiss Federal Environmental Agency, <http://www.hydrodaten.admin.ch/d/2087.htm>, Access date 7.1.2009.
- BFS, 2005. Arealstatistik Schweiz: Zahlen – Fakten – Analysen. Bundesamt für Statistik, Neuchâtel.
- Boardman, J.W., 1995. Analysis, understanding and visualization of hyperspectral data as convex sets in n -space. In: *Imaging Spectrometry Conference*, Orlando, FL.
- Boardman, J.W., 1998. Leveraging the high dimensionality of AVIRIS data for improved subpixel target unmixing and rejection of false positives: mixture tuned matched filtering. In: *Annual JPL Airborne Earth Science Workshop*, Pasadena, CA.
- Boardman, J.W., Kruse, F.A., 1994. Automated spectral analysis – a geological example using AVIRIS data, North Grapevine Mountains, Nevada. In: *10th Thematic Conference on Geologic Remote Sensing – Exploration, Environment, and Engineering*, San Antonio, TX.
- De Asis, A.M., Omasa, K., 2007. Estimation of vegetation parameter for modeling soil erosion using linear spectral mixture analysis of Landsat ETM data. *ISPRS Journal of Photogrammetry and Remote Sensing* 62, 309–324.
- De Asis, A.M., Omasa, K., Oki, K., Shimizu, Y., 2008. Accuracy and applicability of linear spectral unmixing in delineating potential erosion areas in tropical watersheds. *International Journal of Remote Sensing* 29, 4151–4171.
- De Jong, S.M., 1994. Derivation of vegetative variables from a Landsat TM image for erosion modelling. *Earth Surface Processes and Landforms* 19, 165–178.
- De Jong, S.M., Paracchini, M.L., Bertolo, F., Folving, S., Megier, J., De Roo, A.P.J., 1999. Regional assessment of soil erosion using the distributed model SEMMED and remotely sensed data. *Catena* 37, 291–308.
- Descroix, L., Viramontes, D., Vauclin, M., Barrios, J.L.G., Esteves, M., 2001. Influence of soil surface features and vegetation on runoff and erosion in the Western Sierra Madre (Durango, Northwest Mexico). *Catena* 43, 115–135.
- Edwards, D.P., Halvorson, C.M., Gille, J.C., 1999. Radiative transfer modeling for the EOS Terra satellite Measurement of Pollution in the Troposphere (MOPITT) instrument. *Journal of Geophysical Research Atmospheres* 104, 16755–16775.
- Elwell, H.A., Stocking, M.A., 1976. Vegetal cover to estimate soil erosion hazard in Rhodesia. *Geoderma* 15, 61–70.
- Folly, A., Bronsveld, M.C., Clavaux, M., 1996. A knowledge-based approach for C-factor mapping in Spain using Landsat TM and GIS. *International Journal of Remote Sensing* 17, 2401–2415.
- Glenn, N.F., Mundt, J.T., Weber, K.T., Prather, T.S., Lass, L.W., Pettingill, J., 2005. Hyperspectral data processing for repeat detection of small infestations of leafy spurge. *Remote Sensing of Environment* 95, 399–412.
- Green, A.A., Berman, M., Switzer, P., Craig, M.D., 1988. A transformation for ordering multispectral data in terms of image quality with implications for noise removal. *IEEE Transactions on Geoscience and Remote Sensing* 26, 65–74.
- Harris, A.T., Asner, G.P., 2003. Grazing gradient detection with airborne imaging spectroscopy on a semi-arid rangeland. *Journal of Arid Environments* 55, 391–404.
- Harsanyi, J.C., Chang, C.I., 1994. Hyperspectral image classification and dimensionality reduction – an orthogonal subspace projection approach. *IEEE Transactions on Geoscience and Remote Sensing* 32, 779–785.
- Hill, R.A., Foody, G.M., 1994. Separability of tropical rain-forest types in the Tambopata-Candamo reserved zone. *Peru International Journal of Remote Sensing* 15, 2687–2693.
- Isselin-Nondedeu, F., Bedecarrats, A., 2007. Influence of alpine plants growing on steep slopes on sediment trapping and transport by runoff. *Catena* 71, 330–339.
- Konz, N., Schaub, M., Prasuhn, V., Baenninger, D., Alewell, C., 2009. Cesium-137-based erosion-rate determination of a steep mountainous region. *Journal of Plant Nutrition and Soil Science* 172, 615–622.
- Krause, K., 2003. Radiance Conversion of QuickBird Data. Digital Globe, CO, USA.
- Liu, J.G., Mason, P., Hilton, F., Lee, H., 2004. Detection of rapid erosion in SE Spain: a GIS approach based on ERS SAR coherence imagery. *Photogrammetric Engineering and Remote Sensing* 70, 1179–1185.
- Meusburger, K., Alewell, C., 2008. Impacts of anthropogenic and environmental factors on the occurrence of shallow landslides in an alpine catchment (Urseren Valley, Switzerland). *Natural Hazards and Earth System Sciences* 8, 509–520.
- Meusburger, K., Konz, N., Schaub, M., Alewell, C., 2010. Soil erosion modelled with USLE and PESERA using QuickBird derived vegetation parameters in an alpine catchment. *International Journal of Applied Earth Observation and Geoinformation* 12, 208–215.
- Morgan, M.D., 1995. Modeling excess sulfur deposition on wetland soils using stable sulfur isotopes. *Water Air and Soil Pollution* 79, 299–307.
- Mundt, J.T., Glenn, N.F., Weber, K.T., Prather, T.S., Lass, L.W., Pettingill, J., 2005. Discrimination of hoary cress and determination of its detection limits via hyperspectral image processing and accuracy assessment techniques. *Remote Sensing of Environment* 96, 509–517.
- Parker Williams, A., Hunt, E.R., 2002. Estimation of leafy spurge cover from hyperspectral imagery using mixture tuned matched filtering. *Remote Sensing of Environment* 82, 446–456.
- Richter, R., 2005. Atmospheric/topographic correction for satellite imagery. Atcor 2/3 User Guide, version 6.1. Wessling, Germany.
- Roberts, D.A., Smith, M.O., Adams, J.B., 1993. Green vegetation, nonphotosynthetic vegetation, and soils in AVIRIS data. *Remote Sensing of Environment* 44, 255–269.
- Robichaud, P.R., Lewis, S.A., Laes, D.Y.M., Hudak, A.T., Kokaly, R.F., Zamudio, J.A., 2007. Postfire soil burn severity mapping with hyperspectral image unmixing. *Remote Sensing of Environment* 108, 467–480.
- Smith, M.O., Adams, J.B., Sabol, D.E., 1992. Spectral mixture analysis – new strategies for the analysis of multispectral data. In: *2nd Eurocourse on Imaging Spectrometry: A Tool for Environmental Observations*, Ispra, Italy.
- Swisstopo, 2006. Reproduziert mit Bewilligung von swisstopo.
- Theseira, M.A., Thomas, G., Taylor, J.C., Gemmell, F., Varjo, J., 2003. Sensitivity of mixture modelling to end-member selection. *International Journal of Remote Sensing* 24, 1559–1575.
- Thiam, A.K., 2003. The causes and spatial pattern of land degradation risk in southern Mauritania using multitemporal AVHRR-NDVI imagery and field data. *Land Degradation & Development* 14, 133–142.
- Tucker, C.J., 1979. Red and photographic infrared linear combinations for monitoring vegetation. *Remote Sensing of Environment* 8, 127–150.
- Tweddles, S.C., Eschlaeger, C.R., Seybold, W.F., 2000. An Improved Method for Spatial Extrapolation of Vegetative Cover Estimates (USLE/RUSLE C factor) Using LCTA and Remotely Sensed Imagery. USAEC Report No. SFIM-AEC-EQ-TR-200011, ERDC/CERL TR-00-7, CERL, Champaign. US Army of Engineer Research and Development Center, Illinois.
- Van der Meer, F., De Jong, S.M., 2000. Improving the results of spectral unmixing of Landsat thematic mapper imagery by enhancing the orthogonality of end-members. *International Journal of Remote Sensing* 21, 2781–2797.
- Vrieling, A., 2006. Satellite remote sensing for water erosion assessment: a review. *Catena* 65, 2–18.
- Wischmeier, W.H., Smith, D.D., 1978. Predicting Rainfall Erosion Losses – A Guide to Conservation Planning. Agric. Handbook No. 537. Washington, DC.

CHAPTER 6

Soil erosion modelled with USLE and PESERA using QuickBird derived vegetation parameters in an alpine catchment

This chapter has been published in International Journal of Applied Earth Observation and Geoinformation as: *Meusburger K., Konz N., Schaub M. and Alewell C.: Soil erosion modelled with USLE and PESERA using QuickBird derived vegetation parameters in an alpine catchment, 12, 208-215, 2010.*



Contents lists available at ScienceDirect

International Journal of Applied Earth Observation and Geoinformation

journal homepage: www.elsevier.com/locate/jag

Soil erosion modelled with USLE and PESERA using QuickBird derived vegetation parameters in an alpine catchment

K. Meusburger*, N. Konz, M. Schaub, C. Alewell

Institute for Environmental Geosciences, University of Basel, Bernoullistrasse 30, CH-4056 Basel, Switzerland

ARTICLE INFO

Article history:

Received 2 October 2009

Accepted 5 February 2010

Keywords:

Soil erosion

Mountain

Remote sensing

Cs-137

USLE

PESERA

Erosion model

ABSTRACT

The focus of soil erosion research in the Alps has been in two categories: (i) on-site measurements, which are rather small scale point measurements on selected plots often constrained to irrigation experiments or (ii) off-site quantification of sediment delivery at the outlet of the catchment. Results of both categories pointed towards the importance of an intact vegetation cover to prevent soil loss. With the recent availability of high-resolution satellites such as IKONOS and QuickBird options for detecting and monitoring vegetation parameters in heterogeneous terrain have increased. The aim of this study is to evaluate the usefulness of QuickBird derived vegetation parameters in soil erosion models for alpine sites by comparison to Cesium-137 (Cs-137) derived soil erosion estimates. The study site (67 km²) is located in the Central Swiss Alps (Urseren Valley) and is characterised by scarce forest cover and strong anthropogenic influences due to grassland farming for centuries. A fractional vegetation cover (FVC) map for grassland and detailed land-cover maps are available from linear spectral unmixing and supervised classification of QuickBird imagery. The maps were introduced to the Pan-European Soil Erosion Risk Assessment (PESERA) model as well as to the Universal Soil Loss Equation (USLE). Regarding the latter model, the FVC was indirectly incorporated by adapting the C factor. Both models show an increase in absolute soil erosion values when FVC is considered. In contrast to USLE and the Cs-137 soil erosion rates, PESERA estimates are low. For the USLE model also the spatial patterns improved and showed “hotspots” of high erosion of up to 16 t ha⁻¹ a⁻¹. In conclusion field measurements of Cs-137 confirmed the improvement of soil erosion estimates using the satellite-derived vegetation data.

© 2010 Elsevier B.V. All rights reserved.

1. Introduction

Alpine areas have a high potential soil erosion risk associated to the extreme climatic and topographic conditions. The range of soil erosion rates is very uncertain due to the high spatial heterogeneity of erosion risk factors that cause difficulties to extrapolate sediment measurements on plot scale to larger regions (Helming et al., 2005). Several models have been developed for soil loss quantification (e.g. USLE, RUSLE, LISEM, WEPP, PESERA and EROSION-3D). More recently, water erosion models tended to place a greater emphasis on representing the physical processes that are responsible for erosion, but such efforts are scarce for the alpine environment (Cernusca et al., 1998). In the European Alps, only the Universal Soil Loss Equation (USLE) and the Pan-European Soil Erosion Risk Assessment (PESERA) model have been used (Joint Research Center Ispra, 2009a,b). USLE is an empirical model, which allows the prediction of average annual soil loss based on the product of five erosion risk factors (Wischmeier and Smith, 1978). Emerg-

ing geospatial techniques (Desmet and Govers, 1996; Reusing et al., 2000; Wilson and Gallant, 1996) allows extending USLE to entire watersheds and rapid spatial risk assessment, particularly for remote rural areas, where data availability is constrained. PESERA is a simple physically based model with low data demand based on a runoff threshold, which depends on soil properties, the surface and the vegetation cover. The validity of these models has to be carefully considered for alpine regions (Van Rompaey et al., 2003a,b), especially for the empirical USLE model, which was designed for the western U.S. In high relief regions with rugged topography a more detailed scale is needed. Jetten et al. (2003) even stated that there might be more benefit for soil erosion assessment by improving spatial information for model input and validation rather than by adapting models to a specific landscape. Satellite imagery can provide valuable spatial information mainly on vegetation parameters to improve the performance of soil erosion models (De Asis and Omasa, 2007; De Asis et al., 2008; De Jong, 1994; De Jong et al., 1999; Jain et al., 2002; Tweddles et al., 2000). PESERA considers different vegetation-management types and fractional vegetation cover. In USLE, the C factor accounts for vegetation characteristics. The C factor is an empirical factor that is dependent on vegetation type, management and fractional vegetation cover. Several studies

* Corresponding author. Tel.: +41 61 2673631; fax: +41 61 2670479.
E-mail address: Katrin.Meusburger@unibas.ch (K. Meusburger).

focused on the mapping of vegetation parameters using techniques like image classification, NDVI and linear spectral unmixing (De Jong, 1994; De Jong et al., 1999; Liu et al., 2004; Thiam, 2003). The availability of high-resolution satellites such as IKONOS and QuickBird further increased the options for mapping of vegetation parameters.

This paper explores how high resolution maps of fractional vegetation cover (FVC) and land cover improve soil erosion risk mapping using USLE and PESERA in an alpine catchment. High resolution maps of land cover and FVC were obtained from image classification and linear spectral unmixing analysis (Meusburger et al., 2010, this volume). The evaluation of model performance is done by comparing modelled soil erosion estimates to Cesium-137 (Cs-137) measurements. Cs-137 inventories are an established approach to gain integrative soil erosion estimates (He and Walling, 2000; Ritchie and McHenry, 1990; Walling et al., 1999).

2. Site description

The study site (67 km²) is located in the Urseren Valley (46.36°N, –8.32°E) Central Switzerland Alps. The U-shaped valley is characterised by the distinct topography with elevation ranging from 1400 to 3200 m a.s.l. and a mean slope angle of 24.6°. The valley corresponds to a geological fault line that extends NW–SE. The different geologic formations are displayed in Fig. 1. The climate is alpine with a mean air temperature of 3.1 °C and a mean annual rainfall of about 1400 mm per year at the climate station in Andermatt (1901–1961; 1442 m a.s.l.) of MeteoSwiss. The valley is snow covered for 5–6 month (from November to April) with the maximum snow height in March. The river Reuss drains the valley. Its nivo-glacial runoff regime is replenished by summer and early autumn floods. The peak runoff period is in June (BAFU, 2009). The valley mainly consists of cultivated grasslands. Forested areas are limited to protection forests at slopes above villages. Land use is dominated by grazing and, in the lower reaches of the valley, by hay harvesting. Dominant soil types in the catchment classified after WRB (2006) are Podzols, Podzocambisols and Cambisols, often with stagnic properties. On steep valley slopes, Leptosols are common (with rendzic Leptosols on the calcareous substrates). At the valley bottom and lower slopes, clayey gleyic Cambisol, partly stagnic Histosols, Fluvisols and Gleysols developed. The predominant soil texture in the upper 10 cm is silty-loamy sand. The highest soil erosion rates are expected in spring due to the snowmelt on scarce vegetation cover. The dominant soil erosion process is sheet erosion. Rill erosion is of minor importance at our study site. For a more detailed description of the study site, see Meusburger and Alewell (2008).

3. Materials and methods

In order to compare model performance of PESERA and USLE at our alpine study site we applied the models at nine slopes (average slope angle of 37°) with measured long-term soil erosion rates based on Cs-137 method. We evaluated four different model runs: (1) run1 was done with ground truth FVC of the slopes, (2) run2 with 100% FVC, (3) run3 with 0% FVC and (4) run4 with FVC derived from linear spectral unmixing (LSU). For run4, the average FVC of the 7 pixels that match the location of each slope was used.

Further the USLE was applied for the entire catchment using the high resolution (2.4 m) FVC and land-cover map in comparison to low resolution (25 m) land-cover data.

3.1. Model input data

3.1.1. Parameters for the soil erosion model PESERA

The PESERA model (Kirkby et al., 2000, 2003) estimates soil erosion rates by the processes of sheet wash and rill wash on a regional scale. The spatially distributed model is process based and commonly applied as a diagnostic tool for land use and climate change scenarios on an European scale (Gobin et al., 2004). The PESERA works with a regular grid and may be applied to variable scales. As data resolution becomes finer (<100 m) and for single slopes the PESERA-VBA model is recommended and was used in this study (Joint Research Center Ispra, 2009a). The key concept of the model is the separation of precipitation into overland flow and infiltration with a runoff threshold. The runoff threshold value accounts for the effects of surface storage, the dynamic evolution of soil crusting as well as moisture storage within the upper soil layers. In addition to the runoff threshold, two further components determine the erosion estimates: erosion potential and erodibility (Kirkby et al., 2003). Allowance is made for snow accumulation, melting and frozen ground development, using a set of accumulated day-degree terms based on daily temperature data (mean, maximum and minimum). Finally, sediment transport is calculated as

$$S = k q^2 G \quad (1)$$

where k is the soil erodibility, q is the overland flow discharge per unit width and G is the local slope gradient. For more details on the model concept see Kirkby et al. (2003). The climate input parameters of the model are incorporated on a monthly basis for the period of 1986–2007 (corresponding to the time-frame of the Cs-137 method). The monthly outputs were averaged for the according period. The potential evaporation was calculated based on daily mean values of relative humidity, air temperature, global radiation and wind speed using the Penman equation (Penman, 1948). PESERA-VBA offers five soil type categories. We chose medium soil texture (18% < clay < 35% and $\geq 15\%$ sand, or 18% < clay and 15% < sand < 65%) for all our sites. The topography of the single slopes was described by slope angle and curvature. Land use type was set to pasture considering the respective FVC. The ground truth FVC was determined in September 2007 with a mesh of 1 m² (grid size of 0.1 m²). The FVC of each mesh was visually estimated and averaged for the entire square meter. This procedure was repeated 4 times for each slope. The maximum standard deviation was $\sim 5\%$ (Konz et al., 2009b).

3.1.2. Parameters for the soil erosion model USLE

The USLE is given as

$$A = R \times K \times LS \times C \times P \quad (2)$$

where A is the predicted average annual soil loss (t ha^{−1} a^{−1}). R is rainfall-runoff-erosivity factor (N h^{−1}) that quantifies the effects of raindrop impact and reflects the rate of runoff likely to be associated with the rain (Wischmeier and Smith, 1978). The soil erodibility factor K (t h a h MJ^{−1} ha^{−1} mm^{−1}) reflects the ease with which the soil is detached by impact of a splash or surface flow. The parameter LS (dimensionless) accounts for the effect of slope length (L) and slope gradient (S) on soil erosion. The C factor is the cover factor, which represents the effects of all interrelated cover and management variables (Renard et al., 1997). Published values of C (dimensionless) vary from 0.0005 for forest areas with 100% ground cover to 1 for bare soil areas (US Department of Agriculture, 1977). The P factor (dimensionless) is the support practice factor (Wischmeier and Smith, 1978), which is set to 1 because there are no erosion control practices in the study site. The R , K , LS factor basically determine the erosion volume while the C and P factor are reduction factors ranging between 0 and 1.

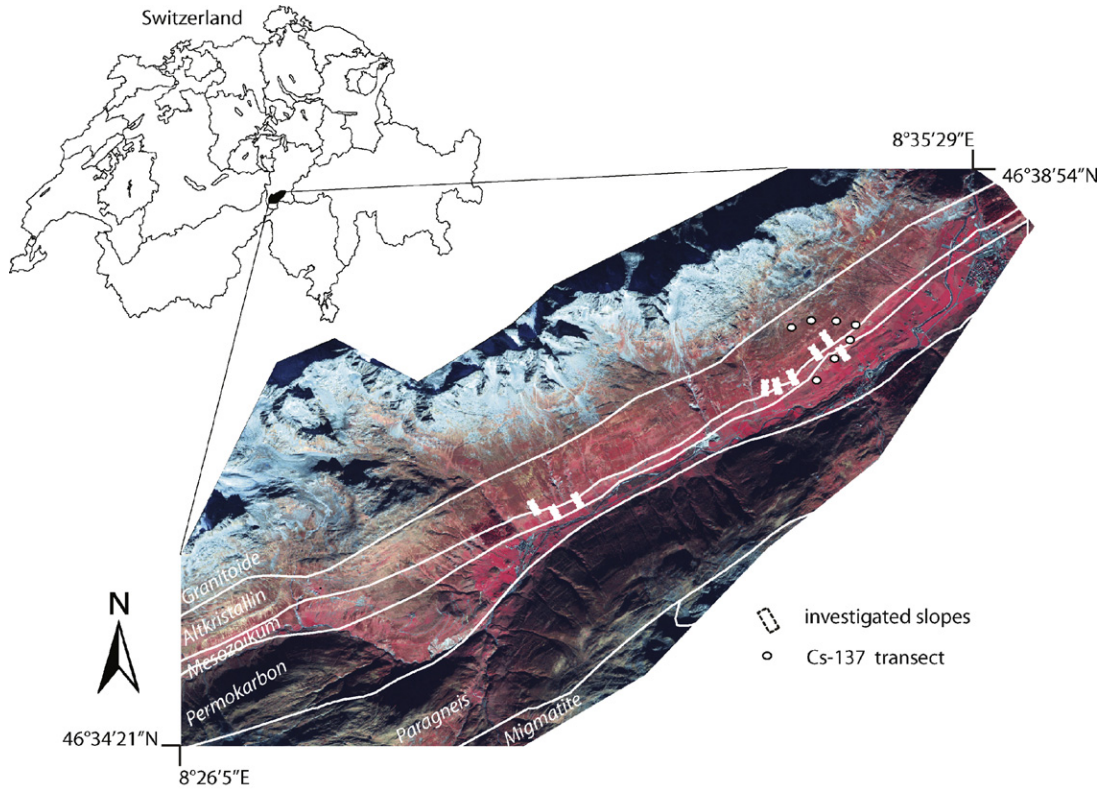


Fig. 1. Geographic location of the QuickBird image (false colour). The white lines separate different geologic formations, the white dots show the locations of the Cs-137 elevation transect and the white rectangles are the slopes used for the model evaluation.

Typically, rainfall erosivity (R) is computed as total storm energy (MJ m^{-2}) multiplied by the maximum 30-min intensity (mm h^{-1}) (Renard et al., 1997). Detailed data on storm intensity is available only for a limited time span (2006–2008), necessitating the use of approximation methods. We used the algorithm of Rogler and Schwertmann (1981) for the determination of the R factor, because the equation was designed for a comparable geographical and meteorological situation in the Bavarian Alps. Rogler and Schwertmann (1981) calculate R as

$$R_r = 0.083 \times N - 1.77 \quad (3)$$

where R_r is the rainfall-runoff factor ($\text{kg m s}^{-2} \text{h}^{-1}$) and N the average annual rainfall (mm). In the Alps some of the precipitation falls as snow, which reduces R factor values. According to Schuepp (1975) the relation between elevation (m a.s.l.) and proportion of snow is

$$f(x) = 0.0264 \times \text{elevation} - 2.0663 \quad (4)$$

The combined equation for the R factor is

$$R = 0.083 \times N \times \left(1 - \frac{0.0264 \times \text{elevation} - 2.0663}{100}\right) - 1.77 \quad (5)$$

The elevation map was derived from the DEM (25 m grid; vertical accuracy in the Alps of ± 3 m (Swisstopo, 2006)). The mean annual precipitation map was derived through inverse distance weighted interpolation of 1 km grid values of the HADES (©Hydrological Atlas of Switzerland, Swiss Federal Office for the Environment).

The soil erodibility factor K ($\text{t ha MJ}^{-1} \text{mm}^{-1}$) was calculated according to Wischmeier and Smith (1978). The calculation of the K factor requires four parameters:

$$K = (27.66 \times m^{1.14} \times 10^{-8} \times (12 - a)) + (0.0043 \times (b - 2)) + (0.0033 \times (c - 3)) \quad (6)$$

in which $m = (\text{silt } (\%) + \text{very fine sand } (\%) \times (100 - \text{clay } (\%)))$, $a = \text{organic matter } (\%)$, $b = \text{structure code: (1) very structured or particulate, (2) fairly structured, (3) slightly structured and (4) solid}$ and $c = \text{profile permeability code: (1) rapid, (2) moderate to rapid, (3) moderate, (4) moderate to slow, (5) slow and (6) very slow}$. Grain size analysis of the upper 10 cm was done for 52 samples at 18 locations with a sedigraph (5100 micromeritics). The organic matter map was derived from measurement of total carbon content at 23 soil profiles with a depth of 40 cm with a Leco CHN analyzer 1000. Measurement reproducibility was better than 0.1%. For the determination of the K factor the values of the upper 10 cm are used.

The C factor was parameterised by assigning a uniform value to each land-cover class. For grassland areas parameterisation was done according to the description of the US Department of Agriculture (1977). A more detailed description is presented in Section 3.2.

The LS factor (dimensionless) was calculated with the DEM according to the procedure described in Renard et al. (1997) because it is also valid for steep slopes between 22% (12.4°) and 56% (29.3°).

In addition, to the application of USLE for the nine slope sections, a parameterisation was done for the entire catchment. Therefore the point measurements needed to be regionalised.

3.1.3. Regionalisation of the USLE parameters to catchment scale

For the K factor, spatial estimates of grain size distribution were derived by assigning the mean value of soil samples within a geologic formation to the entire geologic formation. The geologic map was created based on the definition of geologic formations by Labhart (1999) that was refined by field and air photograph mapping. Using ANOVA we found that organic matter content significantly differs between upland and wetland soils. Thus, we mapped the distribution of organic matter via the occurrence of wetland areas.

Table 1

C factors used for specific land-cover classes (US Department of Agriculture, 1977) for the low resolution land-cover dataset and the QuickBird derived data.

| Land-cover type | C factor for the low resolution dataset | C factor |
|---|---|------------------|
| Bare soil | ^a 0.002 | 0.45 |
| Dwarf-shrub | ^a 0.002 | 0.011 |
| Shrub | 0.003 | 0.003 |
| Grassland | 0.002 | Depending on FVC |
| Forest | 0.0005 | 0.0005 |
| Rock, snow, non-photosynthetic vegetation | 0 | 0 |

^a According land-cover class is not existent, thus, the C factors for grassland were assigned.

The latter was done by selecting all areas with a topographic wetness index > 50 and a slope angle < 8°. The wetland map was verified by comparison to an orthophoto of the study site. Soils above 2000 m.a.s.l. were assumed to exceed organic matter contents of 12% as was found for soil samples in the study site as well as for other alpine regions (Egli et al., 2005; Leifeld et al., 2008). The soil structure parameter map consisted of two categories: for the Mesozoic formation with clayey soils, we set a class value of 3 (lumpy) for all other areas, we used the value 1 (granular). For the profile permeability, we used three categories 1 (rapid) for the alluvium at the valley bottom and debris fans, 5 (slow) for the Mesozoic formation and (2) moderate to rapid for the remaining areas. Structure code and profile permeability code were regionalised with the geomorphology and geology map. The geomorphologic map was generated based on a Quaternary map with a scale of 1:33,000 (Fehr, 1926) and the orthophoto. All data layers were created using ArcGIS (ESRI) version 9.2.

3.2. QuickBird data for vegetation parameterisation

High resolution multispectral QuickBird imagery (pixel resolution = 2.4 m) was used to improve the parameterisation of vegetation. QuickBird standard imagery was acquired on October 17, 2006 (10:51 UTC), under clear sky conditions, over a 67 km² area. The imagery was radiometrically and geo-corrected by the satellite data providers with a published spatial accuracy of 14 m root mean square error (RMSE). Orographic illumination effects

Table 2

Used datasets (*npv, non-photosynthetic vegetation).

| Data type | Model parameters | Source | Samples (n) |
|------------|--|---|---|
| Topography | LS factor map (USLE: plot, catchment) Slope angle (PESERA-VBA) | DEM ©swisstopo | – |
| Climate | R factor map (USLE: plot, catchment) | DEM, mean precipitation data ©Hydrological Atlas of Switzerland Daily climate data of MeteoSwiss: | – |
| Soil | Monthly climate data: precipitation, temperature, pot. evaporation (PESERA-VBA) K factor (USLE: plot) K factor map (USLE: catchment) | Plot grain size analysis Plot organic matter content DEM (topographic wetness index, slope, elevation) Grain size analysis Organic matter content | 9 (3–5 replicates) 9 (3 replicates) 9 (composite sample) 14 (5 replicates) |
| Vegetation | C factor map (USLE: catchment) Land-cover map (USLE: catchment) LSU FVC map (USLE: plot, catchment, PESERA-VBA) Ground truth FVC (USLE: plot, PESERA-VBA) | VECTOR25 dataset ©swisstopo QuickBird imagery QuickBird imagery field measurement | – – – 9 (4 replicates) |
| Evaluation | Cs-137 erosion estimates (USLE: plot, PESERA-VBA) Cs-137 activities (USLE: catchment) | in situ measurement laboratory measurement | 9 (3 replicates) 7 (3 replicates) |

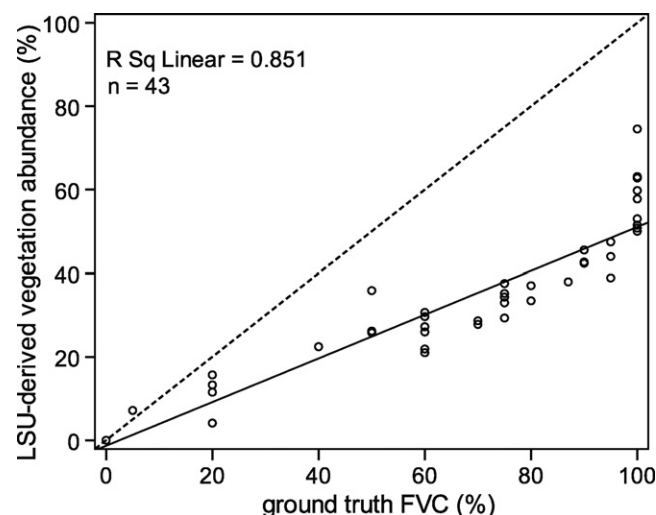


Fig. 2. Scatter plot of LSU-derived vegetation abundances versus the ground truth fractional vegetation cover. Linear regression line is shown.

were corrected using a DEM (25 m grid; ±3 m vertical accuracy in the Alps) and the TOPOCOR module of the Atcor3 software package (Richter, 2005).

Two datasets relevant for vegetation parameterisation result from the analysis of QuickBird imagery, a land-cover map and a FVC map. The land-cover map consists of nine categories: forest, shrub, dwarf-shrub, grassland, non-photosynthetic vegetation, snow, water, bare soil, rock and the artificial category shadow. The overall classification accuracy is 93.3%. In total, 0.81% of the dataset is unclassified. The land-cover classes of bare soil, grassland, rock, snow, water, forest, and shadow have high classification accuracies (82–100%), while classes of dwarf-shrub, shrub, and non-photosynthetic vegetation have lower classification accuracies (67–78%).

The FVC map for the grassland areas was generated by linear spectral unmixing (LSU) of the grassland areas using the endmembers bare soil, grassland and shadow. The resultant vegetation abundance showed significant correlation to ground truth (GT) FVC (Fig. 2) The regression between the 43 ground truth FVC and Quick-

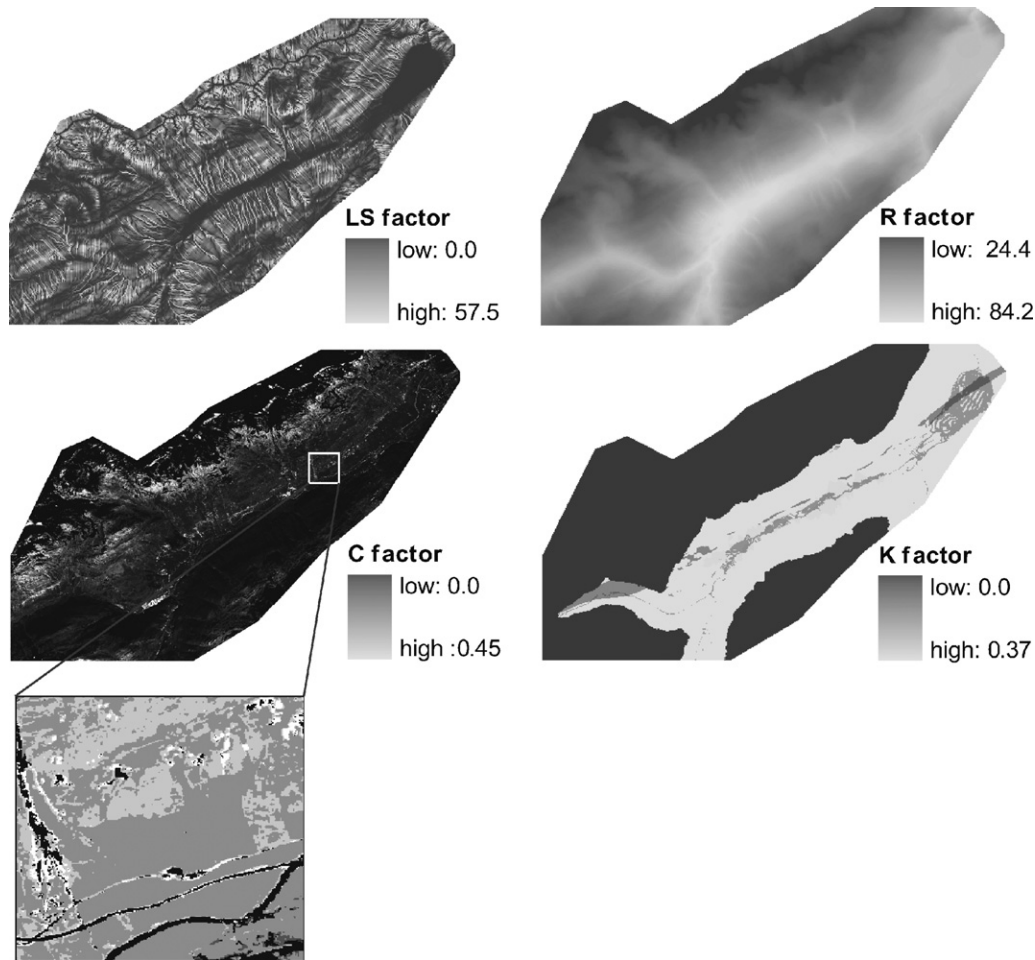


Fig. 3. USLE input factor maps (LS-, R-, K-factor and LSU-derived C factor) and an enlargement for the LSU-derived C factor.

Bird derived vegetation abundance points is given by

$$FVC(GT) = 1.63 \times FVC(LSU) + 12.20 \quad (7)$$

With a coefficient of determination of $r^2 = 0.85$. The mean RMSE value for the image is 0.52. For a detailed description of the analysis see Meusburger et al. (2010, this volume).

Except for the land-cover class grassland uniform C factors are used for single land-cover classes derived from the QuickBird classification. For the land-cover class “grassland”, the following equation was used to implement the FVC (US Department of Agriculture, 1977):

$$C = 0.45 \times e^{-0.0456 \times cv} \quad (8)$$

where cv is the “cover that contacts the surface”. We assume that for grassland cv equals FVC. We will refer to this map as LSU-derived C factor map in the following. The resulting C factors are shown in Table 1 together with the values of the low resolution dataset.

For the application of USLE on catchment scale, comparative analysis of soil erosion estimates between the low resolution land-cover input data (uniform C factors are used for single land-cover classes) and high resolution satellite-derived land-cover data (considering FVC for grassland areas) was conducted (see below). The land-cover dataset (where we will refer to as the “low resolution dataset”) is based on the VECTOR25 dataset available at Swisstopo with a scale of 1:25,000. We used a raster-

based approach for the modelling of soil erosion with a pixel resolution of 25 m for the low resolution dataset and a pixel resolution of 2.4 m equal to the spatial resolution of the QuickBird image.

3.3. Cs-137 measurements

Soil erosion rates estimated with PESERA-VBA and USLE were compared to erosion rates derived from in situ measurements of Cs-137 with a sodium-iodide (NaI) detector 2×2 in. (Sarad, Germany; efficiency at 661 keV is $1.4 \text{ s}^{-1}/(\mu\text{Sv h}^{-1})$). The detector was mounted perpendicular to the ground on a height of 25 cm. Cs-137 concentration was measured for 1 h with 3 replicates per slope section. Spectra evaluation was done with software provided by H. Surbeck, University of Neuchâtel (Switzerland). All measured Cs-137 activities refer to 2007. The mean error for the erosion estimates resulting from analytics and data evaluation is $\pm 30\%$ (Konz et al., 2009b).

To evaluate the USLE estimates for the catchment seven additional Cs-137 measurements (with 3 replicates) along an elevation gradient were done. Here, only the Cs-137 activity of soil samples (upper 10 cm) was determined with a Li-drifted Ge-detector and InterWinner5 gamma spectroscopy software (Schaub et al., 2010). Spearman correlation was used to compare modelled erosion estimates with the Cs-137 activity. For all statistic analysis the software

SPSS was used (SPSS, 2009). A list of the used data is presented in Table 2.

4. Results and discussion

4.1. Comparison of USLE and PESERA-VBA at plot scale

The mean erosion estimates for the nine plots and the four test runs using PESERA-VBA and USLE are shown in Table 3 (columns 3–6) together with the soil erosion estimates from in situ Cs-137 measurements (column 2). PESERA-VBA distinguishes only between 6 soil texture classes and 12 land use types, which is limiting the spatial differentiation. This is especially true for our sites that differ in soil texture, land use and FVC, of which only differences in FVC could be considered. Thus, we will only compare mean values of the nine slopes. The mean erosion rate resulting from in situ Cs-137 measurements is $20.1 \pm 5.8 \text{ t ha}^{-1} \text{ a}^{-1}$. Both models underestimate the Cs-137 derived soil erosion estimates in all runs. With field measured data (column 3), the USLE estimate is $9.6 \text{ t ha}^{-1} \text{ a}^{-1}$, which is only half of Cs-137 based erosion rates. PESERA-VBA computed a soil erosion rate of $0.37 \text{ t ha}^{-1} \text{ a}^{-1}$, which is approximately 50 times less. PESERA-VBA estimates of erosion rates are far too low even with 0% FVC (column 5). Using 100% FVC (column 4), which is done in most soil erosion modelling studies, both models underestimate erosion rates modelled with field measured input data by almost a magnitude (an underestimation of $8.2 \text{ t ha}^{-1} \text{ a}^{-1}$ (85%) and $0.05 \text{ t ha}^{-1} \text{ a}^{-1}$ (86%) for the USLE and the PESERA-VBA, respectively). By introducing the LSU-derived FVC (column 6), the modelled erosion rates of both models approximate the modelled values based on the field measured vegetation cover but still underestimate Cs-137 derived soil erosion rates.

The deviation between the Cs-137 and modelled soil erosion values is high. USLE does not account for winter processes such as snow gliding, snow ablation, avalanches and snowmelt. The latter processes have been discussed as potentially being the crucial confounding factors for soil erosion in the Urseren Valley (Konz et al., 2009a). Surprisingly the deviation is even higher for PESERA-VBA, although snow accumulation and snowmelt are considered and peak erosion occurs in May during snowmelt. The main reason might be the lower sensitivity of PESERA-VBA to changes in FVC, which results in a very small range of erosion estimates between $0.05 \text{ t ha}^{-1} \text{ a}^{-1}$ for 0% FVC and $2.9 \text{ t ha}^{-1} \text{ a}^{-1}$ for 100% FVC. Sprinkling experiments at the sites have shown that 100% FVC almost prevents soil erosion (Merz et al., 2009), which is in accordance with PESERA-VBA. For 0% FVC, on sites with silty-loamy sands and an average slope angle of 37° , higher soil erosion rates are expected. Another possible reason for the underestimation of soil erosion rates for sites with low FVC might be a low erosivity resulting from monthly averaged climate input data in the PESERA-VBA that smoothes out extreme events. Even though a coefficient of variation for the monthly precipitation is considered its impact on soil erosion estimates is low. The empirical USLE Eq. (8) where the impact of FVC is implemented via the C factor seems more suitable than the vegetation growing module of PESERA-VBA at our site. An exponential relationship ($r^2 = 0.93$), similar to the empirical USLE equation, between sediment yield and FVC was found for sprinkling experiments in the valley (Schindler et al., submitted for publication). Moreover, the empirical factors of the USLE equation are based on long-term average values (including extreme events) and the used R and LS factor are adapted to mountainous areas which might explain the higher soil erosion estimates. In general, USLE estimates are closer to the range of measured erosion rates by the

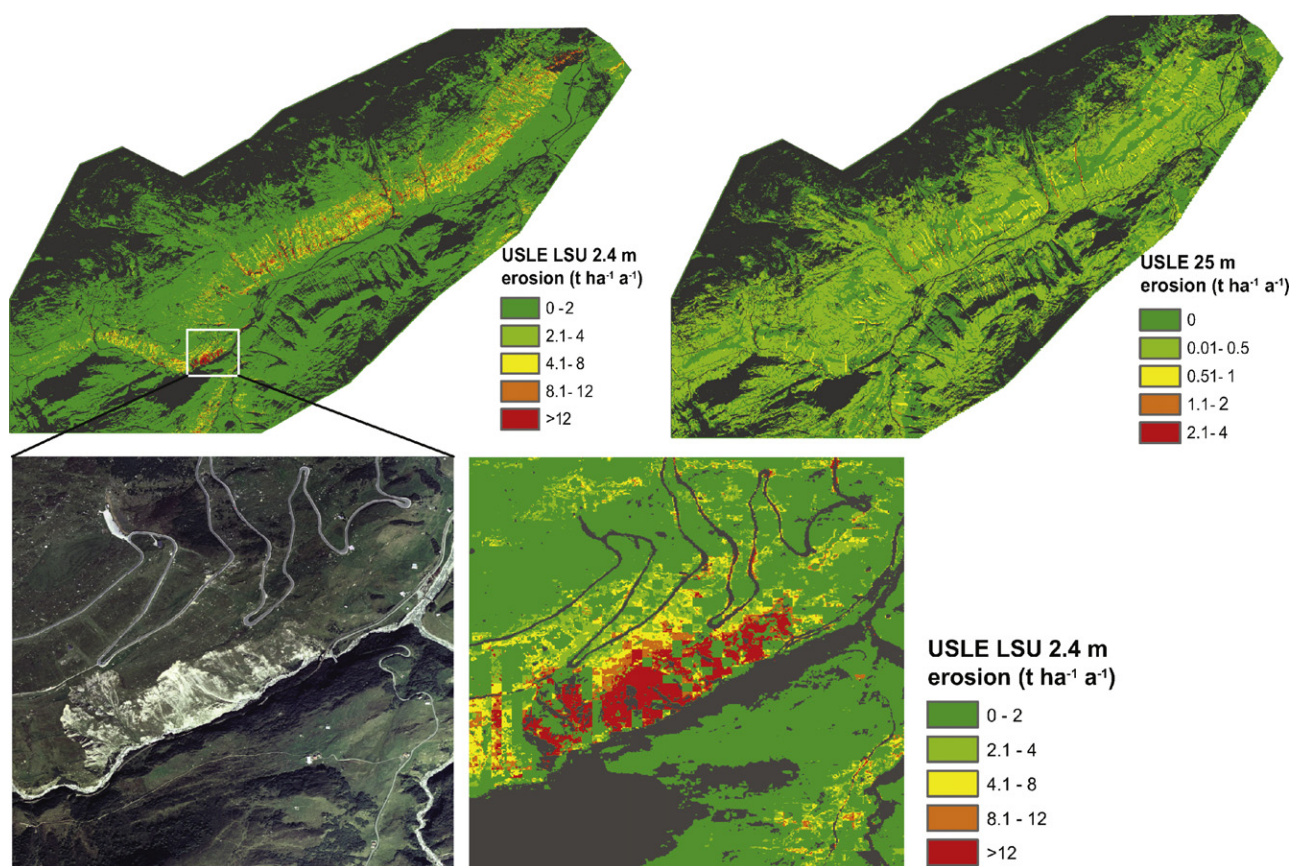


Fig. 4. Estimated soil loss ($\text{t ha}^{-1} \text{ a}^{-1}$) by USLE calculated with the low resolution C factor map (based on the swisstopo land-cover dataset) and the C factor based on the QuickBird derived vegetation data. Below: a visible comparison between the high resolved USLE soil erosion map and the pan-sharpened QuickBird image.

Table 3

Comparison between mean (nine slopes) Cs-137 derived soil erosion rates and mean estimates ($\text{t ha}^{-1} \text{a}^{-1}$) of USLE and PESERA for four different model runs with (1) field measured input data at plot scale, (2) 100% FVC, (3) 0% FVC and (4) LSU-derived FVC.

| Model | Cs-137 erosion estimates | (1) Measured data | (2) 100% FVC | (3) 0% FVC | (4) LSU-derived FVC |
|------------|--------------------------|-------------------|--------------|------------|---------------------|
| USLE | 20.1 ± 5.8 | 9.6 | 1.4 | 201.6 | 11.4 |
| PESERA-VBA | 20.1 ± 5.8 | 0.37 | 0.05 | 2.9 | 0.38 |

Cs-137 method and to visually observed erosion features. Further it showed a high dependency on FVC, which is a decisive parameter in alpine regions (Isselin-Nondedeu and Bedecarrats, 2007).

4.2. USLE erosion estimates for the entire catchment

Grain size analysis for the nine slope sections (with 3–5 replicates each) showed no significant differences between slopes. Mean values are $37.86 \pm 1.10\%$ sand, $48.25 \pm 1.18\%$ silt and $13.09 \pm 0.41\%$ clay. Total carbon content of upland soils is $3.49 \pm 0.17\%$ ($n = 121$) and $24.85 \pm 1.48\%$ ($n = 107$) for wetland soils (note that most wetland soils are influenced by sedimentation of mineral soil particles thus decreasing organic matter content). For the spatial mapping of organic matter content, we worked with two groups: 24.9% for wetlands and 3.5% for the remaining areas. The produced input parameter maps for USLE are displayed in Fig. 3.

K factor values range from 0.0 to $0.368 \text{ t ha MJ}^{-1} \text{ mm}^{-1}$ with the lowest values in elevated areas where skeleton- and organic matter content is high. The values for R range from 24.4 to 84.2 N h^{-1} with the lowest values for elevated areas due to the increasing proportion of snowfall. The LS factor map clearly displays the channel network, where the highest values of about 57.5 are observed in the channels. The LSU-derived C factors are highest for bare soil areas, which are mainly located at the south exposed slope and low for rock outcrops that have no erosion potential (see enlargement in Fig. 3).

The predicted soil erosion estimates are categorized into five classes (Fig. 4). The land-cover types shadow, snow and rock are displayed in black. With the C factor based on the low resolution dataset highest soil erosion values are about $2.8 \text{ t ha}^{-1} \text{a}^{-1}$ and the mean modelled erosion rate for the entire catchment is $0.08 \text{ t ha}^{-1} \text{a}^{-1}$. Highest values are found along the channels in the catchment. The areas in between are characterised by very low erosion rates $< 0.5 \text{ t ha}^{-1} \text{a}^{-1}$. Thus, the former soil erosion map mainly displays the pattern of the LS factor map. The erosion estimates produced with the LSU-derived C factor map range from 0.0 to $16 \text{ t ha}^{-1} \text{a}^{-1}$ with a mean erosion of $1.18 \text{ t ha}^{-1} \text{a}^{-1}$. High erosion rates are concentrated on the south exposed slopes where grassland cover is scarce due to pasturing and at landslides (Meusburger and Alewell, 2009). The highest values occur at spots of bare soil located along rivers, roads and landslides (Fig. 4, lower part). Thus, by visual evaluation of the produced maps the satellite data assisted map is plausible.

In addition, model estimates are compared to Cs-137 activities for seven locations. The Spearman's rank correlation between LSU-assisted USLE outputs and Cs-137 activity is $r = -0.71$ ($n = 7$). For the USLE map based on the low resolution dataset a correlation coefficient of $r = -0.43$ ($n = 7$) is observed. The correlation is negative because the Cs-137 activity is higher with less soil erosion (Sawhney, 1972). Both correlations are not significant due to the small number of sampled locations ($n = 7$ with 3 replicates).

Generally the evaluation with Cs-137 measurements showed that using the LSU-derived C factor increased the correspondence between measured Cs-137 activity and modelled values of soil erosion. Both Cs-137 and USLE give long-term erosion estimates, which

makes the combination of the two methods very suitable. Furthermore, the high resolution input data allows for allocation of field measurements and observed erosion features. This is a necessary requirement in order to validate produced erosion estimates.

5. Conclusion and outlook

Even though USLE is an empirically based model and was not designed for the application in alpine environments the magnitude of erosion estimates seem more plausible than PESERA-VBA derived rates. This might be due to the suitability and high impact of the C factor to overall model outputs at our sites. Several other erosion models also apply this C factor such as the Morgan and Finney method (Morgan et al., 1984), WEPP (NSERL, 1995), ANSWERS (Beasley et al., 1980), SEMMED (De Jong and Riezebos, 1997) and PCARES (Panigbatan, 2001). Thus, improved C factor mapping using remote sensing can provide crucial information to improve spatial soil erosion modelling. PESERA-VBA under estimate the importance and influence of vegetation cover on soil erosion in alpine grasslands.

The QuickBird data could decisively improve vegetation input data for soil erosion risk mapping. On catchment scale (using USLE and high resolution vegetation data), "hotspots" of soil erosion were identified, which allows for more effective soil conservation planning. In addition to direct visual verification of the high resolution USLE map a comparison to soil erosion measurements in the field is possible, which is of crucial importance to validate and adapt soil erosion models. We conclude that even a "simple" empirical erosion model can strongly benefit from using spatial FVC information.

Generally, the suggested approach to model soil erosion with high resolution input data on the catchment scale seems to be promising especially with the perspective to validate the obtained soil erosion risk maps. Model validation is not only critical with respect to the spatial patterns of erosion estimates but also with respect to absolute erosion rates. Consequently, the main profit of high resolution data for soil erosion assessment lies in the ability to directly compare results to ground measurements while at the same time providing soil erosion estimates for entire catchments.

Acknowledgement

This study was funded by the Swiss Federal Office for the Environment (Contract No.: StoBoBio/810.3129.004/05/OX).

References

- Beasley, D.B., Huggins, L.F., Monke, E.J., 1980. ANSWERS—a model for watershed planning. *Transactions of the ASAE* 23, 938–944.
- Cernusca, A., Bahn, M., Chemini, C., Graber, W., Siegwolf, R., Tappeiner, U., Tenhunen, J., 1998. ECOMONT: a combined approach of field measurements and process-based modelling for assessing effects of land-use changes in mountain landscapes. *Ecological Modelling* 113, 167–178.
- De Asis, A.M., Omasa, K., 2007. Estimation of vegetation parameter for modeling soil erosion using linear Spectral Mixture Analysis of Landsat ETM data. *ISPRS Journal of Photogrammetry and Remote Sensing* 62, 309–324.
- De Asis, A.M., Omasa, K., Oki, K., Shimizu, Y., 2008. Accuracy and applicability of linear spectral unmixing in delineating potential erosion areas in tropical watersheds. *International Journal of Remote Sensing* 29, 4151–4171.

- De Jong, S.M., 1994. Derivation of vegetative variables from a landsat TM image for erosion modelling. *Earth Surface Processes and Landforms* 19, 165–178.
- De Jong, S.M., Paracchini, M.L., Bertolo, F., Folving, S., Megier, J., De Roo, A.P.J., 1999. Regional assessment of soil erosion using the distributed model SEMMED and remotely sensed data. *Catena* 37, 291–308.
- De Jong, S.M., Riezebos, H.T., 1997. SEMMED: a distributed approach to soil erosion modeling. In: Spiteri, A. (Ed.), *Remote Sensing '96*. Rotterdam.
- Desmet, P.J.J., Govers, G., 1996. A GIS procedure for automatically calculating the USLE LS factor on topographically complex landscape units. *Journal of Soil and Water Conservation* 51, 427–433.
- Egli, M., Margreth, M., Vökt, U., Fitze, P., Tognina, G., Keller, F., 2005. Modellierung von Bodentypen und Bodeneigenschaften im Oberengadin (Schweiz) mit Hilfe eines Geographischen Informationssystems (GIS). *Geographica Helvetica* 2, 87–97.
- Gobin, A., Jones, R., Kirkby, M., Campling, P., Govers, G., Kosmas, C., Gentile, A.R., 2004. Indicators for pan-European assessment and monitoring of soil erosion by water. *Environmental Science & Policy* 7, 25–38.
- He, Q., Walling, D.E., 2000. Calibration of a field-portable gamma detector to obtain in situ measurements of the ¹³⁷Cs inventories of cultivated soils and floodplain sediments. *Applied Radiation and Isotopes* 52, 865–872.
- Helming, K., Auzet, A.V., Favis-Mortlock, D., 2005. Soil erosion patterns: evolution, spatio-temporal dynamics and connectivity. *Earth Surface Processes and Landforms* 30, 131–132.
- Isselin-Nondedeu, F., Bedecarrats, A., 2007. Influence of alpine plants growing on steep slopes on sediment trapping and transport by runoff. *Catena* 71, 330–339.
- Jain, S.K., Singh, P., Seth, S.M., 2002. Assessment of sedimentation in Bhakra Reservoir in the western Himalayan region using remotely sensed data. *Hydrological Sciences Journal* 47, 203–212.
- Jetten, V., Govers, G., Hessel, R., 2003. Erosion models: quality of spatial predictions. *Hydrological Processes* 17, 887–900.
- Kirkby, M., Robert, J., Irvine, B., Gobin, A., Govers, G., Cerdan, O., Tompaey, A., Le Bissonnais, Y., Daroussin, J., King, D., Montanarella, L., Grimm, M., Vieillefont, V., Puigdefabregas, J., Boer, M., Kosmas, C., Yassoglou, N., Tsara, M., Mantel, S., Van Lynden, G., Hunting, J., 2003. Pan-European Soil Erosion Risk Assessment. Joint Research Centre, ISPRA.
- Kirkby, M.J., Le Bissonnais, Y., Coulthard, T.J., Daroussin, J., McMahon, M.D., 2000. The development of land quality indicators for soil degradation by water erosion. *Agriculture, Ecosystems & Environment* 81, 125–135.
- Konz, N., Bänninger, D., Nearing, M., Alewell, C., 2009a. Does WEPP meet the specificity of soil erosion in steep mountain regions? *Hydrology and Earth System Sciences Discussion* 6, 2153–2188.
- Konz, N., Schaub, M., Prasuhn, V., Bänninger, D., Alewell, C., 2009b. Cesium-137-based erosion-rate determination of a steep mountainous region. *Journal of Plant Nutrition and Soil Science* 172, 615–622.
- Leifeld, J., Zimmermann, M., Fuhrer, J., Conen, F., 2008. Storage and turnover of carbon in grassland soils along an elevation gradient in the Swiss Alps. *Global Change Biology*, doi:10.1111/j.1365-2486.2008.01782.x.
- Liu, J.G., Mason, P., Hilton, F., Lee, H., 2004. Detection of rapid erosion in SE Spain: a GIS approach based on ERS SAR coherence imagery. *Photogrammetric Engineering and Remote Sensing* 70, 1179–1185.
- Merz, A., Alewell, C., Hiltbrunner, E., Bänninger, D., 2009. Plant-compositional effects on surface runoff and sediment yield in subalpine grassland. *Journal of Plant Nutrition and Soil Science*, 9999, NA.
- Meusburger, K., Alewell, C., 2008. Impacts of anthropogenic and environmental factors on the occurrence of shallow landslides in an alpine catchment (Urseren Valley, Switzerland). *Natural Hazards and Earth System Sciences* 8, 509–520.
- Meusburger, K., Alewell, C., 2009. On the influence of temporal change on the validity of landslide susceptibility maps. *Natural Hazards and Earth System Sciences* 9, 1495–1507.
- Meusburger, K., Bänninger, D., Alewell, C., 2010. Estimating vegetation parameter for soil erosion assessment in an alpine catchment by means of QuickBird imagery. *International Journal of Applied Earth Observation and Geoinformation* 12, 201–207.
- Morgan, R.P.C., Morgan, D.D.V., Finney, H.J., 1984. A predictive model for the assessment of soil-erosion risk. *Journal of Agricultural Engineering Research* 30, 245–253.
- NSERL, 1995. USDA-Water Erosion Prediction Project. Hillslope Profile and Watershed Model Documentation. National Soil Erosion Research Laboratory, West Lafayette.
- Paninbatan, E.P., 2001. Geographic information system-assisted dynamic modeling of soil erosion and hydrologic processes at a watershed scale. *Philippine Agricultural Scientist* 84, 388–393.
- Penman, H.L., 1948. Natural evaporation from open water, bare and grass. *Proceedings of the Royal Society of London Series A* 193, 120–145.
- Renard, K.G., Foster, G.R., Weesies, G.A., 1997. Predicting soil erosion by water: a guide to conservation planning with the revised universal soil loss equation (RUSLE). *Agriculture Handbook No. 703*, USDA-ARS.
- Reusing, M., Schneider, T., Ammer, U., 2000. Modelling soil loss rates in the Ethiopian highlands by integration of high resolution MOMS-02/D2-stereo-data in a GIS. *International Journal of Remote Sensing* 21, 1885–1896.
- Richter, R., 2005. Atmospheric/Topographic Correction for Satellite Imagery. Atcor 2/3 User Guide. Version 6.1. Wessling, Germany.
- Ritchie, J.C., McHenry, J.R., 1990. Application of radioactive fallout Cesium-137 for measuring soil-erosion and sediment accumulation rates and patterns—a review. *Journal of Environmental Quality* 19, 215–233.
- Rogler, H., Schwertmann, U., 1981. Rainfall erosivity and isoelement map of Bavaria. *Zeitschrift für Kulturtechnik und Flurbereinigung* 22, 99–112.
- Sawhney, B.L., 1972. Selective sorption and fixation of cations by clay-minerals—review. *Clays and Clay Minerals* 20, 93–100.
- Schaub, M., Konz, N., Meusburger, K., Alewell, C., 2010. Application of in-situ measurement to determine ¹³⁷Cs in the Swiss Alps. *Journal of Environmental Radioactivity*, doi:10.1016/j.jenvrad.2010.02.005.
- Schindler, Y., Alewell, C., Burri, K., Bänninger, D. submitted for publication. Evaluation of a small hybrid rainfall simulator and its application to quantify water erosion on subalpine grassland. *Plant and Soil*.
- Schuepp, M., 1975. Objective weather forecasts using statistical aids in Alps. *Rivista Italiana Di Geofisica E Scienze Affini* 1, 32–36.
- SPSS, 2009. SPSS for Windows 15.0, Rel. 11.0.1. 2001. SPSS Inc., Chicago.
- Swisstopo, 2006. Reproduziert mit Bewilligung von swisstopo.
- Thiam, A.K., 2003. The causes and spatial pattern of land degradation risk in southern Mauritania using multitemporal AVHRR-NDVI imagery and field data. *Land Degradation & Development* 14, 133–142.
- Tweddles, S.C., Eschlaeger, C.R., Seybold, W.F., 2000. An Improved Method for Spatial Extrapolation of Vegetative Cover Estimates (USLE/RUSLE C factor) Using LCTA and Remotely Sensed Imagery. USAEC Report No. SFIM-AEC-EQ-TR-200011, ERDC/CERL TR-00-7, CERL. US Army of Engineer Research and Development Center, Champaign, IL.
- US Department of Agriculture, S.C.S., 1977. Procedure for Computing Sheet and Rill Erosion on Project Areas. Soil Conservation Service, Technical Release No. 51 (Rev. 2).
- Van Rompaey, A.J.J., Bazzoffi, P., Jones, R.J.A., Montanarella, L., Govers, J., 2003a. Validation of Soil Erosion Risk Assessment in Italy. European Commission, Joint Research Centre, Luxembourg.
- Van Rompaey, A.J.J., Vieillefont, V., Jones, R.J.A., Montanarella, L., Verstraeten, G., Bazzoffi, P., Dostal, T., Krassa, J., de Vente, J., Poesen, J., 2003b. Validation of Soil Erosion Estimates at European Scale. European Soil Bureau Research Report No. 13, Luxembourg.
- Walling, D.E., He, Q., Blake, W., 1999. Use of Be-7 and Cs-137 measurements to document short- and medium-term rates of water-induced soil erosion on agricultural land. *Water Resources Research* 35, 3865–3874.
- Wilson, J.P., Gallant, J.C., 1996. EROS: a grid-based program for estimating spatially distributed erosion indices. *Computers & Geosciences* 22, 707–712.
- Wischmeier, W.H., Smith, D.D., 1978. Predicting Rainfall Erosion Losses—A Guide to Conservation Planning. *Agric. Handbook No. 537*, Washington, D.C.
- WRB, 2006. IUSS Working Group World Reference Base for Soil Resources. Food and Agriculture Organization of the United Nations, Rom.

Further reading

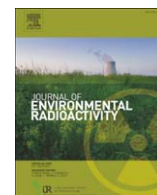
Web References

- BAFU, 2009. BAFU: Hydrological Foundations and Data. Real Time and Historical Data. Swiss Federal Environmental Agency, <http://www.hydrodaten.admin.ch/d/2087.htm> (accessed date 7.1.09).
- Joint Research Center Ispra, 2009a. Nature and extend of soil erosion in Europe. Commiss European Communities, http://eussoils.jrc.it/ESDB_Archive/pesera/pesera.cd/sect.2.2.htm (accessed date: 7.1.09).
- Joint Research Center Ispra. 2009. Soil erosion in the Alps (RUSLE) <<http://eussoils.jrc.ec.europa.eu/library/Themes/Erosion/ClimChalp/Rusle.html>> (accessed date: 7.1.09).

CHAPTER 7

Application of in-situ measurement to determine ^{137}Cs in the Swiss Alps

This chapter has been published in Journal of Environmental Radioactivity as:
Schaub, M., Konz, N., Meusbürger, K., Alewell, C.: *Application of in-situ measurement to determine ^{137}Cs in the Swiss Alps*, 101, 369-376, 2010.



Application of in-situ measurement to determine ^{137}Cs in the Swiss Alps

M. Schaub*, N. Konz¹, K. Meusbürger, C. Alewell

Institute of Environmental Geosciences, University of Basel, Bernoullistrasse 30, CH-4056 Basel, Switzerland

ARTICLE INFO

Article history:

Received 27 August 2009

Received in revised form

5 February 2010

Accepted 15 February 2010

Available online 21 March 2010

Keywords:

Nal detector

GeLi detector

Alps

In-situ measurements

Field application

ABSTRACT

Establishment of ^{137}Cs inventories is often used to gain information on soil stability. The latter is crucial in mountain systems, where ecosystem stability is tightly connected to soil stability. In-situ measurements of ^{137}Cs in steep alpine environments are scarce. Most studies have been carried out in arable lands and with Germanium (Ge) detectors. Sodium Iodide (NaI) detector system is an inexpensive and easy to handle field instrument, but its validity on steep alpine environments has not been tested yet. In this study, a comparison of laboratory measurements with GeLi detector and in-situ measurements with NaI detector of ^{137}Cs gamma soil radiation has been done in an alpine catchment with high ^{137}Cs concentration (Urseren Valley, Switzerland). The aim of this study was to calibrate the in-situ NaI detector system for application on steep alpine slopes. Replicate samples from an altitudinal transect through the Urseren Valley, measured in the laboratory with a GeLi detector, showed a large variability in ^{137}Cs activities at a meter scale. This small-scale heterogeneity determined with the GeLi detector is smoothed out by uncollimated in-situ measurements with the NaI detector, which provides integrated estimates of ^{137}Cs within the field of view (3.1 m^2) of each measurement. There was no dependency of ^{137}Cs on pH, clay content and carbon content, but a close relationship was determined between measured ^{137}Cs activities and soil moisture. Thus, in-situ data must be corrected for soil moisture. Close correlation ($R^2 = 0.86$, $p < 0.0001$) was found for ^{137}Cs activities (in Bq kg^{-1}) estimated with in-situ (NaI detector) and laboratory (GeLi detector) methods. We thus concluded that the NaI detector system is a suitable tool for in-situ measurements in alpine environments. This paper describes the calibration of the NaI detector system for field application under elevated ^{137}Cs activities originating from Chernobyl fallout.

© 2010 Elsevier Ltd. All rights reserved.

1. Introduction

Mountain systems all over the world are unique in their ecology, economy and cultural diversity but at the same time seriously threatened by climate and land use change because of their high sensitivity. One inherent parameter of mountain ecosystem stability is the stability of their soils. Thus, methods to describe and predict soil stability in mountain systems are urgently needed (Alewell et al., 2008; Meusbürger and Alewell, 2009). The measurement of Caesium-137 (^{137}Cs) concentrations is often used to gain important information on the extent of soil erosion in areas where ^{137}Cs occurs either due to nuclear weapon testing and/or the Chernobyl reactor accident in 1986. After deposition, ^{137}Cs is rapidly

and tightly bound to soil fine particles. Redistribution is mainly caused by soil erosion where ^{137}Cs moves with soil particles (e.g. Bonnett, 1990; Ritchie and McHenry, 1990).

Measurement of ^{137}Cs can either be done in the laboratory or in-situ in the field. Advantages and disadvantages of field and laboratory applications of gamma detectors have already been discussed in detail (e.g. Beck et al., 1972; Miller and Shebell, 1993; He and Walling, 2000). Measurement time for in-situ measurements is generally shorter due to the coverage of a representative sampling area in the field which results in a better counting statistics in contrast to small volume soil samples in the laboratory (Table 1; Golosov et al., 2000; Beck et al., 1972). Comparability of in-situ and laboratory measurements has been shown before, but mainly for Ge detectors and/or on arable (mostly tilled) fields with low heterogeneity (Haugen, 1992; Agnesod et al., 2001; Tyler et al., 2001). In general, because of the good resolution of peaks in gamma spectra measured with Ge detectors, these are usually favoured over the NaI detectors whose spectra often show interference of neighbouring peaks (Table 1). However, for application in a mountain environment with difficult accessibility and steep slopes of up

* Corresponding author. Fax: +41 61 267 04 79.

E-mail address: monika.schaub@gmx.ch (M. Schaub).

¹ Present Address: Federal Department of Economic Affairs, Agroscope Reckenholz-Tänikon Research Station ART, Reckenholzstrasse 191, CH-8046 Zürich, Switzerland.

Table 1

Advantages and limitations of in-situ NaI, in-situ HPGe and laboratory Ge detector measurements for their use in our specific environment.

| | In-situ NaI | In-situ HPGe | Laboratory GeLi |
|----------------------|-----------------|-----------------|-----------------|
| Measurement geometry | Area | Area | Soil sample |
| Soil sampling | Non-destructive | Non-destructive | Destructive |
| Measurement time | ca. 1 h | ca. 1 h | ca. 8 h |
| Spectral resolution | Low | High | High |
| Portability | Light weight | Medium weight | Non-Portable |
| Cost | Low | High | High |

to 45°, priorities must be set differently from those of accessible areas and/or for arable lowland sites. Germanium detector systems are usually relatively heavy because of the need for cooling. In contrast to Ge detector systems, NaI detectors have the advantage that they are not only substantially lighter to transport, but also cheaper to purchase and operate (Table 1). However, the compromise is the reduction in spectral resolution that necessitates careful spectral processing (Table 1; Beck et al., 1972; ICRU, 1994). The aim of this study was to find a measurement routine with a NaI detector for mountain regions with high ^{137}Cs concentration which is rather quick and can be handled by one person in the field and which still achieves accurate results.

Knowledge about spatial distribution of ^{137}Cs is crucial not only for the determination of ^{137}Cs inventories but also for the use as a tracer of soil erosion. The vertical distribution of ^{137}Cs in arable soils is influenced by the tillage practice which results in a more or less homogeneous distribution of ^{137}Cs within the tilled layer (Schimmack et al., 1994; Owens et al., 1996; He and Walling, 2000; Ritchie and McCarty, 2003). In untilled soils most of the ^{137}Cs is accumulated at the top of the soil profile or few centimetres below and the content decreases exponentially with depth (Mabit et al., 2008; Ritchie and McHenry, 1990; Owens et al., 1996; Ritchie and McCarty, 2003). It is possible to distinguish areas of net soil loss from net deposition areas by analysing the spatial distribution of ^{137}Cs in the studied area (Mabit et al., 2008; Ritchie and McHenry, 1990). Erosion investigations using ^{137}Cs from weapons testing fallout often assume that ^{137}Cs distribution is relatively homogeneous from the field to small catchment scale (e.g. Walling and Quine, 1991; Wu and Tiessen, 2002; Schoorl et al., 2004; Heckrath et al., 2005). Input of ^{137}Cs through Chernobyl reactor accident was highly dependent on the rainfall pattern which caused high (kilometre to regional scale) heterogeneity in ^{137}Cs distribution (Higgitt et al., 1992; Renaud et al., 2003). For a small catchment or single hillslopes a homogeneous rainfall pattern can be assumed.

There are only few studies about ^{137}Cs in alpine regions (e.g. Hofmann et al., 1995; Albers et al., 1998; Agnesod et al., 2001) which mainly analysed soil samples in the laboratory. Albers et al. (1998) studied the distribution of ^{137}Cs in alpine soils and plants in the German Kalkalpen. They found that 10 years after the fallout from the Chernobyl reactor accident most of the ^{137}Cs was still stored in the top 5 cm of the soil profile and uptake by plants was limited.

This study aims at finding a suitable measurement routine to describe ^{137}Cs activities at eroded and uneroded hillslopes in mountain regions and to provide a method routine for future erosion measurements based on ^{137}Cs activities. Therefore an application-oriented method to give a quick overview of ^{137}Cs distribution in the field had to be developed. In a first step small- and large-scale heterogeneity of ^{137}Cs distribution in the catchment was analysed by measuring soil samples of an altitudinal transect in the laboratory using a GeLi detector. GeLi measurements of soil samples in the laboratory were also made in order to check the comparison with ^{137}Cs specific activity concentrations and their dependency on soil parameters.

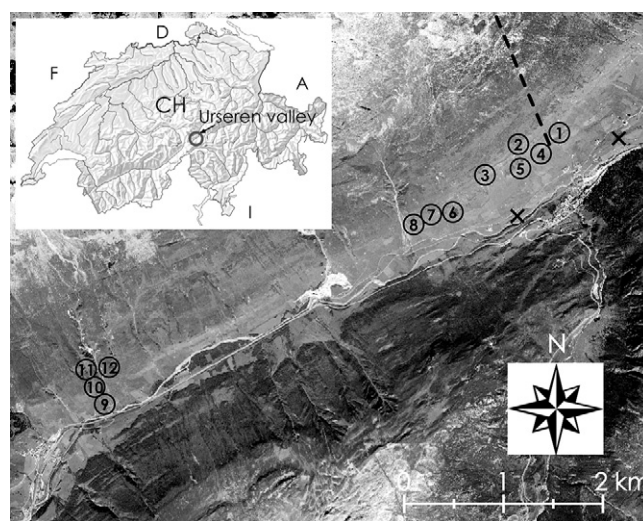


Fig. 1. Aerial photograph of the Urseren Valley in Southern Central Switzerland and location of the sites (numbers), the altitudinal transect (dashed line) and the reference sites (crosses).

Comparison of soil sample measurements in the laboratory (GeLi detector) and in-situ measurements in the field (NaI detector) was done in order to calibrate the field device. Subsequently the calibration of the field device was validated by comparing GeLi laboratory and NaI in-situ measurements of 12 sites.

2. Methods and materials

2.1. Site

The study area is located in the southern part of Central Switzerland (Canton Uri) in the Urseren Valley (Fig. 1). The bottom of the W-E extended mountain valley is approximately 1450 m a.s.l. (above sea level). It is surrounded by mountain ranges of altitudes up to 3200 m a.s.l. The mean annual rainfall is 1516 mm (1986–2007, Source: MeteoSwiss) and the mean annual air temperature is 4.3 °C (1986–2007, Source: MeteoSwiss). The valley mainly consists of cultivated grasslands. Forested areas are limited to protection forests at slopes above villages. Land use is dominated by grazing and, in the lower reaches of the valley, by hay harvesting. The valley is strongly affected by soil erosion. Vegetation cover is disturbed especially on the southern slopes. Soils in the study area mainly consist of podzols and cambisols often with stagic properties (WRB, 2006). For a detailed description of the Urseren Valley see Meusburger and Alewell (2008).

Sampling took place at 12 sites at the south exposed slope (Fig. 1). Sites represent hillslope sections of about 20 m slope length. Mean slope angle of these hillslopes is 36°. Five to nine soil samples were taken at each hillslope section. For laboratory measurements soil samples of a depth of 10 cm were taken as most of the ^{137}Cs is stored in this section (e.g. Schimmack et al., 1989; Owens et al., 1996; Schoorl et al., 2004) and every site was measured three times with in-situ NaI spectrometry. For NaI system calibration, 9 additional soil samples taken from a circular area of 3 m of diameter at one of the sites were measured with the Ge detector system.

Additionally, an altitudinal transect between 1500 and 2050 m a.s.l. and two reference sites with high vegetation cover at sheltered positions behind geomorphologic barriers near the valley bottom (1470 m a.s.l.) were sampled (Fig. 1). From each site, 3 replicate samples were taken within 1 m². The reference sites represent the original ^{137}Cs activity without soil redistribution processes.

Samples were collected during summer seasons 2006 and 2007 using a 72-mm diameter core sampler.

3. Analysis

3.1. Laboratory measurements

Soil samples were dried at 40 °C, passed through a 2-mm sieve and finally ground using a tungsten carbide swing grinder. The ground soil samples were filled into 25-mL sample containers (6.5 cm diameter; Semadeni25) and measured for 8 h. Measurements were done with a Li-drifted Ge detector (GeLi; Princeton

Gamma-Tech, Princeton, NJ, USA) at the Department for Physics and Astronomy, University of Basel. The size of the detector was 48 mm in diameter and 50 mm in length. The relative efficiency was 18.7% (compared to a 3×3 inch NaI detector at a distance of 25 cm between sample and detector). In order to reduce the amount of radiation from background sources in the environment, the samples were shielded by 4-cm-thick lead during measurement. The ^{137}Cs activity concentrations were determined using the InterWinner 5 gamma spectroscopy software (Ortec, Oak Ridge, TN, USA). The energy calibration of the GeLi detector was done using a Eu-152 multi-source with peak line positions at 117.6, 347.6, 773.5, 1108.0 and 1408.9 keV. For efficiency calibration, three reference-samples provided by H. Surbeck (University of Neuchâtel) enriched with known activities of U-238, Th-232 and K-40 were used. These calibration samples were of the same geometry and a comparable density as our analysed soil samples. The resulting measurement uncertainty on ^{137}Cs peak area (at 661 keV) was lower than 15% (error of the measurement at 2-sigma). The minimum detection activity for ^{137}Cs was 0.1 Bq kg^{-1} .

3.2. In-situ measurements

For field measurements a 2×2 inch NaI-scintillation detector (Sarad, Dresden, Germany) was used. The field equipment consists of a detector, a pole, a control unit, a battery and a pocket PC (Fig. 2). The detector was mounted perpendicular to the ground at a height of 25 cm. Usually detectors are mounted 1 m above floor which means that the yield area has, as a rule of thumb, a radius of 10 m. For comparable results the yield area should be flat and should not have irregularities (Laedermann et al., 1998; He and Walling, 2000). As this cannot be fulfilled for such a large area at any site in a mountain region, we decided to use a detector height of 25 cm. The area of yield according to this detector height was determined (see below). For all in-situ measurements, ^{137}Cs concentration was determined for 1 h. Every hillslope section was measured three times. Measurement points were evenly distributed over the slope length of 20 m parallel to the soil sampling transect. Spectra evaluation was done with software provided by H. Surbeck, University of Neuchâtel/Switzerland. Peak area was specified by a gauss function over the region of interest (ROI). The background was separated from the peak area by a straight line between the beginning and end point of the ROI. The ROI was set to include the three interfering peaks Tl-208 at 583.2 keV, Bi-214 at 609.3 keV and ^{137}Cs at 661.7 keV. This multiplet was deconvolved in order to get peak areas of single peaks. In areas with elevated ^{137}Cs activities, interference from natural radionuclides, full energy peaks and secondary scattering of higher energy gamma photons were rather small. In lower activity environments, a more sophisticated processing of the spectra might be required. All measured ^{137}Cs activities refer to 2007. The spectral resolution of the NaI detector was 9.7% at 661.7 keV FWHM.

4. Results & discussion

4.1. Spatial heterogeneity of ^{137}Cs

We tested the small-scale homogeneity of ^{137}Cs distribution in the field by analysing the soil samples taken at meter scale at different altitudes between 1500 m a.s.l. and 2050 m a.s.l. (Fig. 1). Samples were taken at sites with high vegetation cover and no visible erosion and measured with the GeLi detector in the laboratory. The ^{137}Cs activities of the soil samples varied between 47 and 363 Bq kg^{-1} (Fig. 3). On single altitudinal levels a large difference in ^{137}Cs activity was measured for replicate samples within 1 m^2 . Generally, the wide variation of ^{137}Cs concentration at meter

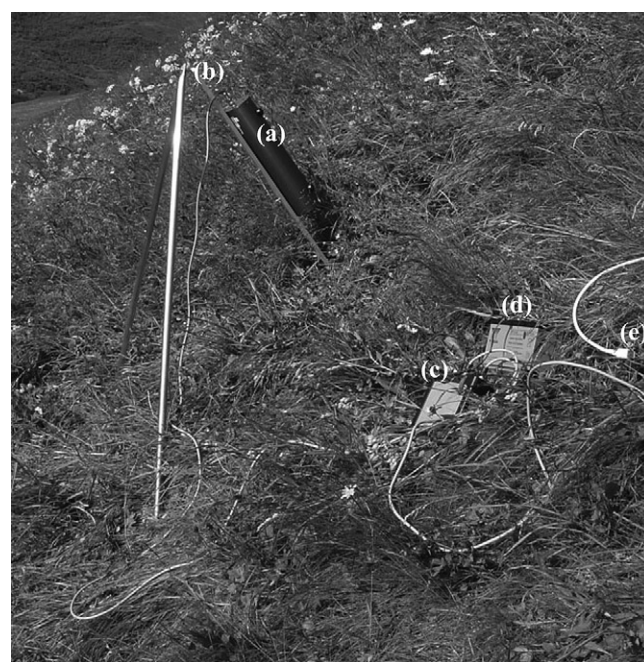


Fig. 2. NaI detector system with its components: (a) detector, (b) pole, (c) control unit, (d) battery and (e) interface to pocket PC.

scale gives evidence that either ^{137}Cs was not evenly deposited and/or not bound homogeneously to soil particles. Another possibility would be secondary transport processes such as erosion and accumulation, which can lead to the high small-scale heterogeneity of ^{137}Cs (He and Walling, 2000). The problem of inhomogeneity in ^{137}Cs distribution has been shown in other studies, but mostly relating to a larger scale (e.g. Clark and Smith, 1988; Albers et al., 1998; Kaste et al., 2006; Machart et al., 2007). According to Machart et al. (2007), the distribution of the radionuclide in the contaminated cloud as well as local inhomogeneities in rainfall intensity or input on a snow layer can be the cause for inhomogeneous small-scale spatial distribution of ^{137}Cs , especially in mountainous terrain. Inhomogeneity in ^{137}Cs distribution may also be due to runoff connected to the rainfall event depositing the ^{137}Cs (Albers et al., 1998). The higher altitudes were still snow-covered at the time of ^{137}Cs deposition (Source: MeteoSchweiz). Therefore, snow melt and runoff processes must be considered as a reason for

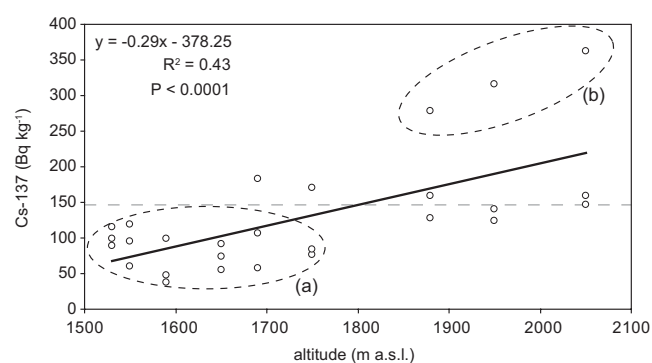


Fig. 3. Altitudinal transect between 1500 and 2050 m a.s.l. with trend line (black). Dashed line represents the ^{137}Cs activity (146.5 Bq kg^{-1}) measured at reference sites. Small-scale variation of ^{137}Cs is demonstrated by the three samples at each altitude. For cluster (a) influence of erosion is possible, cluster (b) is influenced by snow at the time of ^{137}Cs input. Measurement uncertainty is lower than 15%.

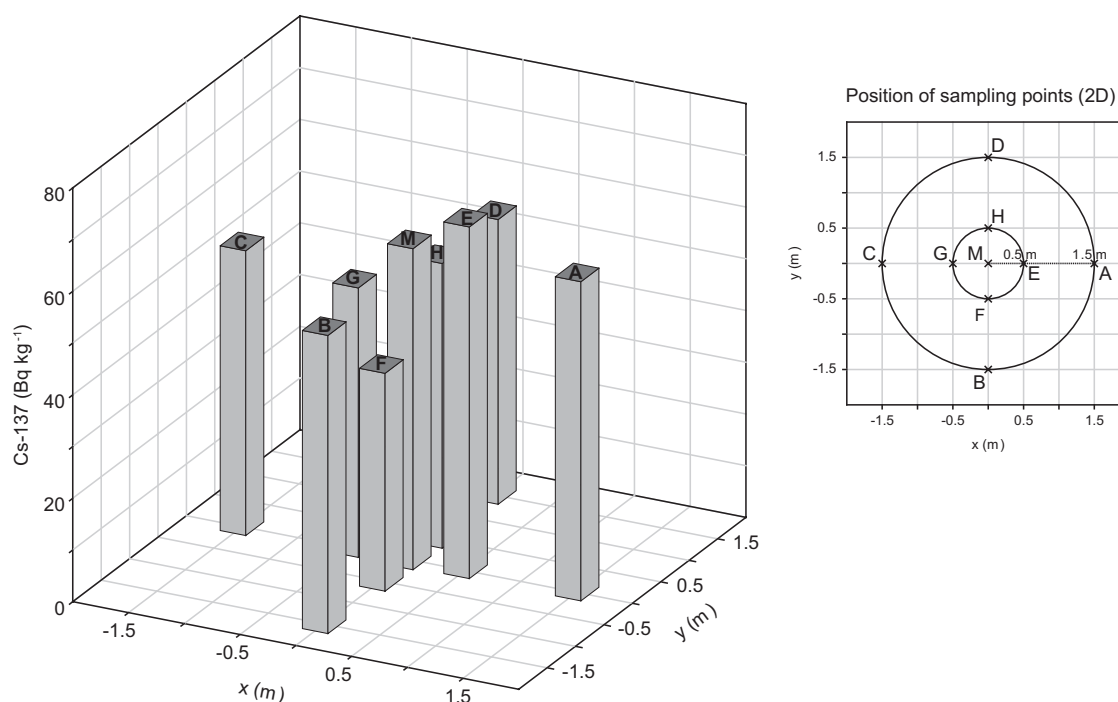


Fig. 4. Spatial heterogeneity of the ^{137}Cs distribution at the calibration site. Measurement uncertainty is lower than 15%.

heterogeneous distribution of ^{137}Cs , also on a small scale (Haugen, 1992). Small-scale heterogeneity in ^{137}Cs activities for replicate samples at altitudes above 1800 m a.s.l. is particularly striking.

For the altitudinal transect, there are two interpretations possible: (i) a linear trend line through all data points shows an increase of ^{137}Cs with altitude (Fig. 3) or (ii) extreme outliers at 1850, 1950 and 2050 m a.s.l. are excluded which results in a homogeneous distribution of ^{137}Cs over 1800 m a.s.l.. A linear trend with altitude would be supported by other studies that have found a dependency of ^{137}Cs on altitude (McGee et al., 1992; Arapis and Karandinos, 2004). However, interference with snow cover (Haugen, 1992) as an explanation for outliers in higher altitudinal levels is also very likely. The remaining data from an altitude above 1800 m a.s.l. were similar to the reference value ($146.4 \pm 19.5 \text{ Bq kg}^{-1}$) determined near the valley bottom (Fig. 3). Even though no erosion damage was visible in the grasslands, the lower activities measured at sites below 1800 m a.s.l. give evidence for soil loss through erosion (cluster a, Fig. 3). This interpretation can be supported by the correspondence of lower ^{137}Cs activities with more intensive land use practice below 1800 m a.s.l. (Meusburger and Alewell, 2008). Small-scale heterogeneity in ^{137}Cs distribution is obvious from replicate samples taken at the same altitudinal level.

4.2. NaI detector calibration and boundary conditions

The ^{137}Cs peak area obtained from measurements with the NaI detector had to be converted to Bq kg^{-1} . This was done by comparison of an in-situ measurement using NaI detector to laboratory measurements using GeLi detector for the samples collected at the same site. However, because measurements from the altitudinal transect have shown large differences in their ^{137}Cs content in replicate samples of the same sites (Fig. 3), small-scale heterogeneity of ^{137}Cs concentration was analysed for the NaI system calibration by laboratory measurement (GeLi detector) of 9 samples (0–10 cm depth) distributed over a 3-m-diameter circular area centred on the position of the NaI in-situ measurement (Fig. 4).

Mean ^{137}Cs concentration was $58.8 \pm 8.2 \text{ Bq kg}^{-1}$ with a maximum at 68.2 Bq kg^{-1} and a minimum at 42.0 Bq kg^{-1} . The mean value of these 9 single measurements (GeLi) was used as a calibration value with which the factor for the conversion of the ^{137}Cs peak area (counts) determined from in-situ measurement (NaI) to Bq kg^{-1} was estimated. This factor allows the conversion from peak area in counts to Bq kg^{-1} for further in-situ measurements at comparable soils in the Urseren Valley. A potential dependency on soil parameters is described below.

In order to estimate the soil volume which is representative for the ^{137}Cs measured in the field, depth and spatial yield of the detector (NaI detector) as well as ^{137}Cs distribution in soil depth were determined. Depth distribution of ^{137}Cs was measured on a subdivided soil core (0–5 cm, 5–10 cm, 10–15 cm, 15–20 cm) by laboratory measurements (GeLi detector). The ^{137}Cs activity decreased exponentially with depth (Fig. 5a). This is a typical distribution for untilled soils (Ritchie and McHenry, 1990; Owens et al., 1996; Ritchie and McCarty, 2003). Over 70% of the total ^{137}Cs inventory of the soil is in the top 10 cm of the soil column (Fig. 5a). This is in accordance with Schimmack and Schultz (2006) who studied the migration of ^{137}Cs deposited after the Chernobyl reactor accident in a grassland for 15 years.

Contribution of radiation from different soil depths to the NaI detector was estimated by repeated measurement of a buried ^{137}Cs point source (7.6 kBq 08/2007) in steps of 2 cm between 0 and 20 cm soil depth by in-situ measurement with the NaI detector mounted 25 cm above the surface. The radiation contributing to the total measured ^{137}Cs activity decreases exponentially with depth (Fig. 5b). Most of the activity comes from the top 10 cm of the soil. Radiation from below 18 cm has a minor influence on the measured surface activity. Considering the ^{137}Cs activity of the soil as well as the depth yield of the NaI detector, the contribution of the top 10 cm of the soil column amounts to 90.3%.

The horizontal coverage of the detector (NaI) was estimated in the field by repeated measurement of a ^{137}Cs point source (15.8 kBq 08/2007) with increasing horizontal distance from the detector which was mounted on 25 cm above ground. The distance was

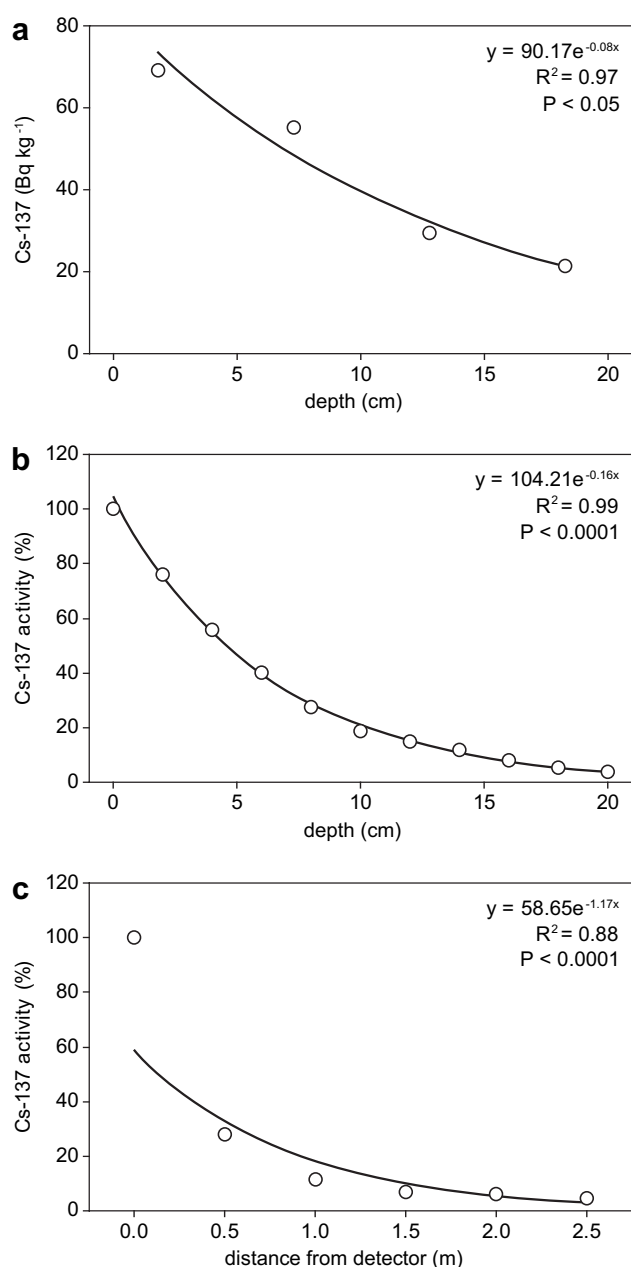


Fig. 5. (a) ^{137}Cs depth profile for an upland soil measured in the laboratory (GeLi detector). (b) Exponential decrease of the ^{137}Cs radiation measured at the surface with increasing burial depth of the point source (NaI detector). ^{137}Cs activity is given as % normalized on the ^{137}Cs activity measured for 0 cm burial depth. (c) Exponential decrease of the measured ^{137}Cs activity with increasing horizontal distance between the point source and the detector (NaI detector). ^{137}Cs activity is given as % normalized on the ^{137}Cs activity measured at 0 m distance from detector. Measurement uncertainty is lower than 15% for measurements with the GeLi detector and lower than 17.3% for measurements with the NaI detector.

increased in 0.5 m steps. For increasing horizontal distance of the point source from the detector ^{137}Cs activity decreases exponentially (Fig. 5c). Under the assumption of a homogeneous distribution, 90% of the measured ^{137}Cs activity origin from a circular area with a radius of 1 m around the detector (3.1 m²).

4.3. Sources of error

Determination of the ^{137}Cs peak position in the spectrum obtained by NaI measurement is subjective. Small changes in start

and end position of the region of interest (ROI) leads to a big variability in peak area. This error on peak area was determined by using the mean standard deviation of peak areas of 20 test spectra each evaluated by eight persons independently. Uncertainty on peak area of measurement was 17.3% at a mean peak area of 2063 counts. Interference with neighbouring peaks may lead to an uncertainty on ^{137}Cs peak area. As spectral deconvolution was processed the same way for all spectra, this uncertainty is thought to be negligible for intercomparison of samples in this study. However, for comparison of absolute values with other studies an uncertainty should be considered.

Knowledge about contribution of pre-Chernobyl ^{137}Cs is important for quantitative estimation of erosion rates because date of input is crucial to know. The contribution of pre-Chernobyl ^{137}Cs originating from above ground nuclear weapon tests in the 1950s and 1960s is not clear for the site Urseren Valley as only little data are available for Switzerland. Riesen et al. (1999) measured samples collected in 1986 before the Chernobyl reactor accident from 12 forested sites distributed over Switzerland. The ^{137}Cs activities of the top soil layers (0–5 cm) were between 2 and 58 Bq kg^{−1} (Riesen et al., 1999). Consequently, after decay with a half-life of 30.17 a, in 2007 only 1–35 Bq kg^{−1} would be left, which means that the maximum contribution of pre-Chernobyl ^{137}Cs might amount to 20% at reference sites.

Additionally, vertical migration must be considered. From literature, migration values between 0.03 and 1.30 cm a^{−1} are known (Schimmack et al., 1989; Arapis and Karandinos, 2004; Schuller et al., 2004; Schimmack and Schultz, 2006; Ajayi et al., 2007). However, our measurements show that in the Urseren Valley most of the ^{137}Cs is still stored in the top 10 cm of the soil profile. Thus, only moderate migration of ^{137}Cs occurred.

4.4. Dependency of ^{137}Cs on different soil parameters

The ^{137}Cs content of the soil was plotted versus pH, clay content, soil moisture and organic carbon content (Fig. 6). There are two groups of soil differing in pH, one with a pH between 4 and 5 and one with a pH around 7 (Fig. 6a). Neither an overall dependency of ^{137}Cs content on pH was found, nor within the single groups. This is in accordance with Livens and Loveland (1988) who relate the pH range between 4 and 7 to conditions of immobile ^{137}Cs . No correlation between clay content and ^{137}Cs content was calculated due to different sites forming different clusters (Fig. 6b). Niesiobedzka (2000) found a positive dependency of ^{137}Cs on clay content for soils with very low clay contents, under 3%. Higher ^{137}Cs with higher clay content are consistent with the theory of the clay's higher binding capacity and strength. No dependency of ^{137}Cs on total organic carbon content was found (Fig. 6c). Dependency of ^{137}Cs on soil moisture was estimated by repeated measurement of a soil sample at different moisture levels with the NaI detector in the laboratory. The sample was sealed in a plastic bag during measurement time to keep moisture constant. Soil moisture shows a clear influence on the measured ^{137}Cs activity (Fig. 6d). Therefore, soil moisture was measured parallel to in-situ measurements in order to correct data with soil moisture using an EC-5 soil moisture sensor (DecagonDevices, Pullman, WA, USA). Measured soil moisture in the field at the time of in-situ measurements varied from 5 to 12%, which represents a shielding of gamma activity by 3–7%.

4.5. Validation of the in-situ NaI measurements

In-situ and laboratory determination of ^{137}Cs activity of 12 sites were compared in order to check the validity of the calibration of the NaI detector system. The mean value of all soil samples (0–10 cm) of one site measured in the laboratory (GeLi detector)

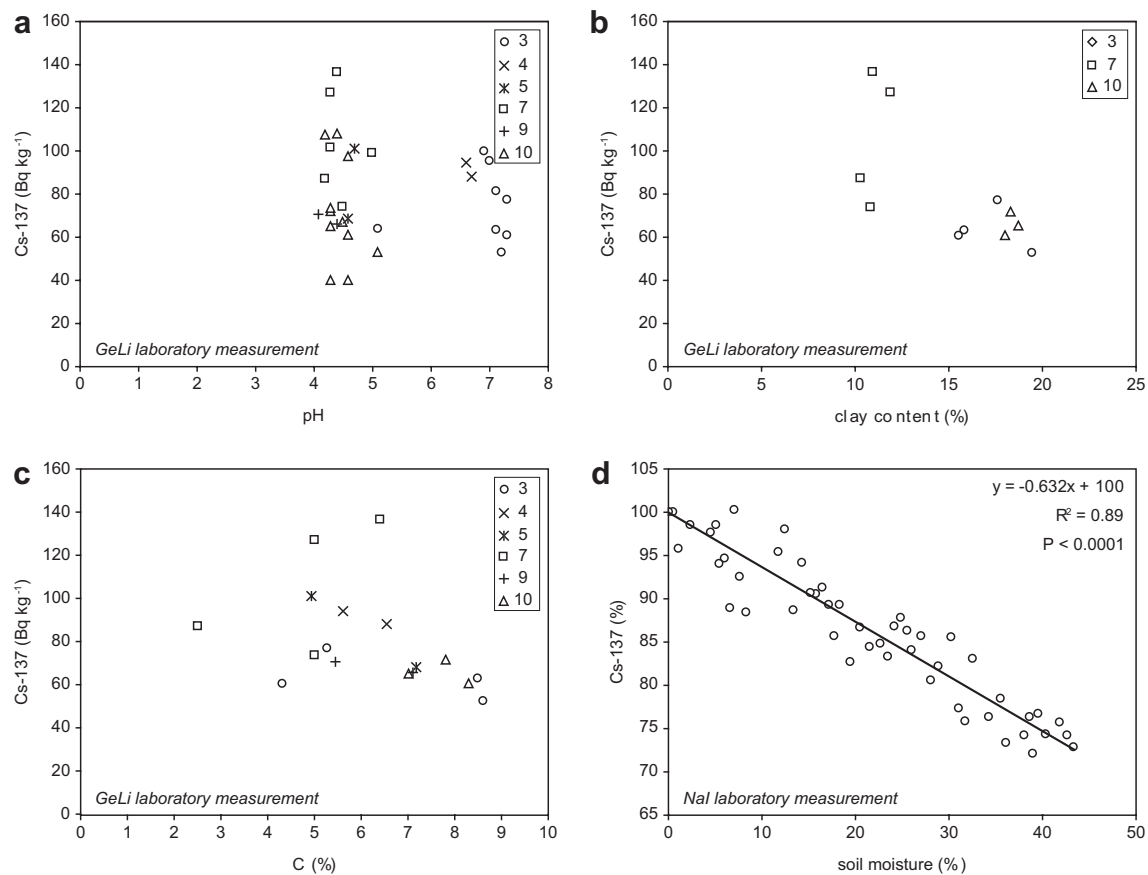


Fig. 6. Dependency of ¹³⁷Cs on (a) pH (GeLi detector), (b) clay content (GeLi detector), (c) carbon content (GeLi detector) and (d) soil moisture (Nal detector) (3, 4, 5, 7, 9, 10 stand for different sampling sites). ¹³⁷Cs activity in figure (d) is given as % normalized on the ¹³⁷Cs activity measured for 0% soil moisture. Measurement uncertainty is lower than 15% for measurements with the GeLi detector and lower than 17.3% for measurements with the Nal detector.

was checked against the mean value of the in-situ measurements (Nal detector) at the same sites (Table 2, Fig. 7). A good correspondence of ¹³⁷Cs activities determined by in-situ Nal measurements and laboratory GeLi measurements was found ($R^2 = 0.86$). In Fig. 7, standard deviations for both laboratory measurements with GeLi detector and in-situ measurement with Nal detector are given. Note that the large variation of ¹³⁷Cs activities for GeLi detector measurements at single sites is due to spatial heterogeneity in ¹³⁷Cs distribution (see above). In-situ measurements generally have a smaller standard deviation because the detector integrates over a measurement area of 3.1 m² (Table 2, Fig. 7). The close correlation

between in-situ and laboratory measurements shows that both methods give good averages of ¹³⁷Cs activities at alpine hillslopes. Our results are supported by Haugen (1992) and Tyler et al. (2001) who have found similar correspondences for cultivated fields. Despite the fact that our estimations do not include an exact calculation of the basic conditions concerning ¹³⁷Cs flux and detector response (e.g. Beck et al., 1972; Miller and Shebell, 1993), the achieved results with low calculating effort are equal to laboratory measurements (GeLi detector) of several soil samples. The Nal in-situ measurements provide a quick and easy method to determine ¹³⁷Cs inventories in regions with high ¹³⁷Cs concentration.

Table 2
¹³⁷Cs data of all sites for measurements with GeLi and Nal detector. Measurement uncertainty is lower than 15% for measurements with the GeLi detector and lower than 17.3% for measurements with the Nal detector.

| site | GeLi | | | | Nal | | | |
|------|-----------------------------|-----------------------------|-----------------------------|-----------------------------|-----------------------------|-----------------------------|-----------------------------|-----------------------------|
| | Mean (Bq kg ⁻¹) | S.d. (Bq kg ⁻¹) | Min. (Bq kg ⁻¹) | Max. (Bq kg ⁻¹) | Mean (Bq kg ⁻¹) | S.d. (Bq kg ⁻¹) | Min. (Bq kg ⁻¹) | Max. (Bq kg ⁻¹) |
| 1 | 74 | 31 | 43 | 134 | 73 | 1 | 72 | 74 |
| 2 | 135 | 59 | 69 | 266 | 148 | 3 | 144 | 150 |
| 3 | 104 | 49 | 53 | 178 | 108 | 12 | 95 | 119 |
| 4 | 92 | 25 | 60 | 145 | 76 | 23 | 56 | 106 |
| 5 | 92 | 24 | 49 | 133 | 99 | 29 | 70 | 135 |
| 6 | 114 | 25 | 77 | 131 | 119 | 14 | 103 | 130 |
| 7 | 134 | 67 | 54 | 261 | 128 | 33 | 105 | 166 |
| 8 | 111 | 50 | 50 | 160 | 132 | 24 | 114 | 159 |
| 9 | 66 | 16 | 41 | 85 | 64 | 11 | 53 | 64 |
| 10 | 64 | 19 | 38 | 91 | 64 | 5 | 59 | 68 |
| 11 | 86 | 26 | 55 | 113 | 84 | 13 | 70 | 94 |
| 12 | 71 | 29 | 41 | 128 | 90 | 12 | 83 | 104 |

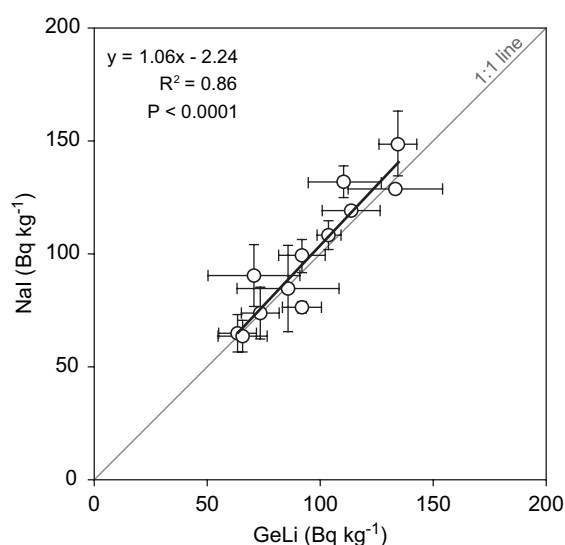


Fig. 7. Comparison of ^{137}Cs activities determined by in-situ (NaI detector) and laboratory measurements (GeLi detector). Error bars are standard errors on the mean estimate. They include the uncertainty in ^{137}Cs activity due to heterogeneity in ^{137}Cs distribution. Measurement uncertainty is comparable for both detectors with 15% for the GeLi detector and 17.3% for the NaI detector.

For measurements of similar soils in the same catchment only one factor for conversion of ^{137}Cs peak area obtained by NaI in-situ measurement to Bq kg^{-1} must be estimated. However, knowledge about the soils in a catchment might be crucial as the conversion factor most likely has to be adapted to differing soils. Another limitation of this method is the poor spectral resolution of NaI detectors which needs experience in spectra evaluation. Because of this poor spectral resolution the application of NaI in-situ measurements is limited to areas with relatively high ^{137}Cs activity.

Spatial small-scale distribution and especially vertical distribution of ^{137}Cs in grasslands is much more variable than in arable lands where ^{137}Cs is mechanically homogenised by tillage. Therefore, interpretation of in-situ data of alpine grasslands is subject to errors relating to the spatial heterogeneity. Our data show that ^{137}Cs varied greatly over a small scale. Consequently, either the number of soil samples per site must be increased or in-situ measurements which smooth out irregularities must be done in order to achieve a representative ^{137}Cs activity of a site. Collecting large numbers of samples in the field does not seem appropriate for sensitive mountain soils seriously affected by soil erosion. Especially in regions where soil restoration takes hundreds of years, non-destructive in-situ measurements should be favoured. Furthermore, large numbers of soil samples are always connected to the problem of adequate homogenizing which is problematic in densely rooted soils, soils with varying soil texture and/or organic content.

Based on the results of this study, in-situ measurements with NaI detector enable a determination of a mean ^{137}Cs activity of a single hillslope section and at the same time an estimation of the erosion state in a steep alpine catchment characterised by elevated ^{137}Cs activities originating from Chernobyl fallout. For an application of the method in the Urseren Valley see Konz et al. (2009).

5. Conclusion

The ^{137}Cs distribution in the Alps is very heterogeneous especially on a small scale (meter scale) which was shown by GeLi laboratory measurements. In alpine areas the steep terrain with

low accessibility hampers the use of the heavy and mostly non-portable Ge detectors in the field, hence NaI detector system offers a good alternative. Further, in-situ measurements are non-destructive which is important particularly at sites strongly affected by soil erosion. For the in-situ measurements, a NaI detector was mounted 25 cm above ground integrating over a measurement area of 3.1 m^2 . No dependency of ^{137}Cs on pH, carbon content and clay content was found, but in-situ measurements must be corrected for soil moisture. The NaI detector which is a quick and easy to apply method was successfully applied to an alpine grassland with strong heterogeneity in ^{137}Cs distribution. The use of NaI detectors in the field is a valid and rather quick alternative for extensive soil sampling (correspondence to GeLi laboratory measurements $R^2 = 0.86$). In addition small-scale heterogeneity of ^{137}Cs activity obtained in GeLi laboratory measurements is averaged spatially by NaI in-situ measurements.

Acknowledgements

This work was financially supported by the Swiss National Science Foundation (SNF), project no. 200020-113331 and by the State Secretariat for Education and Research (SER), in the framework of the European COST action 634: "On- and Off-site Environmental Impacts of Runoff and Erosion".

We would like to thank H. Surbeck (University of Neuchâtel) for help with spectra evaluation and provision of software and samples for detector calibration, S. Estier (Federal Office of Public Health FOPH) for helpful discussion and J. Jourdan and D. Sacker (Department of Physics and Astronomy, University of Basel) for access to and help with the GeLi detector.

References

- Agnesod, G., Lazzaron, R., Operti, C., Zappa, C., 2001. Accuracy of field spectrometry in estimating Cs-137 contamination in high altitude alpine soils. *Radiation Protection Dosimetry* 97, 329–332.
- Ajayi, I.R., Fischer, H.W., Burak, A., Qwasmeh, A., Tabot, B., 2007. Concentration and vertical distribution of Cs-137 in the undisturbed soil of southwestern Nigeria. *Health Physics* 92, 73–77.
- Albers, B.P., Rackwitz, R., Schimmack, W., Bunzl, K., 1998. Transect survey of radiocesium in soils and plants of two Alpine pastures. *The Science of the Total Environment* 216, 159–172.
- Alewell, C., Meusburger, K., Brodbeck, M., Bänninger, D., 2008. Methods to describe and predict soil erosion in mountain regions. *Landscape and Urban Planning* 88, 46–53.
- Arapis, G.D., Karandinos, M.G., 2004. Migration of Cs-137 in the soil of sloping semi-natural ecosystems in Northern Greece. *Journal of Environmental Radioactivity* 77, 133–142.
- Beck, H.L., Decampo, J., Gogolak, C., 1972. In: H. a. S. Laboratory & U.S.A.E. Commission (Ed.), *In Situ Ge(Li) and NaI(Tl) Gamma-ray Spectrometry*, p. 75.
- Bonnett, P.J.P., 1990. A review of the erosional behavior of radionuclides in selected drainage basins. *Journal of Environmental Radioactivity* 11, 251–266.
- Clark, M.J., Smith, F.B., 1998. Wet and dry deposition of Chernobyl releases. *Nature* 332, 245–249.
- Golovov, V.N., Walling, D.E., Kvasnikova, E.V., Stukin, E.D., Nikolaev, A.N., Panin, A.V., 2000. Application of a field-portable scintillation detector for studying the distribution of ^{137}Cs inventories in a small basin in Central Russia. *Journal of Environmental Radioactivity* 48, 79–94.
- Haugen, L.E., 1992. Small-scale variation in deposition of radiocesium from the Chernobyl fallout on cultivated grasslands in Norway. *Analyst* 117, 465–468.
- He, Q., Walling, D.E., 2000. Calibration of a field-portable gamma detector to obtain in situ measurements of the Cs-137 inventories of cultivated soils and flood-plain sediments. *Applied Radiation and Isotopes* 52, 865–872.
- Heckrath, G., Djurhuus, J., Quine, T.A., Van Oost, K., Govers, G., Zhang, Y., 2005. Tillage erosion and its effect on soil properties and crop yield in Denmark. *Journal of Environmental Quality* 34, 312–324.
- Higgitt, D.L., Froehlich, W., Walling, D.E., 1992. Applications and limitations of Chernobyl radiocesium measurements in a Carpathian erosion investigation, Poland. *Land Degradation & Rehabilitation* 3, 15–26.
- Hofmann, W., Gastberger, M., Türk, R., 1995. Bodenflechten der alpinen Höhenstufe als Bioindikator für radioaktiven Fallout. *Umweltbundesamt, Wien*, p. 28.
- ICRU, 1994. Gamma-ray spectrometry in the environment. In: *ICRU Report 53*. International Commission on Radiation Units and Measurements, Bethesda, MD, USA, p. 84.

- Kaste, J.M., Heimsath, A.M., Hohmann, M., 2006. Quantifying sediment transport across an undisturbed prairie landscape using cesium-137 and high resolution topography. *Geomorphology* 76, 430–440.
- Konz, N., Schaub, M., Prasuhn, V., Alewell, C., 2009. Cs-137-based erosion-rate determination of a steep mountainous region. *Journal of Plant Nutrition and Soil Science* 172, 615–622.
- Laedermann, J.-P., Byrde, F., Murith, C., 1998. In-situ gamma-ray spectrometry: the influence of topography on the accuracy of activity determination. *Journal of Environmental Radioactivity* 38, 1.
- Livens, F.R., Loveland, P.J., 1988. The influence of soil properties on the environmental mobility of caesium in Cumbria. *Soil Use and Management* 4, 69–75.
- Mabit, L., Benmansour, M., Walling, D.E., 2008. Comparative advantages and limitations of the fallout radionuclides ^{137}Cs , $^{210}\text{Pb}_{\text{ex}}$ and ^7Be for assessing soil erosion and sedimentation. *Journal of Environmental Radioactivity* 99, 1700–1807.
- Machart, P., Hofmann, W., Türk, R., Steger, F., 2007. Ecological half-life of ^{137}Cs in lichen in an alpine region. *Journal of Environmental Radioactivity* 97, 70–75.
- McGee, E.J., Colgan, P.A., Dawson, D.E., Rafferty, B., Okeeffe, C., 1992. Effects of topography on cesium-137 in montane peat soils and vegetation. *Analyst* 117, 461–464.
- Meusburger, K., Alewell, C., 2008. Impacts of anthropogenic and environmental factors on the occurrence of shallow landslides in an alpine catchment (Urseren Valley, Switzerland). *Natural Hazards and Earth System Sciences* 8, 509–520.
- Meusburger, K., Alewell, C., 2009. The influence of land use change on the validity of landslide susceptibility maps. *Natural Hazards and Earth System Sciences* 9, 1495–1507.
- Miller, K.M., Shebell, P., 1993. In Situ Gamma-ray Spectrometry: a Tutorial for Environmental Radiation Scientists. E.M. Laboratory & U.S.D. o. Energy, United States. 45.
- Niesiobedzka, K., 2000. Mobile forms of radionuclide Cs-137 in sandy soils in northeastern Poland. *Polish Journal of Environmental Studies* 9, 133–136.
- Owens, P.N., Walling, D.E., He, Q.P., 1996. The behaviour of bomb-derived caesium-137 fallout in catchment soils. *Journal of Environmental Radioactivity* 32, 169–191.
- Renaud, P., Pourcelot, L., Métivier, J.-M., Morello, M., 2003. Mapping of ^{137}Cs deposition over eastern France 16 years after the Chernobyl accident. *The Science of the Total Environment* 309, 257–264.
- Riesen, T.K., Zimmermann, S., Blaser, P., 1999. Spatial distribution of Cs-137 in forest soils of Switzerland. *Water Air and Soil Pollution* 114, 277–285.
- Ritchie, J.C., McCarty, G.W., 2003. ^{137}Cs and soil carbon in a small agricultural watershed. *Soil & Tillage Research* 69, 45–51.
- Ritchie, J.C., McHenry, J.R., 1990. Application of radioactive fallout cesium-137 for measuring soil-erosion and sediment accumulation rates and patterns – a review. *Journal of Environmental Quality* 19, 215–233.
- Schimmack, W., Bunzl, K., Flessa, H., 1994. Short-term and long-term effects of ploughing on the vertical distribution of radiocaesium in two Bavarian soils. *Soil Use and Management* 10, 164–168.
- Schimmack, W., Bunzl, K., Zelles, L., 1989. Initial rates of migration of radionuclides from the Chernobyl fallout in undisturbed soils. *Geoderma* 44, 211–218.
- Schimmack, W., Schultz, W., 2006. Migration of fallout radiocaesium in a grassland soil from 1986 to 2001-Part 1: activity-depth profiles of Cs-134 and Cs-137. *Science of the Total Environment* 368, 853–862.
- Schoorl, J.M., Boix Fayos, C., de Meijer, R.J., van der Graaf, E.R., Veldkamp, A., 2004. The Cs-137 technique applied to steep Mediterranean slopes (Part I): the effects of lithology, slope morphology and land use. *Catena* 57, 15–34.
- Schuller, P., Bunzl, K., Voigt, G., Ellies, A., Castillo, A., 2004. Global fallout Cs-137 accumulation and vertical migration in selected soils from South Patagonia. *Journal of Environmental Radioactivity* 71, 43–60.
- Tyler, A.N., Davidson, D.A., Grieve, I.C., 2001. In situ radiometric mapping of soil erosion and field-moist bulk density on cultivated fields. *Soil Use and Management* 17, 88–96.
- Walling, D.E., Quine, T.A., 1991. Use of ^{137}Cs measurements to investigate soil erosion on arable fields in the UK: potential applications and limitations. *Journal of Soil Science* 42, 147–165.
- WRB, 2006. World Reference Base for Soil Resources 2006. Reports No. 103, second ed. World Soil Resources, FAO, Rome.
- Wu, R.G., Tiessen, H., 2002. Effect of land use on soil degradation in alpine grassland soil, China. *Soil Science Society of America Journal* 66, 1648–1655.

CHAPTER 8

Final remarks and outlook

Soil erosion seriously threatens mountain slopes. In order to have a better understanding of soil degradation processes and its extent new approaches are needed for monitoring and prediction of soil erosion and soil erosion risk areas. In this study we tested the potential of GIS and remote sensing methods for the assessment of soil loss by landslides and sheet erosion. One focus of the study was to develop mapping tools for landslides and sheet erosion in mountainous regions. The second focus was to implement the elaborated data from GIS and image mapping in commonly used erosion risk assessment models (logistic regression model, USLE, PESERA) thereby testing the suitability and validity of the models by referring to the identified causes.

8.1. Causes for soil erosion and monitoring

We found that the Urseren Valley is characterised by a high natural susceptibility to landslides. Geology, slope and stream density were identified with multivariate analysis as plausible factors to explain the spatial variation of landslides (chapter 4). However, the strong increase of the landslide area of 92% within 45 years indicated that dynamic factors like climate and land use decisively influence the landslide pattern that we observe today (chapter 3). The analysis of the time-series related to the increase in landslide occurrence revealed that the increase of extreme rainfall events and the increased stocking of the pastures are likely to have enhanced the landslide hazard. In addition to stocking numbers, the change in management practices is decisive. Extensively used or abandoned areas with recently emerging shrub vegetation show low landslide densities in the Urseren Valley and were not responsible for the landslide trend. Although we cannot infer quantitative relationships between landslide hazard and anthropogenic impacts, our data indicate the changes during the last decades duplicated the extent of landslide hazard. Erosion rates by landslides are generally unknown due to the lack of historic

spatial data. The temporal data on spatial landslide occurrence allowed a rough estimate of the erosion rate by landslides of $0.6 \text{ t ha}^{-1} \text{ a}^{-1}$ for the study site (30 km^2) during the last 45 years (chapter 3). Even though this soil loss might be low compared to arable areas ($2\text{--}4 \text{ t ha}^{-1} \text{ a}^{-1}$ as a limit value in the Swiss soil protection guideline (BAFU, 2001)), the areal damage is critical and may persist for decades.

For sheet erosion, the decisive impact of fractional vegetation cover was proved by Cs-137 measurement. The application of the USLE and PESERA model further confirmed the strong influence of vegetation cover. A sensitivity analysis of PESERA (see Appendix) showed that PESERA is not very sensitive for small changes in vegetation cover, which is in contrast to the field measurements made and also to observations in literature. USLE soil erosion rates of up to $16 \text{ t ha}^{-1} \text{ a}^{-1}$ were in the range of the Cs-137 measurements (chapter 6). Thus, for single slopes measures to reduce soil loss by sheet erosion as well as for landslides are needed. The mean sheet erosion rate for the entire catchment is $1.18 \text{ t ha}^{-1} \text{ a}^{-1}$, which is approximately twice as high as the erosion rate by landslides. However, a direct comparison has to be considered with caution because the erosion rates refer to different time periods. Overall, looking at soil erosion rates of the two processes averaged over larger areas and time spans there is no need for action. However, for single slopes limit values of the Swiss soil protection guidelines are exceeded. Thus, the following methods to distinguish differences in soil erosion risk within a catchment are urgently needed.

8.2. Methodological approach: Erosion monitoring and risk assessment

GIS overlay techniques combined with multivariate analysis are commonly used for spatial landslide susceptibility predictions. The technique is established and was applied for many mountain areas all over the world (Ohlmacher and Davis, 2003; Van Den Eeckhaut et al., 2006; Zhou et al., 2002). However, there are only few studies considering potential temporal trends in landslide occurrence. Temporal trends were shown to reduce the validity of the predictions made on the assumption of static behaviour of susceptibility and triggering factors. This dissertation implies that the validity of commonly used static landslide susceptibility maps under changing environmental conditions is questionable. Slopes that are predicted as stable can rapidly and mostly unnoticed increase in landslide susceptibility. Thus, it was shown that it is crucial to understand the dynamic of landslide causal factors in order to guarantee validity of landslide susceptibility maps (chapter 4).

The simultaneous change of several dynamic landslide causal factors poses great problems to identify causal relationships and thereby new emerging risk zones by statistical methods. Moreover, the knowledge of the impact of different land use on landslide susceptibility is limited. With the proposed approach (chapter 4) to analyse multitemporal spatial data by comparing susceptibility maps for two points in time it was possible to identify new emerging risk areas. In addition, the spatial pattern of the shift in landslide susceptibility allowed better inference on the potential causes. In

general, there is still great discussion about the impact of different land use types and management practices on landslide susceptibility. Applying the described techniques for further case studies might greatly improve our knowledge.

The small scale heterogeneity of land-cover features make high demands for remote sensing in alpine environments. High spatial resolutions are needed, however, so far high resolution data was exclusively used for validation of either coarse to medium resolution satellite systems or of soil erosion risk models by visual comparison. The problem of coarse scale erosion assessments is the inability to compare the obtained results to actual field measured soil loss. However, images with higher spatial resolution might resolve this problem and allow for a direct allocation of image data to field measurements. Thus, the applicability of high resolution QuickBird data for mapping land-cover features that are relevant for soil erosion was tested. The satellite mapping successfully identified the typical land-cover types of alpine regions. This automatic detection enabled a quicker mapping compared to the digitizing of air photographs. Despite the limitations of QuickBird imagery for linear spectral unmixing approaches, for grassland areas relative abundance of ground components (grassland and bare soil) could be mapped (chapter 5).

Further, the high resolution land-cover and FVC data was used for the erosion risk models USLE and PESERA. Cs-137 derived soil erosion rates exceeded the PESERA estimates more than fifty times. USLE produced more plausible soil erosion estimates compared to the Cs-137 measurement. Still the modelled erosion rate was only half, which might be due to the missing implementation of snow melt peak events in spring. The difference in the performance of the two models might be attributed to the different sensitivity of the models to vegetation cover. The C factor of USLE, which accounts for changes in vegetation cover is highly sensitive while PESERA (designed for a European scale) accounts for small differences in fractional vegetation cover to a lesser extend. USLE was also designed for different environments, hence, it is uncertain whether it describes the main processes of soil erosion in alpine regions correctly. For instance, USLE does not account for snowmelt that is known to be a peak erosion event. Nonetheless, including small adaptations for the alpine environment might be of great potential. Former erosion estimates for alpine environments were relatively low due to the assumption of a 100% vegetation cover. By the usage of QuickBird data it was possible to identify "hotspots" of erosion. It was shown that even a "simple" model can strongly benefit from using more spatial information. Overall, the great profit of high resolution data for soil erosion assessment lies in the ability to directly compare results to ground measurement while at the same time providing estimates for entire catchments. Thus, this approach (chapter 6) might provide great potential for the validation of regional scale models by linking regional model scale with plot measurement scale.

8.3. Outlook

It could be shown that GIS and remote sensing are powerful tools for soil erosion detection and analysis of soil erosion risk and causes. Still several tasks remain to be pursued:

The elaborated methods for the Urseren Valley need in a next step to be transferred to other alpine catchments.

1. In order to validate the landslide susceptibility mapping method developed in the Urseren Valley.
2. With the objective to separate and quantify the effect of climate- and land use change on the magnitude of landslide hazard and the distribution of landslide susceptibility zones. The role of land use and climate also might be clarified by the application of physically based slope stability models, which may allow quantifying and separating the effect of climate and land use change with plausible scenarios. The ERT measurements could help to parameterise the model (Appendix).
3. To evaluate the history and actual state of landslide susceptibility in order to estimate future landslide activity with respect to various alpine areas.
4. For sheet erosion it remains to be tested whether the FVC mapping approach with a single image is valid for other alpine areas. Given this prerequisite, the application of the method for different alpine regions provides great potential for the validation of regional scale models.

The benefit of QuickBird data for landslide risk assessment needs to be tested.

1. The detailed land-cover map with the additional land-cover classes (dwarf-shrub and bare soil) in combination with the FVC map might be a significant predictor for landslide susceptibility. Repetitive measurement of this parameter might account for changes in land use.
2. An automatic bivariate landslide mapping procedure that would ease landslide susceptibility assessment could be tested. The approach was already successfully applied for the mapping of gullies (Vrieling et al., 2007)

So far, soil loss from landslides, which is decisive in mountainous areas, is not considered in regional assessments of soil erosion and, therefore soil erosion rates by the process of landslides are unknown. Even though, landslides are a well noticed threat to mountain areas their relevance for soil loss is almost unnoticed. Thus, a future requirement would be to develop soil erosion models that include the process of landslide and can account for temporal variations of causal factors by means of historic data and repetitive satellite imagery.

Yet, the high cost of QuickBird imagery impedes the usage for larger regions with repetitive measurement. However, with the launch of Rapid Eye in August 2008 high resolution data (5 m pixel) is available with larger coverage and thus shorter repetition time. This is of special interest for soil erosion monitoring on a regional scale and for updating risk assessments. Further, with repetitive imagery it might be possible to relate the temporal developments to causes and risks of sheet erosion (parallel to the approach presented for landslides in chapter 4). The higher spectral resolution of

Rapid Eye might also improve the mapping of bare soil areas and allow for spectral unmixing with other vegetation types as for instance dwarf-shrubs. This would be a big step in the direction of developing a monitoring system of soil erosion for alpine environments, which in future could help avoid damages.

BIBLIOGRAPHY 9

- Adams, J.B., Sabol, D.E., Kapos, V., Almeida Filho, R., Roberts, D.A., Smith, M.O. and Gillespie, A.R., **1995**. Classification of multispectral images based on fractions of endmembers: Application to land-cover change in the Brazilian Amazon. *Remote Sensing of Environment*, 52 (2): 137-154.
- Agnesod, G., Lazzaron, R., Operti, C. and Zappa, C., **2001**. Accuracy of field spectrometry in estimating Cs-137 contamination in high altitude alpine soils, Workshop on Physical Agents and Measurements in the Environment. Nuclear Technology Publ, Ivrea, Italy, pp. 329-332.
- Ahnert, F., **2003**. Einführung in die Geomorphologie. UTB, Stuttgart, 440 pp.
- Ajayi, I.R., Fischer, H.W., Burak, A., Qwasmeh, A. and Tabot, B., **2007**. Concentration and vertical distribution of Cs-137 in the undisturbed soil of southwestern Nigeria. *Health Physics*, 92 (1): 73-77.
- Albers, B.P., Rackwitz, R., Schimmack, W. and Bunzl, K., **1998**. Transect survey of radiocesium in soils and plants of two Alpine pastures. *Science of the Total Environment*, 216 (1-2): 159-172.
- Alewell, C. and Gehre, M., **1999**. Patterns of stable S isotopes in a forested catchment as indicators for biological S turnover. *Biogeochemistry*, 47 (3): 319-333.
- Alewell, C. and Novak, M., **2001**. Spotting zones of dissimilatory sulfate reduction in a forested catchment: the S-34-S-35 approach. *Environmental Pollution*, 112 (3): 369-377.
- Alewell, C., Meusburger, K., Brodbeck, M. and Bänninger, D., **2008**. Methods to describe and predict soil erosion in mountain regions. *Landscape and Urban Planning*, 88 (2-4): 46-53.
- Ammer, U., Breitsameter, J. and Zander, J., **1995**. Contribution of mountain forests towards the prevention of surface runoff and soil-erosion. *Forstwissenschaftliches Centralblatt*, 114 (4-5): 232-249.
- Amundson, R., Austin, A.T., Schuur, E.A.G., Yoo, K., Matzek, V., Kendall, C., Uebersax, A., Brenner, D. and Baisden, W.T., **2003**. Global patterns of the isotopic composition of soil and plant nitrogen. *Global Biogeochemical Cycles*, 17 (1).
- Andre, M.F., **1998**. Depopulation, land-use change and landscape transformation in the French Massif Central. *Ambio*, 27 (4): 351-353.
- Angehrn, **1996**. Hydrogeologische Grundlagen - Urserental. Geologisches Büro Dr. P. Angehrn AG im Auftrag von: Amt für Umweltschutz - Abteilung Gewässerschutz, Altdorf.
- Arapis, G.D. and Karandinos, M.G., **2004**. Migration of Cs-137 in the soil of sloping semi-natural ecosystems in Northern Greece. *Journal of Environmental Radioactivity*, 77 (2): 133-142.
- Asner, G.P. and Heidebrecht, K.B., **2000**. Spectral unmixing of vegetation, soil and dry carbon cover in arid regions: comparing multispectral and hyperspectral observations, International Workshop on Land Cover/Land Use Change and Water Management in Arid Regions. Taylor & Francis Ltd, Beer Sheva, Israel, pp. 3939-3958.
- Asselman, N.E.M., Middelkoop, H. and van Dijk, P.M., **2003**. The impact of changes in climate and land use on soil erosion, transport and deposition of suspended sediment in the river Rhine. *Hydrological Processes*, 17 (16): 3225-3244.

- Atkinson, P.M. and Massari, R., **1998**. Generalized linear modelling of landslide susceptibility in the central Apennines. *Computers & Geosciences*, 24: 373– 385.
- Ayalew, L. and Yamagishi, H., **2005**. The application of GIS-based logistic regression for landslide susceptibility mapping in the Kakuda-Yahiko Mountains, Central Japan. *Geomorphology*, 65 (1-2): 15.
- Ayalew, L., Yamagishi, H., Marui, H. and Kanno, T., **2005**. Landslides in Sado Island of Japan: Part II. GIS-based susceptibility mapping with comparisons of results from two methods and verifications. *Engineering Geology*, 81 (4): 432-445.
- Backhaus, K., **2006**. Multivariate Analysemethoden: Eine anwendungsorientierte Einführung. Springer, Berlin, 830 pp.
- BAFU, **2001**. Article 18 of the Ordinance of 7 December 1998. Relating to Agricultural Terminology (SR 910.91). *Swiss Federal Office for the Environment (German: BAFU)*.
- BAFU, **2007**, Hydrological foundations and data. Real time and historical data, Swiss Federal Environmental Agency, <http://www.hydrodaten.admin.ch/d/2087.htm>, Access date: 7.1.2009.
- BAFU, **2009**, BAFU: Hydrological foundations and data. Real time and historical data, Swiss Federal Environmental Agency, <http://www.hydrodaten.admin.ch/d/2087.htm>, Access date: 7.1.2009.
- Bänninger, D., **2007**. Technical Note: Water flow routing on irregular meshes. *Hydrology and Earth System Sciences*, 11: 1243-1247.
- Bätzing, W., **1996**. Landwirtschaft im Alpenraum - Ansätze für eine Synthesedarstellung. In: Europäische Akademie Bozen (Hrsg.): Landwirtschaft im Alpenraum - unverzichtbar, aber zukunftslos. Blackwell Wissenschaftsverlag, Berlin, 229-242 pp.
- Baur, P., Müller, P. and Herzog, F., **2007**. Alpweiden im Wandel. *AGRAR Forschung*, 14 (6): 254-259.
- BBC, **2000**, Soil loss threatens food prospects, <http://news.bbc.co.uk/2/hi/science/nature/758899.stm>, Access date: 7.1.2009.
- Beasley, D.B., Huggins, L.F. and Monke, E.J., **1980**. ANSWERS - A model for watershed planning. *Transactions of the Asae*, 23 (4): 938-944.
- Beck, H.L., De Campo, J. and Gogolak, C., **1972**. In situ Ge(Li) and NaI(Tl) gamma-ray spectrometry. In: H.a.S. Laboratory and U.S.A.E, 75 pp.
- Beniston, M., **2006**. Mountain weather and climate: A general overview and a focus on climatic change in the Alps. *Hydrobiologica*, 562: 3-16.
- Beven, K. and Kirkby, M., **1979**. A physically based, variable contributing area model of basin hydrology. *Bulletin of Hydrolic Sciences*, 24: 43-69.
- BFS, **2001**. The changing face of landuse. Landuse statistics of Switzerland. Bundesamt für Statistik, Bern.
- BFS, **2005**. Arealstatistik Schweiz: Zahlen - Fakten - Analysen. Bundesamt für Statistik, Neuchâtel.
- Boardman, J.W. and Kruse, F.A., **1994**. Automated spectral analysis - a geological example using AVIRIS data, North Grapevine Mountains, Nevada, 10th Thematic Conference on Geologic Remote Sensing - Exploration, Environment, and Engineering. Environmental Research Inst Michigan, San Antonio, Tx, pp. I407-I418.
- Boardman, J.W., **1995**. Analysis, understanding and visualization of hyperspectral data as convex sets in n-space. In: M.R. Descour, J.M. Mooney, D.L. Perry and I. L. (Editors), Imaging Spectrometry Conference. Spie - Int Soc Optical Engineering, Orlando, Florida, pp. 14-22.
- Boardman, J.W., **1998**. Leveraging the high dimensionality of AVIRIS data for improved subpixel target unmixing and rejection of false positives: Mixture tuned matched filtering, Annual JPL Airborne Earth Science Workshop. In R. O. Green (Ed.), Summaries of the Seventh Annual JPL Airborne Earth Science Workshop, Pasadena, California.
- Bonnett, P.J.P., **1990**. A review of the erosional behavior of radionuclides in selected drainage basins. *Journal of Environmental Radioactivity*, 11 (3): 251-266.
- Brassel, P. and Brändli, U., **1999**. Schweizerisches Forstinventar. Ergebnisse der Zweitaufnahme 1993–1995. Birmensdorf, Eidgenössische Forschungsanstalt für Wald, Schnee und Landschaft, Bern.

- Brunetti, M., Maugeri, M., Nanni, T., Auer, I., Bohm, R. and Schoner, W., **2006**. Precipitation variability and changes in the greater Alpine region over the 1800-2003 period. *Journal of Geophysical Research - Atmospheres*, 111.
- Buck, B.J. and Monger, H.C., **1999**. Stable isotopes and soil-geomorphology as indicators of Holocene climate change, northern Chihuahuan Desert. *Journal of Arid Environments*, 43 (4): 357-373.
- Bunza, G., **1989**. Oberflächenabfluss und Bodenabtrag in alpinen Grassökosystemen. *Verhandlungen der Gesellschaft fuer Oekologie*, 12: 101-109.
- Can, T., Nefeslioglu, H.A., Gokceoglu, C., Sonmez, H. and Duman, T.Y., **2005**. Susceptibility assessments of shallow earthflows triggered by heavy rainfall at three catchments by logistic regression analyses. *Geomorphology*, 72 (1-4): 250.
- Carrara, A., **1983**. Multivariate models for landslide hazard evaluation. *Journal of the international association for mathematical geology*, 15 (3): 403-426.
- Carrara, A., Cardinali, M., Detti, R., Guzzetti, F., Pasqui, V. and Reichenbach, P., **1991**. GIS techniques and statistical-models in evaluating landslide hazard. *Earth Surface Processes and Landforms*, 16 (5): 427-445.
- Carrara, A., Guzzetti, F., Cardinali, M. and Reichenbach, P., **1998**. Current limitations in modeling landslide hazard. *Proceedings of IAMG'98*: 195-203.
- Carrara, A., Crosta, G. and Frattini, P., **2003**. Geomorphological and historical data in assessing landslide hazard. *Earth Surface Processes and Landforms*, 28 (10): 1125-1142.
- Carson, M.A., **1971**. The mechanics of erosion. Pion Ltd., London, 174 pp.
- Catchrisk, **2006**, INTERREG IIIB Alpine Space Programme, <http://www.alpinespace.org/catchrisk.html>, Access date: 7.1.2009.
- Cernusca, A., Bahn, M., Chemini, C., Graber, W., Siegwolf, R., Tappeiner, U. and Tenhunen, J., **1998**. ECOMONT: a combined approach of field measurements and process-based modelling for assessing effects of land-use changes in mountain landscapes. *Ecological modelling*, 113: 167-178.
- Chung, C.F. and Fabbri, A.G., **2003**. Validation of spatial prediction models for landslide hazard mapping. *Natural Hazards*, 30 (3): 451-472.
- Claessens, L., Lowe, D.J., Hayward, B.W., Schaap, B.F., Schoorl, J.M. and Veldkamp, A., **2006**. Reconstructing high-magnitude/low-frequency landslide events based on soil redistribution modelling and a Late-Holocene sediment record from New Zealand. *Geomorphology*, 74 (1-4): 29-49.
- Claessens, L., Schoorl, J.M. and Veldkamp, A., **2007**. Modelling the location of shallow landslides and their effects on landscape dynamics in large watersheds: An application for Northern New Zealand. *Geomorphology*, 87 (1-2): 16-27.
- Clark, M.J. and Smith, F.B., **1988**. Wet and dry depositions of chernobyl releases. *Nature*, 332 (6161): 245-249.
- Clerici, A., Perego, S., Tellini, C. and Vescovi, P., **2006**. A GIS-based automated procedure for landslide susceptibility mapping by the Conditional Analysis method: the Baganza valley case study (Italian Northern Apennines). *Environmental Geology*, 50 (7): 941-961.
- ClimChAlps, **2006**. Climate Change, Impacts and Adaption Strategies in the Alpine Space. *The Clim Ch Alps Partnership*: 1-32.
- Collison, A., Wade, S., Griffiths, J. and Dehn, M., **2000**. Modelling the impact of predicted climate change on landslide frequency and magnitude in SE England. *Engineering Geology*, 55 (3): 205-218.
- Dai, F.C. and Lee, C.F., **2002**. Landslide characteristics and slope instability modeling using GIS, Lantau Island, Hong Kong. *Geomorphology*, 42 (3-4): 213.
- Davis, J.C., Chung, C.J. and Ohlmacher, G.C., **2006**. Two models for evaluating landslide hazards. *Computers & Geosciences*, 32 (8): 1120-1127.
- De Asis, A.M. and Omasa, K., **2007**. Estimation of vegetation parameter for modeling soil erosion using linear Spectral Mixture Analysis of Landsat ETM data. *ISPRS Journal of Photogrammetry and Remote Sensing*, 62 (4): 309-324.
- De Asis, A.M., Omasa, K., Oki, K. and Shimizu, Y., **2008**. Accuracy and applicability of linear spectral unmixing in delineating potential erosion areas in tropical watersheds. *International Journal of Remote Sensing*, 29 (14): 4151-4171.

- De Jong, S.M., **1994**. Derivation of Vegetative Variables from a Landsat TM Image for Erosion Modelling. *Earth Surface Processes and Landforms*, 19 (2): 165-178.
- De Jong, S.M. and Riezebos, H.T., **1997**. SEMMED: a distributed approach to soil erosion modeling. In: A. Spiteri, Editor, Remote Sensing '96, Rotterdam 199-204 pp.
- De Jong, S.M., Paracchini, M., L., Bertolo, F., Folving, S., Megier, J. and De Roo, A.P.J., **1999**. Regional assessment of soil erosion using the distributed model SEMMED and remotely sensed data. *Catena*, 37: 291-308.
- De Roo, A. and Jetten, V., **1999**. Calibrating and validating the LISEM model for two data sets from the Netherlands and South Africa. *Catena*, 37: 477-493.
- De Vente, J., Poesen, J., Verstraeten, G., Van Rompaey, A. and Govers, G., **2008**. Spatially distributed modelling of soil erosion and sediment yield at regional scales in Spain. *Global and Planetary Change*, 60: 393-415.
- Descroix, L., Viramontes, D., Vauclin, M., Barrios, J.L.G. and Esteves, M., **2001**. Influence of soil surface features and vegetation on runoff and erosion in the Western Sierra Madre (Durango, Northwest Mexico). *Catena*, 43 (2): 115-135.
- Descroix, L. and Gautier, E., **2002**. Water erosion in the southern French alps: climatic and human mechanisms. *Catena*, 50 (1): 53-85.
- Descroix, L. and Mathys, N., **2003**. Processes, spatio-temporal factors and measurements of current erosion in the French Southern Alps: A review. *Earth Surface Processes and Landforms*, 28 (9): 993-1011.
- Desmet, P.J.J. and Govers, G., **1996**. A GIS procedure for automatically calculating the USLE LS factor on topographically complex landscape units. *Journal of Soil and Water Conservation*, 51 (5): 427-433.
- Domermuth, C., **1995**. Beschleunigte Bodenabtragungsvorgänge in der Kulturlandschaft des Nationalparks Berchtesgaden. Ursachen und Auswirkungen aufgezeigt am Beispiel des Jennergebiets. *Forstwissenschaftliches Centralblatt*, 114: 285-292.
- Dotterweich, M., **2008**. The history of soil erosion and fluvial deposits in small catchments of central Europe: Deciphering the long-term interaction between humans and the environment - A review, 39th Annual Binghamton Geomorphology Symposium. Elsevier Science Bv, Austin, TX, pp. 192-208.
- Douglas, T., Critchley, D. and Park, G., **1996**. The deintensification of terraced agricultural land near Trevelez, Sierra Nevada, Spain. *Global Ecology and Biogeography*, 4 (4-5): 258-270.
- Edwards, D.P., Halvorson, C.M. and Gille, J.C., **1999**. Radiative transfer modeling for the EOS Terra satellite Measurement of Pollution in the Troposphere (MOPITT) instrument. *Journal of Geophysical Research-Atmospheres*, 104 (D14): 16755-16775.
- EEA, **2000**. Down to earth: Soil degradation and sustainable development in Europe - A challenge for the 21st century Document Actions. European Environment Agency, Copenhagen.
- Egli, M., Margreth, M., Vökt, U., Fitze, P., Tognina, G. and Keller, F., **2005**. Modellierung von Bodentypen und Bodeneigenschaften im Oberengadin (Schweiz) mit Hilfe eines Geographischen Informationssystems (GIS). *Geographica Helvetica*, 2: 87-97.
- Elwell, H.A. and Stocking, M.A., **1976**. Vegetal cover to estimate soil erosion hazard in Rhodesia. *Geoderma*, 15 (1): 61-70.
- Ermini, L., Catani, F. and Casagli, N., **2005**. Artificial Neural Networks applied to landslide susceptibility assessment. *Geomorphology*, 66 (1-4): 327.
- Fabbri, A.G., Chung, C.-J.F., Cendrero, A. and Remondo, J., **2003**. Is Prediction of Future Landslides Possible with a GIS? *Natural Hazards*, 30 (3): 487-503.
- Fehr, W., **1926**. Geologische Karte der Urserenzone, Beiträge zur geologischen Karte der Schweiz. Kommissionsverlag: A. Franke A.G., Bern.
- Felix, R. and Johannes, B., **1995**. Bodenerosionsuntersuchungen auf Testparzellen im Kalkhochgebirge. *Mitteilungen der Österreichischen Geographischen Gesellschaft*, 137: 76-92.
- Folly, A., Bronsveld, M.C. and Clavaux, M., **1996**. A knowledge-based approach for C-factor mapping in Spain using Landsat TM and GIS. *International Journal of Remote Sensing*, 17 (12): 2401 - 2415.

- Frankenberg, P., Geier, B., Proswitz, E., Schütz, J. and Seeling, S., **1995**. Untersuchungen zu Bodenerosion und Massenbewegungen im Gunzesrieder Tal/Oberallgäu. *European Journal of Forest Research*, 114 (1): 214-231.
- Frei, C., Calanca, P., Schär, C., Wanner, H., Schaedler, B., Haeberli, W., Appenzeller, C., Neu, U., Thalmann, E., Ritz, C. and Hohmann, R., **2007**. Grundlagen. Klimaänderungen und die Schweiz 2050 - Erwartete Auswirkungen auf Umwelt, Gesellschaft und Wirtschaft.
- Fuhrer, J., Beniston, M., Fischlin, A., Frei, C., Goyette, S., Jasper, K. and Pfister, C., **2006**. Climate risks and their impact on agriculture and forests in Switzerland. *Climatic Change*, 79 (1): 79-102.
- GarciaRuiz, J.M., Lasanta, T., RuizFlano, P., Ortigosa, L., White, S., Gonzalez, C. and Marti, C., **1996**. Land-use changes and sustainable development in mountain areas: A case study in the Spanish Pyrenees. *Landscape Ecology*, 11 (5): 267-277.
- Gellrich, M. and Zimmermann, N.E., **2007**. Investigating the regional-scale pattern of agricultural land abandonment in the Swiss mountains: A spatial statistical modelling approach. *Landscape and Urban Planning*, 79 (1): 65-76.
- Gibbs, M., Thrush, S. and Ellis, J., **2001**. Terrigenous clay deposition on estuarine sandflats: Using stable isotopes to determine the role of the mud crab, *Helice crassa* Dana, in the recovery process. *Isotopes in Environmental Health Studies*, 37 (2): 113-131.
- Glade, T., **2003**. Landslide occurrence as a response to land use change: a review of evidence from New Zealand. *Catena*, 51 (3-4): 297-314.
- Glenn, N.F., Mundt, J.T., Weber, K.T., Prather, T.S., Lass, L.W. and Pettingill, J., **2005**. Hyperspectral data processing for repeat detection of small infestations of leafy spurge. *Remote Sensing of Environment*, 95 (3): 399-412.
- Gobin, A., Jones, R., Kirkby, M., Campling, P., Govers, G., Kosmas, C. and Gentile, A.R., **2004**. Indicators for pan-European assessment and monitoring of soil erosion by water. *Environmental Science & Policy*, 7 (1): 25-38.
- Gomez, H. and Kavzoglu, T., **2005**. Assessment of shallow landslide susceptibility using artificial neural networks in Jabonosa River Basin, Venezuela. *Engineering Geology*, 78 (1-2): 11-27.
- Gorsevski, P.V., Gessler, P.E., Boll, J., Elliot, W.J. and Foltz, R.B., **2006**. Spatially and temporally distributed modeling of landslide susceptibility. *Geomorphology*, 80 (3-4): 178-198.
- Graf, C., Boell, A. and Graf, F., **2003**. Pflanzen im Einsatz gegen Erosion und oberflächennahe Rutschungen. Eidgenössische Forschungsanstalt WSL, Birmensdorf.
- Gray, D.H. and Leiser, H.T., **1982**. Biotechnical slope protection and erosion control. Van Nostrand Reinhold, New York, 288 pp.
- Green, A.A., Berman, M., Switzer, P. and Craig, M.D., **1988**. A Transformation for ordering multispectral data in terms of image quality with implications for noise removal. *IEEE Transactions on Geoscience and Remote Sensing*, 26 (1): 65-74.
- Greenway, D.R., **1987**. Vegetation and slope stability. In: Anderson, M.G., Richards, K.S. (Eds.), *Slope Stability*. Wiley, Chichester, New York, 187-230 pp.
- Guardian, **2004**, Soil erosion as big a problem as global warming, say scientists, <http://www.guardian.co.uk/world/2004/feb/14/science.environment>., Access date: 7.1.2009.
- Guzzetti, F., Carrara, A., Cardinali, M. and Reichenbach, P., **1999**. Landslide hazard evaluation: a review of current techniques and their application in a multi-scale study, Central Italy. *Geomorphology*, 31 (1-4): 181.
- Guzzetti, F., Reichenbach, P., Ardizzone, F., Cardinali, M. and Galli, M., **2006**. Estimating the quality of landslide susceptibility models. *Geomorphology*, 81 (1-2): 166-184.
- Harris, A.T. and Asner, G.P., **2003**. Grazing gradient detection with airborne imaging spectroscopy on a semi-arid rangeland. *Journal of Arid Environments*, 55 (3): 391-404.
- Harris, D., Horwath, W.R. and van Kessel, C., **2001**. Acid fumigation of soils to remove carbonates prior to total organic carbon or carbon-13 isotopic analysis. *Soil Science Society of America Journal*, 65 (6): 1853-1856.
- Harsanyi, J.C. and Chang, C.I., **1994**. Hyperspectral image classification and dimensionality reduction - an orthogonal subspace projection approach. *IEEE Transactions on Geoscience and Remote Sensing*, 32 (4): 779-785.

- Haugen, L.E., **1991**. Small-scale variation in deposition of radiocesium from the Chernobyl fallout on cultivated grasslands in Norway, 27th International Colloquium on Spectroscopy. Royal Soc Chemistry, Norway, pp. 465-468.
- He, Q. and Walling, D.E., **2000**. Calibration of a field-portable gamma detector to obtain in situ measurements of the ¹³⁷Cs inventories of cultivated soils and floodplain sediments. *Applied Radiation and Isotopes*, 52 (4): 865-872.
- Heckrath, G., Djurhuus, J., Quine, T.A., Van Oost, K., Govers, G. and Zhang, Y., **2005**. Tillage erosion and its effect on soil properties and crop yield in Denmark. *Journal of Environmental Quality*, 34 (1): 312-324.
- Helming, K., Auzet, A.V. and Favis-Mortlock, D., **2005**. Soil erosion patterns: evolution, spatio-temporal dynamics and connectivity. *Earth Surface Processes and Landforms*, 30 (2): 131-132.
- Helsel, D.R., Mueller, D.K. and Slack, J.R., **2006**. Computer Program for the Kendall Family of Trend Tests. *Scientific Investigations Report 2005-5275*: 4.
- Herbst, M., Eschenbach, C. and Kappen, L., **1999**. Water use in neighbouring stands of beech (*Fagus Sylvatica* L.) and black alder (*Alnus glutinosa* (L.) Gaertn.). *Ann. For. Sci.*, 56: 107-120.
- Hill, R.A. and Foody, G.M., **1994**. Separability of tropical rain-forest types in the Tambopata-Candamo reserved zone, Peru *International Journal of Remote Sensing*, 15 (13): 2687-2693.
- Höchtel, F., Lehringer, S. and Konold, W., **2005**. "Wilderness": what it means when it becomes a reality--a case study from the southwestern Alps. *Landscape and Urban Planning*, 70 (1-2): 85-95.
- Hofmann, W., Gastberger, M. and Türk, R., **1995**. Bodenflechten der alpinen Höhenstufe als Bioindikator für radioaktiven Fallout. Umweltbundesamt, Wien.
- Horton, P., Schaefli, A., Mezghani, B., Hingray, B. and Musy, A., **2006**. Assessment of climate-change impacts on alpine discharge regimes with climate model uncertainty. *Hydrological Processes*, 20: 2091-2109.
- Hufschmidt, G., Crozier, M. and Glade, T., **2005**. Evolution of natural risk: research framework and perspectives. *Natural Hazards and Earth System Sciences*, 5: 375-387.
- IPCC, **2007**. Climate Change 2007: The physical science basis. Summary for policymakers. 661 10th session of working group I of the IPCC, Paris.
- Irigaray, C., Fernández, T., El Hamdouni, R. and Chacón, J., **2007**. Evaluation and validation of landslide-susceptibility maps obtained by a GIS matrix method: examples from the Betic Cordillera (southern Spain). *Natural Hazards*, 41 (1): 61-79.
- Isselin-Nondedeu, F. and Bedecarrats, A., **2007**. Influence of alpine plants growing on steep slopes on sediment trapping and transport by runoff. *Catena*, 71: 330-339.
- Jain, S.K., Singh, P. and Seth, S.M., **2002**. Assessment of sedimentation in Bhakra Reservoir in the western Himalayan region using remotely sensed data. *Hydrological Sciences Journal-Journal Des Sciences Hydrologiques*, 47 (2): 203-212.
- Jasper, K., Calanca, P., Gyalistras, D. and Fuhrer, J., **2004**. Differential impacts of climate change on the hydrology of two alpine river basins. *Climate Research*, 26: 113-129.
- Jenny, H., **1994**. Factors of Soil Formation. A System of Quantitative Pedology. Dover Press. (Reprint, with Foreword by R. Amundson, of the 1941 McGraw-Hill publication), New York.
- Jetten, V., Govers, G. and Hessel, R., **2003**. Erosion models: quality of spatial predictions. *Hydrological Processes*, 17: 887-900.
- Joint Research Center Ispra, **2008**, Land Management & Natural hazards unit, Commiss European Communities, <http://eussoils.jrc.ec.europa.eu/library/themes/LandSlides>, Access date: 7.1.09.
- Joint Research Center Ispra, **2009a**, Soil erosion in the Alps (RUSLE), <http://eussoils.jrc.ec.europa.eu/library/Themes/Erosion/ClimChalp/Rusle.html>, Access date:
- Joint Research Center Ispra, **2009b**, Nature and extend of soil erosion in Europe, Commiss European Communities, http://eussoils.jrc.it/ESDB_Archive/pesera/pesera_cd/sect_2_2.htm, Access date: 7.1.2009.

- Kaegi, H.U., **1973**. Die traditionelle Kulturlandschaft im Urserental: Beitrag zur alpinen Kulturgeographie, University of Zurich, Switzerland, 212 pp.
- Kanungo, D.P., Arora, M.K., Sarkar, S. and Gupta, R.P., **2006**. A comparative study of conventional, ANN black box, fuzzy and combined neural and fuzzy weighting procedures for landslide susceptibility zonation in Darjeeling Himalayas. *Engineering Geology*, 85 (3-4): 347-366.
- Karl, J., **1977**. Oberflächenabfluss und Bodenabtrag auf brachliegenden extensiv genutzten Flächen. DVWK (Deutscher Verband für Wasserwirtschaft und Kulturbau), 34.
- Karl, J., Porzelt, M. and Bunza, G., **1985**. Oberflächenabfluss und Bodenabtrag bei künstlichen Starkniederschlägen. DVWK (Deutscher Verband für Wasserwirtschaft und Kulturbau), 71: 37-102.
- Kaste, J.M., Heimsath, A.M. and Hohmann, M., **2006**. Quantifying sediment transport across an undisturbed prairie landscape using cesium-137 and high resolution topography. *Geomorphology*, 76 (3-4): 430-440.
- Kendall, C., **1998**. Tracing nitrogen sources and cycling in catchments. In: C. Kendall and J.J. McDonnell (Editors), *Isotope Tracers in Catchment Hydrology*. Elsevier Science B.V., Amsterdam, pp. 519-576.
- Kirkby, M., Robert, J., Irvine, B., Gobin, A., Govers, G., Cerdan, O., Tompaey, A., Le Bissonnais, Y., Daroussin, J., King, D., Montanarella, L., Grimm, M., Vieilefont, V., Puigdefabregas, J., Boer, M., Kosmas, C., Yassoglou, N., Tsara, M., Mantel, S., Van Lynden, G. and Hunting, J., **2003**. Pan-European Soil Erosion Risk Assessment. Joint Research Centre, ISPRA.
- Kirkby, M.J., Le Bissonnais, Y., Coulthard, T.J., Daroussin, J. and McMahon, M.D., **2000**. The development of land quality indicators for soil degradation by water erosion. *Agriculture, Ecosystems & Environment*, 81 (2): 125-135.
- Knödel, K., Krummel, H. and Lange, G., **1997**. Handbuch zur Erkundung des Untergrundes von Deponien und Altlasten. Band 3: Geophysik. SpringerVerlag.
- Komac, M., **2006**. A landslide susceptibility model using the Analytical Hierarchy Process method and multivariate statistics in perialpine Slovenia. *Geomorphology*, 74 (1-4): 17.
- Konz, N., Bänninger, D., Nearing, M. and Alewell, C., **2009a**. Does WEPP meet the specificity of soil erosion in steep mountain regions? *Hydrology and Earth System Sciences Discussion*, 6: 2153-2188.
- Konz, N., Schaub, M., Prasuhn, V., Bänninger, D. and Alewell, C., **2009b**. Cesium-137-based erosion-rate determination of a steep mountainous region. *Journal of Plant Nutrition and Soil Science*, 172 (5): 615-622.
- Konz, N., Schaub, B., Prasuhn, V. and Alewell, C., **submitted a**. Cs-137 based erosion rate determination of a steep mountainous region. *Journal of Plant nutrition and soil science*.
- Krause, K., **2003**. Radiance Conversion of QuickBird data.: Digital Globe. Colorado. USA.
- Krohmer, J. and Deil, U., **2003**. Dynamic and conservative landscapes? Present vegetation cover and land-use changes in the Serra de Monchique (Portugal). *Phytocoenologia*, 33 (4): 767-799.
- Krouse, R.H. and Grinenko, V.A., **1991**. Stable Isotopes: Natural and Anthropogenic Sulphur in the Environment. Scope 43. John Wiley and Sons, Chichester.
- Küttel, M., **1990a**. Der subalpine Schutzwald im Urserental - ein inelastisches Ökosystem. *Botanica Helvetica*, 100/2.
- Küttel, M., **1990b**. Zur Vegetationsgeschichte des Gotthardgebietes. *Mitteilungen der Naturforschenden Gesellschaft Luzern*, 31: 100-111.
- Labhart, T.P., **1999**. Planbeilage: Geologisch-tektonische Übersichtskarte Aarmassiv, Gotthardmassiv und Tavetscher Zwischenmassiv. In: S. Löw and R. Wyss (Editors), *Vorerkundung und Prognose der Basistunnels am Gotthard und am Lötschberg*. Balkema A. A., Rotterdam.
- Laedermann, J.P., Byrde, F. and Murith, C., **1998**. In-situ gamma-ray spectrometry: the influence of topography on the accuracy of activity determination. *Journal of Environmental Radioactivity*, 38 (1).
- Lange, E., **1994**. Intergration of computerized visual simulation and visual assessment in environmental-planning. *Landscape and Urban Planning*, 30 (1-2): 99-112.

- Langenscheidt, E., **1995**. The Jenner area of the Berchtesgaden-National-Park - short description and results of soil-erosion monitoring. *Forstwissenschaftliches Centralblatt*, 114 (4-5): 282-284.
- Lasanta, T., González-Hidalgo, J.C., Vicente-Serrano, S.M. and Sferi, E., **2006**. Using landscape ecology to evaluate an alternative management scenario in abandoned Mediterranean mountain areas. *Landscape and Urban Planning*, 78 (1-2): 101-114.
- Leifeld, J., Zimmermann, M., Fuhrer, J. and Conen, F., **2008**. Storage and turnover of carbon in grassland soils along an elevation gradient in the Swiss Alps. *Global Change Biology*, doi: 10.1111/j.1365-2486.2008.01782.x.
- Liu, J.G., Mason, P., Hilton, F. and Lee, H., **2004**. Detection of rapid erosion in SE Spain: A GIS approach based on ERS SAR coherence imagery. *Photogrammetric Engineering And Remote Sensing*, 70 (10): 1179-1185.
- Livens, F.R. and Loveland, P.J., **1988**. The influence of soil properties on the environmental mobility of caesium in Cumbria. *Soil Use and Management*, 4 (3): 69-75.
- Loke, M.H., **2000**. Electrical imaging surveys for environmental and engineering studies - A practical guide to 2-D and 3-D surveys. , <http://www.geoelectrical.com>, Access date: 7.1.2009.
- Luginbuhl, J.-M., Green, J.T., Poore, M.H. and Conrad, A.P., **2000**. Use of goats to manage vegetation in cattle pastures in the Appalachian region of North Carolina. *Sheep & Goat Research Journal* 16: 124-135.
- Machart, P., Hofmann, W., Turk, R. and Steger, F., **2007**. Ecological half-life Of Cs-137 in lichens in an alpine region. *Journal of Environmental Radioactivity*, 97 (1): 70-75.
- Markart, G., Kohl, B., Gallmetzer, W. and Pramstraller, A., **2000**. Wirkungen von Begrünungen auf das Abflussverhalten in Wildbacheinzugsgebieten bei Starkregen, Internationales Symposium INTERPRAEVENT, Villach / Österreich., pp. 53 - 64.
- Matisoff, G., Bonniwell, E.C. and Whiting, P.J., **2002**. Soil erosion and sediment sources in an Ohio watershed using beryllium-7, cesium-137, and lead-210. *Journal of Environmental Quality*, 31 (1): 54-61.
- McGee, E.J., Colgan, P.A., Dawson, D.E., Rafferty, B. and Okeeffe, C., **1992**. Effects of topography on cesium-137 in montane peat soils and vegetation. *Analyst*, 117 (3): 461-464.
- Merz, A., Alewell, C., Hiltbrunner, E. and Bänninger, D., **2009**. Plant-compositional effects on surface runoff and sediment yield in subalpine grassland. *Journal of Plant Nutrition and Soil Science*, 9999 (9999): NA.
- Meusburger, K. and Alewell, C., **2008**. Impacts of anthropogenic and environmental factors on the occurrence of shallow landslides in an alpine catchment (Urseren Valley, Switzerland). *Natural Hazards and Earth System Sciences*, 8: 509-520.
- Meusburger, K. and Alewell, C., **2009**. On the influence of temporal change on the validity of landslide susceptibility maps. *Natural Hazards and Earth System Sciences*, 9: 1495-1507.
- Meusburger, K., Bänninger, D. and Alewell, C., **submitted-a**. Estimating vegetation parameter for soil erosion assessment in an alpine catchment by means of QuickBird imagery. *International Journal of Applied Earth Observation and Geoinformation*: submitted.
- Meusburger, K., Konz, N., Schaub, M. and Alewell, C., **submitted-b**. Soil erosion modelled with USLE and PESERA using QuickBird derived vegetation parameters in an alpine catchment. *International Journal of Applied Earth Observation and Geoinformation*: submitted.
- Miller, K.M. and Shebell, P., **1993**. In situ gamma-ray spectrometry: A tutorial for environmental radiation scientists, United States.
- Millward, A.A. and Mersey, J.E., **1999**. Adapting the RUSLE to model soil erosion potential in a mountainous tropical watershed. *Catena*, 38: 109-129.
- Morgan, M.D., **1995**. Modeling excess sulfur deposition on wetland soils using stable sulfur isotopes. *Water Air and Soil Pollution*, 79 (1-4): 299-307.
- Morgan, R.P.C., Morgan, D.D.V. and Finney, H.J., **1984**. A PREDICTIVE MODEL FOR THE ASSESSMENT OF SOIL-EROSION RISK. *Journal of Agricultural Engineering Research*, 30 (3): 245-253.

- Mössmer, E.M., **1985**. Einflussfaktoren für die Blaikenerosion auf beweideten und aufgelassenen Almflächen im kalkalpinen Bereich der Landkreise Miesbach und Rosenheim. Forstliche Forschungsberichte München.
- Mottet, A., Ladet, S., Coque, N. and Gibon, A., **2006**. Agricultural land-use change and its drivers in mountain landscapes: A case study in the Pyrenees. *Agriculture, Ecosystems & Environment*, 114 (2-4): 296-310.
- Mundt, J.T., Glenn, N.F., Weber, K.T., Prather, T.S., Lass, L.W. and Pettingill, J., **2005**. Discrimination of hoary cress and determination of its detection limits via hyperspectral image processing and accuracy assessment techniques. *Remote Sensing of Environment*, 96 (3-4): 509-517.
- Nadim, F., Kjekstad, O., Peduzzi, P., Herold, C. and Jaedicke, C., **2006**. Global landslide and avalanche hotspots. *Landslides*, 3 (2): 159-173.
- Nearing, M., Foster, G., Lane, L. and Finkner, S., **1989**. A process-based soil erosion model for USDA - water erosion prediction project technology. *Transactions of the American Society of Agricultural Engineers*, 32 (5): 1587-1593.
- Newesely, C., Tasser, E., Spadinger, P. and Cernusca, A., **2000**. Effects of land-use changes on snow gliding processes in alpine ecosystems. *Basic and Applied Ecology*, 1 (1): 61-67.
- Niesiobedzka, K., **2000**. Mobile forms of radionuclide Cs-137 in sandy soils in northeastern Poland. *Polish Journal of Environmental Studies*, 9 (2): 133-136.
- Niwas, S., **1974**. Theoretical resistivity sounding results over a transition layer model. *Geophysical Prospecting*, 22 (2): 279-296.
- NSERL, **1995**. USDA-Water Erosion Prediction Project. Hillslope Profile and Watershed Model Documentation. National Soil Erosion Research Laboratory, West Lafayette.
- OcCC/ProClim-, **2007**. Klimaänderungen und die Schweiz 2050 - Erwartete Auswirkungen auf Umwelt, Gesellschaft und Wirtschaft. OcCC/ProClim-.
- Ohlmacher, G.C. and Davis, J.C., **2003**. Using multiple logistic regression and GIS technology to predict landslide hazard in northeast Kansas, USA. *Engineering Geology*, 69 (3-4): 331.
- Okin, G.S., **2007**. Relative spectral mixture analysis - A multitemporal index of total vegetation cover. *Remote Sensing of Environment*, 106 (4): 467-479.
- Owens, P.N., Walling, D.E. and He, Q., **1996**. The behaviour of bomb-derived caesium-137 fallout in catchment soils. *Journal of Environmental Radioactivity*, 32 (3): 169-191.
- Paningbatan, E.P., **2001**. Geographic information system-assisted dynamic modeling of soil erosion and hydrologic processes at a watershed scale. *Philippine Agricultural Scientist*, 84 (4): 388-393.
- Papanicolaou, A.N., Fox, J.F. and J., M., **2003**. Soil fingerprinting in the Palouse Basin, USA using stable carbon and nitrogen isotopes. *International Journal of Sediment Research*, 18 (2): 278-284.
- Parker Williams, A. and Hunt, E.R., **2002**. Estimation of leafy spurge cover from hyperspectral imagery using mixture tuned matched filtering. *Remote Sensing of Environment*, 82 (2-3): 446-456.
- Peng, W., Wheeler, D.B., Bell, J.C. and Krusemark, M.G., **2003**. Delineating patterns of soil drainage class on bare soils using remote sensing analyses. *Geoderma*, 115 (3-4): 261.
- Penman, H.L., **1948**. Natural evaporation from open water, bare and grass. *Proc R Soc Lond Ser A*, 193: 120-145.
- Petley, D., Hearn, G., Hart, A., Rosser, N., Dunning, S., Owen, K. and Mitchell, W., **2007**. Trends in landslide occurrence in Nepal. *Natural Hazards*, 43 (1): 23-44.
- Piégay, H., Walling, D.E., Landon, N., He, Q.P., Liébault, F. and Petiot, R., **2004**. Contemporary changes in sediment yield in an alpine mountain basin due to afforestation (The upper Drome in France). *Catena*, 55: 183-212.
- Remondo, J., González, A., De Terán, J.R.D., Cendrero, A., Fabbri, A. and Chung, C.-J.F., **2003**. Validation of Landslide Susceptibility Maps; Examples and Applications from a Case Study in Northern Spain. *Natural Hazards*, 30 (3): 437-449.
- Renard, K.G., Foster, G.R. and Weesies, G.A., **1997**. Predicting soil erosion by water; a guide to conservation planning with the revised universal soil loss equation (RUSLE). Agriculture Handbook No. 703, USDA-ARS, 703, 404 pp.

- Reusing, M., Schneider, T. and Ammer, U., **2000**. Modelling soil loss rates in the Ethiopian Highlands by integration of high resolution MOMS-02/D2-stereo-data in a GIS. *International Journal of Remote Sensing*, 21 (9): 1885-1896.
- Richter, R., **2005**. Atmospheric / topographic correction for satellite imagery. Atcor 2/3 user guide. version 6.1, Wessling, Germany.
- Rickli, C., Zimmerli, P. and Böll, A., **2001**. Effects of vegetation on shallow landslides: an analysis of the events of August 1997 in Sachseln, Switzerland. *International Conference on Landslides. Causes, Impacts and Countermeasures*: 575-584.
- Riesen, T.K., Zimmermann, S. and Blaser, P., **1999**. Spatial distribution of Cs-137 in forest soils of Switzerland. *Water Air and Soil Pollution*, 114 (3-4): 277-285.
- Ritchie, J.C. and McHenry, J.R., **1990**. Application of radioactive fallout cesium-137 for measuring soil-erosion and sediment accumulation rates and patterns - a review. *Journal of Environmental Quality*, 19 (2): 215-233.
- Ritchie, J.C. and McCarty, G.W., **2003**. (137)Cesium and soil carbon in a small agricultural watershed. *Soil & Tillage Research*, 69 (1-2): 45-51.
- Ritzmann-Blickenstorfer, H., **1996**. Historische Statistik der Schweiz. Chronos Verlag, Zürich.
- Roberts, D.A., Smith, M.O. and Adams, J.B., **1993**. Green vegetation, nonphotosynthetic vegetation, and soils in AVIRIS data. *Remote Sensing of Environment*, 44 (2-3): 255-269.
- Robichaud, P.R., Lewis, S.A., Laes, D.Y.M., Hudak, A.T., Kokaly, R.F. and Zamudio, J.A., **2007**. Postfire soil burn severity mapping with hyperspectral image unmixing. *Remote Sensing of Environment*, 108 (4): 467-480.
- Rogiers, N., Eugster, W., Furger, M. and Siegwolf, R., **2005**. Effect of land management on ecosystem carbon fluxes at a subalpine grassland site in the Swiss Alps. *Theoretical and Applied Climatology*, 80 (2-4): 187-203.
- Rogler, H. and Schwertmann, U., **1981**. Rainfall erosivity and isoerodent map of Bavaria. *Zeitschrift für Kulturtechnik und Flurbereinigung*, 22 (2): 99-112.
- Russi, A., **2006**. Erhebung der Viehzahlen in Ursern. Kooperation Urseren: Talkanzlei Ursern, Andermatt.
- Santacana, N., Baeza, B., Corominas, J., De Paz, A. and Marturia, J., **2003**. A GIS-based multivariate statistical analysis for shallow landslide susceptibility mapping in La Pobla de Lillet area (Eastern Pyrenees, Spain). *Natural Hazards*, 30 (3): 281-295.
- Sawhney, B.L., **1972**. Selective sorption and fixation of cations by clay-minerals - review. *Clays and Clay Minerals*, 20 (2): 93-100.
- Schaub, M., Konz, N., Meusburger, K. and Alewell, C., **submitted**. Application of in-situ measurement to determine 137-Cs in the Swiss Alps. *Journal of Environmental Radioactivity*: submitted.
- Schaub, M. and Alewell, C., **submitted a**. Stable carbon isotopes as an indicator for soil degradation in an alpine environment (Urseren Valley, Switzerland). *European Journal of Soil Sciences*.
- Schauer, T., **1975**. Die Blaikenbildung in den Alpen. *Schriftreihe Bayerisches Landesamt für Wasserwirtschaft*: 1-29.
- Schauer, T., **1981**. Vegetations veränderungen und Florenverlust auf Skipisten in den bayrischen Alpen. *Jahrbuch des Vereins zum Schutze der Bergwelt e.V München*: 149-179.
- Schimmack, W., Bunzl, K. and Zelles, L., **1989**. Initial rates of migration of radionuclides from the Chernobyl fallout in undisturbed soils. *Geoderma*, 44 (2-3): 211-218.
- Schimmack, W., Steindl, H. and Bunzl, K., **1998**. Variability of water content and of depth profiles of global fallout Cs-137 in grassland soils and the resulting external gamma-dose rates. *Radiation and Environmental Biophysics*, 37 (1): 27-33.
- Schimmack, W. and Schultz, W., **2006**. Migration of fallout radiocaesium in a grassland soil from 1986 to 2001 - Part 1: Activity-depth profiles of Cs-134 and Cs-137. *Science of the Total Environment*, 368 (2-3): 853-862.
- Schindler, Y., Alewell, C., Burri, K. and Bänninger, D., **submitted**. Evaluation of a small hybrid rainfall simulator and its application to quantify water erosion on subalpine grassland. *Catena*: submitted.
- Schmidli, J. and Frei, C., **2005**. Trends of heavy precipitation and wet and dry spells in Switzerland during the 20th century. *International Journal of Climatology*, 25: 753-771.

- Schmidt, J., Von Werner, M. and Michael, A., **1999**. Application of the EROSION 3D model to the CATSOP watershed, The Netherlands. *Catena*, 37: 449-456.
- Schmidt, J. and Dikau, R., **2004**. Modeling historical climate variability and slope stability. *Geomorphology*, 60 (3-4): 433-447.
- Schneeberger, N., Burgi, M. and Kienast, P.D.F., **2007**. Rates of landscape change at the northern fringe of the Swiss Alps: Historical and recent tendencies. *Landscape and Urban Planning*, 80 (1-2): 127-136.
- Schoorl, J.M., Boix Fayos, C., de Meijer, R.J., van der Graaf, E.R. and Veldkamp, A., **2004**. The Cs-137 technique applied to steep Mediterranean slopes (Part I): the effects of lithology, slope morphology and land use. *Catena*, 57 (1): 15-34.
- Schroter, D., Cramer, W., Leemans, R., Prentice, I.C., Araujo, M.B., Arnell, N.W., Bondeau, A., Bugmann, H., Carter, T.R., Gracia, C.A., de la Vega-Leinert, A.C., Erhard, M., Ewert, F., Glendining, M., House, J.I., Kankaanpää, S., Klein, R.J.T., Lavorel, S., Lindner, M., Metzger, M.J., Meyer, J., Mitchell, T.D., Reginster, I., Rounsevell, M., Sabate, S., Sitch, S., Smith, B., Smith, J., Smith, P., Sykes, M.T., Thonicke, K., Thuiller, W., Tuck, G., Zaehle, S. and Zierl, B., **2005**. Ecosystem service supply and vulnerability to global change in Europe. *Science*, 310 (5752): 1333-1337.
- Schuepp, M., **1975**. Objective weather forecasts using statistical aids in Alps. *Rivista Italiana Di Geofisica E Scienze Affini*, 1: 32-36.
- Schuller, P., Bunzl, K., Voigt, G., Ellies, A. and Castillo, A., **2004**. Global fallout Cs-137 accumulation and vertical migration in selected soils from South Patagonia. *Journal of Environmental Radioactivity*, 71 (1): 43-60.
- Shrestha, D.P., Zinck, J.A. and Van Ranst, E., **2004**. Modelling land degradation in the Nepalese Himalaya. *Catena*, 57 (2): 135.
- Shrimali, S.S., Aggarwal, S.P. and Samra, J.S., **2001**. Prioritizing erosion-prone areas in hills using remote sensing and GIS – a case study of the Sukhna Lake catchment, Northern India. *International Journal of Applied Earth Observation and Geoinformation*, 3 (1): 54.
- SilvaProtect-CH, **2006**. Dokumentation zu Projektphase I und II. Bundesamt für Umwelt - Abteilung Gefahrenprävention.
- SilvaProtect-CH, **2008**, <http://www.bafu.admin.ch/naturgefahren/01920/01964/index.html?lang=de>, Access date: 7.1.2009.
- SLF, **2007**. Swiss Federal Institute for Snow and Avalanche Research Davos.
- Smith, M.O., Adams, J.B. and Sabol, D.E., **1992**. Spectral mixture analysis - new strategies for the analysis of multispectral data. In: J.M.J. Hill (Editor), 2nd Eurocourse on Imaging Spectrometry: A Tool for Environmental Observations. Kluwer Academic Publ, Ispra, Italy, pp. 125-143.
- Sparling, G., Ross, D., Trustrum, N., Arnold, G., West, A., Speir, T. and Schipper, L., **2003**. Recovery of topsoil characteristics after landslip erosion in dry hill country of New Zealand, and a test of the space for time hypothesis. *Soil Biology & Biochemistry*, 35: 1575-1586.
- SPSS, **2009**. SPSS for Windows 15.0, Rel. 11.0.1. 2001. Chicago: SPSS Inc.
- Strunk, H., **2003**. Soil degradation and overland flow as causes of gully erosion on mountain pastures and in forests. *Catena*, 50 (2-4): 185-198.
- Suezen, M.L. and Doyuran, V., **2004**. Data driven bivariate landslide susceptibility assessment using geographical information systems: a method and application to Asarsuyu catchment, Turkey. *Engineering Geology*, 71: 303-321.
- Swisstopo, **2006**. Reproduziert mit Bewilligung von swisstopo. (BA071108, Zürich).
- Tappeiner, U., Tasser, E., Leitinger, G. and Tappeiner, G., **2006**. Landnutzung in den Alpen: historische Entwicklung und zukünftige Szenarien. In: Die Alpen im Jahr 2020, 1. Innsbruck university press, 23-39 pp.
- Tarboton, D., **1997**. A new method for the determination of flow directions and upslope areas in grid digital elevation models. *Water Resources Research*, 33 (2): 309-319.
- Tasser, E. and Tappeiner, U., **2002**. Impact of land use changes on mountain vegetation. *Applied Vegetation Science*, 5 (2): 173-184.

- Tasser, E., Mader, M. and Tappeiner, U., **2003**. Effects of land use in alpine grasslands on the probability of landslides. *Basic and Applied Ecology*, 4 (3): 271-280.
- Tasser, E., Walde, J., Tappeiner, U., Teutsch, A. and Noggler, W., **2007**. Land-use changes and natural reforestation in the Eastern Central Alps. *Agr. Ecosyst. Environ.*, 118 (1-4): 115-129.
- Theseira, M.A., Thomas, G., Taylor, J.C., Gemmell, F. and Varjo, J., **2003**. Sensitivity of mixture modelling to end-member selection. *International Journal of Remote Sensing*, 24 (7): 1559 - 1575.
- Thiam, A.K., **2003**. The causes and spatial pattern of land degradation risk in southern Mauritania using multitemporal AVHRR-NDVI imagery and field data. *Land Degradation & Development*, 14 (1): 133-142.
- Troxler, J., Chatelain, C. and Schwery, M., **2004**. Technical and economical evaluation of grazing systems for high altitude sheep pastures in Switzerland. *Grassland Science in Europe*, 9: 590-592.
- Tucker, C.J., **1979**. Red and photographic infrared linear combinations for monitoring vegetation. *Remote Sensing of Environment*, 8 (2): 127- 150.
- Tweddles, S.C., Eschlaeger, C.R. and Seybold, W.F., **2000**. An Improved Method for Spatial Extrapolation of Vegetative Cover Estimates (USLE/RUSLE C factor) using LCTA and Remotely Sensed Imagery. USAEC report No. SFIM-AEC-EQ-TR-200011, ERDC/CERL TR-00-7, CERL, Champaign. US Army of Engineer Research and Development Center, Illinois.
- Tyler, A.N., Davidson, D.A. and Grieve, I.C., **2001**. In situ radiometric mapping of soil erosion and field-moist bulk density on cultivated fields. *Soil Use and Management*, 17 (2): 88-96.
- US Department of Agriculture, S.C.S., **1977**. Procedure for computing sheet and rill erosion on project areas. Soil Conservation Service, Technical Release No. 51 (Rev. 2).
- Van-Camp, L., Bujarrabal, B., Gentile, A.-R., Jones, R.J.A., Montanarella, L., Olazabal, C. and Selvaradjou, S.-K., **2004**. Reports of the Technical Working Groups Established under the Thematic Strategy for Soil Protection. European Soil Bureau, Luxembourg.
- Van Den Eeckhaut, M., Vanwalleghem, T., Poesen, J., Govers, G., Verstraeten, G. and Vandekerckhove, L., **2006**. Prediction of landslide susceptibility using rare events logistic regression: A case-study in the Flemish Ardennes (Belgium). *Geomorphology*, 76 (3-4): 392-410.
- Van der Knijff, J.M., Jones, R.J.A. and Montanarella, L., **2000**. Soil Erosion Risk Assessment in Italy. European Soil Bureau, Luxembourg.
- Van der Meer, F. and De Jong, S.M., **2000**. Improving the results of spectral unmixing of Landsat Thematic Mapper imagery by enhancing the orthogonality of end-members. *International Journal of Remote Sensing*, 21 (15): 2781-2797.
- Van Rompaey, A.J.J., Verstraeten, G., Van Oost, K., Govers, G. and Poesen, J., **2001**. Modelling mean annual sediment yield using a distributed approach. *Earth Surface Processes and Landforms*, 26: 1221-1236.
- Van Rompaey, A.J.J. and Govers, G., **2002**. Data quality and model complexity for regional scale soil erosion prediction. *International Journal of Geographical Information Science*, 16: 663-680.
- Van Rompaey, A.J.J., Bazzoffi, P., Jones, R.J.A., Montanarella, L. and Govers, J., **2003a**. Validation of Soil Erosion Risk Assessment in Italy. European Commission, Joint Research Centre, Luxembourg.
- Van Rompaey, A.J.J., Vieillefont, V., Jones, R.J.A., Montanarella, L., Verstraeten, G., Bazzoffi P., Dostal, T., Krasa, J., de Vente, J. and Poesen, J., **2003b**. Validation of Soil Erosion Estimates at European scale. European Soil Bureau Research Report No.13, Luxembourg.
- Van Westen, C.J., **2000**. The modelling of landslide hazard using GIS. *Surveys in Geophysics*, 21: 241-255.
- Van Westen, C.J. and Lulie Getahun, F., **2003**. Analyzing the evolution of the Tessina landslide using aerial photographs and digital elevation models. *Studies on Large Volume Landslides*, 54 (1-2): 77.

- Vanacker, V., Vanderschaeghe, M., Govers, G., Willems, E., Poesen, J., Deckers, J. and De Bievre, B., **2003**. Linking hydrological, infinite slope stability and land-use change models through GIS for assessing the impact of deforestation on slope stability in high Andean watersheds. *Geomorphology*, 52 (3-4): 299-315.
- Varnes, D.J., **1984**. Landslide hazard zonation: A review of principles and practice, Paris.
- Von Wyl, B., **1988**. Düngung an steilen Hängen vergrößert das Risiko von Erdrutschen. *Mitteilungen der Naturforschenden Gesellschaft Luzern*, 30: 324-335.
- Vrieling, A., **2006**. Satellite remote sensing for water erosion assessment: A review. *Catena*, 65 (1): 2-18.
- Vrieling, A., Rodrigues, S.C., Bartholomeus, H. and Sterk, G., **2007**. Automatic identification of erosion gullies with ASTER imagery in the Brazilian Cerrados. *International Journal of Remote Sensing*, 28 (12): 2723-2738.
- Walling, D.E. and Quine, T.A., **1991**. Use of ¹³⁷Cs measurements to investigate soil erosion on arable fields in the UK: potential applications and limitations. *Journal of Soil Science*, 42 (1): 147-165.
- Walling, D.E., He, Q. and Blake, W., **1999**. Use of Be-7 and Cs-137 measurements to document short- and medium-term rates of water-induced soil erosion on agricultural land. *Water Resources Research*, 35 (12): 3865-3874.
- Wang, Y., Huntington, T.G., Osher, L.J., Wassenaar, L.I., Trumbore, S.E., Amundson, R.G., Harden, J.W., McKnight, D.M., Schiff, S.L., Aiken, G.R., Lyons, W.B., R.O., A. and J.S., B., **1998**. Carbon cycling in terrestrial environments. In: C. Kendall and J.J. McDonnell (Editors), *Isotope Tracers in Catchment Hydrology*. Elsevier B.V., Amsterdam, pp. 577-610.
- Wiedmer, E. and Senn-Irlet, B., **2006**. Biomass and primary productivity of an *Alnus viridis* stand – a case study from the Schächental valley, Switzerland. *Botanica Helvetica*, 116: 55-64.
- Wills, C.J. and McCrink, T.P., **2002**. Comparing landslide inventories: The map depends on the method. *Environmental & Engineering Geoscience*, 8 (4): 279-293.
- Wilson, J.P. and Gallant, J.C., **1996**. EROS: A grid-based program for estimating spatially-distributed erosion indices. *Computers & Geosciences*, 22 (7): 707-712.
- Wischmeier, W.H. and Smith, D.D., **1978**. Predicting Rainfall Erosion Losses - A Guide to Conservation Planning. Agric. Handbook No. 537, Washington D.C.
- WRB, **2006**. IUSS Working Group World reference base for soil resources. Food and Agriculture Organization of the United Nations, Rom.
- Wu, R.G. and Tiessen, H., **2002**. Effect of land use on soil degradation in alpine grassland soil, China. *Soil Science Society of America Journal*, 66 (5): 1648-1655.
- Wyss, R., **1986**. Die Urseren-Zone - Lithostatigraphie und Tektonik. *Eclogae Geologicae Helveticae*, 79 (3): 731-767.
- Yesilnacar, E. and Topal, T., **2005**. Landslide susceptibility mapping: A comparison of logistic regression and neural networks methods in a medium scale study, Hendek region (Turkey). *Engineering Geology*, 79 (3-4): 251.
- Zapata, F., **2003**. The use of environmental radionuclides as tracers in soil erosion and sedimentation investigations: recent advances and future developments. *Soil & Tillage Research*, 69 (1-2): 3-13.
- Zêzere, J.L., Reis, E., Garcia, R., Oliveira, S., Rodrigues, M.L., Vieira, G. and Ferreira, A.B., **2004**. Integration of spatial and temporal data for the definition of different landslide hazard scenarios in the area north of Lisbon (Portugal). *Natural Hazards and Earth System Sciences*, 4 (1): 133-146.
- Zhou, C.H., Lee, C.F., Li, J. and Xu, Z.W., **2002**. On the spatial relationship between landslides and causative factors on Lantau Island, Hong Kong. *Geomorphology*, 43 (3-4): 197-207.
- Zinck, J.A., Lopez, J., Metternicht, G.I., Shrestha, D.P. and Vazquez-Selem, L., **2001**. Mapping and modelling mass movements and gullies in mountainous areas using remote sensing and GIS techniques. *International Journal of Applied Earth Observation and Geoinformation*, 3 (1): 43.

APPENDIX

Some additional results

10.1. Modelling soil erosion of an alpine grassland

For the PESERA (Pan-European Soil Erosion Risk Assessment) model, which is an established conceptual model, I explored the local sensitivity of the input parameter with respect to the model output. A local sensitivity analysis quantifies the effect of small variations of an input on an output compared to a base case. The base case are measured field parameters at the test site in the Urseren Valley for the year 2006 (Konz et al., submitted a). For the base case a mean precipitation of 1095 mm, a mean temperature of 6.15°C, a slope of 55%, a fractional vegetation cover of 50% and a qualitative erodibility value of 5 was used. In PESERA the erodibility value is connected to soil types by means of pedo-transfer functions. Precipitation- and slope values ranging from plus 100% to minus 100% of the base case value were used. The mean air temperature is ranging from -3.85°C to 16.15°C and fractional vegetation cover (FVC) from 0% to 100%. For the base case the curves concentrate in one point/output for runoff and erosion. For our base case the erosion rate is 2.96 t ha⁻¹ a⁻¹ and runoff 317 mm (Figure 1-1).

The PESERA model shows a high sensitivity to temperature for both runoff and erosion. This might be due to the general low temperatures of our base case. Small temperature shifts can have strong effects on vegetation, for instance, by reducing the temperature the vegetation module of PESERA stops the growing of vegetation. Moreover, temperature plays also a decisive role whether precipitation falls as snow or rain. The erosion output is also strongly influenced by FVC, however, FVC values > 50% show only weak sensitivity. Runoff increases with increasing slope angle. Erosion increases for slope angles > 55%. The amount of precipitation only slightly affected runoff for our base case. The relation between runoff and precipitation might be stronger for different vegetation types and lower FVC. Erosion slightly increases for decreasing precipitation probably due to a reduced growth of vegetation. Without precipitation no erosion is observed due to the lack of the transport and detaching trigger. The erodibility does not affect runoff, which seems plausible. Erosion output is only slightly increased with increasing erodibility.

Except for the low sensitivity of precipitation and FVC > 50% to runoff and erosion, the relation between model input parameters and produced output are plausible. For our base case the effect of precipitation might be underestimated due to an overestimation of the protective effect of vegetation and snow cover.

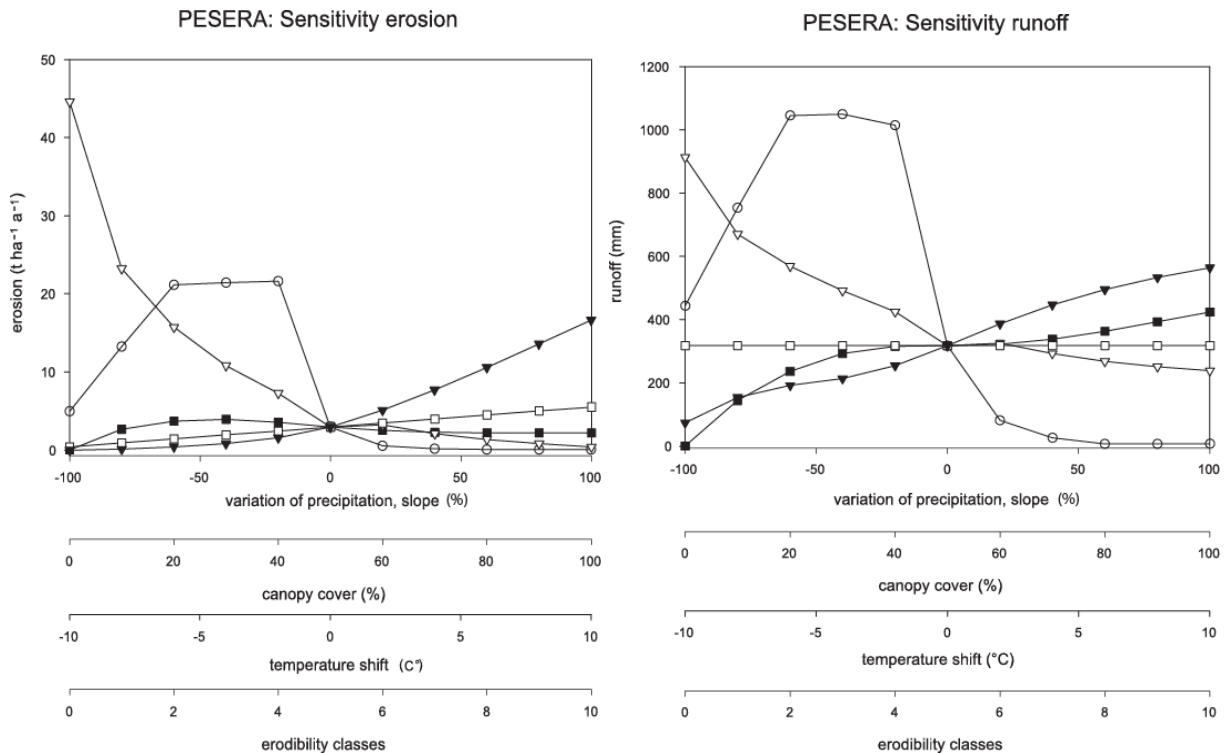


Figure 10-1. Local sensitivities of erosion and runoff in the PESERA model.

10.2. Digital soil mapping – a decision tree approach

During field courses with students in the Urseren Valley over 160 soil profiles have been mapped according to the "Bodenkundliche Kartieranleitung KA5". The data has a great bias due to the change of students over the years. Nonetheless, we could establish a knowledge-based conceptual model of the soil type distribution in the valley. According to Jenny (1994) soil properties are determined by following factors: regional climate, potential biota, topography, parent material and time. In order to map soil types it is in a first step necessary to derive proxies for these parameters for the entire catchment and second to implement the conceptual model in order to classify the dataset. The decision tree derived from the conceptual model is shown in Figure 10-2.

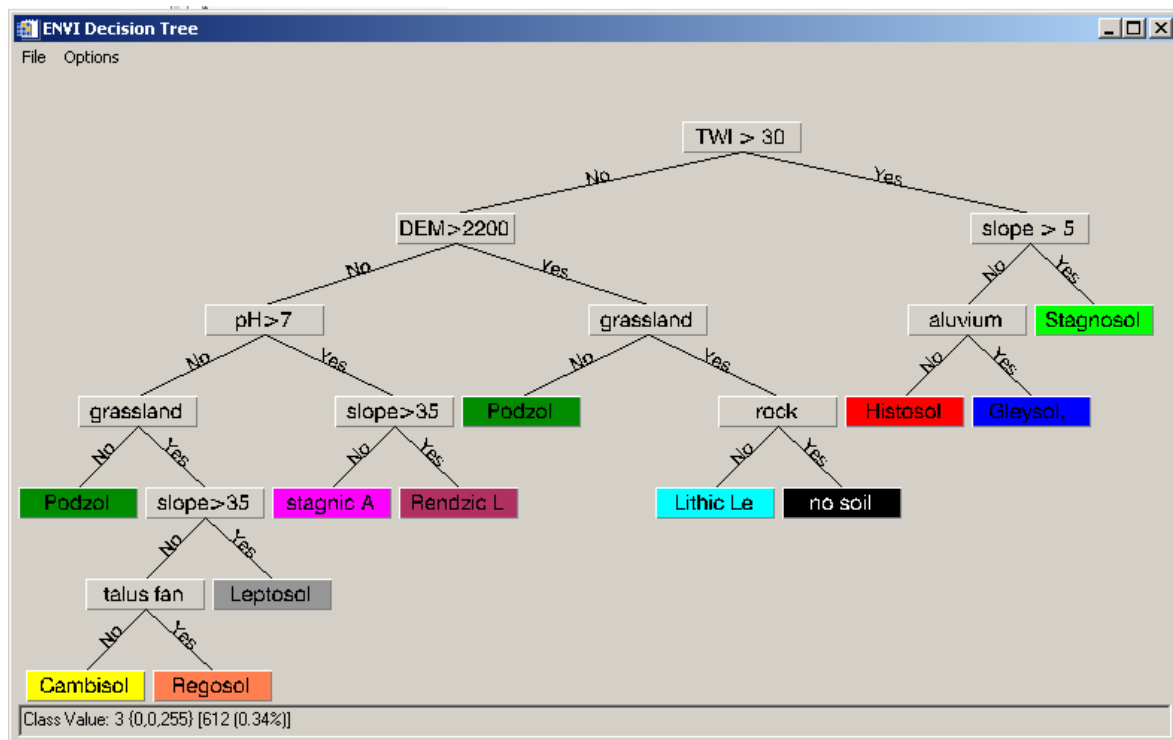


Figure 10-2. Decision tree used for the digital mapping of dominant soil types in the Urseren Valley.

The parameter climate was represented by the DEM, which was subdivided into two classes: DEM > 2200 m a.s.l. above this height Lithic Leptosols are prevalent. The topographic wetness index (TWI), developed by Beven and Kirkby (1979), is a proxy for water availability. In a first step we separated potential wet soils from dry soils by a threshold of TWI > 30. Water influenced soils are Stagnosol, Histosol, Gleysol and Fluvisol. The later three only occur at flat terrain (slope angle < 5°). Further, it was assumed that Gleysols and Fluvisols occur exclusively on the valley alluvium. Slope is the most relevant topographic parameter: above a slope angle of 40°, depending on the parent material, different A/C- soils occur. Regosols can also occur on talus fans, where time was too short to develop Cambisols. This seems to be true for parts of the talus fan with a slope angle > 5°. For parent material, we used a map with 2 classes separating siliceous material from calcareous (pH > 7). Finally, we used the land-cover map of the QuickBird classification (chapter 5) to separate grassland from the remaining cover types (dwarf-shrubs, shrubs, forest). Cambisols are predominant for grassland. For the remaining vegetation types Podzols are predominant. The decision tree was executed using ENVI 4.3 software (Research Systems Inc., Boulder, CO). The resulting soil type map is shown in Figure 10-3. A validation of the map is still required.

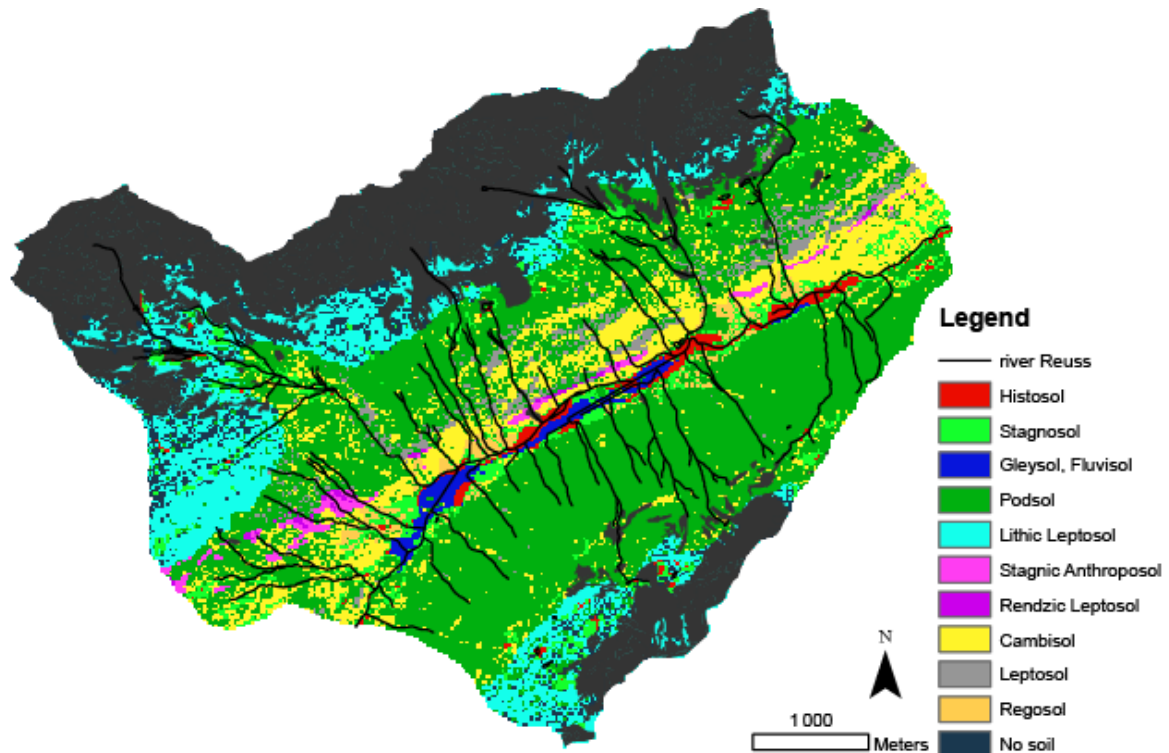


Figure 10-3. Digital soil map of the Urseren Valley showing the distribution of the 10 predominant soil types.

10.3. Electrical Resistivity Tomography (ERT)

The purpose of the ERT is to determine the resistivity distribution of the subsurface by making measurements on the surface (Loke, 2000). This method provides insight to the subsurface structure without affecting or even destroying it. Due to the high density of ions inside a matrix pore, it can be assumed that electric conductivity is stronger influenced by porosity and electrical conductivity of the water than by the surrounding matrix material. Therefore, Ski Niwas (1974), conclude that measured resistivity mainly reflects hydrologic conditions. The effect of porosity and water content on the electrical resistivity is expressed by Archie's law (Knödel et al., 1997):

$$\frac{\sigma_w}{\sigma_f} = F = \varepsilon * p_e^{-m} \quad (9-1)$$

- σ_w = conductivity of the water [-],
- σ_f = conductivity of the formation as a whole [-],
- F = „formation factor“, related to the volume and tortuosity of the pore space,
- ε = empirical constant, typically 1 for unconsolidated sediments,
- m = empirical constant, typically 2 for unconsolidated sediments,
- p_e = effective porosity, the fraction of interconnected pore space.

The interpretation of resistivity data is difficult, because without the knowledge about the depth of different materials, it is not possible to calculate the resistivity of the materials and without the knowledge of the specific resistivity of the different materials, no depth can be assigned to the different layers. To solve this problem the use of inversion-software program is necessary to calculate via a subsurface picture with “pseudo” depth and “pseudo” resistivities a “true” image of the subsurface. Therefore, a top down approach is used. With the assumption that the upper layer consists of only one resistivity a “true” depth is calculated. Based on this information the second and the following layer are calculated. In this manner, a model of the subsurface is generated which shows which resistivity response fits best to the measured resistivities. The quality of the fit is represented by the root mean squared (RMS). Essential for the correct interpretation is to keep in mind how the image of the subsurface is created. Errors develop for example due to the 3-dimensional nature of resistivity data, which are transformed to point data and again interpolated to two-dimensional images.

The analysis of the measured resistivity collected with Syscal Kid was performed by a commercial inversion-software-program RES2dinv. We measured a profile with landslides (site Hospental) and without landslides (site Realp) during dry conditions (no precipitation for three days). The comparison of the two profiles shows an opposed vertical distribution of resistivity. For the landslide site, resistivities are low for the upper layer and low for the subjacent layer (Figure 10-4).

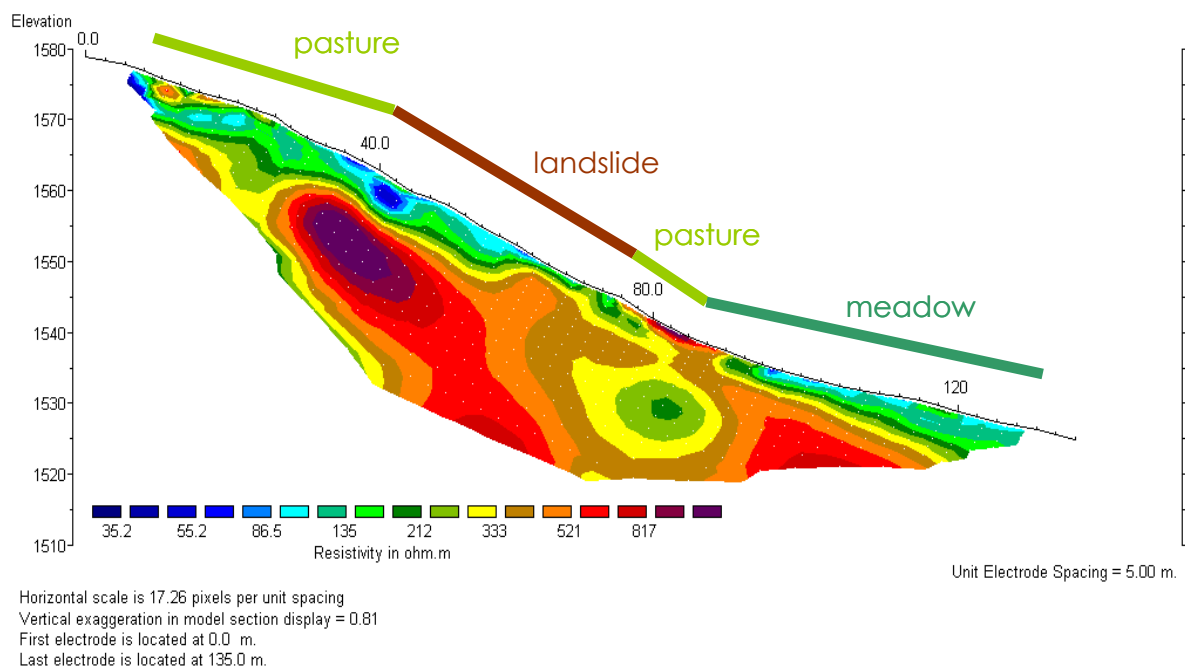


Figure 10-4. ERT transect at landslide slope in Hospental (Dipole-dipole | 5 m spacing | 28 electrodes | RMS error 5.7 % | 22.09.06) during dry conditions.

Only a small section of high resistivities below the landslide area reaches up to the surface. Whether this section was already present before the landslide potentially impeding lateral drainage of the slope is not known. In general, the very low

resistivities in the upper section point to an accumulation of water above a less permeable layer. This assumption is strengthened by a second measurement after a rainfall event of 17.2 mm, where we see a further decrease of resistivity below the landslide area and at the foot of the slope (Figure 10-5).

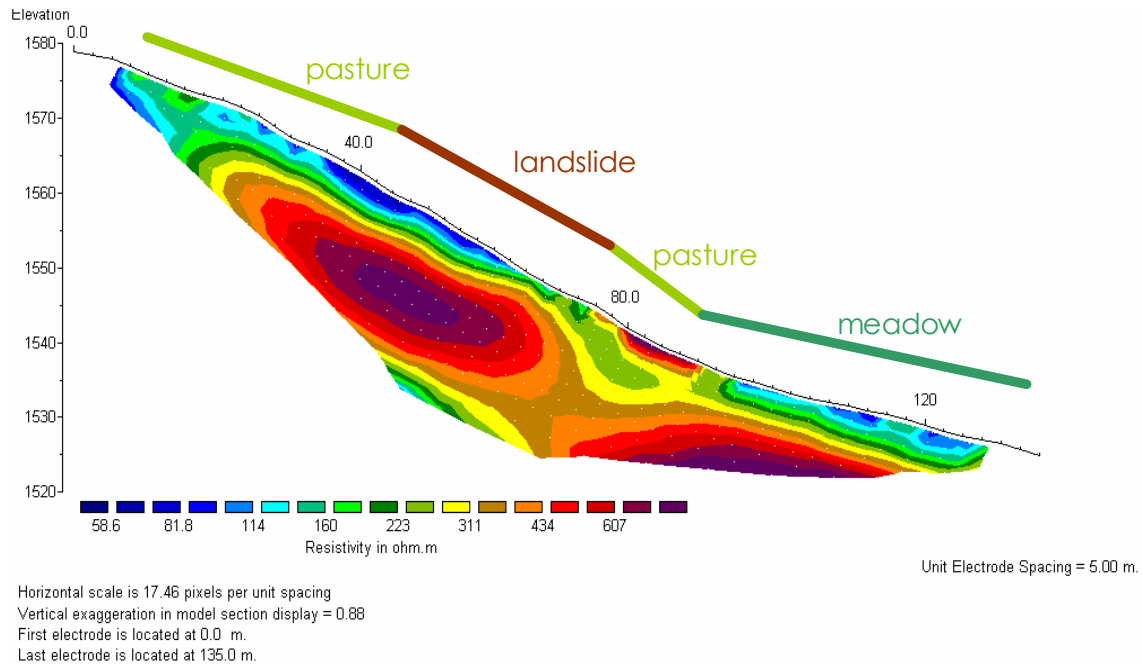


Figure 10-5. ERT transect at landslide slope in Hospental (Dipole-dipole | 5 m spacing | 28 electrodes | RMS error 1.9 % | 26.09.06) during wet conditions.

The site without landslide is characterised by higher resistivities (Figure 10-6), which might be due to difference in parent material. Both sites are located on the Mesozoic formation, however, the Realp site is covered by siliceous moraine and debris material. The amount of stored pore water and the conductivity of the pore water itself might be lower for this material. Lower resistivity in the subjacent layer suggests drainage of the slope water.

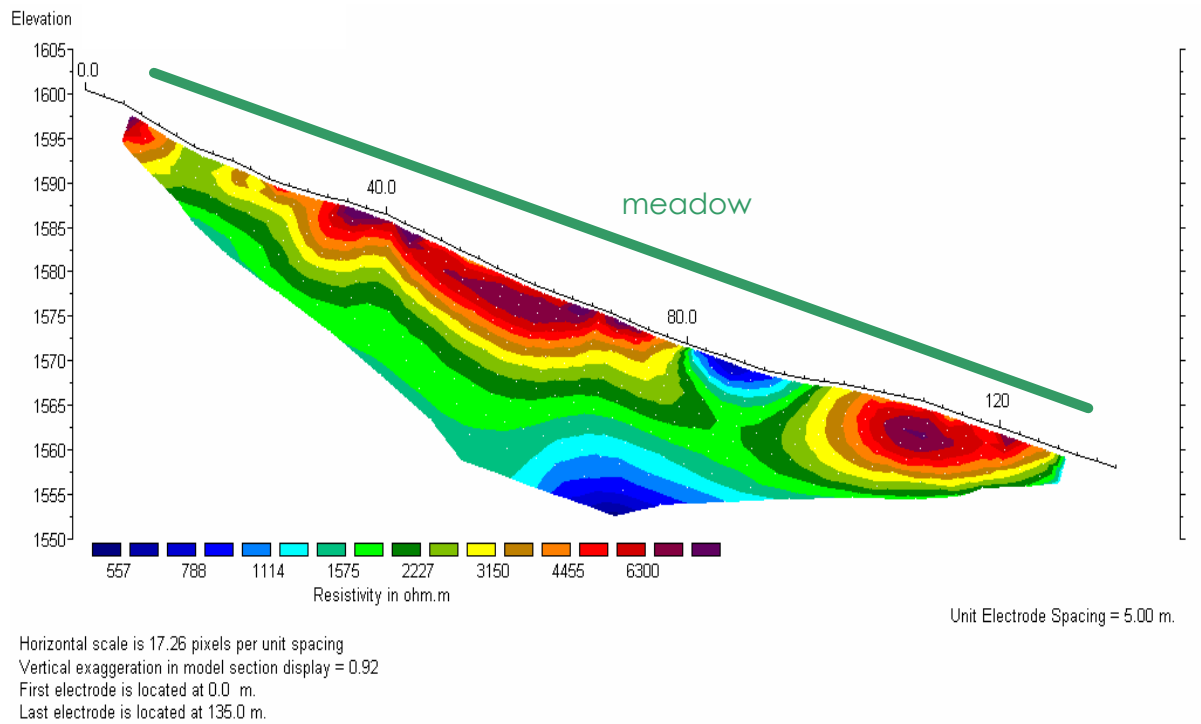


Figure 10-6. ERT transect at landslide slope in Realp (Dipole-dipole | 5 m spacing | 28 electrodes | RMS error 3.3 % | 26.09.06) during wet conditions.

ACKNOWLEDGEMENTS

Am Ende meiner Dissertation möchte ich mich bei jenen bedanken, die mich bei dieser anspruchsvollen und interessanten Aufgabe unterstützt haben.

Danke...

... Christine Alewell, neben der fachlichen Unterstützung vor allem für die angenehme Arbeitsatmosphäre.

... Jean-Pierre Clement für die unkomplizierte Zusammenarbeit und für die Möglichkeit zur Fortführung dieser Arbeit.

... Dominik Bänninger, der jederzeit bereitwillig Hilfe bei aussichtslosen Problemen bot.

... Nadine Konz und Monika Schaub, die meine Arbeit nicht nur mit zahlreichen Leckereien sondern auch mit viel Humor versüsst haben.

... der ganzen UGW-Gruppe für unterhaltsame Kaffeepausen.

CURRICULUM VITAE

Katrin Meusbürger

born on 4th July 1978 in Waldshut, Germany

Education

| | |
|-------------|---|
| 1985 – 1989 | Grundschule, Berau, Germany |
| 1989 – 1995 | Realschule, Tiengen, Germany |
| 1995 – 1998 | Justus-Liebig Gymnasium, Waldshut, Germany |
| 1998 – 1999 | Master student in Chemistry at the Albert-Ludwigs University Freiburg i.Br., Germany |
| 1999 – 2005 | Master student in Hydrology at the Albert-Ludwigs University Freiburg i.Br., Germany (Supervised by Prof. Dr. Christian Leibundgut) |
| 2005 – 2009 | PhD-Student, Institute of Environmental Geosciences, University of Basel, Switzerland (Supervised by Prof. Dr. Christine Alewell) |

Work experience and courses

| | |
|--------------|---|
| AUG-OKT/2001 | Internship at the Eidgenössischen Anstalt für Wasserversorgung, Abwasserreinigung und Gewässerschutz (EAWAG), Zürich, Switzerland |
| SEP-OKT/2003 | Participation at ASTHyDA International Study Course on Hydrological Droughts, Alterra, Wageningen, Netherlands |
| JAN-MAR/2003 | Internship at the National Institute of Water and Atmospheric Research (NIWA), Christchurch, New Zealand |
| FEB-JUL/2005 | Research assistant at the Institute of Hydrology, Albert-Ludwigs University, Freiburg i.Br., Germany |